

Aus der Professur für Bodenphysik  
der Agrar- und Umweltwissenschaftlichen Fakultät

## **Groundwater Defluoridation: Fixed-Bed Column Systems Packed with Rock Materials**

Kumulative Dissertation

zur

Erlangung des akademischen Grades  
Doktor der Ingenieurwissenschaften (Dr.-Ing.)

an der Agrar- und Umweltwissenschaftliche Fakultät  
der Universität Rostock

vorgelegt von

Wondwosen Sime Geleta, geb. am 30.06.1983  
in Fitch, Oromia, Äthiopien

Rostock, 2023



Dieses Werk ist lizenziert unter einer  
Creative Commons Namensnennung - Weitergabe unter gleichen  
Bedingungen 4.0 International Lizenz.

## **Gutachter**

### **Prof. Dr. Bernd Lennartz**

Professur für Bodenphysik  
Agrar- und Umweltwissenschaften Fakultät  
Universität Rostock  
Justus Von Liebig Weg 6, 18051 Rostock, Germany

### **Prof. Dr.-Ing. Esayas Alemayehu**

Professor of Water and Environmental Engineering  
Faculty of Civil and Environmental Engineering  
Jimma University, Jimma Institute of Technology  
P. O. BOX 378, Jimma, Ethiopia

### **Prof. Dr.-Ing. habil. Jens Tränckner**

Professur für Wasserwirtschaft  
Agrar- und Umweltwissenschaften Fakultät  
Universität Rostock  
Satower Straße 48, 18059 Rostock, Germany

### **Dr. Shimelis Kebede**

Associate Professor of Chemical/ Environmental Engineering  
Addis Ababa University, Addis Ababa Institute of Technology  
School of Chemical and Bio Engineering  
St. George IV Street, P.O.BOX 385, Addis Ababa, Ethiopia

**Eingereicht am:** 02.01.2023

**Verteidigt am:** 10.11.2023

**Wissenschaftliche Betreuer:**

**Prof. Dr. Bernd Lennartz**

Professur für Bodenphysik

Agrar- und Umweltwissenschaften Fakultät

Universität Rostock

Justus Von Liebig Weg 6, 18051 Rostock, Germany

**Prof. Dr.-Ing. Esayas Alemayehu**

Professur für Wasserversorgung und Umwelttechnik

Bau- und Umwelttechnik Fakultät

Universität Jimma

P.O.BOX 378, Jimma, Oromia, Äthiopien

# Table of Contents

<b>List of Figures</b> .....	v
<b>List of Tables</b> .....	vii
<b>List of Symbols and Abbreviations</b> .....	viii
<b>Eidesstattliche Erklärung</b> .....	xi
<b>Dedicatory</b> .....	xii
<b>Acknowledgments</b> .....	xiii
<b>Summary</b> .....	xiv
<b>Zusammenfassung</b> .....	xvi
<b>1. General Introduction</b> .....	1
1.1. Background .....	1
1.2. Groundwater and Geogenic Pollutants .....	1
1.3. Benefits and Health Effects of Fluoride.....	2
1.4. Fluoride Occurrence.....	5
1.5. Fluoride Treatment Technologies .....	8
1.5.1. Adsorbent Materials for Water Defluoridation .....	11
1.5.1.1. Activated Alumina (AA).....	11
1.5.1.2. Bone Char (BC) .....	12
1.5.1.3. Volcanic Rocks .....	14
1.6. Aim and Scope of the Study .....	15
1.7. Hypothesis and Key Questions .....	17
1.8. Research Objectives.....	17
1.9. Experimental Setups and Conceptual Framework .....	18
1.10. Structure of the Dissertation .....	18
<b>2. Volcanic Rock Materials for Defluoridation of Water in Fixed-Bed Column Systems</b> .....	21
2.1. Introduction.....	22
2.2. Materials and Methods.....	24
2.2.1. Materials .....	24
2.2.2. Preparations of Adsorbents .....	24
2.2.3. Preparations of Adsorbate.....	24
2.2.4. Adsorbent Characterizations .....	25
2.2.4.1. Crystalline Structures.....	25
2.2.4.2. Chemical Composition.....	25
2.2.4.3. Fourier Transform Infrared (FTIR) Analysis.....	25
2.2.4.4. Scanning Electron Microscope (SEM) Analysis.....	25

2.2.4.5.	Determination of pH and Point of Zero Charges ( $\text{pH}_{\text{PZC}}$ ) .....	25
2.2.4.6.	BET Analysis .....	26
2.2.5.	Column Adsorption Experimental Set-up and Procedures .....	26
2.2.6.	Modeling and Analysis of Fixed-Bed Column Data .....	27
2.2.7.	Fixed-Bed Column Breakthrough Curve Modeling .....	29
2.2.7.1.	Thomas Model .....	30
2.2.7.2.	Adams-Bohart model .....	30
2.3.	Results and Discussions .....	31
2.3.1.	Characterization of Adsorbents .....	31
2.3.1.1.	Crystalline Structures and Material Properties and Experimental Conditions .....	31
2.3.1.2.	Chemical Composition .....	32
2.3.1.3.	Fourier Transform Infrared (FTIR) Analysis .....	33
2.3.1.4.	Scanning Electron Microscope (SEM) analysis .....	34
2.3.1.5.	pH and Point of Zero Charges ( $\text{pH}_{\text{PZC}}$ ) .....	35
2.3.2.	Effect of Adsorbents Particle Size .....	35
2.3.3.	Effect of Influent pH .....	36
2.3.4.	Effect of Flow Rate .....	39
2.3.5.	Application of the Thomas Model .....	40
2.3.6.	Application of the Adams-Bohart Model .....	42
2.3.7.	Comparison of Different Adsorbents on Fluoride Removal .....	43
2.4.	Conclusions .....	43
<b>3.</b>	<b>Enhanced Defluoridation of Water Using Zirconium-Coated Pumice in Fixed-Bed Adsorption Columns .....</b>	<b>45</b>
3.1.	Introduction .....	46
3.2.	Materials and Methods .....	48
3.2.1.	Adsorbent Preparations .....	48
3.2.1.1.	Natural Pumice .....	48
3.2.1.2.	Coating of VPum with Zirconium .....	48
3.2.2.	Chemicals and Reagents .....	49
3.2.3.	Adsorbent Characterizations .....	49
3.2.3.1.	Crystalline Structure .....	49
3.2.3.2.	Chemical Composition .....	49
3.2.3.3.	Fourier Transform Infrared (FT-IR) Analysis .....	49
3.2.3.4.	Surface Area ( $S_{\text{BET}}$ ) and Pore-Size Distribution Analysis .....	49
3.2.3.5.	Scanning Electron Microscope (SEM) Analysis .....	50
3.2.3.6.	pH and Point of Zero Charges ( $\text{pH}_{\text{PZC}}$ ) .....	50

3.2.3.7.	Surface Acidity/Basicity Analysis .....	50
3.2.4.	Fixed-Bed Column Adsorption Studies .....	50
3.2.5.	Analysis of Column Data .....	51
3.2.6.	Breakthrough Curve Modeling .....	52
3.2.6.1.	Thomas Model .....	53
3.2.6.2.	Adams-Bohart Model.....	53
3.3.	Results and Discussions .....	54
3.3.1.	Characterization of Adsorbents.....	54
3.3.1.1.	Crystalline Structure .....	54
3.3.1.2.	Chemical Composition.....	55
3.3.1.3.	Fourier Transform Infrared (FTIR) Analysis .....	56
3.3.1.4.	Surface Area ( $S_{\text{BET}}$ ) and Pore-Size Distribution Analysis.....	57
3.3.1.5.	Scanning Electron Microscope (SEM) Analysis.....	57
3.3.1.6.	pH and Point of Zero Charges ( $\text{pH}_{\text{PZC}}$ ) .....	58
3.3.1.7.	Surface Acidity/Basicity Analysis .....	59
3.3.2.	Effect of Experimental Conditions on Fluoride Removal.....	59
3.3.2.1.	Initial Solution pH.....	59
3.3.2.2.	Flow Rate .....	61
3.3.3.	Application of the Thomas Model .....	62
3.3.4.	Application of the Adams-Bohart Model.....	64
3.3.5.	Performance of various Adsorbents on Fluoride Uptake .....	65
3.4.	Conclusions.....	66
<b>4.</b>	<b>Fixed-bed Adsorption: Comparisons of Virgin and Zirconium Oxide–Coated Scoria for the Removal of Fluoride from Water .....</b>	<b>67</b>
4.1.	Introduction.....	68
4.2.	Materials and Methods.....	70
4.2.1.	Adsorbent Preparations .....	70
4.2.2.	Coating of Zirconium Oxide onto Virgin Scoria (VSco).....	70
4.2.3.	Chemicals and Reagents .....	71
4.2.4.	Characterizations of the Materials .....	71
4.2.5.	Fixed-bed Column Adsorption Studies .....	72
4.2.6.	Analysis of Column Data.....	73
4.2.6.1.	Breakthrough Curve .....	73
4.2.7.	Breakthrough Curve Modeling .....	74
4.2.7.1.	Thomas Model .....	75
4.2.7.2.	Adams-Bohart Model.....	75

<b>4.3. Results and Discussions .....</b>	<b>76</b>
4.3.1. Characterization of Adsorbents.....	76
4.3.2. Influence of Experimental Parameters on Fluoride Removal .....	81
4.3.2.1. Influence of Initial Solution pH .....	81
4.3.2.2. Influence of Initial Flow Rate .....	83
4.3.3. Application of the Thomas Model .....	85
4.3.4. Application of the Adams-Bohart Model.....	87
4.3.5. Fluoride Adsorption Performance of Different Adsorbents.....	89
4.4. Conclusions.....	90
<b>5. Synthesis, General Outlook, Limitations, and Recommendations for Further study .....</b>	<b>92</b>
5.1. Overview.....	92
5.2. Synthesis .....	92
5.2.1. Physiochemical Characteristics of the Adsorbents .....	92
5.2.2. Effect of Experimental Conditions on Fluoride Removal.....	94
5.2.2.1. Effect of Adsorbent Particle Size.....	94
5.2.2.2. Effect of pH.....	95
5.2.2.3. Effect of Flow Rate .....	97
5.2.2. Application of the Thomas and Adams-Bohart Models.....	98
5.3. General Outlook, Limitations, and Recommendations for Further Study .....	101
<b>References.....</b>	<b>103</b>
<b>Appendices: Supplementary materials .....</b>	<b>118</b>

## List of Figures

<b>Figure 1.1</b> Illustration of fluoride problem: example for the image of dental (left image) and skeletal (right image) fluorosis (Eawag, 2015).....	5
<b>Figure 1.2</b> Estimated probability for fluoride concentration in groundwater exceeding 1.5 mg/L (Amini et al., 2008).....	6
<b>Figure 1.3</b> Fluoride concentration profile in Ethiopian drinking water sources (MacDonald et al., 2009) .....	7
<b>Figure 1.4</b> Activated alumina (AA) grains (Eawag, 2015) .....	11
<b>Figure 1.5</b> Bone char material (Salifu, 2017).....	13
<b>Figure 1.6</b> Experimental setups and conceptual framework .....	18
<b>Figure 2.1</b> XRD patterns for (a) virgin pumice (VPum) and (b) virgin scoria (VSco).....	32
<b>Figure 2.2</b> Fourier-transform infrared (FTIR) for (a) VPum and (b) VSco.....	34
<b>Figure 2.3</b> SEM micrographs for (a) VPum and (b) VSco .....	34
<b>Figure 2.4</b> Determination of pH point of zero charges (pH <sub>PZC</sub> ) for (a) VPum and (b) VSco .....	35
<b>Figure 2.5</b> Effect of particle sizes on the breakthrough behavior of fluoride in (a) VPum and (b) VSco at (pH 2.00; influent fluoride concentration 10 mg/L (C <sub>0</sub> : 10 mg/L); flow rate 1.25 mL/min (Q <sub>0</sub> : 1.25 mL/min; bed depth 10 cm) .....	37
<b>Figure 2.6</b> Effect of pH on the breakthrough behavior of fluoride in (a) VPum: 0.075–0.425 mm and (b) VSco: < 0.075 mm (C <sub>0</sub> : 10 mg/L; Q <sub>0</sub> : 1.25 mL/min; bed depth 10 cm).....	38
<b>Figure 2.7</b> Effect of influent flow rate on the breakthrough behavior of fluoride in (a) VPum: 0.075–0.425 mm and (b) VSco: < 0.075 mm (pH 2; C <sub>0</sub> : 10 mg/L; bed depth 10 cm).....	40
<b>Figure 3.1</b> The geographical location of natural pumice (VPum) sample collections .....	48
<b>Figure 3.2</b> XRD patterns for (a) VPum and Zirconium–coated pumice (Zr–Pu) (b) before and (c) after adsorption.....	55
<b>Figure 3.3</b> Fourier–transform infrared (FT–IR) for (a) VPum; Zr–Pu (b) before and (c) after adsorption.....	57
<b>Figure 3.4</b> SEM micrographs of (a) VPum; Zr– Pu (b) before and after (c) adsorption.....	58
<b>Figure 3.5</b> Effect of solution pH on the breakthrough performance of fluoride onto Zr–Pu (initial fluoride concentration 10 mg/L (C <sub>0</sub> : 10 mg/L); initial flow rate 1.25 mL/min (Q <sub>0</sub> : 1.25 mL/min); bed depth 10 cm).....	60
<b>Figure 3.6</b> Effect of initial flow rate on the breakthrough performance of fluoride onto Zr–Pu (pH 2; C <sub>0</sub> : 10 mg/L; bed depth 10 cm).....	62
<b>Figure 3.7</b> Experimental (exp.) and simulated (cal.; Thomas model) breakthrough curves of fluoride for Zr–Pu at different (a) pH values (C <sub>0</sub> : 10 mg/L; Q <sub>0</sub> : 1.25 mL/min; bed depth 10 cm) and (b) initial flow rates, Q <sub>0</sub> (pH 2; C <sub>0</sub> : 10 mg/L; bed depth 10 cm) .....	63
<b>Figure 3.8</b> Experimental (exp.) and simulated (cal.; Adams-Bohart model) breakthrough curves of fluoride for Zr–Pu at different (a) pH values (C <sub>0</sub> : 10 mg/L; Q <sub>0</sub> : 1.25 mL/min; bed depth 10 cm) and (b) Q <sub>0</sub> (pH 2; C <sub>0</sub> : 10 mg/L; bed depth 10 cm).....	64
<b>Figure 4.1</b> Sampling site of virgin scoria (VSco).....	71
<b>Figure 4.2</b> XRD patterns for (a) VSco; zirconium oxide-coated scoria (ZrOCSco) (b) before and (c) after adsorption experiment.....	77
<b>Figure 4.3</b> Fourier-transform infrared (FT-IR) for (a) VSco; ZrOCSco (b) before, and (c) after adsorption experiment.....	78
<b>Figure 4.4.</b> SEM image of (a) VSco and (b) ZrOCSco before adsorption experiments. ....	80
<b>Figure 4.5.</b> TGA-DTA thermograms of (a) VSco and (b) ZrOCSco before adsorption experiments. ....	81
<b>Figure 4.6</b> Effect of solution pH on fluoride breakthrough (a) VSco and (b) ZrCSc (initial fluoride concentration 10 mg/L (C <sub>0</sub> : 10 mg/L); initial flow rate 1.25 mL/min (Q <sub>0</sub> : 1.25 mL/min); bed depth 10 cm).....	81
<b>Figure 4.7</b> Effect of initial flow rate on the fluoride breakthrough (a) VSco and (b) ZrOCSco (pH 2; C <sub>0</sub> : 10 mg/L; bed depth 10 cm).....	84



<b>Figure 4.8</b> Experimental (exp.) and simulated (cal.; Thomas model) breakthrough curves of fluoride for ZrOCSs at different (a) pH ( $C_0$ : 10 mg/L; $Q_0$ : 1.25 mL/min; bed depth 10 cm) and (b) Initial flow rate, $Q_0$ (pH 2; $C_0$ : 10 mg/L; bed depth 10 cm) .....	85
<b>Figure 4.9</b> Experimental (exp.) and simulated (cal.; Thomas model) breakthrough curves of fluoride for VScO at different (a) pH ( $C_0$ : 10 mg/L; $Q_0$ : 1.25 mL/min; bed depth 10 cm) and (b) Initial flow rate, $Q_0$ (pH 2; $C_0$ : 10 mg/L; bed depth 10 cm) .....	86
<b>Figure 4.10</b> Experimental (exp.) and simulated (cal.; Adams-Bohart model) breakthrough curves of fluoride for ZrOCSs at different (a) pH ( $C_0$ : 10 mg/L; $Q_0$ : 1.25 mL/min; bed depth 10 cm) and (b) $Q_0$ (pH 2; $C_0$ : 10 mg/L; bed depth 10 cm) .....	87
<b>Figure 4.11</b> Experimental (exp.) and simulated (cal.; Adams-Bohart model) breakthrough curves of fluoride for VScO at different (a) pH ( $C_0$ : 10 mg/L; $Q_0$ : 1.25 mL/min; bed depth 10 cm) and (b) $Q_0$ (pH 2; $C_0$ : 10 mg/L; bed depth 10 cm) .....	88
<b>Figure 4.11</b> Experimental (exp.) and simulated (cal.; Adams-Bohart model) breakthrough curves of fluoride for VScO at different (a) pH ( $C_0$ : 10 mg/L; $Q_0$ : 1.25 mL/min; bed depth 10 cm) and (b) $Q_0$ (pH 2; $C_0$ : 10 mg/L; bed depth 10 cm) .....	89
<b>Figure 5.1</b> Effects of particle sizes on the adsorption performance of VScO and VPum (pH 2.00; $C_0$ : 10 mg/L; $Q_0$ : 1.25 mL/min; bed depth 10 cm) .....	95
<b>Figure 5.2</b> Effects of solution pH on the adsorption performance of the adsorbents (particle sizes: 0.075 – 0.425 mm; $C_0$ : 10 mg/L; $Q_0$ : 1.25 mL/min; bed depth 10 cm) .....	96
<b>Figure 5.3</b> Effects of initial flow rate on the adsorption performance of the adsorbents (particle sizes: 0.075 – 0.425 mm; pH: 2.00; bed depth 10 cm) .....	98

## List of Tables

<b>Table 1.1</b> Level of fluoride in drinking water and its related health effects (modified from Salifu et.al, (Salifu, 2017), and Edmunds & Smedley (Edmunds & Smedley, 2014)) .....	4
<b>Table 1.2</b> Regulations and recommendations for fluoride concentrations from some organizations or countries (Edmunds & Smedley, 2014).....	4
<b>Table 2.1</b> Material properties and experimental conditions .....	32
<b>Table 2.2</b> Fixed-bed column parameters obtained for fluoride adsorption onto VPum and VSco .....	37
<b>Table 2.3</b> Thomas model parameters for fluoride adsorption onto VPum and VSco .....	41
<b>Table 2.4</b> Adams–Bohart model parameters for fluoride adsorption onto VPum and VSco .....	42
<b>Table 2.5</b> Comparison of other adsorbents with VPum and VSco.....	43
<b>Table 3.1</b> Elemental and oxide compositions of natural pumice (VPum) and Zr–Pu.....	56
<b>Table 3.2</b> Textural properties of VPum and Zr–Pu.....	57
<b>Table 3.3</b> Fixed-bed column parameters obtained for defluoridation by zirconium–coated pumice (Zr–Pu) and on VPum (recent study) (Geleta et al., 2021b) .....	60
<b>Table 3.4</b> Thomas model parameter values for defluoridation by Zr–Pu, and VPum (Geleta et al., 2021b)....	63
<b>Table 3.5</b> Adams-Bohart model parameter values for defluoridation by Zr–Pu, and VPum (Geleta et al., 2021b).....	64
<b>Table 3.6</b> Fluoride adsorption capacity of various adsorbents .....	65
<b>Table 4.1</b> Elemental and oxide compositions of virgin scoria (VSco) and zirconium oxide-coated scoria (ZrOCSc) .....	79
<b>Table 4.2</b> Fixed-bed column parameters obtained for defluoridation by VSco and ZrOCSc .....	82
<b>Table 4.3</b> Thomas model parameter values for the defluoridation by VSco and ZrOCSc.....	86
<b>Table 4.4</b> Adams-Bohart model parameter values for defluoridation by ZrOCSc and VSco.....	89
<b>Table 4.5</b> Fluoride uptake capacity of some reported adsorbents .....	90

## List of Symbols and Abbreviations

A	Cross-Sectional Area of the Fixed-bed [cm <sup>2</sup> ]
Al <sub>2</sub> O <sub>3</sub>	Aluminum oxide [-]
Al	Aluminum [-]
A <sub>pa</sub>	Integrated peak areas for the amorphous components [-]
As	Arsenic [-]
BDST	Bed Depth Service Time
BET	Brunauer-Emmett-Teller
Ca	Calcium [-]
C <sub>ad</sub>	Adsorbed fluoride concentration [mgL <sup>-1</sup> ]
Cal.	Simulated/Calculated [-]
C <sub>b</sub>	Breakthrough concentration [mgL <sup>-1</sup> ]
C <sub>d</sub>	Cadmium [-]
Cm	Measured crystallinity [%]
Co	Cobalt [-]
C <sub>o</sub>	Initial solute concentration [mgL <sup>-1</sup> ]
C <sub>pa</sub>	Integrated peak areas for the crystalline components [-]
Cr	Chromium [-]
C <sub>t</sub>	Solute concentration at the time, t [mgL <sup>-1</sup> ]
Cu	Copper [-]
Cu K $\alpha$	Copper K $\alpha$ emission [-]
CuO	Copper oxide [-]
DAAD	Deutscher Akademischer Austauschdienst
DTA	Differential Thermal Analysis [-]
EBCT	Empty Bed Contact Time [min]
EC	European Commission
exp.	Experimental [-]
Fe <sub>2</sub> O <sub>3</sub>	Iron oxide [-]
Fe	Iron [-]
FTIR	Fourier-Transforms Infrared Spectroscopy [-]
GV	Guideline value
MCLG	Maximum contaminant level goal
MDPI	Multidisciplinary Digital Publishing Institute
H	Column Height [cm]
h	Hour [-]
H <sub>B</sub>	Used bed length [cm]
HCl	Hydrochloric acid [-]
H <sub>T</sub>	Total bed height [cm]
ICP-OES	Inductively coupled plasma-optical emission spectroscopy [-]
IUPAC	International Union of Pure and Applied Chemistry
K <sub>2</sub> O	Potassium Oxide [-]
K	Potassium [-]
K <sub>AB</sub>	Adams-Bohart kinetic constant [Lmin <sup>-1</sup> .mg <sup>-1</sup> ]

KBr	Potassium bromide [-]
$K_T$	Thomas rate constant [ $L \text{min}^{-1} \cdot \text{mg}^{-1}$ ]
kV	kilo volt [-]
L	Liter [-]
m	Mass of dry adsorbent [kg]
mA	Milliamp [-]
$m_{\text{ads}}$	Dry mass of adsorbent [g]
Mg	Magnesium [-]
MgO	Magnesium Oxide [-]
mL	milliliter [-]
MnO	Manganese Oxide [-]
MTZ/ $H_{\text{UNB}}$	Mass Transfer Zone/Unused Bed Length [cm]
$\text{Na}(\text{AlSi}_3\text{O}_8)$	Albite low/Albite high [-]
$\text{Na}_2\text{O}$	Sodium Oxide [-]
Na	Sodium [-]
NaF	Sodium Fluoride [-]
NaOH	Sodium Hydroxide [-]
NEERI	National Environmental Engineering Research Institute
Ni	Nickel [-]
$\text{NH}_4\text{OH}$	Ammonium hydroxide
NiO	Nickel oxide [-]
NMR	Nuclear Magnetic Resonance Spectrometer [-]
$P_b$	Lead [-]
$\text{pH}_{\text{PZC}}$	pH Point of Zero Charges [-]
Psize	Particle size [mm]
Q	Flow rate [ $\text{cm}^3 \text{min}^{-1}$ ]
$q_b$	Fluoride uptake at breakthrough [ $\text{mg kg}^{-1}$ ]
$q_e$	Equilibrium fluoride uptake [ $\text{mg kg}^{-1}$ ]
$q_{\text{total}}$	Total amount of fluoride adsorbed [ $\text{mg kg}^{-1}$ ]
$R^2$	Coefficient of determination [-]
SEM	Scanning Electron Microscope [-]
Si	Silicon [-]
$\text{SiO}_2$	Silicon Oxide [-]
t	Time [min]
$t_b$	Breakthrough time [min]
$t_e$	Exhaustion time [min]
TGA	Thermogravimetric Analysis [-]
$\text{TiO}_2$	Titanium oxide [-]
$t_{\text{total}}$	Total flow time until saturation of the bed [min]
U.S.EPA	U.S. Environmental Protection Agency
$v$	Linear flow rate [ $\text{mL min}^{-1}$ ]
$V_b$	Breakthrough volume [mL]
$V_B$	Fixed-bed volume [ $\text{cm}^3$ ]
$V_e$	Effluent volume [mL]

$V_f$	Filter (superficial) velocity [ $\text{cm min}^{-1}$ ]
$V_I$	Effective (interstitial) velocity [ $\text{cm min}^{-1}$ ]
VPum	Virgin pumice [-]
VSco	Virgin scoria [-]
$V_t$	Bulk volume [ $\text{cm}^3$ ]
$V_v$	Void volume [ $\text{cm}^3$ ]
$W_{\text{dry}}$	Weight of dry adsorbent [g]
$W_{\text{sat}}$	Weight of saturated adsorbent [g]
$W_{\text{total}}$	The total amount of fluoride sent to a packed column [mg]
WHO	World Health Organization
XRD	X-ray diffraction [-]
XRF	X-ray fluorescence [-]
XPS	X-ray Photoelectron Spectroscopy [-]
Z	Column bed depth [cm]
ZnO	Zinc oxide [-]
ZrCSc	Zirconium-coated scoria [-]
$\text{ZrOCl}_2 \cdot 8\text{H}_2\text{O}$	zirconium (IV) oxychloride octahydrate
Zr – Pu	Zirconium-coated pumice [-]
Å	Angstrom [-]
$\varepsilon_b$	The total porosity of the adsorbent [-]
$\rho_b$	Bulk density [ $\text{gmcm}^{-3}$ ]

## **Eidesstattliche Erklärung**

Hiermit erkläre ich durch eigenhändige Unterschrift, die vorliegende Dissertation selbstständig verfasst und keine anderen als die angegebenen Quellen und Hilfsmittel verwendet zu haben. Die aus den Quellen direkt oder indirekt übernommenen Gedanken sind als solche kenntlich gemacht. Die Dissertation ist in dieser Form noch keiner anderen Prüfungsbehörde vorgelegt worden.

Jimma, 02.01.2023

Geleta, Wondwosen sime



---

Ort, Datum

---

Unterschrift der Doktorandin/des Doktoranden

## **Dedictory**

**To God:** for allowing me to reach this stage and providing me with the well-being necessary to achieve my goals.

**To my dear sister:** this thesis is dedicated in memory of my dear sister Getenesh Sime Geleta.

**To all my dear family:** for encouraging and helping me throughout my study.

**To all my friends and colleagues:** for supporting me practically and emotionally.

## **Acknowledgments**

First and foremost, I would like to thank ALMIGHTY GOD for allowing me to reach this level and providing me with the health and well-being needed to achieve my goals. I would like to express my heartfelt gratitude to my supervisors: Prof. Dr. Bernd Lennartz (Chair of Soil Physics at the Faculty of Agricultural and the Environmental Sciences University of Rostock, Germany) and Prof. Dr.-Ing. Esayas Alemayehu (Professor of Water and Environmental Engineering at the Faculty of Civil and Environmental Engineering, Jimma Institute of Technology, Jimma University, Ethiopia) for their patience and very valuable guidance in bringing this research to the successful completion of the thesis in this current form. I am also very grateful to Mrs. Evelyn Boltzmann who kindly helped and supported me in measuring the experimental test samples results produced in this research study. I extend my gratitude to Dr. Agrar. Wakene Chewaka and Dr. Aberham Hailu for their keen support and editing of my document. My special thanks also go to my colleagues at the Chair of Soil Physics, Faculty of Agricultural and Environmental Sciences, University of Rostock, Germany, including Dr. Agrar. Haojie Liu, Mrs. Miaorun Wang, Mr. Erwin Don Racasa, Dr. Agrar. Andreas Bauwe, Mr. Tilo Hartwig, and others for their kind help and support.

Furthermore, I am greatly indebted to DAAD and the Ethiopian Ministry of Education for providing me with a scholarship during my research work, as well as to Jimma University, Jimma Institute of Technology School of Chemical Engineering, for their encouragement and support.

I would like to express my utmost gratitude to my family and friends for their support and prayers.



## Summary

Fluoride intoxication is one of the drinking water quality parameters of concern worldwide; the excess ( $> 1.5$  mg/L, WHO guideline value) of which pollutes groundwater resources and makes them unsuitable for human consumption due to the associated adverse health effects. Therefore, the search for suitable, low-cost, and locally available materials to reduce excess fluoride levels in groundwater remains critical to minimize its adverse health effects in drinking water. There are various methodologies for the treatment of fluoride-laden water; however, adsorption is recognized as one of the most effective methods due to its simplicity of design and low cost. Numerous adsorbents have indeed been examined and reported for the adsorption of fluoride-laden water. However, many of the materials suffer from one of the following issues: time-consuming synthesis procedures, high manufacturing costs, scarcity of raw materials, and a short lifetime, making them impractical to apply in low-income countries (e.g., as in the case of Ethiopia). Therefore, this dissertation aimed to explore the possibility of using unmodified and surface-modified adsorbents derived from low-cost and easily accessible volcanic rock materials (virgin pumice (VPum) and virgin scoria (VSco)) for the treatment of fluoride-laden groundwater in flow-through fixed-bed column adsorption systems. The first part of the research examined the use of unmodified VPum and VSco at various experimental conditions such as particle sizes, initial solution pH, and initial volumetric flow rates. The second and third constituents of the research goal evaluated the use of surface-modified VPum and VSco, respectively under various initial solution pH and initial volumetric flow rates. Surface modification of the low-cost materials was achieved by zirconium oxide coating onto the adsorbent's particle sizes ranging from 0.075 to 0.425 mm using 0.1 M  $\text{ZrOCl}_2 \cdot 8\text{H}_2\text{O}$  as the Zirconium-bearing solution. Hence, two different types of zirconium-modified adsorbents were produced: zirconium oxide-coated pumice (Zr – Pu) and zirconium oxide-coated scoria (ZrOCSc). The physicochemical properties of the adsorbents were characterized using various techniques: X-ray diffraction (XRD), X-ray fluorescence (XRF) analysis, scanning electron microscopy (SEM), Fourier transform infrared (FTIR) analysis, Brunauer-Emmett-Teller (BET) specific surface area, inductively coupled plasma-optical emission spectroscopy (ICP-OES), and pH point of zero charges ( $\text{pH}_{\text{PZC}}$ ). This provided vital information on the fluoride adsorption mechanism of the adsorbents. Simultaneous thermogravimetric and differential thermal analysis (TGA/DTA) of VSco and ZrOCSc were also carried out to understand their thermal resistance using DTG-60H. The column tests were conducted in a small-scale cylindrical filter column with an internal diameter of 8.1 cm and a height of 10 cm. Ion chromatography (IC) has been used to determine the remaining fluoride in the effluent solution. The obtained experimental results were analyzed/modeled using two widely used and well-known models: Thomas and Adams-Bohart models. Nonlinear optimization techniques were employed to determine the best fit and obtain the associated model parameters. The obtained model parameters could provide a better understanding and vital information for process design and scale-up. The first, second, and third components of the study evaluated the fluoride adsorption performance of VPum and VSco, Zr – Pu and VPum, and ZrOCSc and VSco, respectively.

The maximum adsorption capacity of 110 mg/kg for VPum (particle sizes: 0.075–0.425 mm) and 22 mg/kg (particle sizes: < 0.075 mm) for VScO were achieved at a low solution pH (2.00) and flow rate (1.25 mL/min). The results revealed that reducing the particle size of an adsorbent is a significant controlling factor in fluoride-VScO and fluoride-VPum systems at particle sizes of 0.075 and 0.075–0.425 mm, respectively. However, the effect of particle size on adsorption capacity is more pronounced for VScO than VPum. This implies that VPum loses internal porosity at the smallest particle size (<0.075 mm) due to damage to the continuum pore space (skeletal structure) when compared to fine particle size (0.075–0.425 mm). Using zirconium coating on the particle surface of VPum and VScO was influential in creating zirconium-based active sites for fluoride adsorption from aqueous solutions. The Zr – Pu had a maximum adsorption capacity of 225 mg/kg (2.05 times the adsorption capacity of VPum: 110 mg/kg), while ZrOCSc retained the maximum removal capacity of 58 mg/kg, which is 4.46 times higher than VScO (13 mg/kg) at a lower pH of 2 and an initial flow rate of 1.25 mL/min. The experimental results indicated that electrostatic attraction and surface complexation are the principal adsorption mechanisms for binding fluoride ions to the adsorbents. Furthermore, VPum and Zr-Pu beds showed higher removal efficiency than VScO and ZrOCSc beds under the same experimental conditions. The experimental adsorption data was well-matched by the Thomas and Adams-Bohart models with correlation coefficients ( $R^2$ ) of  $\geq 0.967$  for fluoride-modified volcanic rock systems and  $\geq 0.897$  for fluoride-unmodified volcanic rock systems. The values of the Thomas rate constant ( $K_T$ ) and Adams-Bohart rate constant ( $K_{AB}$ ) decreased as the influent flow rate decreased but, the adsorption capacity per mass of the bed of the adsorbents predicted by the Thomas model ( $q_0$ ; mg/kg) and the adsorption capacity per volume of the bed predicted by Adams-Bohart model ( $N_0$ ; mg/L) increased. An increase in  $N_0$  and  $q_0$  values with decreasing flow rates is ascribed to the increase in EBCT due to the direct proportion of the adsorption capacity to the interaction time. The derived model parameters could be used to upscale the design of the three developed adsorbent-based defluoridation filters without the need for additional experimentation. The fluoride adsorption performance of modified materials had been enhanced than that of unmodified ones, suggesting that the coating of VPum and VScO with zirconium could account for the improved activity and, hence, adsorption capacity.

This dissertation highlights the potential of unmodified and surface-modified adsorbents made from low-cost, readily available volcanic rock materials for removing excess fluoride from drinking water and groundwater. Further study is necessary to determine the feasibility of this method, including the impact of other ions and the ability to regenerate used adsorbents.

## Zusammenfassung

Die Belastung des Grundwassers mit Fluorid ist aufgrund geologischer Gegebenheiten an vielen Orten weltweit z.B. im Ostafrikanischen Graben zu beobachten. Die Nutzung des Grundwassers als Trinkwasser bei zu hohen Fluoridkonzentrationen ( $> 1,5 \text{ mg/L}$ , WHO-Richtwert) kann zu erheblichen Gesundheitsproblemen führen. Daher ist die Suche nach geeigneten, kostengünstigen und lokal verfügbaren Materialien zur Verringerung des überschüssigen Fluoridgehalts im Grundwasser nach wie vor von entscheidender Bedeutung, um die gesundheitsschädlichen Auswirkungen von Fluorid im Trinkwasser zu minimieren. Es gibt verschiedene Methoden zur Aufbereitung von fluoridbelastetem Wasser; die Adsorption gilt jedoch aufgrund ihrer Einfachheit und geringen Kosten als eine der wirksamsten Methoden. In der Tat wurden zahlreiche Adsorptionsmittel für die Aufbereitung von fluoridhaltigem Wasser untersucht und beschrieben. Viele der Materialien sind jedoch problembehaftet: zeitaufwändige Syntheseverfahren, hohe Herstellungskosten, Rohstoffknappheit und kurze Lebensdauer, was ihre Anwendung in Ländern mit niedrigem Einkommen (z. B. in Äthiopien) unpraktisch macht. In dieser Dissertation wurde daher die Möglichkeit untersucht, unmodifizierte und oberflächenmodifizierte Adsorbentien aus kostengünstigen und leicht zugänglichen vulkanischen Gesteinsmaterialien (Bimsstein (VPum) und Schlacke (VScO)) für die Aufbereitung von fluoridhaltigem Grundwasser in Durchfluss-Festbett-Adsorptionssystemen zu verwenden. Im ersten Teil der Untersuchung wurde der Einsatz von unmodifiziertem VPum und VScO unter verschiedenen Versuchsbedingungen wie Partikelgröße, anfänglicher pH-Wert der Lösung und anfängliches Durchflussvolumen bewertet. Im zweiten und dritten Teil des Forschungsvorhabens wurde die Verwendung von oberflächenmodifiziertem VPum und VScO unter verschiedenen anfänglichen pH-Werten der Lösung und anfänglichen Volumenströmen untersucht. Die Oberflächenmodifikation der kostengünstigen Materialien wurde durch Beschichtung mit Zirkoniumoxid auf den Partikelgrößen des Adsorptionsmittels von 0,075 bis 0,425 mm unter Verwendung von 0,1 M  $\text{ZrOCl}_2 \cdot 8\text{H}_2\text{O}$  als zirkoniumhaltige Lösung erreicht. Auf diese Weise wurden zwei verschiedene Arten von zirkoniummodifizierten Adsorbentien hergestellt: zirkoniumoxidbeschichteter Bimsstein (Zr-Pu) und zirkoniumoxidbeschichtete Schlacke (ZrOCSc). Die physikochemischen Eigenschaften der Adsorbentien wurden mit verschiedenen Techniken charakterisiert: Röntgenbeugung (XRD), Röntgenfluoreszenzanalyse (XRF), Rasterelektronenmikroskopie (SEM), Fourier-Transform-Infrarotanalyse (FTIR), spezifische Oberfläche nach Brunauer-Emmett-Teller (BET), induktiv gekoppelte plasma-optische Emissionsspektroskopie (ICP-EOS) und pH-Nullpunktladung (pHPZC). Die Analysen lieferten wichtige Informationen über den Fluoridadsorptionsmechanismus. Simultane thermogravimetrische und Differentialthermoanalysen (TGA/DTA) von VScO und ZrOCSc wurden ebenfalls durchgeführt, um ihre thermische Beständigkeit zu verstehen.

Die Säulenversuche wurden mit kleinen zylindrischen Filtersäulen mit einem Innendurchmesser von 8,1 cm und einer Höhe von 10 cm durchgeführt. Die Ionenchromatographie (IC) wurde eingesetzt, um das verbleibende Fluorid in der Ablauflösung zu bestimmen. Die erzielten Versuchsergebnisse wurden mit zwei weit verbreiteten

und bekannten Modellen analysiert/modelliert: Thomas- und Adams-Bohart-Modell. Nichtlineare Optimierungstechniken wurden eingesetzt, um die beste Anpassung zu erzielen und um Modellparameterwerte abzuleiten. Die erhaltenen Modellparameter können ein besseres Verständnis und wichtige Informationen für die Prozessgestaltung und das Scale-up liefern. In den drei Abschnitten der Studie wurde die Fluoridadsorptionsleistung von VPum und VScO, Zr-Pu und VPum bzw. ZrOCSc und VScO bewertet.

Die maximale Adsorptionskapazität von 110 mg/kg für VPum (Partikelgrößen: 0,075-0,425 mm) und 22 mg/kg (Partikelgrößen: < 0,075 mm) für VScO wurde bei einem niedrigen pH-Wert der Lösung (2,00) und einer Durchflussrate von 1,25 ml/min erreicht. Die Ergebnisse zeigen, dass die Verringerung der Partikelgröße eines Adsorptionsmittels ein wichtiger Kontrollfaktor in Fluorid-VScO- und Fluorid-VPum-Systemen bei Partikelgrößen von 0,075 bzw. 0,075-0,425 mm ist. Die Auswirkung der Partikelgröße auf die Adsorptionskapazität ist jedoch bei VScO stärker ausgeprägt als bei VPum. Die Zirkoniumbeschichtung erhöhte bei beiden getesteten Materialien die Adsorptionskapazität. Zr-Pu hatte eine maximale Adsorptionskapazität von 225 mg/kg (das 2,05-fache der Adsorptionskapazität von VPum: 110 mg/kg), während mit ZrOCSc eine maximale Entfernungskapazität von 58 mg/kg erreicht wurde, was 4,46-mal höher ist als bei VScO (13 mg/kg) bei einem pH-Wert von 2 und einer anfänglichen Durchflussrate von 1,25 mL/min. Die experimentellen Ergebnisse zeigten, dass elektrostatische Anziehung und Oberflächenkomplexierung die wichtigsten Adsorptionsmechanismen für die Bindung von Fluoridionen an die Adsorbentien sind. Außerdem zeigten VPum- und Zr-Pu-Materialien unter denselben experimentellen Bedingungen eine höhere Entfernungseffizienz als VScO- und ZrOCSc-Filtersäulen. Die experimentellen Adsorptionsdaten wurden durch die Thomas- und Adams-Bohart-Modelle mit Korrelationskoeffizienten ( $R^2$ ) von  $\geq 0,967$  für fluoridmodifizierte vulkanische Gesteinssysteme und  $\geq 0,897$  für fluoridunmodifizierte vulkanische Gesteinssysteme gut wiedergegeben. Die Werte der Thomas-Ratenkonstante ( $K_T$ ) und der Adams-Bohart-Ratenkonstante ( $K_{AB}$ ) verringerten sich mit abnehmendem Zufluss, während die nach dem Thomas-Modell vorhergesagte Adsorptionskapazität pro Masse des Adsorptionsmittels ( $q_0$ ; mg/kg) und die nach dem Adams-Bohart-Modell vorhergesagte Adsorptionskapazität pro Volumen der Säule ( $N_0$ ; mg/L) zunahm. Die abgeleiteten Modellparameter können für die Auslegung der von Defluoridierungsfiltren auf Adsorptionsbasis verwendet werden, ohne dass zusätzliche Experimente erforderlich sind.

Diese kumulative Dissertation unterstreicht, dass unmodifizierte und oberflächenmodifizierte Adsorbentien, die aus leicht zugänglichen und kostengünstigen vulkanischen Gesteinsmaterialien gewonnen werden, geeignet sind, überschüssiges Fluorid aus Trinkwasser/Grundwasser zu entfernen. Weitere Untersuchungen der Materialien, wie z. B. die Wirkung konkurrierender Ionen und die Regeneration verbrauchter Adsorbentien, sind erforderlich, um zu bestätigen, dass die Defluoridierung von Grundwasser mit Vulkangestein eine nachhaltige Methode ist.

# 1. General Introduction

## 1.1. Background

Since the 1990s, there have been tremendous steps in providing safe sources of drinking water to people around the globe. In 2015, 91 % of the world's population had access to improved (although not inherently safe) sources of drinking water compared to 76 % in 1990. More people have access to water through piped connections, public taps, protected wells, and boreholes ([WHO and UNICEF, 2015](#)). Access to clean water is not only crucial to human development and welfare but is also a fundamental human right. The provision of clean drinking water is considered vital and essential for overall growth and development, including adequate nutrition, education, gender equality, and, most importantly, poverty eradication in low-income countries ([UNICEF & WHO, 2019](#); [WHO and UNICEF, 2015](#)). However, there is still a significant need to upgrade supplies of safe drinking sources of water in both developed and low-income countries. The per capita supply of drinking water is expected to be reduced by one-third by 2035. By 2025, around 34 % of the world's population will face an acute shortage of drinking water ([Gupta & Ayoob, 2016](#)). This unfortunate situation is reflected in the scarcity of good quality water in many parts of the world. As a result, the global water supply system is under pressure on both the demand and supply sides. Early in the twenty-first century, the conventional ways of utilizing and valuing water underwent a radical change due to the severe scarcity of drinking water supplies and heightened competition. Therefore, the scarcity of water and insufficient access to potable water sources are expected to be the most challenging and critical environmental problems of the future in maintaining and determining the quality of life on Earth ([Ayoob et al., 2008](#); [Gupta & Ayoob, 2016](#)).

One of the most severe issues in low-income countries regarding the provision of safe drinking water is usually related to the low quality of the water source and the need for treatment. In low-income countries, there are several issues related to water treatment. One of them is the high costs of investment, operation, and maintenance, and another is the complexity of some processes which necessitate special equipment, facilities, and skilled human power that are not readily accessible, especially in rural areas ([Banerjee, 2015](#); [Teng et al., 2009](#)). Due to financial constraints, the development of low-cost and effective water treatment technologies is considered critical.

## 1.2. Groundwater and Geogenic Pollutants

Groundwater is considered the safest of all available drinking water sources on the surface of the earth. As a result, half of the world's population is dependent on groundwater sources for drinking and survival ([Mengistu et al., 2021](#)). Furthermore, in many communities, these sources tend to be the only economically viable option for drinking, as they provide safe quality water and a stable quantity of

water relative to surface sources. Due to the crucial role that groundwater plays in the existence of the majority of the human population in the world, critical concerns about its availability, safety, and purity have emerged for many habitations around the globe (Ayoob & Gupta, 2006; WHO and UNICEF, 2004). In recent years, the entry of geogenic contaminants, such as fluoride, into groundwater aquifers has become a primary environmental concern worldwide. This situation is critical in low-income countries such as Ethiopia. According to the report from the Central Statistical Agency of Ethiopia (CSAE, 2017), high fluoride concentrations ( $> 1.5$  mg/L) in groundwater impacted 3.8 % of the population. The presence of a high level of fluoride in drinking water raises a great concern, as it initiates fluorosis in various proportions, thereby reducing the quality of human life. Fluoride poisoning is believed to be a threat to people in more than 35 countries around the world. The number of people at risk of fluorosis has most likely surpassed 200 million (Geleta et al., 2021b; Zhang et al., 2019). As a result, fluoride in groundwater is one of the most pressing issues affecting groundwater quality in the world today, and it requires some levels of treatment.

### 1.3. Benefits and Health Effects of Fluoride

Fluoride has both negative and positive impacts on human health, depending on the dose and duration of exposure (Kumari et al., 2020, 2021). The consumption of fluoride at low concentrations (1.5 mg/L) is an essential micronutrient for the healthy development of bone and dental enamel (Ye et al., 2018). For instance, fluoride's unique ability to avert and even reverse adverse dental health effects has been well documented (Whitford, 1996). If ingested in drinking water at an optimal concentration (0.5 – 1.5 mg/L), it can decrease the occurrence of tooth decay, especially in children under the age of eight years. It protects the tooth from decay by preventing bacteria from producing acid. The oral bacteria (most notably such as streptococcus mutans, streptococcus sobrinus, and lactobacilli) ingest food particles or sugar (sucrose) on the tooth's surface as their source of energy and convert it to lactic acid via fermentation. These species can have high levels of lactic acid, which, when in contact with the tooth, can induce the dissolution of minerals from the enamel (a highly mineralized cellular tissue that protects the teeth from decay). The tooth enamel becomes thin and susceptible to decay as it loses its mineral content (primarily hydroxyapatite and calcium phosphate). Preventing the chemical processes (mineral dissolution/breakdown) that lead to tooth decay by inhibiting the action of decay-causing bacteria (by fluoride) from producing the necessary acidic environment around the enamel is beneficial. Furthermore, fluoride is a re-mineralization agent that can aid in the removal of lost minerals from damaged enamel which leads to reversing the development of dental caries. Fluoride can bind to hydroxyapatite crystals in tooth enamel which makes the enamel more substantial and more resistant to demineralization, resulting in resistance to decay (Whitford, 1996).

However, it is detrimental to human and animal bones when it is ingested beyond the permitted concentration limit ( $> 1.5$  mg/L) for extended periods (Tao et al., 2020). Fluoride has several mechanisms of detrimental effects (Salifu, 2017; Whitford, 1996). Around 75 – 90 % of fluoride is adsorbed as it reaches the human body, mainly via the ingestion of water and, to a lesser degree, food and dental products (Fawell et al., 2006; Salifu, 2017). As fluoride ions are consumed, they combine with hydrogen ions in the gastrointestinal mucosa to form hydrofluoric acid (HF) under acidic conditions in the stomach. The production of HF induces nausea, diarrhea, vomiting, gastric intestinal inflammation, and abdominal pain. About 40 % of the fluoride consumed is adsorbed as HF in the stomach, and the remaining fluoride is adsorbed in the intestine. As soon as it is absorbed into the bloodstream, fluoride is easily distributed throughout the body and tends to concentrate in calcium-rich areas such as bone and teeth (dentin and enamel) (Firempong et al., 2013; Salifu, 2017). When consumed at relatively high levels (1.5 – 4 mg/L), it causes dental fluorosis, especially among children. Even though the mechanisms underlying the formation of dental fluorosis are unknown, Whitford (1996) claims that there is evidence that the processes include effects on the ameloblasts, which deposit tooth enamel. Ameloblasts are cells that secrete enamel proteins (enamelin and amelogenin) that mineralize to form tooth enamel during tooth formation in childhood. These cells are known to be extremely sensitive to their surroundings and bodily stressors (such as those experienced during childhood) can disrupt their work, causing a delay in enamel development. Excess fluoride exposure (1.5-4 mg/L) to children (aged 2 to 8) who are still mineralizing in their adult teeth is thought to be a type of stressor that disrupts enamel production and contributes to the formation of dental fluorosis (Fawell et al., 2006; Firempong et al., 2013; Whitford, 1996). The most common symptom of long-term exposure to high-fluoride water is dental fluorosis, which appears as discolored, blackened, mottled, or chalky white teeth. Dental fluorosis results from excessive fluoride exposure during childhood when the teeth were developing (Fawell et al., 2006). On the contrary, these results are not visible if the teeth are fully developed before overexposure to fluoride. As a result, just because adults have no symptoms of dental fluorosis may not mean their fluoride consumption is within acceptable limits, and they could be at risk of other fluoride-related health problems.

Fluoride can affect the mineralization of bones at higher levels ( $> 4$  mg/L), resulting in serious and permanent bone and joint deformations known as skeletal fluorosis (Fawell et al., 2006; Whitford, 1996). Scattered pain and swelling in the joints are early signs of skeletal fluorosis. Skeletal fluorosis symptoms include headaches, stomachaches, and muscle fatigue. The spine, main joints, muscles, and nervous system are all weakened due to osteosclerosis (the hardening and calcification of the bones) (UNICEF, 2009). In addition to skeletal and dental fluorosis, excessive fluoride ingestion can cause nonskeletal manifestations. However, these are sometimes ignored due to the belief that excessive

fluoride only affects bone and teeth. Fluoride contamination can also cause Alzheimer's, arthritis, thyroid problems, and other health problems (Kumari et al., 2019). High levels of fluoride can cause serious problems leading to death as a result of respiratory paralysis, dysrhythmia (abnormal heartbeat), or cardiac arrest (Table 1.1) (Firempong et al., 2013; Salifu, 2017).

**Table 1.1** Level of fluoride in drinking water and its related health effects (modified from Salifu et.al, (Salifu, 2017), and Edmunds & Smedley (Edmunds & Smedley, 2014))

Fluoride concentrations (mg/L)	Chronic health effects
Nil	Limited growth and fertility
< 0.5	Dental Caries
0.5 – 1.5	Promotes dental health/prevents tooth decay
1.5 – 4	Dental fluorosis
> 4	Dental/skeletal fluorosis
> 10	Crippling fluorosis
> 50	Thyroid changes
> 100	Growth retardation
> 120	Effects on kidney
~50 - 250	Death

From Table 1.1, chronic use of drinking water with concentrations beyond 1.5 mg/L is considered to be detrimental to health. The WHO (WHO, 2011) guideline value for fluoride in drinking water remains at 1.5 mg/L. Many countries also use this value as a national standard for drinking water (Table 1.2). The US Environmental Protection Agency (EPA) has set the primary standard (enforceable limit) for fluoride in drinking water at 4 mg/L. In contrast, the secondary standard (unenforceable) for drinking water from the United States is 2 mg/L. The standard limit in China is 1 mg/L, while the national limit in Tanzania is high as 8 mg/L, indicating enforcement challenges in a country with regionally high fluoride levels and an issue of water shortage.

**Table 1.2** Regulations and recommendations for fluoride concentrations from some organizations or countries (Edmunds & Smedley, 2014)

Organization/ Country	Limit/guideline	Level (mg/L)	Comment
WHO	Guideline value (GV)	1.5	2011 guidelines, as previous
U.S.EPA	Maximum contaminant level goal (MCLG)	4	Enforceable regulation
U.S.EPA	Secondary standard	2	Guideline intended to protect against dental fluorosis; not enforceable
EC	Maximum permissible value	1.5	1998 regulations
Canada	National Standard	1.5	
India	National Standard	1.5	'Acceptable' limit 1.0 mg/L
China	National Standard	1	
Tanzania	National Standard	8	Interim standard
Ethiopia	National Standard	1.5	Maximum permissible



Aside from the health risks, drinking water with high fluoride levels may have significant psychological and social implications, including young adult matrimonial issues (Salifu, 2017). Due to the increased water intake and, therefore, further ingestion of excess fluoride, the effects of fluoride in drinking water are greater in areas with elevated temperatures at a given concentration. As seen in Figure 1.1, excessive fluoride concentration in drinking water above the WHO guideline limit of 1.5 mg/L can lead to dental fluorosis (mottling and pitting of teeth) (left) and skeletal fluorosis (right).



**Figure 1.1** Illustration of fluoride problem: example for the image of dental (left image) and skeletal (right image) fluorosis (Eawag, 2015)

#### 1.4. Fluoride Occurrence

Fluorine is the lightest member of the halogen group and is considered one of the most reactive elements of the periodic table (Fawell et al., 2006). It is the most electronegative of all elements (Hem, 1985), so it has a strong tendency to gain a negative charge and form a fluoride anion ( $F^-$ ) in solution, which is the only oxidation state found in nature (Hem, 1985). Fluorine is the thirteenth most common element in the Earth's crust (representing about 0.06-0.09 percent of the Earth's crust) and exists as fluoride in over 300 minerals, of which fluorite ( $CaF_2$ ), cryolite ( $Na_3AlF_6$ ), and fluorapatite ( $Ca_5(PO_4)_3F$ ) are the most widely known. Its presence in natural waters is directly proportional to the concentration and solubility of these fluoride-containing minerals. Most natural waters have fluoride concentrations that are below the WHO's recommended limit for fluoride in drinking water (1.5 mg/L, (WHO, 2011)). However, excessive fluoride levels in groundwater are still an issue in many regions of the world (Figure 1.2).

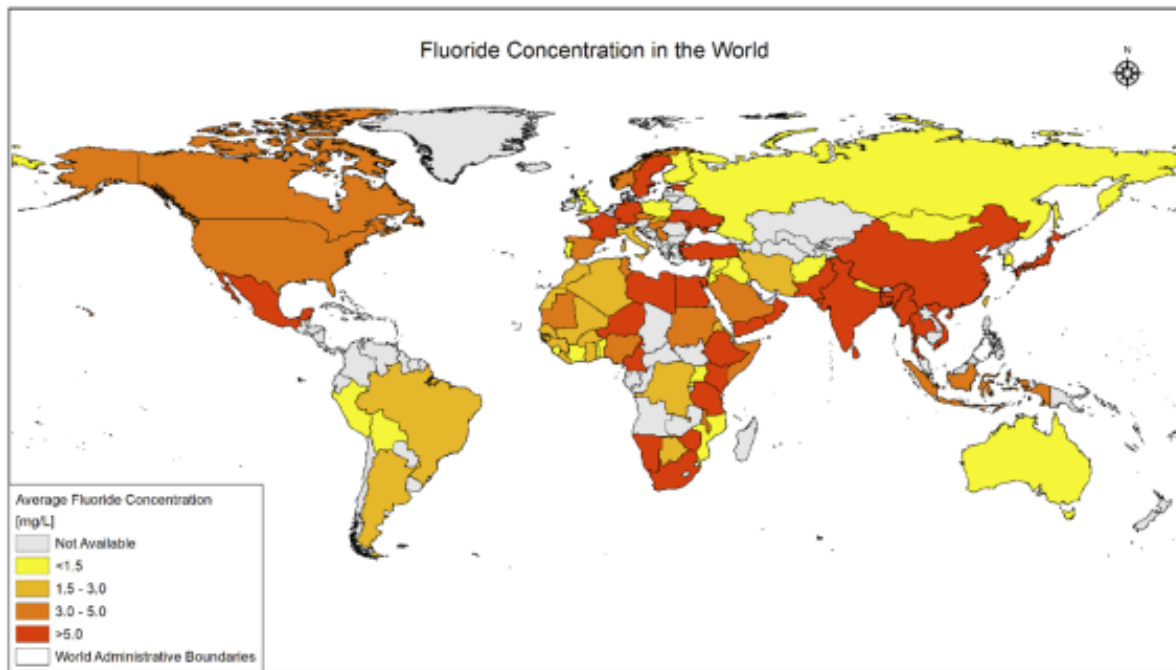


**Figure 1.2** World map depicting fluoride concentration (in mg/L) in groundwater ([Ahmad et al., 2022](#))

High concentrations of geogenic fluoride in groundwater ( $> 1.5$  mg/L) are associated with various geological and climatic conditions. These are granitic basements, arid climates, and alkaline volcanic rocks. Groundwater with elevated dissolved fluoride concentrations can be found in granitic basement aquifers containing a high proportion of high-fluoride minerals, like apatites, micas, or amphiboles (e.g., in India, and Sri Lanka). High fluoride concentrations can also be caused by arid climates with slow groundwater penetration and flow rates, as well as long water-rock reaction times. Alkaline volcanic areas (e.g., the East African Rift valley) have some of the highest fluoride concentrations due to the presence of high-fluoride hyperalkaline volcanic rocks. Fluoride is also introduced to groundwater through high-fluoride geothermal solutions ([Eawag, 2015](#); [Edmunds & Smedley, 2014](#)). The accumulation of fluoride or excessive fluoride levels can be obtained due to low calcium levels which are not sufficient to remove from the solution by precipitating into  $\text{CaF}_2$ . Such conditions can be found in alkaline groundwater, where sodium bicarbonate regulates its chemistry. Furthermore, groundwater associated with granitic rocks has a low calcium content. Ethiopia is one of the East African countries with a large community residing where excess fluoride is becoming a major concern, particularly along the central Rift of the country ([Rango et al., 2017](#); [Žáček et al., 2015](#)). The dissolution of fluoride-containing minerals has increased the amount of fluoride in parent rocks and soils in the Ethiopian main Rift valley, which is usually associated with high bicarbonate and low calcium levels ([Demelash et al., 2019](#); [Rango et al., 2010](#)). In Ethiopia's main Rift valley, fluoride levels in wells are typically up to ten times higher than the WHO standard, which puts millions of Ethiopians at risk of severe fluoride ion toxicity ([Rango et al., 2017](#); [Tekle-Haimanot et al., 2006](#)).

Therefore, these high fluoride concentrations in the drinking water of Ethiopia need special attention (Figure 1.3).

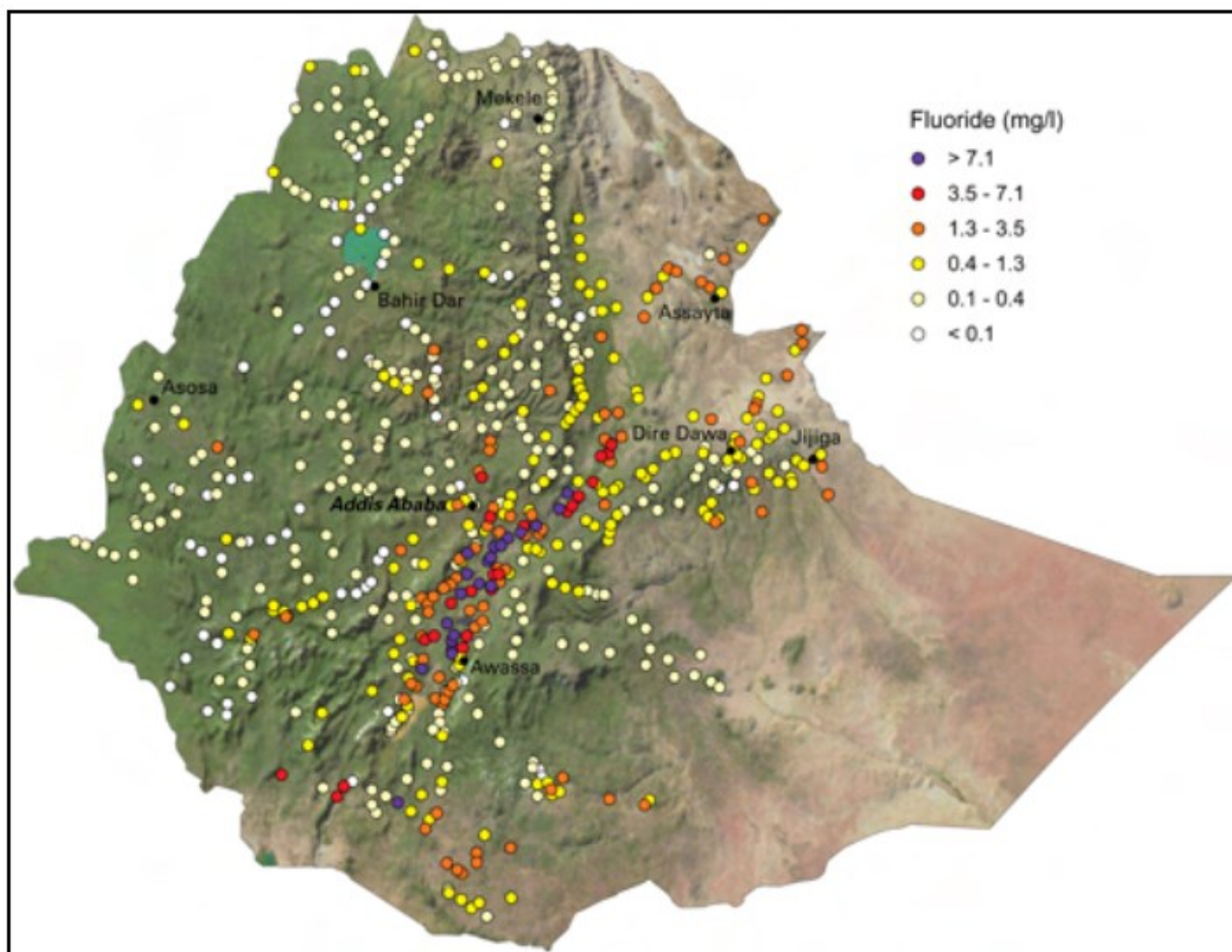


**Figure 1.3** Fluoride concentration profile in Ethiopian drinking water sources (MacDonald et al., 2009)

Aside from natural geological sources of fluoride enrichment in groundwater, a variety of human activities contribute to fluoride pollution. However, quantitative data on fluoride release into the environment from anthropogenic sources are scarce. Fluoride is discharged into the environment through exhaust gases, wastewater, and solid waste from a variety of industrial processes (WHO, 2002), which include: the production of glass, brick, and ceramic; manufacturing of semiconductors, steel, aluminum, copper, nickel, and aluminum smelters; and the production and use of phosphate fertilizer (Bhatnagar et al., 2011; WHO, 2002). The effluents from these industries can raise fluoride concentrations in water by tens to thousands of mg/L, far exceeding the WHO recommendation (1.5 mg/L) (Bhatnagar et al., 2011; Fawell et al., 2006). As a result, techniques for removing fluoride ions from drinking water must be developed to keep the concentration in the water below 1.5 mg/L.

### 1.5. Fluoride Treatment Technologies

Due to irreversible risk and the lack of proven successful treatments for fluorosis, the removal of excessive fluoride levels from drinking water as a protective measure is very critical (Sarkar et al., 2007). Defluoridation technologies have been developed in a variety of locations around the world. However, they have some limitations such as expensiveness, regular maintenance, and complicated operational procedures that make their use impractical in most situations, especially in low-income countries (Geleta et al., 2021b; WHO, 2011). Based on the underlying defluoridation mechanism, the most common defluoridation technologies can be categorized into three groups. These are the precipitation and coagulation, membrane, and adsorption processes.

**Precipitation and Coagulation Techniques:** Fluoride can be extracted from a solution using precipitation and coagulation methods, followed by precipitate settling (or flotation). Typically, the addition of chemicals that act as precipitating agents is required. Contact precipitation, the Nalgonda technique, and electrocoagulation are all well-known coagulation or precipitation techniques.

**Contact Precipitation Techniques:** the method works by introducing calcium (Ca) and phosphate ( $\text{PO}_4$ ) compounds into raw water, with fluoride uptake accomplished through both sorption and precipitation reactions when the fluoride comes in contact with hydroxyapatites (e.g., bone char). Contact precipitation has a high defluoridation capacity (Fawell et al., 2006; Feenstra et al., 2007; Salifu, 2017). The precipitation of calcium fluoride and/or fluorapatite in a solution containing calcium, phosphate, and fluoride is theoretically possible. The precipitation mechanism, however, is impractical because of the slow reaction kinetics. Though the exact mechanism of defluoridation by this method is not explored, it is believed that the bone char catalyzes the precipitation of calcium fluoride and/or fluorapatite. Bone char also serves as a filter media for the precipitate, allowing the defluoridation process to take place (Fawell et al., 2006; Salifu, 2017). Some of the drawbacks of the contact process are: (i) the method is new and still under study and has only been used on a domestic level in Tanzania and Kenya so far (Eawag, 2015), (ii) the method necessitates chemicals and skilled personnel, which is sometimes problematic and impractical when used for water defluoridation in rural communities in low-income countries, (iii) the use of bone char as a contact bed has the same drawbacks as bone char in the defluoridation process (Fawell et al., 2006; Feenstra et al., 2007).

**Nalgonda Technique:** the use of alum as a coagulant for defluoridation was first proposed in the United States in the 1930s. It was later adapted and called the 'Nalgonda Technique' by the National Institute of Environmental Engineering Research (NEERI) in India in the 1970s (Eawag, 2015). The method has been considered to be the most known and well-established method of defluoridation. A



coagulation-flocculation process needs alum (aluminum sulfate,  $\text{Al}_2(\text{SO}_4)_3 \cdot 18\text{H}_2\text{O}$ ) and lime (calcium hydroxide,  $\text{Ca}(\text{OH})_2$ ). Alum is applied as a coagulant to fluoride-contaminated water under efficient mixing conditions. This causes insoluble aluminum hydroxide ( $\text{Al}(\text{OH})_3$ ) micro-flocs to form, which then coalesce into large settleable flocks. The uptake of fluoride is achieved by the electrostatic attraction of negatively charged fluoride ions ( $\text{F}^-$ ) in a solution to aluminum hydroxide particles, then isolated from water through sedimentation and filtration (Dysart, 2008; Fawell et al., 2006). When alum is mixed with water, it produces an acidic solution. To achieve a neutral pH, the simultaneous addition of lime ( $\text{Ca}(\text{OH})_2$ ) is needed (Dysart, 2008; Fawell et al., 2006; Meenakshi & Maheshwari, 2006). Some of the drawbacks of the Nalgonda process are: (i) insufficient defluoridation efficiency when the fluoride levels in feed water are high (Fawell et al., 2006; Feenstra et al., 2007), (ii) It generates large quantities of sludge that is toxic and needs to be disposed of properly, (iii) its operational cost is high (Meenakshi & Maheshwari, 2006), (iv) the use of aluminum sulfate as a coagulant raises the concentration of sulfate ions, which can have cathartic symptoms (i.e. accelerated defecation) (Meenakshi & Maheshwari, 2006; Salifu, 2017), (v) excess sulfate concentrations (about 600 mg/L), which could result from the use of aluminum sulfate, may affect the treated water test (Eawag, 2015; Fawell et al., 2006). As a result, consumers may choose to bypass the treatment unit and drink the raw water directly, or they may return to their old (i.e., polluted water sources) (vi) excess residual aluminum in treated water can cause dangerous dementia disease as well as neurobehavioral, structural and biochemical changes (Meenakshi & Maheshwari, 2006). It could also affect the respiratory, cardiovascular, endocrine, and reproductive systems. The high level of aluminum in drinking water has also been associated with Alzheimer's disease (Salifu, 2017; Sarkar et al., 2007).

**Electrocoagulation Technique:** For a long time, the electrocoagulation (EC) process has been used to remove fluoride and other ions from industrial wastewater (Aoudj et al., 2015; Govindan et al., 2015; Hu et al., 2008; Shen et al., 2003; Zuo et al., 2008), and it is now gaining attention as a viable technology for fluoride removal from drinking water in low-income countries. The three basic technologies electrochemistry, coagulation, and precipitation are combined in the electrocoagulation method. The metal (e.g., aluminum) plates serve as anode and cathode in this process. As an electrical potential is applied to the electrodes, current flows into the electrodes, and  $\text{Al}^{3+}$  is released at the anode, where it reacts with water at neutral pH to form  $\text{Al}(\text{OH})_3$ , a fluoride-loving compound. The resulting  $\text{Al}(\text{OH})_3\text{F}$  flocs settle at the bottom of the solution and can be removed as sludge. The defluoridation efficiency relies on the initial fluoride concentration, initial pH of the influent solution, and current density (Ghosh et al., 2008; Gwala et al., 2011; Zhao et al., 2011; Zuo et al., 2008).

Some of the shortcomings of the electrocoagulation process are (Eawag, 2015): (i) the presence of high  $\text{SO}_4^{2-}$  concentrations in raw water could inhibit the uptake of fluoride, (ii) the amount of aluminum in treated water might be higher than the WHO's recommended limit (200  $\mu\text{g/L}$ ), (iii) requires the use of high-cost electrical energy, (iv) requires skilled human power.

**Membrane Methods/ Reverse Osmosis (RO):** Reverse osmosis uses a semipermeable membrane that allows water to pass through, but not ions or larger molecules. In principle, water molecules migrate through the membrane along a concentration gradient from a low to a high concentration of dissolved salt during the osmosis process. In reverse osmosis, the opposite result is desired: pressure is applied to force feed water through a semipermeable membrane, removing solutes (including fluoride) through rejection by the membrane based on particle size and electrical charges. The technique is a physical process that works in the opposite direction of natural osmosis by applying pressure to the concentrated side of a membrane to overcome osmotic pressure. This membrane separation technology has been perceived to be highly effective for defluoridation. It has a fluoride uptake capacity of 85-95%, and the US-EPA has recommended it as one of the best available defluoridation techniques (Dysart, 2008; Feenstra et al., 2007).

The reverse osmosis method is also known to have some drawbacks such as (i) the process is very complex, especially for rural water supply in low-income countries, as it needs special equipment, a continuous supply of electricity, and skilled human power (Dysart, 2008), (ii) it requires high capital, operational, and maintenance cost (Meenakshi & Maheshwari, 2006), (iii) the method eliminates the majority of ions present in the water, although some of the ions are needed as essential minerals for the human body (Eawag, 2015; Meenakshi & Maheshwari, 2006), (iv) it is difficult to dispose of concentrate containing rejected pollutants (fluoride), (v) membrane fouling due to the accumulation of particulate matter, collides, bacteria and organic material. To control fouling, a pre-filtration step or conventional pre-treatment (e.g., coagulation and disinfection) may be required. Chemical cleaning is also needed to restore the permeability of the fouled membranes (Eawag, 2015), and (vi) substantial water loss (usually 10-35 percent) (Meenakshi & Maheshwari, 2006).

**Adsorption-Based Technologies:** Adsorption is the accumulation of substances at an interface or surface. The adsorbate is the material that is adsorbed and the adsorbent is the adsorbing phase. Adsorption mechanisms can be physisorption, chemisorption, or both. A physisorbed species is not bound to a specific location; rather, it is free of translational motion within the interface. At low temperatures, physisorption may be significant, and it develops low adsorption energy, indicating that the adsorbate is loosely held with the adsorbent. If the adsorbate has a chemical interaction with the

adsorbent, the process is known as chemisorption. The adsorbed molecules are attached to the surface by forming strong localized bonds at the active centers of the adsorbent. Ion exchange can be thought of as exchange adsorption, which occurs when ions of one substance concentrate at a surface due to electrostatic attraction to charged sites on the surface (Ayoob & Gupta, 2007; Zhang & Stanforth, 2005). Lately, adsorption or ion exchange is one of the most widely used methods and is quite attractive due to its applicability for defluoridation even at low concentrations, relative ease of operation, and low cost, as well as flexibility and simplicity of design (Liu et al., 2018; Yadav et al., 2018). Fluoride-polluted water is passed through a column packed with an adsorbent, and the adsorbed bed may be back-washed for reuse after saturation.

#### 1.5.1. Adsorbent Materials for Water Defluoridation

The suitability of the defluoridation technique is mainly dependent on the availability of a suitable adsorbent (Chen et al., 2010; Maliyekkal et al., 2006; Salifu, 2017; Sarkar et al., 2006). The most commonly used materials are activated alumina (AA) and bone char.

##### 1.5.1.1. Activated Alumina (AA)

The process, which uses activated alumina as a filter media, has been designated the Best Available Technique for water defluoridation by the United States Environmental Protection Agency (US- EPA) (Dysart, 2008). The method, which was first used in the 1930s, is still widely used and has become the method of choice for removing fluoride from water in developed countries such as the United States and Australia. The technology has also gained traction in some low-income and low-middle-income countries, especially India, where it is being spread in villages with UNICEF's support. The technique has a defluoridation efficiency of approximately 85 – 95 % (Dysart, 2008; Feenstra et al., 2007; Salifu, 2017).

Activated alumina (AA) is a granular type of aluminum oxide ( $\text{Al}_2\text{O}_3$ ) that can be used as a filter to remove a variety of pollutants from water, such as fluoride (Figure 1.3).



**Figure 1.4** Activated alumina (AA) grains (Eawag, 2015)

The media is made by thermally treating hydrated alumina granules in a regulated manner to create a highly porous material. It primarily comprises a mixture of amorphous and crystalline phases of aluminum oxide known as the aluminum trihydrate. Alumina has a high pH point of zero charges ( $\text{pH}_{\text{PZC}} \sim 8.2$ ), meaning that it can adsorb a wide range of negatively charged particles, including fluoride ions (Dysart, 2008; Fawell et al., 2006). The surface of AA becomes hydrated when it comes into contact with water, forming  $\text{Al}(\text{OH})_3$  with surface hydroxide groups ( $\equiv\text{Al}-\text{OH}$ ). As shown below in Equation 1, negatively charged ions can replace the hydroxyl ( $\text{OH}^-$ ) ion.



The defluoridation capacity of alumina is highly pH-dependent; hence activated alumina-based defluoridation systems often require pH adjustment to optimize fluoride removal (Dysart, 2008; Fawell et al., 2006). Overall, defluoridation is most effective when the pH is between 5 and 6 (Dysart, 2008; Salifu, 2017). When the pH rises above 7 the fluoride removal capacity of activated alumina media decreases. This is due to the exchange reaction between surface hydroxyl groups, and the adsorbing fluoride becomes less favorable since silicates and hydroxides in solution compete more effectively with the fluoride ion for exchange sites on the surface of activated alumina. At pH 5, activated alumina dissolves in the acidic environment, resulting in media loss and, consequently, a decrease in fluoride adsorption capacity (Dysart, 2008; Meenakshi & Maheshwari, 2006). As activated alumina is used for defluoridation, it is gradually exhausted and needs to be regenerated. The regeneration process is taken place by exposing the media to an alkaline solution, usually caustic soda ( $\text{NaOH}$ ), to remove the fluoride and restore the adsorption capacity of the media. As the defluoridation capacity is strongly sensitive to pH,  $\text{H}_2\text{SO}_4/\text{HCl}$  is subsequently used to neutralize and activate the media. Approximately 5-10% of the alumina is lost during each regeneration period, resulting in a 30-40% reduction in the adsorption capacity of the media. Therefore, the media usually must be replaced before three to four regenerations (Dysart, 2008; Fawell et al., 2006). Some of the drawbacks that have been identified with the activated alumina technique are (i) for non-developed nations, the technology is costly to obtain, run and maintain for long-term use (Eawag, 2015; Fawell et al., 2006), (ii) its defluoridation capacity is relatively low in less purified AA products (Fawell et al., 2006; Meenakshi & Maheshwari, 2006), and (iii) concentrations of fluoride ions in the spent regeneration solution are high (Fawell et al., 2006; Salifu, 2017).

#### 1.5.1.2. Bone Char (BC)

Bone charcoal (Figure 1.4) is a porous, blackish granular material used as a defluoridation filter media. It was used in the United States from the 1940s to the 1960s and is considered the oldest known

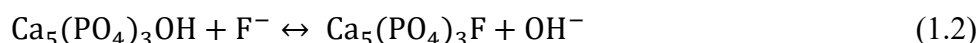


defluoridation agent. It has been successfully used as a filter material to remove excessive fluoride from drinking water in Thailand and some African countries (e.g. Kenya and Tanzania) (Dysart, 2008; Eawag, 2015; Fawell et al., 2006).



**Figure 1.5** Bone char material (Salifu, 2017)

The adsorptive mechanism of bone char (BC) in removing fluoride from the water allows fluoride ions to exchange with hydroxide ions ( $\text{OH}^-$ ) at the surface of the main mineral constituent of BC (hydroxyapatite,  $\text{Ca}_5(\text{PO}_4)_3\text{OH}$ ), releasing  $\text{OH}^-$  into the solution as shown in Equation (2) (Eawag, 2015).



Bone char is produced by heating in specially built kilns at temperatures ranging from 300 to 500 °C for approximately 10 days in a controlled air supply, leading to the highest removal capacity with no organic remains (CDN (Catholic Diocese of Nakuru) & Müller, 2007; Eawag, 2015). Calcium phosphate (57-80%), calcium carbonate (6-10%), and activated carbon (7-10%) are the main ingredients in bone charcoal (Fawell et al., 2006; Feenstra et al., 2007). The quality of the bone char and particle size determine the defluoridation performance of the filter material. The higher the defluoridation capacity, the smaller the particles (Mjengera & Mkongo, 2003). It was reported that the well-prepared bone char filters can reduce fluoride concentrations from over 6 mg/L to less than 0.1 mg/L after adsorption, with a defluoridation capacity of about 1.2 mg/g (e.g. in Kenya) (Eawag, 2015). Some drawbacks that have been identified using bone char as a filter media for defluoridation are: (i) Due to religious or cultural concerns, the use of animal bones as a filter media may not be suitable in certain areas (Eawag, 2015; Fawell et al., 2006), (ii) treated water can have an unpleasant taste when using low-quality bone char with high organic content. This could turn off consumers and lead to complete rejection of the bone char treatment technique (Dysart, 2008; Eawag, 2015; Feenstra et al., 2007), (iii) the method is contingent on the local availability of sufficient quantities of bones as raw material for the preparation of the filter media (Dysart, 2008; Fawell et al., 2006).

In addition to the common adsorbents mentioned above, numerous adsorbent materials have been investigated for the removal of fluoride (Chen et al., 2010; Ghanbarian et al., 2020; Kennedy & Arias-Paic, 2020; Maliyekkal et al., 2006; Sarkar et al., 2006; Su et al., 2020). Many of these, however, have either a time-consuming synthesis procedure, high processing costs, limited raw material availability, or limited lifespan, making them unsuitable for use in underdeveloped countries where fluoride concentrations in water are high (Kumari et al., 2021). Thus, for the long-term defluoridation of drinking water, the search for suitable fluoride adsorbents with local production capacity remains a critical problem in low-income countries. The adsorbent materials used in this study are discussed in the following section.

#### 1.5.1.3. Volcanic Rocks

Rocks are any natural solid mass composed of minerals and/or mineraloids. They are classified into igneous, sedimentary, and metamorphic rocks according to their chemical and mineral composition, the texture of the constituent particles, and the formation process (Warner, 1990). Plutonic or intrusive rocks are formed when magma slowly cools and crystallizes within the Earth's crust (e.g., granite), while volcanic or extrusive rocks are formed when magma reaches surfaces as fragmented ejecta or lava. Furthermore, igneous rocks are classified as *felsic*, *intermediate*, or *mafic*. These are mainly chemical classes; however, lava chemistry tends to correlate with magma temperature, viscosity, and eruption type. The chemical composition of the rock mass is an important determining factor in the formation of minerals in the rock mass because certain minerals can only be formed when the necessary elements are present in the rock. Among more than 3000 known minerals, only the nine minerals can account for 95 percent of the crust which includes (i) four *felsic*: quartz ( $\text{SiO}_3$ ), muscovite ( $\text{KAl}_2(\text{AlSi}_3\text{O}_{10}(\text{F}, \text{OH})_2)$ ), orthoclase ( $\text{KAlSi}_3\text{O}_8$ ), and Na-plagioclase/albite ( $\text{NaAlSi}_3\text{O}_8$ ); and (ii) five *mafic*: biotite ( $\text{K}(\text{Fe}, \text{Mg})_3\text{AlSi}_3\text{O}_{10}(\text{F}, \text{OH})_2$ ), Amphibole ( $\text{Ca}_2(\text{Mg}, \text{Fe}, \text{Al})_5(\text{Al}, \text{Si})_8\text{O}_{22}(\text{OH})_2$ ), pyroxene ( $(\text{Ca}, \text{Na})(\text{Mg}, \text{Fe}, \text{Al})(\text{Al}, \text{Si})_2\text{O}_6$ ), Ca-plagioclase ( $\text{CaAl}_2\text{Si}_2\text{O}_8$ ), and olivine ( $(\text{Mg}, \text{Fe})_2\text{SiO}_4$ ) (Manville et al., 1998).

Recently, volcanic rocks have received a lot of attention for pollutant removal due to their valuable properties such as high surface area, low cost, easy accessibility, good mechanical resistance, and availability in large quantities (Alemayehu & Lennartz, 2009). Volcanic rocks often have a vascular texture, which is the result of voids left by volatiles escaping from the molten lava. Accordingly, they can be classified into two textures: microvascular (Pumice) and macrovascular (scoria). Pumice is a finely porous rock frothy with air bubbles, whereas scoria is a rough rock that resembles furnace slag (Alemayehu & Lennartz, 2009). Pumice is often formed from rhyolite magma (Alemayehu & Lennartz, 2009), but it can also develop from trachytic or dacitic magma. It has been used in water

and wastewater treatment processes due to its high porosity and low specific gravity (Aregu et al., 2018). Scoria is a vesicular pyroclastic rock with basaltic compositions that range in color from reddish-brown to black and is denser than VPum, somewhat porous with high surface area and strength. Both volcanic rocks are found in abundance in Europe (Italy, etc.), Central America, Southeast Asia (Indonesia, etc.), and East Africa (Ethiopia, Eritrea, etc.) (Alemayehu & Lennartz, 2009; Aregu et al., 2018). A few studies have found surface modification of these volcanic rocks might also perform better as an adsorbent for water contaminants (Dehghani et al., 2017; Sepehr et al., 2013b).

#### 1.6. Aim and Scope of the Study

In many parts of the world, groundwater is the primary and favored source of potable water for many rift communities in rural and urban areas. However, over 200 million people on the globe, including in East Africa, are drinking fluoride-containing groundwater beyond the permissible limit ( $> 1.5\text{mg/L}$ ), which has a serious consequence on people's welfare (Geleta et al., 2021b; Zhang et al., 2019). In the East African rift, fluorosis is the most prevalent geochemical disease, affecting over 80 million people (Geleta et al., 2021b; Kut et al., 2016; Mohan et al., 2017a). Ethiopia is among the East African countries with a large population where too much fluoride is becoming a major concern, particularly along the main rift of the country (Rango et al., 2017; Žáček et al., 2015). The World Health Organization (WHO) identified 28 countries in 2006 in which high fluoride limits in potable water were linked to dental fluorosis and skeletal fluorosis. The most affected countries were India, Ethiopia, and China (Datturi et al., 2017; Fawell et al., 2006; Susheela & Bhatnagar, 2002). The issue of excessive fluoride in the groundwater in the Ethiopian Rift valley has been intensified by weathering of primary rocks and the leaching of fluoride-containing minerals in the soils, which is usually linked to low calcium content and high bicarbonate concentrations (Demelash et al., 2019; Rango et al., 2010). In the Ethiopian rift valley wells, concentrations usually range from 1 to 10 times higher than the WHO norm of  $1.5\text{ mg/L}$ , placing an estimated 10 million Ethiopians at risk of high exposure to fluoride ions in the area (Rango et al., 2017; Tekle-Haimanot et al., 2006). To overcome this problem, defluoridation techniques such as Nalgonda and bone char have been attempted in the Ethiopian Rift Valley areas (Datturi et al., 2017). However, due to a variety of concerns related to the availability of sorbent, the efficacy of the sorbent, and social and technological issues, the attempted approaches are ineffective or unable to resolve the existing problem. Thus, the inability to accelerate the provision of safe drinking water to the population, particularly for Ethiopian Rift valley communities, due to the presence of high fluoride levels in the groundwater supply remains the most pressing issue. Due to the harmful health effects of high fluoride levels in drinking water on populations primarily in low-income countries, the search for low-cost and appropriate technology for the uptake of fluoride from drinking

water remains very crucial. Among the fluoride removal techniques, adsorption is still the most widely employed and most appropriate method, due to its applicability for pollutant uptake even at low concentrations, relative ease of operation, low cost, flexibility, and simplicity of design. On the other hand, the suitability of the defluoridation technique is mainly dependent on the availability of a suitable adsorbent (Chen et al., 2010; Maliyekkal et al., 2006; Salifu, 2017; Sarkar et al., 2006). An adsorbent could be considered appropriate if it has good functional and economic viability for sustainable use in groundwater defluoridation, especially in low-income nations. Such adsorbents could have some characteristic features such as good adsorption performance, local availability in large quantities, good mechanical resistance and high porosity, low investment cost, and being environmentally friendly (Alemayehu & Lennartz, 2009; Geleta et al., 2021b).

Various materials have been studied for the uptake of fluoride from water such as; manganese-oxide-coated alumina (Maliyekkal et al., 2006), laterite (Sarkar et al., 2007), granular ceramic (Chen et al., 2010), La (III)-Al (III)-activated carbon modified by chemical route (Su et al., 2020), biomaterial functionalized cerium nanocomposite (Nehra et al., 2020), Quaternized Palm Kernel Shell (QPKS) (Abu Bakar et al., 2019), bone char and activated alumina (Kennedy & Arias-Paic, 2020), bone char (Alkurdi et al., 2019), renewable biowaste (Rajkumar et al., 2019),  $\text{MgFe}_2\text{O}_4$  -chitosan-CaAl nanohybrid (Ghanbarian et al., 2020), carbon nanotube composite (Araga et al., 2019). However, many of these are suffering from either time-taking synthesis procedures, high processing costs, availability of raw materials, or short lifespan which makes them impractical to be applied in the rift valleys which are essentially impacted by high fluoride concentrations in the water (Geleta et al., 2021b; Kumari et al., 2021).

Activated alumina (AA) is the most suitable and widely used - considered the industry standard for fluoride uptake from drinking water in developed countries. However, in most low-income countries, it is both costly and scarce, and regeneration and disposal of the exhausted adsorbent are the major problems (Maliyekkal et al., 2006). For sustainable defluoridation of drinking water, especially in low-income nations, the quest for suitable fluoride adsorbents with a capacity to produce locally remains critical.

This study aimed to investigate the use of natural and surface-modified adsorbents derived from locally available volcanic rock materials (VPum and VSco) for the defluoridation of fluoride-laden water using fixed-bed column systems. The rock samples were collected from volcanic cones of the main Rift valley area of Ethiopia, around 50-100 km East of Addis Ababa. The rocks are indigenous volcanic rocks of different chemical and mineralogical compositions. The rocks are representative of the Ethiopian Rift valley, readily available in approximately 1/3 of the area of the country (Alemayehu

et al., 2011; Aregu et al., 2018). The fluoride uptake capacities of the unmodified and surface-modified adsorbents were investigated in small-scale laboratory column tests. Many characterization techniques and well-known fixed-bed adsorption models were employed to analyze the physicochemical characteristics and fluoride uptake properties/capacities of the natural and surface-modified adsorbents and the mechanism of fluoride uptake.

### 1.7. Hypothesis and Key Questions

It was hypothesized that complete adsorption of fluoride ions from fluoride-laden water by unmodified and surface-modified adsorbents derived from volcanic rock materials to attain acceptable limits (< 1.5 mg/L, WHO guideline value) of fluoride ions in the drinking water is attainable under appropriate experimental conditions.

The key research questions were:

- (i) Could volcanic rock materials be employed for the defluoridation of drinking water?
- (ii) Can surface modification of volcanic rock materials improve both the adsorbent characteristics and fluoride ions adsorption performance?

### 1.8. Research Objectives

The general research objective of this thesis was to investigate the use of natural and surface-modified adsorbents derived from locally (Ethiopia) available volcanic rock materials (virgin pumice (VPum) and virgin scoria (VSco)) for the defluoridation of fluoride-laden drinking water using fixed-bed column systems. Specific objectives were formulated as follows:

- (i) To investigate the use of locally available and easily accessible materials (Volcanic rocks: VPum and VSco) as an adsorbent for sustainable defluoridation of drinking water.
- (ii) To assess and compare the fluoride adsorption performance of surface-modified pumice (Zr – Pu) and unmodified pumice (VPum) for viable removal of fluoride from drinking water.
- (iii) To investigate and compare the fluoride removal capacity of surface-modified scoria (ZrOCSc) and unmodified one (VSco) for long-term drinking water defluoridation.
- (iv) To investigate the effects of experimental conditions such as initial pH, adsorbent particle sizes, and initial flow rate on the fluoride uptake behavior of the adsorbents.
- (v) To characterize the physicochemical parameters of the adsorbents, including mineralogy, surface morphology, functional group, specific surface area, thermal behavior, and  $\text{pH}_{\text{PZC}}$ .

- (vi) To compare the adsorption characteristics of the adsorbents.
- (vii) To fit experimental data to kinetic models to characterize fluoride uptake onto the adsorbents.

### 1.9. Experimental Setups and Conceptual Framework

The experiments in the present study were conducted in a laboratory-based setting. The diagram (Figure 1.6) below depicts the general flow of the experiments, beginning with sample collection and ending with discussions, conclusions, and recommendations.

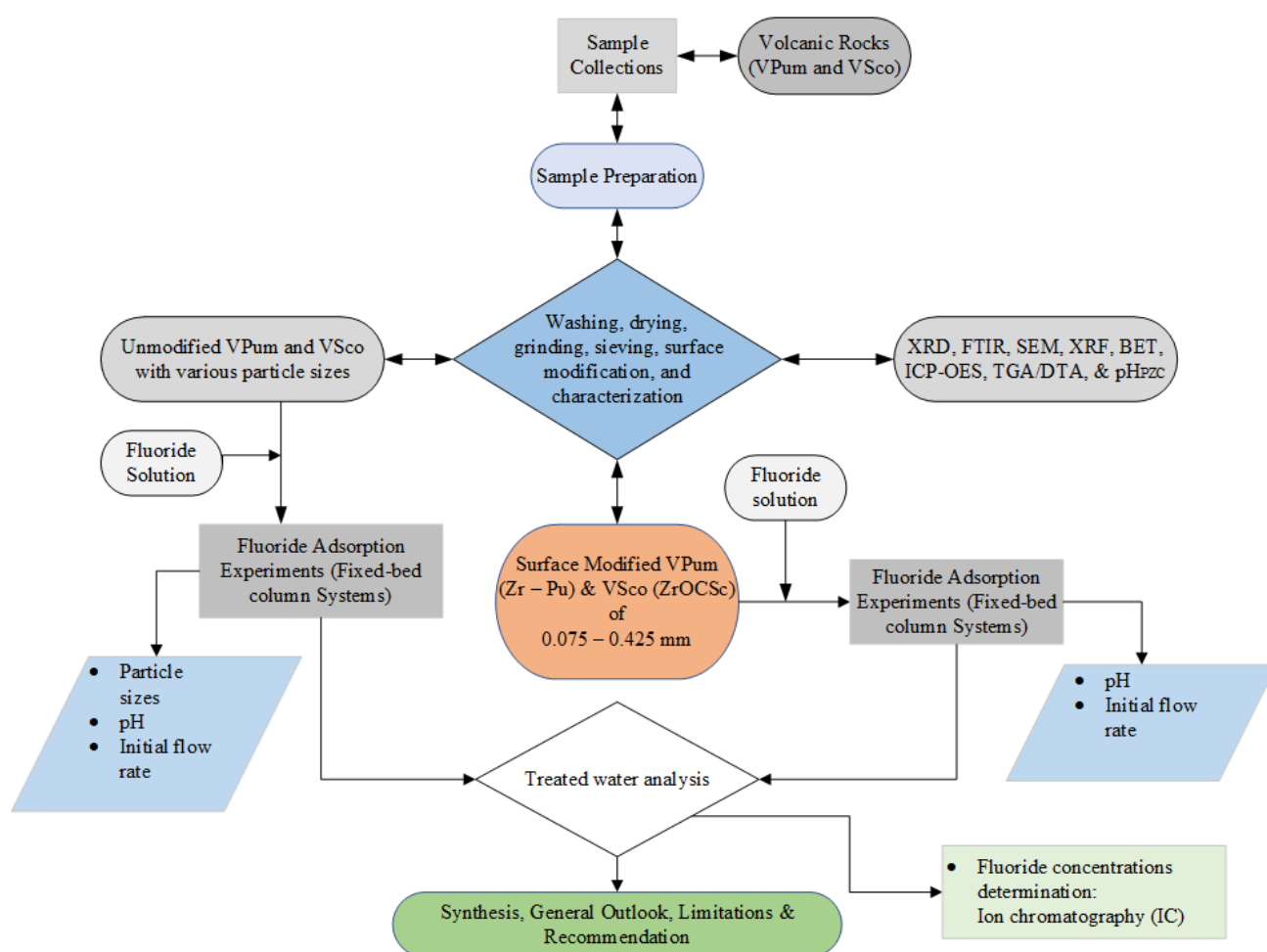


**Figure 1.6** Experimental setups and conceptual framework

### 1.10. Structure of the Dissertation

This work is a cumulative dissertation with five chapters: three first-authored published articles in peer-reviewed international journals (Geleta et al., 2021b, 2021c, 2022) that contain the findings of various segments of the study, in addition to the introductory chapter (Chapter 1) and synthesis, general outlook, limitations, and recommendations chapter (Chapter 5).

After the introductory chapter (the current chapter), [Chapter 2](#), focuses on the investigation of the efficiency of volcanic rocks, virgin pumice (VPum) and virgin scoria (VSco), for fluoride uptake in fixed-bed column adsorption experiments and modeling breakthroughs under different experimental conditions. The adsorption properties of the two adsorbents (VPum and VSco) were also compared. This chapter comprises the following publication;

Geleta, W. S.; Alemayehu, E.; Lennartz, B., **2021**. Volcanic Rock Materials for Defluoridation of Water in Fixed-Bed Column Systems. *Molecules* 26, 977. doi:10.3390/molecules26040977

*Contribution W.S. Geleta: prepared the adsorbents, designed and conducted the adsorption experiments, analyzed the data, and prepared the manuscript*

The following two chapters ([3 & 4](#)) show the findings from laboratory investigations on the synthesis of fluoride adsorbents for water defluoridation, which could have sustainable applicability in fluorotic areas of underdeveloped countries, based on surface modifications of easily available volcanic rock materials (VPum and VSco).

Thus, [Chapter 3](#) focuses on the surface modification by the zirconium coating process using pumice as a base and testing the efficiency of the synthesized adsorbent, zirconium-coated pumice (Zr-Pu) for fluoride uptake in fixed-bed column adsorption systems and breakthrough curves modeling at various experimental parameters. The adsorption characteristics of unmodified/virgin pumice (VPum) and Zr – Pu were also compared. This chapter comprises the following publication;

Geleta, W. S.; Alemayehu, E.; Lennartz, B., **2021**. Enhanced Defluoridation of Water Using Zirconium-Coated Pumice in Fixed-Bed Adsorption Columns. *Materials* 14, 6145. doi.org/10.3390/ma14206145

*Contribution W.S. Geleta: prepared the adsorbents, designed and conducted the adsorption experiments, analyzed the data, and prepared the manuscript*

[Chapter 4](#) similarly focuses on the surface modification by the zirconium oxide coating process using scoria as a base and testing the efficiency of the synthesized adsorbent, zirconium-coated scoria (ZrOCSco) for fluoride uptake in continuous flow-through fixed-bed column adsorption systems and the modeling of breakthrough curves at different experimental conditions. The chapter also presents the comparative analysis of the adsorption characteristics of unmodified/virgin scoria (VSco) and ZrOCSco. This chapter comprises the following publication;



Geleta, W.S.; Alemayehu, E.; Lennartz, B., **2022**. Fixed-Bed Adsorption: Comparisons of Virgin and Zirconium Oxide-Coated Scoria for the Removal of Fluoride from Water. *Molecules* 27, 2527. doi:10.3390/molecules27082527

*Contribution W.S. Geleta: prepared the adsorbents, designed and conducted the adsorption experiments, analyzed the data, and prepared the manuscript*

And at the last,

[Chapter 5](#) presents the synthesis, general outlook, limitations, and recommendations for further study.



## 2. Volcanic Rock Materials for Defluoridation of Water in Fixed-Bed Column Systems

Wondwosen Sime Geleta <sup>1,2</sup>, Esayas Alemayehu <sup>3,4, \*</sup> and Bernd Lennartz <sup>2, \*</sup>

<sup>1</sup> School of Chemical Engineering, Jimma Institute of Technology, Jimma University, P.O. Box 378, Jimma, Oromia, Ethiopia

<sup>2</sup> Faculty of Agricultural and Environmental Sciences, University of Rostock, Justus-Von-Liebig-Weg 6, 18059 Rostock, Germany

<sup>3</sup> Faculty of Civil and Environmental Engineering, Jimma Institute of Technology, Jimma University, P.O. Box 378, Jimma, Oromia, Ethiopia

<sup>4</sup> Africa Center of Excellence for Water Management, Addis Ababa University, 1176 Addis Ababa, Ethiopia

\*Correspondence

***Molecules* (2021) 26: 977**

**Abstract:** Consumption of drinking water with a high concentration of fluoride (>1.5 mg/L) causes detrimental health problems and is a challenging issue in various regions around the globe. In this study, a continuous fixed-bed column adsorption system was employed for the defluoridation of water using volcanic rocks: virgin pumice (VPum) and virgin scoria (VSco), as adsorbents. The XRD, SEM, FTIR, BET, XRF, ICP-OES, and pH Point of Zero Charges (pH<sub>PZC</sub>) analyses were performed for both adsorbents to elucidate the adsorption mechanisms and the suitability for fluoride removal. The effects of particle size of adsorbents, solution pH, and flow rate on the adsorption performance of the column were assessed at room temperature, constant initial concentration, and bed depth. The maximum removal capacity of 110 mg/kg for VPum and 22 mg/kg for VSco were achieved at particle sizes of 0.075–0.425 mm and <0.075 mm, respectively, at a low solution pH (2.00) and flow rate (1.25 mL/min). The fluoride breakthrough occurred late and the treated water volume was higher at a low pH and flow rate for both adsorbents. The Thomas and Adams–Bohart models were utilized and fitted well with the experimental kinetic data and the entire breakthrough curves for both adsorbents. Overall, the results revealed that the developed column is effective in handling water containing excess fluoride. Additional testing of the adsorbents including regeneration options is, however, required to confirm that the defluoridation of groundwater employing volcanic rocks is a safe and sustainable method.

**Keywords:** adsorption; breakthrough curve; defluoridation; up-flow mode; volcanic rocks

## 2.1. Introduction

Credible evidence from scientific literature substantiates both the beneficial and detrimental effects of fluoride on human health with only a narrow range between intake associated with these effects (Kumari et al., 2020, 2021). Consumptions of fluoride in low concentrations ( $<1.0$  mg/L) are an essential micronutrient for the healthy development of bone and dental enamel (Ye et al., 2018); however, it leads to the development of fluorosis if it is consumed beyond the permissible limit ( $>1.5$  mg/L) (WHO, 2011).

In many parts of the world, groundwater sources are the single largest supply of drinking water. For many rift communities, it may be the only economically viable option for drinking water. In the Ethiopian rift valley, about 40% of deep and shallow wells are contaminated with up to 26 mg/L of fluoride (Fufa et al., 2013; Rango et al., 2017). The weathering of primary rocks and leaching of fluoride-containing minerals in soils yield fluoride-rich groundwater in the Ethiopian Rift, which is generally associated with a low calcium content and high bicarbonate concentrations (Demelash et al., 2019; Rango et al., 2010).

Globally, more than 200 million people, including Ethiopia, rely on groundwater with a fluoride concentration above the permissible level (Cai et al., 2016; WHO, 2011; Ye et al., 2018). According to the Central Statistical Agency of Ethiopia report (CSAE, 2017), 3.8% of the population is affected by high-level fluoride concentrations ( $>1.5$  mg/L) in groundwater, which is used for drinking purposes. In general, fluorosis turns out to be the most widespread geochemical-based disease in the East African rift, affecting more than 80 million people (Kut et al., 2016; Mohan et al., 2016; Shen & Schäfer, 2015; Smedley et al., 2002). Thus, due to the health effect of high fluoride in groundwater, it is essential to reduce excess fluoride concentrations to the allowable limit ( $<1.5$  mg/L).

So far, various technologies such as coagulation/precipitation, electro-coagulation, membrane separations, ion exchange, and adsorption had been attempted for efficient defluoridation of groundwater (Araga et al., 2019; Gill et al., 2014; Manna et al., 2018; Waghmare & Arfin, 2015). Some of the shortfalls of these techniques include expensiveness, fouling issues, regular maintenance, and complicated operational procedures. In comparison to the techniques mentioned above, the adsorption methodology is still one of the most widely applied methods, taking the lead in high removal efficiency, cost-effectiveness, ease of operation, simplicity of design, and availability of large varieties of adsorbents (Liu et al., 2018; Yadav et al., 2018).

Various adsorbents have been investigated and reported for the removal of excess fluoride from water in an effective manner. Some of the widely employed adsorbents are La (III)-Al (III)-activated carbon

modified by chemical route (Su et al., 2020), biomaterial functionalized cerium nanocomposite (Nehra et al., 2020), Quaternized Palm Kernel Shell (QPKS) (Abu Bakar et al., 2019), bone char and activated alumina (Kennedy & Arias-Paic, 2020), bone char (Alkurdi et al., 2019), renewable biowaste (Rajkumar et al., 2019),  $\text{MgFe}_2\text{O}_4$ –chitosan–CaAl nanohybrid (Ghanbarian et al., 2020), carbon nanotube composite (Araga et al., 2019), Neem Oil-Phenolic Resin Treated Bio-sorbent (Manna et al., 2018), etc. However, many of these suffer from either time-consuming synthesis procedures, high processing costs, availability of raw materials, or short lifespan, which makes them impractical to be applied in the rift valleys that are essentially impacted by high fluoride concentration in water (Kumari et al., 2021). Consequently, efforts have been made to obtain easily accessible and long-lasting, low-cost, and efficient adsorbents that may be applied for the purification of water in low-income countries such as Ethiopia.

In recent years, volcanic rocks (VPum and VSco) have received significant interest for pollutant removal due to their valuable properties such as high surface area, low cost, easy accessibility, good mechanical resistance, and availability in large quantities (Alemayehu & Lennartz, 2009). The source of these rocks is volcanic magma that formed during volcanic eruptions. Pumice (VPum) is a finely porous rock frothy with air bubbles; Scoria (VSco) is a rough rock that seems like a furnace slag (Alemayehu & Lennartz, 2009). VPum is often formed from rhyolite magma (Alemayehu & Lennartz, 2009), it can also develop from trachytic or dacitic magma. Due to its high porosity and low specific gravity, it has been used for water and wastewater treatment processes (Aregu et al., 2018). VSco is a vesicular pyroclastic rock with basaltic compositions, reddish-brown to black, denser than VPum, and somewhat porous with high surface area and strength. Both volcanic rocks are found in abundance in Europe (Italy, etc.), Central America, Southeast Asia (Indonesia, etc.), and East Africa (Ethiopia, Eritrea, etc.) (Alemayehu & Lennartz, 2009; Aregu et al., 2018). Although several studies have been conducted on the application of volcanic rocks for pollutants-laden wastewaters (Alemayehu & Lennartz, 2009; Aregu et al., 2018; Asere et al., 2017a; Asere et al., 2017b), very little research has been directed to the defluoridation of groundwater using volcanic rocks.

Previously, defluoridation research has been conducted on batch experiments using natural adsorbents (Birhane et al., 2014; Fufa et al., 2013). The sorption capacity of adsorbents gained from batch equilibrium is valuable in giving basic information about the effectiveness of the adsorbents. Nevertheless, the data obtained from batch studies may not be appropriate for continuous processes where the contact time for the achievement of equilibrium might be insufficient (Viswanathan & Meenakshi, 2010). Consequently, studies by different authors (Monash & Pugazhenth, 2010; Patel, 2019; US EPA, 1983) reveal that the continuous processes mode (fixed-bed column set-up) yields

reliable information about the breakthrough time, appropriate adsorption conditions, and the stability of the adsorption performance which can then be used to evaluate the potential of prepared adsorbents for industrial applications ([Kumari et al., 2021](#)). Therefore, there is an interest to conduct adsorption studies in a flow-through system.

The primary objectives of the current work were to (i) investigate the fluoride sorption capacity of VPum and VSco in a fixed-bed column set-up, (ii) compare the adsorption properties of both adsorbents with each other, (iii) assess the fluoride adsorption mechanisms with respect to varying solution pH, adsorbent particle size, and flow rate, (iv) deeper analyze the adsorption processes employing mathematical models such as the Adams–Bohart and Thomas model, and (v) finally verify the suitability of the models for the design of flow-through systems for the removal of fluoride from aqueous solutions.

## 2.2. Materials and Methods

### 2.2.1. Materials

In this study, rock samples were collected from volcanic cones (VPum: 8°10' N 39°50' E; VSco: 8°33' N 39°16' E) of the Main Rift Valley area of Oromia Regional State, East Showa Zone, Ethiopia, around 50–100 km East of Addis Ababa. The rocks are readily available in approximately 1/3 of the country's total area and are, thus, a preferred adsorption material because of very low supply costs ([Alemayehu et al., 2011, 2017; Aregu et al., 2018](#)).

### 2.2.2. Preparations of Adsorbents

The rock samples (VPum and VSco) were washed repeatedly with deionized water until all water-soluble compounds and dust were removed, and thereafter dried at 55 °C for 48 h ([Asere et al., 2017b; Kwon et al., 2010](#)). After cooling samples down to room temperature, they were crushed with a mortar and sieved using different mesh sizes: silt (<0.075 mm), fine sand (0.075–0.425 mm), and medium sand (0.425–2.00 mm) ([Alemayehu & Lennartz, 2009; Liu & Evett, 2003](#)). All prepared samples were packed in air-tight plastic bags and stored at a cool and dry place for further use

### 2.2.3. Preparations of Adsorbate

All glassware and bottles were thoroughly washed and rinsed with deionized water before usage. The chemicals used were analytical grade reagents and a fluoride stock solution (1000 mg/L) was prepared freshly by dissolving 2.21 g of anhydrous NaF (Merck KGaA, Darmstadt, Germany) in 1000 mL of deionized water. The synthetic fluoride solution of desired concentrations was made by diluting the stock solution. 0.1M of NaOH and/or 0.1 M HCl solutions were used to adjust the pH values of the

fluoride solution utilized in the column experimental experiments.

#### 2.2.4. Adsorbent Characterizations

##### 2.2.4.1. Crystalline Structures

The crystalline structures of the adsorbents were analyzed by an X-ray diffractometer (XRD-7000, Drawell, Shanghai, China) with Cu K $\alpha$  as a radiation source (1.54056 Å) generated at 30 kV and 25 mA instrument. The diffractograms were gained with a step width of 2 $\theta$  and a scan rate of 0.04°/min.

##### 2.2.4.2. Chemical Composition

The elemental composition of the adsorbents was analyzed using inductively coupled plasma-optical emission spectroscopy (ICP-OES). X-ray fluorescence (XRF) spectroscopy was used to obtain information on the oxide contents of the adsorbents.

##### 2.2.4.3. Fourier Transform Infrared (FTIR) Analysis

FTIR spectra of the samples were run on KBr pellets. The spectra were recorded over a range of 5000 to 400 cm<sup>-1</sup> at a resolution of 0.1 cm<sup>-1</sup> in a PerkinElmer spectrometer (UNSW Sydney, Australia) using a lithium tantalite (LiTaO<sub>3</sub>) detector.

##### 2.2.4.4. Scanning Electron Microscope (SEM) Analysis

A scanning electron microscope (SEM) (JCM-6000plus, Version 0.2, Peabody, Massachusetts, USA), operated at 15 kV, was used to determine the morphologies of VPum and VSco. The characteristics of the adsorbents were compared.

##### 2.2.4.5. Determination of pH and Point of Zero Charges (pH<sub>PZC</sub>)

The pH of the adsorbents was determined using a pH meter in a 1:10 adsorbent/water ratio as per the standard method (Fufa et al., 2013). The pH at the point of zero charges (pH<sub>PZC</sub>) of the adsorbents was examined based on the standard method. For this effect, 250 mL of 0.01 M NaCl solution as an electrolyte was positioned in a vessel, thermostated at 298 K, and N<sub>2</sub> was bubbled through the solution to stabilize the pH by preventing the dissolving of CO<sub>2</sub> from the air. In 6 Erlenmeyer flasks, 25 mL of the electrolyte was introduced and the pH was adjusted to the required value (2.00, 4.00, 6.00, 8.00, 10.00, and 12.00) by adding 0.1 M NaOH or 0.1 M HCl. The same procedure and method were performed for blank electrolyte solution (0.01 M NaCl). In each beaker, 0.25 g of the rock samples were added and shaken for 48 h. The suspension was subsequently filtrated and the final pH was determined. The point of zero charges (pH<sub>PZC</sub>) was found at the intersection point by plotting the initial pH versus the final pH.

#### 2.2.4.6. BET Analysis

The specific surface area ( $S_{BET}$ ) of the adsorbents was measured using a nitrogen gas adsorption-desorption technique at 77 K using surface analyzer equipment (Micrometrics/Gemini-2372). The samples were degassed at 300 °C under vacuum for at least 6 h before analysis. The Brunauer-Emmett-Teller (BET) equation was used to obtain a specific surface area ( $S_{BET}$ ). The  $S_{BET}$  values of the two adsorbents (VPum and VScO) are compared.

#### 2.2.5. Column Adsorption Experimental Set-up and Procedures

Continuous fixed-bed column adsorption studies were carried out to assess the dynamic behavior of fluoride removal by using VPum and VScO. Continuous flow adsorption experiments were conducted in a small-scale cylindrical column of 8.1 cm internal diameter and 10 cm height with an empty bed volume of 515 cm<sup>3</sup>. The column was filled with a weighted amount of adsorbent of different particle sizes (silt: < 0.075 mm, fine sand: 0.075–0.425 mm, and medium sand: 0.425–2.00 mm). The same particle size was used if controlling parameters such as pH and flow rate were tested. The bed was conditioned with deionized water (pH: 7.00–7.30) for 12 h (overnight) to ensure a closely packed adsorbent and to avoid the potential occurrence of voids, channeling, or cracking, which can significantly affect the performance of the column.

A synthetic fluoride solution with a concentration of 10 mg/L was pumped to a packed bed column in up-flow mode to avoid channeling caused by gravity. The influent volumetric flow rate varied between experiments but was held constant in a given experiment using an adjustable peristaltic pump (MS-REGLO, Labortechnik-Analytic, Switzerland). The experiments were conducted at room temperature ( $25 \pm 2$  °C). The effluent column sample was collected using an automatic fraction collector (RFI, MA-RON GmbH, Germany). The constant flow rate was verified by collecting and quantifying the effluent solution at regular time intervals. The column operation was stopped when the concentrations of the fluoride in the effluent exceeded 90% of its initial concentrations. Ion chromatography (930 Compact IC Flex, Metrohm, Switzerland) was used to quantify fluoride concentrations. The instrument uses 3.2 mmol/L Na<sub>2</sub>CO<sub>3</sub>/1.0 mmol/L NaHCO<sub>3</sub> as eluent, Metrosep A Supp 5–150/4.0 column, and a standard conductivity detector to measure the conductivity of the effluent solutions. The fluoride concentration was measured in the calibration range of 0.2–200 mg/L, containing inline dilution, inline dialysis, eluent degasser, CO<sub>2</sub> suppressor, and chemical suppressor. Suppression in IC maximizes the detection sensitivity of fluoride ions while reducing the background conductivity of the eluent.

The maximum tolerable breakthrough concentration ( $C_b$ ) was 1.5 mg/L (15% of the influent initial

concentration of 10 mg/L), which is recommended by WHO ([WHO, 2011](#)) as a maximum acceptable level for drinking water.

The effect of experimental parameters such as particles size (silt: < 0.075 mm, fine sand: 0.075–0.425 mm, and medium sand: 0.075–0.425 mm), influent solution pH (2.00, 4.00, and 6.00), and influent volumetric flow rate (1.25, 2.50, and 3.75 mL/min) on breakthrough behavior and amount of fluoride removed were examined.

#### 2.2.6. Modeling and Analysis of Fixed-Bed Column Data

A fixed-bed column adsorption performance is well described through the breakthrough curve concept ([Aksu et al., 2007](#)). The time of solute breakthrough and the shape of the breakthrough curve are important indicators for the operational adsorption processes; the breakthrough curve is directly linked to the viability and economics of the adsorption process ([Chen et al., 2015](#); [Golie & Upadhyayula, 2016](#)). The breakthrough patterns and according parameters are dependent on the operating conditions of the fixed-bed column such as adsorbent particle size, influent flow rate, and pH of the influent solution. Nevertheless, the pH value may not influence the breakthrough curve in a situation such as when using strongly basic anion exchangers. The primary and significant attribute is the sorbent selectivity to the pollutant, as well as the dynamic exchange capacity and full dynamic capacity of the column ([Gennaro et al., 2020](#)). To investigate the performance of the column and to scale up, the determination of breakthrough parameters is crucial. The breakthrough curves expressed in terms of the ratio of effluent to influent adsorbate concentration ( $C_t/C_o$ ) as a function of time or effluent volume for a given height of the bed reflect the absorbed fluoride from the solution. Time equivalent to stoichiometric capacity (exhaustion time) and time equivalent to usable capacity (breakthrough time) is shown in Equations (2.1) and (2.2), respectively ([Golie & Upadhyayula, 2016](#); [Yagub et al., 2015](#)).

$$t_e = \int_{t=0}^{t=t_{total}} \left(1 - \frac{C_t}{C_o}\right) dt \quad (2.1)$$

$$t_b = \int_{t=0}^{t_b} \left(1 - \frac{C_b}{C_o}\right) dt \quad (2.2)$$

where  $t_e$  is exhaustion time (min),  $t_b$  is the breakthrough time (min) at which  $C_t = C_b$  (mg/L) (for the present system,  $C_b = 1.5$  mg/L).

The total value of fluoride adsorbed ( $q_{total}$ : mg) from the column for a given feed concentration and the flow rate was obtained from the area (A) under the breakthrough curve by integrating the adsorbed fluoride concentration  $C_{ad}$  ( $C_{ad} = C_o - C_t$ ) (mgL<sup>-1</sup>) versus  $t$  (min) and can be obtained from Equation

(2.3) (Chen et al., 2012; Paudyal et al., 2013).

$$q_{\text{total}} = \frac{QA}{1000} = \frac{Q}{1000} \int_{t=0}^{t=t_{\text{total}}} C_{\text{ad}} dt \quad (2.3)$$

where  $t_{\text{total}}$ , and  $Q$  are the total flow time until saturation of the bed (min), and volumetric flow rate (mL/min), respectively.

Equilibrium fluoride uptake ( $q_e$ : mg kg<sup>-1</sup>) (maximum capacity of the column) in the column is calculated by Equation (2.4) as the total amount of fluoride adsorbed ( $q_{\text{total}}$ ) per kilogram of dry adsorbent mass ( $m$ ) at the end of the total flow time (Chen et al., 2012).

$$q_{\text{eq}} = \frac{q_{\text{total}}}{m} \quad (2.4)$$

The effluent volume ( $V_e$ ) and treated effluent volume or breakthrough volume ( $V_b$ ) of the solution can be found from Equations (2.5) and (2.6), respectively.

$$V_e = Qt_e \quad (2.5)$$

$$V_b = Qt_b \quad (2.6)$$

where  $V_e$  is the total effluent volume at exhaustion time (mL),  $V_b$  is the total effluent volume at the breakthrough time (mL),  $Q$  is the volumetric flow rate (mL/min),  $t_e$  and  $t_b$  are exhaustion and breakthrough time (min), respectively.

The Mass Transfer Zone (MTZ) or unused bed length ( $H_{\text{UNB}}$ ) can be obtained from Equation (2.7) (Golie & Upadhyayula, 2016; Yagub et al., 2015).

$$\text{MTZ} = H_T \left( \frac{t_e - t_b}{t_e} \right) \quad (2.7)$$

where  $H_T$  is total bed height (cm),  $t_e$  (min) is exhaustion time, and  $t_b$  is breakthrough time (min).

The Empty Bed Contact Time (EBCT), which measures the critical depth and the contact time between the solid phase adsorbent and the liquid phase, can be obtained from Equation (2.8).

$$\text{EBCT} = \frac{V_B}{Q} \quad (2.8)$$

where  $V_B$  is the volume of a fixed bed (mL) and  $Q$  is the flow rate (mL/min).

The bulk density ( $\rho_b$ : gm.cm<sup>-3</sup>), which measures the adsorbent compaction status, and the particle



density ( $\rho_p$ : gm.cm<sup>-3</sup>) of the adsorbent can be obtained from Equations (2.9) and (2.10), respectively (Worch, 2012).

$$\rho_b = \frac{m_{ads}}{V_t} \quad (2.9)$$

$$\rho_p = \frac{m_{ads}}{V_t - V_v} \quad (2.10)$$

where  $m_{ads}$  is the dry mass of adsorbent (mg), and  $V_t$  is the bulk volume (cm<sup>3</sup>) which includes the volume of adsorbent ( $V_B$ :cm<sup>3</sup>) and the pore space between the adsorbent particles or void volume ( $V_v$ :cm<sup>3</sup>).

The void volume ( $V_v$ :cm<sup>3</sup>) of the adsorbent can be found from Equation (2.11) (Worch, 2012).

$$V_v = \frac{W_{sat} - W_{dry}}{\rho_w} \quad (2.11)$$

where  $w_{dry}$  is the weight of dry adsorbent (g),  $W_{sat}$  is the weight of saturated adsorbent (g), and  $\rho_w$  is the density of water (g cm<sup>-3</sup>).

The total porosity of the adsorbent ( $\epsilon_b$ ) can be obtained from Equation (2.12) (Worch, 2012).

$$\epsilon_b = 1 - \frac{\rho_b}{\rho_p} \quad (2.12)$$

The filter (superficial) velocity ( $V_f$ : cm min<sup>-1</sup>) and effective (interstitial) velocity ( $V_I$ : cm min<sup>-1</sup>) can be found from Equations (2.13) and (2.14), respectively (Worch, 2012).

$$V_f = \frac{Q}{A} \quad (2.13)$$

$$V_I = \frac{Q}{A \times \epsilon_b} \quad (2.14)$$

where  $A$  is the cross-sectional area of the fixed-bed (cm<sup>2</sup>) and  $Q$  is the flow rate (cm<sup>3</sup>min<sup>-1</sup>).

#### 2.2.7. Fixed-Bed Column Breakthrough Curve Modeling

The successive operation of a small-scale column towards industrial applications can be well elucidated with the help of some models. Various models have been reported for predicting the breakthrough performance in fixed-bed adsorption (Mohan et al., 2017b; Salifu, 2017). In this study, the two most important and widely used mathematical models, the Thomas model and the Adams–Bohart model, have been applied to the column experimental data for describing the dynamic behavior

of fluoride adsorption using VPum and VScO in a fixed-bed column filter.

#### 2.2.7.1. Thomas Model

The Thomas model (Thomas, 1944) is one of the most extensively employed kinetic models to predict fixed-bed column performance. In addition to the prediction of the breakthrough curve for the effluent, the model can be used to determine the maximum uptake of adsorbate and adsorption rate constant (Thomas, 1944). The non-linear form of the Thomas model can be described as follows Equation (2.15), (Singh et al., 2016).

$$\frac{C_t}{C_o} = \frac{1}{1 + \exp \left[ K_T q_o \frac{m}{Q} - K_T C_o t \right]} \quad (2.15)$$

where  $C_o$  (mg/L) is the initial solute concentration,  $C_t$  (mg/L) is the solute concentration at the time,  $t$ ,  $Q$  (L/min) is the volumetric flow rate,  $q_o$  (mg/kg) is the maximum solid-phase concentration of solute (maximum column adsorption capacity),  $K_T$  is the Thomas rate constant (L/min mg), and  $m$  (kg) is the packed dry mass of the adsorbent in a fixed-bed.

#### 2.2.7.2. Adams–Bohart model

The Adams–Bohart model (Bohart & Adams, 1920) was developed for the analysis of the dynamics of fixed-bed based on the assumption that the adsorption rate is proportional to both the residual adsorbent and adsorbate concentration. The nonlinear form of the Adams–Bohart model (Equation (2.16)) (Chu, 2020), was used for the prediction of breakthrough curves and model parameters.

$$\frac{C_t}{C_o} = \frac{1}{1 + \exp \left[ K_{AB} N_o \frac{Z}{v} - K_{AB} C_o t \right]} \quad (2.16)$$

Where  $K_{AB}$  (L/mg min) is the kinetic constant,  $v$  (mL/min) is the linear flow rate,  $Z$  (cm) is a column bed depth, and  $N_o$  (mg/L) is the saturation concentration (adsorption capacity of the adsorbent per unit volume of the bed), and time  $t$  (min) ranges from the start to fluoride breakthrough point. The linear flow rate was determined by Equation (2.17).

$$v = \frac{Q}{A} \quad (2.17)$$

where  $Q$  (cm<sup>3</sup>/min) is the volumetric flow rate, and  $A$  (cm<sup>2</sup>) is the cross-sectional area of the bed (García-sánchez et al., 2013; Han et al., 2009; Quintelas et al., 2013).

## 2.3. Results and Discussions

### 2.3.1. Characterization of Adsorbents

#### 2.3.1.1. Crystalline Structures and Material Properties and Experimental Conditions

The crystalline phases of VPum and VScO were characterized using the X-ray diffraction (XRD) instrumental technique. The mineralogical composition of the adsorbents was characterized by matching the X-ray diffractogram (Figure 2.1a (VPum), b (VScO)) with the database of the X'pert HighScore Plus software package (Version: 2.2b (2.2.2)). The results showed that the main crystalline phases in VScO were Silicon Oxide (SiO<sub>2</sub>), Albite low (Na(AlSi<sub>3</sub>O<sub>8</sub>)), whereas Hematite (Fe<sub>2</sub>O<sub>3</sub>) and Silicon Oxide (SiO<sub>2</sub>) and Albite high (Na(AlSi<sub>3</sub>O<sub>8</sub>)) are the dominant components of VPum. The presence of crystalline phases in VPum samples can be ascribed to the peaks at  $2\theta = 24.9^\circ, 27.6^\circ, 27.7^\circ, 37.7^\circ, 41.9^\circ, 58.0^\circ, 64.9^\circ$  and  $65.0^\circ$ , while that of VScO sample appeared at  $2\theta = 22.2^\circ, 23.9^\circ, 23.9^\circ, 28.2^\circ, 30.0^\circ, 33.9^\circ$ , and  $35.8^\circ$ . The detected dome in both samples between  $2\theta = 10^\circ$  and  $40^\circ$  is an indication of amorphous material. The amorphous phase(s) present in the adsorbents was estimated by the calibration method. This method makes use of the integrated counts associated with the amorphous and crystalline fractions (Equation (2.18)) (Rowe & Brewer, 2018).

$$C_m(\%) = \left[ \frac{C_{pa}}{A_{pa} + C_{pa}} \right] \times 100 \quad (2.18)$$

where  $C_m$  is the measured crystallinity,  $C_{pa}$  and  $A_{pa}$  are the integrated peak areas for the crystalline and amorphous components, respectively. The results revealed that the presence of the amorphous phase (s) in VPum and VScO is 89% and 68%, respectively.

The greater fraction of amorphous phase(s) in VPum compared with VScO possibly originates from simultaneous rapid cooling and depressurization of high-temperature volcano lava. The depressurization produces bubbles by lowering the boiling point of the lava. The simultaneous cooling then freezes the bubbles in the matrix of VPum. Due to rapid cooling, crystals do not have enough time to grow. A similar observation has been reported from the XRD analysis of pumice in previous studies (Li et al., 2010; Sepehr et al., 2014).

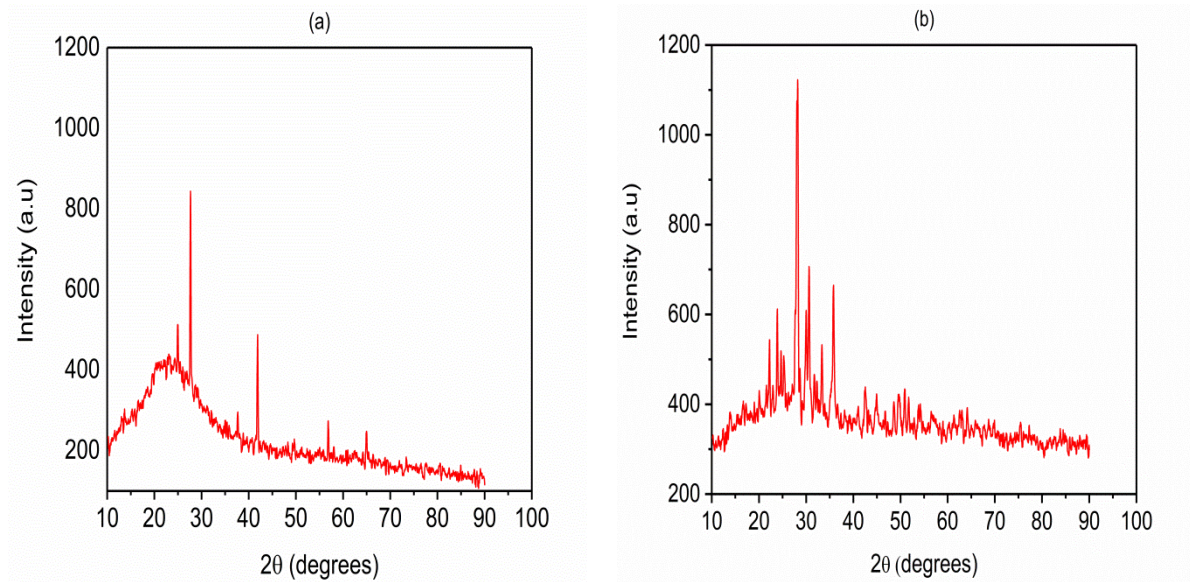


**Figure 2.1** XRD patterns for (a) virgin pumice (VPum) and (b) virgin scoria (VSco)

Additionally, the results of material properties and experimental conditions were summarized in Table 2.1 as shown below.

**Table 2.1** Material properties and experimental conditions

Parameters	Virgin scoria (VSco)			Virgin pumice (VPum)		
	<0.075	0.075–0.425	0.425–2.00	<0.075	0.075–0.425	0.425–2.00
Particle size (mm)						
Mass of adsorbents, $m_{ads}$ (gm)	737.90	763.90	680.50	376.40	265.90	186.40
Bulk density, $\rho_b$ (gm cm <sup>-3</sup> )	1.43	1.48	1.32	0.73	0.52	0.36
Particle density, $\rho_s$ (gm cm <sup>-3</sup> )	2.37	2.33	1.94	1.61	1.31	0.64
Void volume, $V_v$ (cm <sup>3</sup> )	203.70	187.20	164.70	281.10	311.80	222.30
Total porosity, $\epsilon$	0.40	0.36	0.32	0.55	0.61	0.43
Flow rate, $Q$ (cm <sup>3</sup> min <sup>-1</sup> )	1.25	2.50	3.75	1.25	2.50	3.75
Empty Bed Contact Time, $EBCT$ (min)	412.00	206.00	137.33	412.00	206.00	137.33
Filter (Superficial) velocity, $V_f$ (cm min <sup>-1</sup> )	0.02	0.05	0.07	0.02	0.05	0.07
Effective (Interstitial) velocity, $V_I$ (cm min <sup>-1</sup> )	0.06	0.13	0.23	0.05	0.08	0.17

### 2.3.1.2. Chemical Composition

The chemical analysis revealed that the major elements in VPum and VSco, as determined by ICP-OES (Table A2.1), are Si, Al, and Fe. Other elements were present in comparatively smaller quantities or below the detection limit of the instrument. In our previous study (Alemayehu & Lennartz, 2009), the XRF measurement (Table A2.1) indicated that the oxides of Si, Fe, and Al were the major constituents of both VPum and VSco.

However, the chemical composition of the adsorbents might change in time due to weathering processes. Consequently, representative samples have to be checked for possible changes induced due

to weathering.

#### 2.3.1.3. Fourier Transform Infrared (FTIR) Analysis

The FTIR spectrums of VPum (Figure 2.2a) and VScO (Figure 2.2b) at wavelengths ranging from 4000 to 400  $\text{cm}^{-1}$  are shown in Figure 2.2. Due to the symmetric stretching vibration of Si-O-Si, the absorption band at  $\sim 1045.75 \text{ cm}^{-1}$  can be assigned to the characteristic peak of  $(\text{SiO}_4)^{2-}$  groups in the FTIR spectrum of VPum (Sepehr et al., 2014), whereas the band located at  $\sim 1011.5$  in the FTIR spectrum of VScO can be belongs to the asymmetric stretching vibration of T-O-Si, T = Si or Al (Pirsaheb et al., 2018). In the FTIR spectrum of VPum, the peaks at  $\sim 781$  and  $\sim 695.25$  belong to bending vibrations of Si-O-Si bond (Li et al., 2010), whereas the band shown in the FTIR spectrum of VScO at  $\sim 759$  is related to the stretching vibration of 6-fold coordinated Al(VI)-OH and 6-fold coordinated Al(VI)-O (Djobo et al., 2014). The small peaks shown in the FTIR spectrum of VScO at  $\sim 572$  and  $\sim 539.25$  can be attributed to the symmetric stretching of Si-O-Si and Al-O-Si (Panias et al., 2007; Pirsaheb et al., 2018), whereas the small band at  $\sim 465$  belongs to bending vibrations of Si-O-Si and O-Si-O (Panias et al., 2007). Certain peaks like the broadening peak at  $\sim 3602.5 \text{ cm}^{-1}$  in the FTIR spectrum of VPum and sharper peak at  $\sim 2369.75 \text{ cm}^{-1}$  in the FTIR spectrum of VScO belong to the asymmetric stretching vibration of -OH bond can be allocated to adsorbed water molecules, whereas the peak at  $\sim 1645.75 \text{ cm}^{-1}$  in VPum can be allocated to the bending vibration of H-O-H bond (Li et al., 2010; Panias et al., 2007; Sepehr et al., 2014). The most characteristic difference observed between the FTIR spectrum of VPum and the FTIR spectra of VScO concerning the band is attributed to the asymmetric stretching vibration of the -OH bond. This band that appeared as a broad band at about  $\sim 3602.5 \text{ cm}^{-1}$  in the FTIR spectrum of VPum becomes sharper and shifts to lower frequencies ( $\sim 2369.75 \text{ cm}^{-1}$ ) in the FTIR spectrum of VScO indicating that there is a high-water content in VPum and could be correlated with less mechanical strength than VScO. Similar observations have been reported for a different system (Panias et al., 2007).



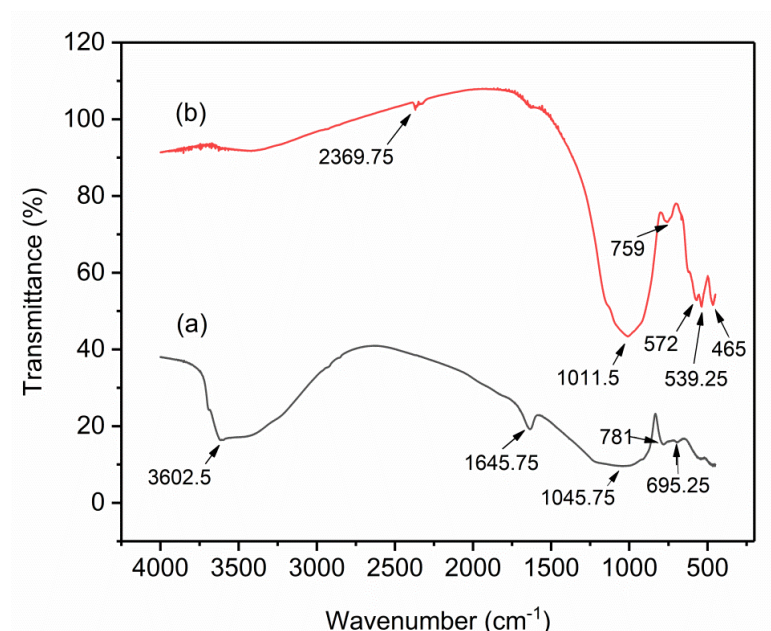


**Figure 2.2** Fourier-transform infrared (FTIR) for (a) VPum and (b) VScO

#### 2.3.1.4. Scanning Electron Microscope (SEM) analysis

The VPum (Figure 2.3a) and VScO (Figure 2.3b) SEM micrographs allowed direct observation of the surface morphology of the adsorbents with a magnification of  $\times 100$ . The structure of VPum showed that the surface of VPum had an interconnected porous surface (Asgari et al., 2012; Li et al., 2010), while VScO had an irregular shape and fibrous cavities (or pores). In addition, it may be said that these pores in VScO were either closed or in open forms (pores) (Moradi et al., 2015). As seen from the micrographs of the adsorbents, VPum had an interconnected inner porous surface (as indicated in Figure 2.3a, red-colored), while VScO (Figure 2.3b) is dominated by the dead-end pores. Consequently, the interconnected internal pore structure in VPum allows for better fluoride accessibility and, hence, better adsorption capacity than VScO.

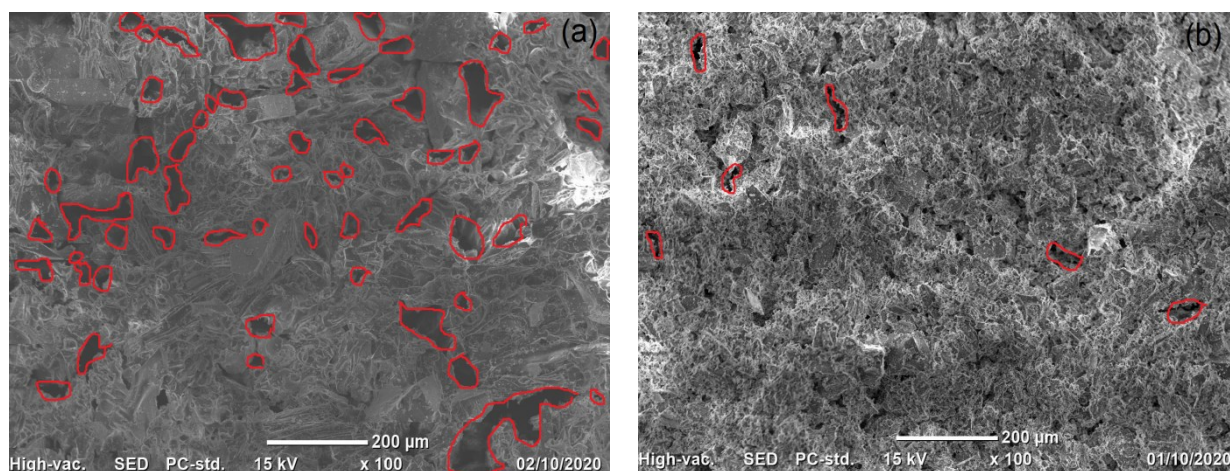


**Figure 2.3** SEM micrographs for (a) VPum and (b) VScO

### 2.3.1.5. pH and Point of Zero Charges ( $pH_{PZC}$ )

The pH of the rock samples in water was found to be 6.65 and 7.20 for VPum and VScO, respectively. The point of zero charges ( $pH_{PZC}$ ) of the adsorbents was identified as 6.85 for VPum and 6.98 for VScO at the intersection of the graph of the initial pH vs. the final pH (Figure 2.4). The slight difference observed in the adsorbents  $pH_{PZC}$  is related to their different characteristics. As can be seen from Table A2.1, the two volcanic rocks (VPum and VScO) have different chemical compositions, which also influence the surface charge of the adsorbents. This is in agreement with previous studies (Asere et al., 2017b; Souza et al., 2012), showing the effect of chemical composition on the zeta potential of different materials. Below these values ( $pH < 6.85$  for VPum and  $< 6.98$  for VScO), the surface of the adsorbents is positively charged. Thus, if the  $pH < pH_{PZC}$ , fluoride could possibly be adsorbed onto the surface of the adsorbents by coulombic attraction (Ayoob & Gupta, 2009; Fufa et al., 2013; Salifu et al., 2013). In addition, the curve for the blank experiment (for blank electrolyte solution 0.01 M NaCl) of both adsorbents is shown in Figure 2.4. As seen from the blank curve (Figure 2.4), a pH change without adding the adsorbents was obtained, which confirmed that sorbent dosing is not the only factor to fluctuates the pH of the solution.

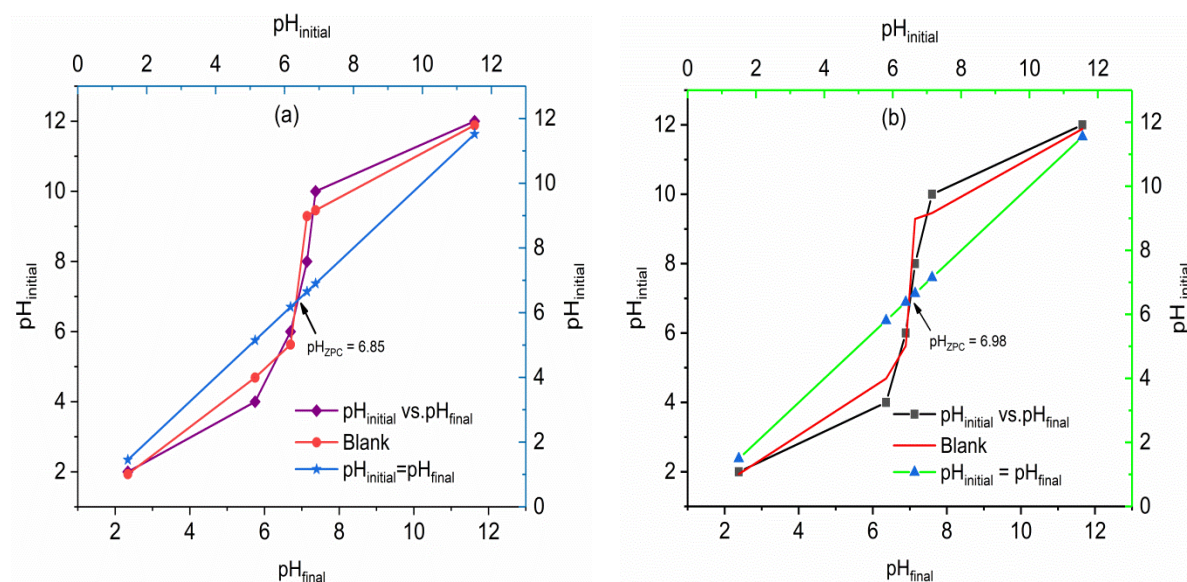


**Figure 2.4** Determination of pH point of zero charges ( $pH_{PZC}$ ) for (a) VPum and (b) VScO

### 2.3.2. Effect of Adsorbents Particle Size

The effect of the particles size on the breakthrough behavior of fluoride was investigated for both VScO and VPum with grain size classes of silt to medium sand ( $< 0.075$ ,  $0.075-0.425$ ,  $0.425-2.00$  mm), while maintaining the same initial fluoride concentration (10 mg/L), bed depth (10cm), initial flow rate (1.25 mL/min), as well as solution pH (2.00) (Figure 2.5a (VPum), b (VScO)). As seen from Figure 2.5a (VPum) and b (VScO), on reducing the particle size from medium ( $0.425-2.00$  mm) to silt

(< 0.075 mm) the breakthrough and exhaustion time noticeably increased for VScO, while the breakthrough and exhaustion time was high for VPum at a fine particle size (0.075–0.425 mm). The resulting breakthrough and removal of fluoride parameters are tabulated in Table 2.2. As can also be seen from Table 2.2, the amount of total adsorbed fluoride ( $q_{\text{tot}}$ ) and the uptake of fluoride were high at silt (< 0.075 mm) and fine (0.075–0.425 mm) particle size for VScO and VPum, respectively. The smaller particle sizes provide large surface areas and/or sorption sites are more readily available. The results showed that the reduction of particle size of an adsorbent is a significant controlling factor in the fluoride–VScO system (at a particle size of < 0.075 mm the fluoride uptake was high). A similar effect was observed for VPum (at a particle size of 0.075–0.425 mm the fluoride sorption capacity was high). However, the effect of particle size on the adsorption capacity is more pronounced for VScO than VPum. That means the pore spaces are more readily available in VPum as compared to VScO, showing that the pore space of VPum is a continuum (skeletal structure) while the pore space of VScO is dominated by dead-end pores. This infers that VPum loses its internal porosity at the smallest particle size (< 0.075 mm) since the continuum pore space (skeletal structure) is damaged when compared to the fine particle size (0.075–0.425 mm) and resulting in smaller internal pore surface areas; consequently, the removal capacity of the adsorbent decreased. On the other hand, the pore space is not readily available in VScO (i.e., the internal pore space of VScO is dominated by dead-end pores). VScO at the smallest particle size (< 0.075 mm) is, therefore, expected to have a large surface area, which leads to higher removal capacity compared to the fine particle size (0.075–0.425 mm). A similar observation was reported for both adsorbents based on a batch adsorption experiment (Alemayehu & Lennartz, 2009), and a similar remark was also drawn for pumice in the previous study (Li et al., 2010). Moreover, the BET specific surface area ( $S_{\text{BET}}$ ) of the adsorbents was determined. As expected, VPum (3.50 m<sup>2</sup>/g) has a larger surface area than VScO (2.49 m<sup>2</sup>/g). Thus, all experiments other than the effect of particle sizes were conducted at a particle size of < 0.075 mm for VScO and 0.075–0.425 mm for VPum.

### 2.3.3. Effect of Influent pH

The influent solution's pH can noticeably affect the anions sorption on the adsorbents by changing the degree of ionization, the ion speciation, and the adsorbent's surface charge. Therefore, the effect of solution pH on the adsorption of fluoride using VPum and VScO was investigated at different pH (2.00, 4.00, and 6.00) by a separate set of fixed-bed adsorption columns. The breakthrough curves obtained for both adsorbents are shown in Figure 2.6a, b for a fixed inlet flow rate of 1.25 mL/min, influent fluoride concentration of 10 mg/L, column bed depth of 10 cm, and a particle size of < 0.075 mm for VScO and 0.075–0.425 mm for VPum.



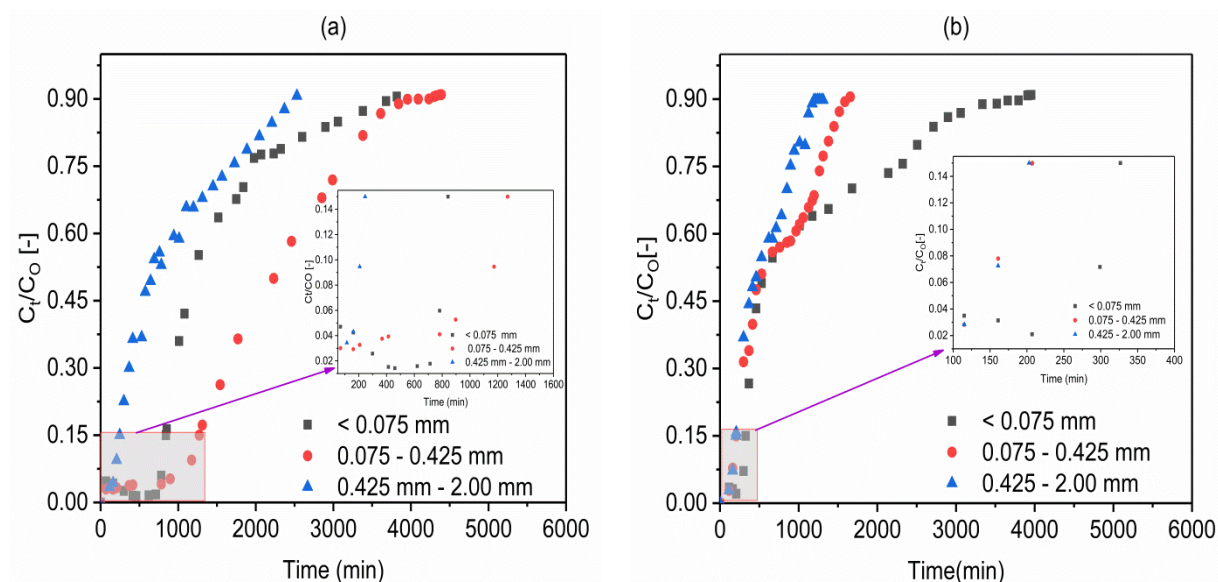


**Figure 2.5** Effect of particle sizes on the breakthrough behavior of fluoride in (a) VPum and (b) VScO at (pH 2.00; influent fluoride concentration 10 mg/L ( $C_0$ : 10 mg/L); flow rate 1.25 mL/min ( $Q_0$ : 1.25 mL/min; bed depth 10 cm)

**Table 2.2** Fixed-bed column parameters obtained for fluoride adsorption onto VPum and VScO

VPum.	H (cm)	$C_0$ (mg/L)	$Q_0$ (mL/min)	pH	Particles size ( $P_{size}$ ) (mm)	$t_b$ (min)	$t_e$ (min)	$V_b$ (mL)	$V_e$ (mL)	MTZ (cm)	EBCT (min)	$q_{tot}$ (mg)	$q_e$ (mg/kg)
	10	10	1.25	2.00	< 0.075	816	1623	1019.64	2033.41	4.99	412	20.28	59.6
	10	10	1.25	2.00	0.075–0.425	1206	2339	1507.50	2923.70	4.84	412	29.24	109.9
	10	10	1.25	2.00	0.425–2.00	235	1013	293.23	1265.89	7.68	412	12.67	67.9
	10	10	1.25	4.00	0.075–0.425	278	500	347.50	625	4.44	412	6.25	23.51
	10	10	1.25	6.00	0.075–0.425	135	315	168.75	393.75	5.71	412	3.94	14.81
	10	10	2.50	2.00	0.075–0.425	215	634	538.47	1585.16	6.60	206	7.93	29.8
	10	10	3.75	2.00	0.075–0.425	75	359	282.69	1346.42	7.90	137	4.49	16.89
VScO	H (cm)	$C_0$ (mg/L)	$Q_0$ (mL/min)	pH	Particles size ( $P_{size}$ ) (mm)	$t_b$ (min)	$t_e$ (min)	$V_b$ (mL)	$V_e$ (mL)	MTZ (cm)	EBCT (min)	$q_{tot}$ (mg)	$q_e$ (mg/kg)
	10	10	1.25	2.00	< 0.075	415	1286	518.03	1607.60	6.77	412	16.08	22
	10	10	1.25	2.00	0.075–0.425	199	760	248.99	849.80	7.38	412	9.50	12.4
	10	10	1.25	2.00	0.425–2.00	231	591	288.17	739.12	6.10	412	7.39	10.9
	10	10	1.25	4.00	< 0.075	296	487	370	608.75	3.92	412	6.09	8.2
	10	10	1.25	6.00	< 0.075	227	393	283.75	491.25	4.22	412	4.91	6.7
	10	10	2.50	2.00	< 0.075	185	445	462.95	1113.19	5.84	206	5.57	7.5
	10	10	3.75	2.00	< 0.075	69	249	256.82	931.87	7.24	137	3.10	4.2

$t_b$  = breakthrough time,  $t_e$  = exhaustion time,  $V_b$  = total effluent volume at a breakthrough time,  $V_e$  = total effluent volume at exhaustion time MTZ = Mass Transfer Zone, EBCT = Empty Bed Contact Time,  $q_{total}$  = total amount of fluoride adsorbed from the column,  $q_e$  = equilibrium fluoride uptake per kg of adsorbent.

As can generally be observed from Figures 2.6a, b, the adsorption capacity of the adsorbents noticeably increased with decreasing pH. As can also be seen from Table 2 (VPum and VScO), the total amount of fluoride adsorbed ( $q_{tot}$ ) was high for VPum (29.24 mg) and 16.08 mg for VScO at lower pH of 2, and the breakthrough time decreased from 1206 to 135 min for VPum and 415 to 227 min for VScO with an increase in pH from 2 to 6. The volume of water treated at the breakthrough time was higher at a pH of 2.00 (1507.5 mL for VPum and 518.03 mL for VScO) than 4.00 (347.5 mL for VPum and

370 mL for VScO) and 6.00 (168.75 mL for VPum and 283.75 mL for VScO). This concludes the occurrence of the breakthrough time was longer, the amount of fluoride adsorbed, and the treated water volume was high for a pH of 2.00. As pH varies, surface charge also varies; the sorption of charged species is affected. Therefore, the performance of adsorbents for better adsorption at low pH may be the result of the presence of a large number of  $H^+$  ions at low pH values, and hence neutralize the negatively charged adsorbent surface (Alemayehu et al., 2011), consequently dropping the interference of the adsorption of fluoride. In addition, this reality can be elucidated based on the pH value at the point of zero charges of the adsorbents ( $pH_{PZC} = 6.85$  (VPum) and 6.98 (VScO)).

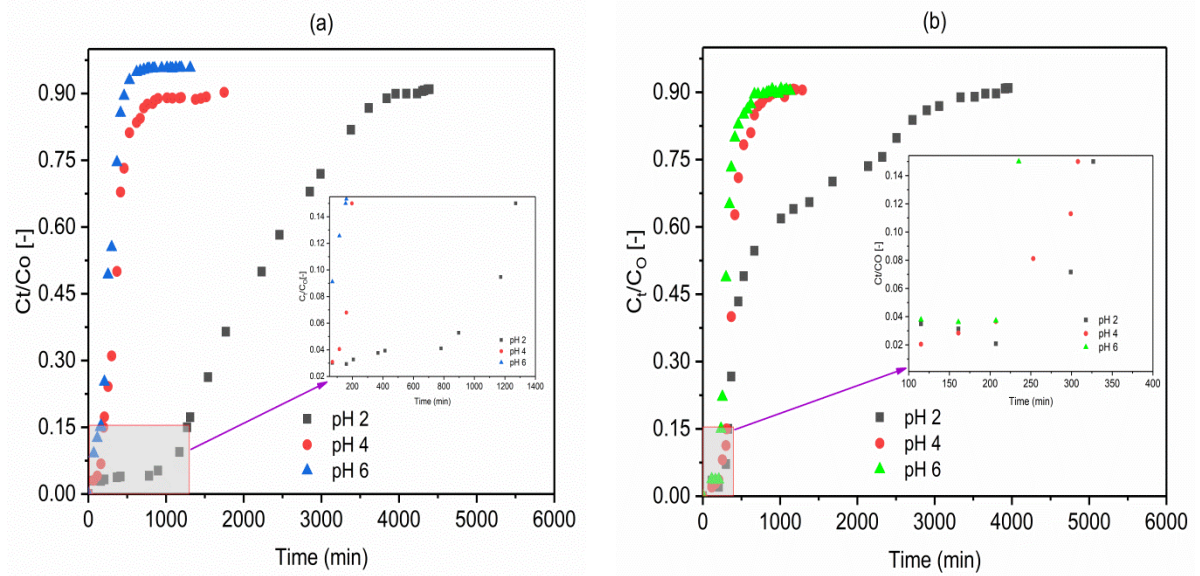
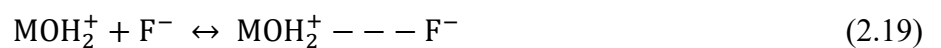


**Figure 2.6** Effect of pH on the breakthrough behavior of fluoride in (a) VPum: 0.075–0.425 mm and (b) VScO: < 0.075 mm ( $C_0$ : 10 mg/L;  $Q_0$ : 1.25 mL/min; bed depth 10 cm)

Moreover, the decrease in the adsorption of fluoride at pH 4.00 and 6.00 could also be due to the decrease in the number of  $H^+$  or electrostatic repulsion of fluoride by negatively charged adsorbent surface (Chen et al., 2011; Salifu et al., 2013).

Hence, the sorption of fluoride ions is due to an electrostatic phenomenon and surface complexation that perform independently or together for the adsorption of fluoride ions on the adsorbents. The removal mechanism at  $pH < pH_{PZC}$  is presumably due to the columbic attraction of fluoride by positive surface charges (Equation (2.19)) and/or ligand exchange reactions of fluoride with surface hydroxyl groups (Equation (2.20)).



where, M represents Fe, Al, Si, Ca, Mg, etc.

In this study, an increment in the final pH (pH  $\sim$ 7.20) was observed after the completion of the adsorption experiment, which is consistent with the columbic or ligand exchange type adsorption mechanism shown in Equations (2.19) and (2.20) (Salifu et al., 2013). This can be further explained by the capacity of the adsorbents to maintain a neutral pH after adsorption (Alemayehu & Lennartz, 2010; Fufa et al., 2013). The capacity to maintain neutral effluent solution pH could be from the amphoteric nature of oxides in both adsorbents ( $\text{Al}_2\text{O}_3$ ,  $\text{Fe}_2\text{O}_3$ ,  $\text{TiO}_2$ , etc.) when compared with the effect of basic metallic oxides (Table A2.1). This type of observation was reported for the removal of pollutants in a previous study (Fufa et al., 2013). Furthermore, the elemental compositions of exchangeable cations also play a critical role in fluoride uptake during defluoridation (Obijole et al., 2019). There might be a slight increase in electro conductivities of the final solutions, which might not influence the adsorption process (Sepehr et al., 2013a). However, additional testing of the effluent solution for various compounds may be required to draw definite conclusions.

It is noted that the effect of pH on the adsorption capacity may be due to the shared impact of pH on the nature of the adsorbent surface, the existence of the adsorbed pollutant (fluoride ion), and the added acid and base to the working solution to adjust its pH. In this study, the optimum and effective removal of fluoride takes place at a pH of 2.00; hence, all experiments other than the effect of pH were conducted at a pH of 2.00 for both adsorbents.

#### 2.3.4. Effect of Flow Rate

The effect of flow rate on the adsorption of fluoride using VPum and VScO was examined at the flow rates of 1.25, 2.50, and 3.75 mL/min whereas the bed depth (10 cm), influent solution pH (2.00), initial fluoride concentration (10 mg/L), and adsorbents particle size ( $< 0.075$  mm (VScO) and 0.075–0.425 mm (VPum)) were held constant. As indicated in Figure 2.7a (VPum) and b (VScO), the breakthrough curves become steeper and shifted to the origin with an increasing flow rate while the breakthrough time decreased. The use of a high flow rate decreases the contact time of fluoride in the solution with the adsorbents, thereby allowing earlier breakthroughs to occur. Additionally, increasing the flow rate from 1.25 to 3.75 mL/min decreased the volume of water treated from 1507.5 to 282.69 mL and 518.03 to 256.03 mL for VPum and VScO, respectively (Table 2.2).

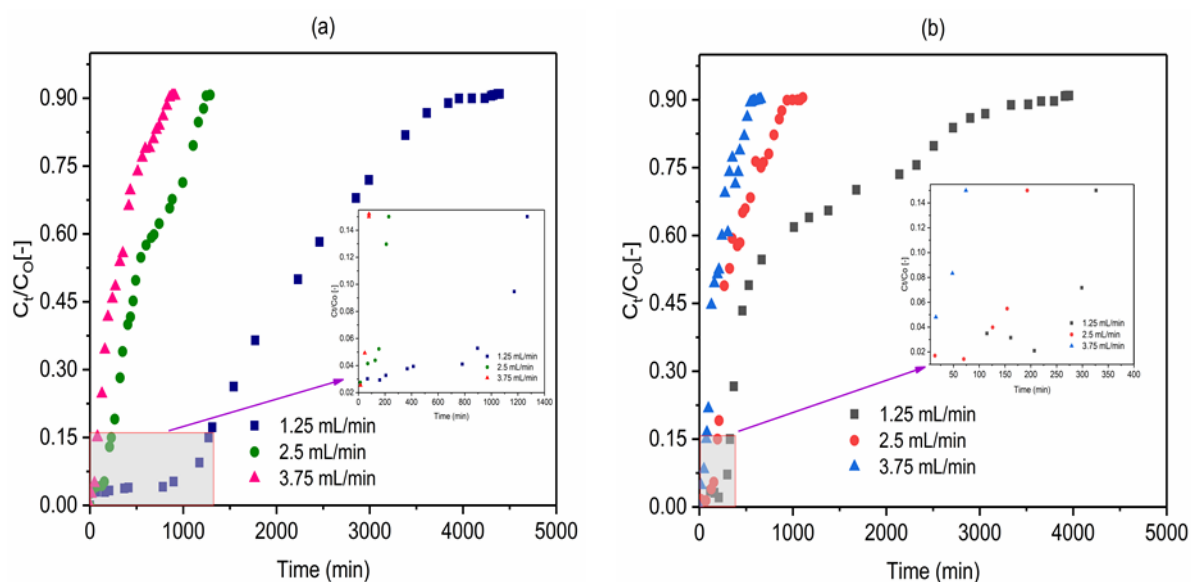


**Figure 2.7** Effect of influent flow rate on the breakthrough behavior of fluoride in (a) VPum: 0.075–0.425 mm and (b) VScO: < 0.075 mm (pH 2;  $C_0$ : 10 mg/L; bed depth 10 cm)

This was further supported by Mass Transfer Zone (MTZ) (Table 2.2) which increased with increasing flow rate. The total fluoride adsorbed ( $q_{tot}$ ) increased from 4.49 mg to 29.24 mg for VPum and from 3.10 mg to 16.08 mg for VScO (Table 2.2) as the flow rate decreased from 3.75 to 1.25 mL/min. This results in the increase of the adsorption performance of the column from 17 to 110 mg/kg and 4.2 to 22 mg/kg for VPum and VScO, respectively (Table 2.2). The increase in sorption efficiency at a low flow rate shows that the adsorbates have sufficient time to penetrate and diffuse deeply into the pores of the adsorbents; hence, intraparticle mass transfer controls the sorption process. This was also verified by MTZ (Table 2.2) or unused bed, which decreased with decreasing flow rate. In general, at the lower flow rate, the contact time between the adsorbent and the fluoride was higher, resulting in an increased breakthrough time and treated water volume for the continuous column adsorption system. A similar type of observation was reported by various authors for fixed-bed column systems (Aksu et al., 2007; Golie & Upadhyayula, 2016; Paudyal et al., 2013). In this study, the optimum and effective removal of fluoride takes place at a flow rate of 1.25 mL/min; so, all experiments other than the effect of flow rate were performed at a flow rate of 1.25 mL/min.

### 2.3.5. Application of the Thomas Model

The values of the Thomas model parameters,  $K_T$  and  $q_0$  for both adsorbents shown in Table 2.3 for different experimental parameters were found from the non-linear optimization techniques according to Equation (2.15). The non-linear plots of the experimental (designated as exp.) and simulated (designated as cal.) breakthrough curves based on the Thomas model for VPum (a) and VScO (b) at different particle sizes (Figure A2.1), influent pH (Figure A2.2), and influent volumetric flow rate (Figure A2.3) were provided in Supplementary Materials. The results of  $K_T$ ,  $q_0$ , and correlation

coefficient ( $R^2$ ) are shown in Table 2.3 for VPum and VScO. From the results, it can be seen that the values of  $R^2$  range from 0.897 to 0.993 for VPum and 0.901 to 0.973 for VScO.

**Table 2.3** Thomas model parameters for fluoride adsorption onto VPum and VScO

VPum	H (cm)	C <sub>o</sub> (mg/L)	Q (mL/min)	pH	P <sub>size</sub> (mm)	K <sub>T</sub> (L/min.mg) (x10 <sup>4</sup> )	q <sub>0</sub> (cal.) (mg/kg)	q <sub>e</sub> (exp.) (mg/kg)	R <sup>2</sup>
	10	10	1.25	2.00	< 0.075	2.199	48.6	59.6	0.950
	10	10	1.25	2.00	0.075–0.425	1.440	109.9	109.9	0.993
	10	10	1.25	2.00	0.425–2.00	1.840	57.9	67.9	0.897
	10	10	1.25	4.00	0.075–0.425	8.289	17.83	23.51	0.977
	10	10	1.25	6.00	0.075–0.425	12.099	13.08	14.81	0.995
	10	10	2.50	2.00	0.075–0.425	3.565	55.81	29.8	0.953
	10	10	3.75	2.00	0.075–0.425	5	45.82	16.9	0.962
VScO	H (cm)	C <sub>o</sub> (mg/L)	Q (mL/min)	pH	P <sub>size</sub> (mm)	K <sub>T</sub> (L/min.mg) (x10 <sup>4</sup> )	q <sub>0</sub> (cal.) (mg/kg)	q <sub>e</sub> (exp.) (mg/kg)	R <sup>2</sup>
	10	10	1.25	2.00	< 0.075	1.23	19	22	0.901
	10	10	1.25	2.00	0.075–0.425	2.213	13.4	12.4	0.931
	10	10	1.25	2.00	0.425–2.00	3.310	10.1	10.9	0.956
	10	10	1.25	4.00	< 0.075	10.140	7.06	8.2	0.973
	10	10	1.25	6.00	< 0.075	15.520	5.42	6.7	0.965
	10	10	2.50	2.00	< 0.075	5.263	13.3	7.5	0.929
	10	10	3.75	2.00	< 0.075	7.220	11.2	4.2	0.944

The high values of  $R^2$  indicate there were no significant disparities between the experimental data points and calculated data by the Thomas model for all particle sizes, influent solution pH, and influent volumetric flow rate. The observed differences between the experimental data and calculated data from the Thomas model may be due to the characteristic attribute weakness in the model. The Thomas model does not consider the external (film) and intra-particle diffusions in the adsorption system and, therefore, proposes adsorbate–adsorbent surface reactions to control the adsorption rate, hence the breakthrough. However, nearly all adsorption operations are typically not limited to surface reaction kinetics but are also controlled by external and/or intra-particle diffusion (Ghorai & Pant, 2005; Salifu, 2017). Thus, the perceived disparities in this study indicate external and/or intra-particle mass transfer may be the rate-controlling steps in fluoride adsorption in a fixed-bed column onto the adsorbents. Similar observations were drawn with the kinetic study of fluoride under fixed-bed conditions onto modified pumice (Salifu, 2017). As shown in Table 2.3, the value of the Thomas rate constant ( $K_T$ ) increased as the influent flow rate increased but the value of the maximum solid-phase concentration ( $q_0$ ) decreased. A related type of investigation on Thomas constants for different systems was reported by various authors (Han et al., 2007; Yagub et al., 2015).

### 2.3.6. Application of the Adams–Bohart Model

The parameter values of the Adams–Bohart model,  $K_{AB}$  and  $N_0$ , as depicted in Table 2.4 for VPum and VScO were similarly determined by non-linear regression analysis according to Equation (2.16).

**Table 2.4** Adams–Bohart model parameters for fluoride adsorption onto VPum and VScO

VPum	H (cm)	$C_0$ (mg/L)	Q (mL/min)	pH	$P_{size}$ (mm)	$K_{AB}$ (L/min.mg) ( $\times 10^4$ )	$N_0$ (mg/L)	$R^2$
	10	10	1.25	2.00	< 0.075	2.187	35.55	0.950
	10	10	1.25	2.00	0.075–0.425	1.439	56.85	0.993
	10	10	1.25	2.00	0.425–2.00	1.741	20.77	0.911
	10	10	1.25	4.00	0.075–0.425	8.289	9.22	0.995
	10	10	1.25	6.00	0.075–0.425	12.099	6.76	0.953
	10	10	2.50	2.00	0.075–0.425	3.565	29.68	0.962
	10	10	3.75	2.00	0.075–0.425	5.000	22.74	0.995
VScO	H(cm)	$C_0$ (mg/L)	Q (mL/min)	pH	$P_{size}$ (mm)	$K_{AB}$ (L/min.mg) ( $\times 10^4$ )	$N_0$ (mg/L)	$R^2$
	10	10	1.25	2.00	< 0.075	1.233	27.27	0.886
	10	10	1.25	2.00	0.075–0.425	2.213	17.68	0.886
	10	10	1.25	2.00	0.425–2.00	3.310	13.41	0.956
	10	10	1.25	4.00	< 0.075	10.145	10.13	0.969
	10	10	1.25	6.00	< 0.075	15.518	7.77	0.980
	10	10	2.50	2.00	< 0.075	5.263	19.72	0.929
	10	10	3.75	2.00	< 0.075	7.221	15.36	0.944

From the results presented in Table 2.4, it can be realized that the values of  $R^2$  range from 0.911 to 0.993 for VPum and 0.886 to 0.969 for VScO. The high values of  $R^2$  designate the applicability of the Adams–Bohart model for describing the entire sorption mechanisms of fluoride onto VPum and VScO under a continuous fixed-bed flow process.

In a similar fashion with the Thomas model, the comparison of the non-linear plots of the experimental and calculated breakthrough curve, based on the Adams–Bohart model, are generally in good agreement for VPum (a) and VScO (b) at different particle sizes (Figure A2.4), influent solution pH (Figure A2.5), and influent flow rate (Figure A2.6) respectively. Only minor disparities were noticed at lower pH (2.00) and particle sizes of 0.075–0.425 mm and < 0.075 mm for VPum and VScO, respectively. As seen in Table 2.4, the values of the kinetic constants were affected by the influent flow rate and increased with increasing flow rate. This presented that external mass transfer in the entire fluoride adsorption mechanisms in the fixed-bed column dominates the overall system kinetics (Quintelas et al., 2013; Salifu, 2017). In general, both the Adams–Bohart and the Thomas models could predict very well the entire region of the breakthrough curves for the fluoride-VScO and fluoride-VPum systems. In addition, both the Adams–Bohart model (Equation (2.16)) and the Thomas model



(Equation (2.15)) are mathematically the same and, therefore, gave similar fit quality.

### 2.3.7. Comparison of Different Adsorbents on Fluoride Removal

A comparison has been made between volcanic rocks (VPum and VSco) used in this study and previously reported adsorbents for fluoride removal in a fixed-bed column system. The results for some adsorbents are presented in Table 2.5.

**Table 2.5** Comparison of other adsorbents with VPum and VSco

Adsorbents	Surface area (m <sup>2</sup> g <sup>-1</sup> )	Bed depth (cm)	Fluoride in (mgL <sup>-1</sup> )	Adsorption capacity (mg F <sup>-</sup> g <sup>-1</sup> )	Adsorption capacity per surface area (mg.m <sup>-2</sup> )	References
Cement paste aluminum modified iron oxide	NA*	20	15	0.149	-	(Kang et al., 2007)
Acid-treated bentonite (GHB)	NA	10.5	4	0.139	-	(García-sánchez et al., 2013)
MnO <sub>2</sub> -coated Tamarind Fruit Shell	24.5	28	2.85	0.169	0.0069	(Ma et al., 2011)
kanuma mud	NA	6	2	0.883	-	(Sivasankar et al., 2010)
Activated alumina (Grade OA-25)	144.01	10	20	1.560	0.0108	(Chen et al., 2011)
VPum	250	10	5	0.74	0.0029	(Ghorai & Pant, 2004)
VSco	3.5	10	10	0.110	0.0314	This study
	2.49	10	10	0.022	0.0088	This study

NA\*: Not available.

As can be seen from these results in Table 2.5, the natural VPum used is comparable to cement paste and aluminum-modified iron oxide in terms of defluoridation capacity. Values of adsorption capacity per unit surface area are, however, higher for VPum than those of acid-treated bentonite (GHB), kanuma mud, and activated alumina; and higher for VSco than acid-treated bentonite (GHB) and activated alumina (Grade OA-25) (Table 2.5). Both adsorbents are available in abundance in all parts of the world and are readily available in approximately 1/3 of Ethiopia's total area and are, hence, favored adsorption materials because of very low supply costs. The adsorbents used are primarily part of the natural environment. However, to improve the specific surface area and hence the defluoridation capacity, surface modification of the natural volcanic rocks may be appropriate.

## 2.4. Conclusions

In this study, the removal of fluoride from aqueous solutions was examined in a continuous fixed-bed adsorption column system using VPum and VSco. The characterization investigations were performed using XRD, SEM, FTIR, BET, XRF, and ICP-OES equipment to reveal the mechanisms of adsorption and the suitability of the adsorbents for fluoride removal. The pH<sub>PZC</sub> is 6.98 for VSco and 6.85 for VPum. The effects of process parameters such as adsorbent particle size, influent pH, and influent

volumetric flow rate on the performance of the adsorption process in a column were evaluated. The maximum removal capacity of 110 mg/kg for VPum and 22 mg/kg for VScO were achieved at a particle size of 0.075–0.425 mm and < 0.075 mm, respectively, at a lower solution pH (2.00) and flow rate (1.25 mL/min). The increase in adsorbent particle size, solution pH, and flow rate decreases the breakthrough and saturation time of the column bed and, consequently, lowers the amount of fluoride removal by VScO. The breakthrough and exhaustion time on VPum was high at a particle size of 0.075–0.425 mm, at lower solution pH and flow rate similar to that of VScO. Thus, in order to attain optimum performance, suitable experimental parameters are significant for the operation of the adsorption column. The Thomas and Adams–Bohart models were applied to the experimental data to estimate the breakthrough curves and to determine fixed-bed column kinetic parameters. Both the Adam–Bohart and the Thomas models could predict very well the entire region of the breakthrough curves for the fluoride-VScO and fluoride-VPum system. The results show that VPum and VScO could be used in a fixed-bed adsorption column for the removal of excess fluoride from water. The supply cost of the two adsorbents is very low; nevertheless, an overall cost analysis of the purification system is very important as it has implications for the feasibility (technical and economic) of the adsorption method. Additional testing of the adsorbents including representative samples test for possible compositional, mineralogical, and textural changes in time due to weathering, leaching test, competitive ions effects, and regeneration options is required to confirm that the defluoridation of groundwater employing volcanic rocks is a safe and sustainable method.



### 3. Enhanced Defluoridation of Water Using Zirconium-Coated Pumice in Fixed-Bed Adsorption Columns

Wondwosen Sime Geleta <sup>1,2</sup>, Esayas Alemayehu <sup>3,4, \*</sup> and Bernd Lennartz <sup>2, \*</sup>

<sup>1</sup> School of Chemical Engineering, Jimma Institute of Technology, Jimma University, P.O. Box 378, Jimma, Oromia, Ethiopia

<sup>2</sup> Faculty of Agricultural and Environmental Sciences, University of Rostock, Justus-Von-Liebig-Weg 6, 18059 Rostock, Germany

<sup>3</sup> Faculty of Civil and Environmental Engineering, Jimma Institute of Technology, Jimma University, P.O. Box 378, Jimma, Oromia, Ethiopia

<sup>4</sup> Africa Center of Excellence for Water Management, Addis Ababa University, 1176 Addis Ababa, Ethiopia

\*Correspondence

**Materials (2021) 14: 6145**

**Abstract:** Millions of people across the globe suffer from health issues related to high fluoride levels in drinking water. The purpose of this study was to test modified pumice as an adsorbent for the purification of fluoride-containing waters. The adsorption of fluoride onto zirconium-coated pumice (Zr–Pu) adsorbent was examined in fixed-bed adsorption columns. The coating of zirconium on the surface of VPum was revealed by X-ray diffractometer (XRD), Inductively coupled plasma-optical emission spectroscopy (ICP-EOS), and X-ray fluorescence (XRF) techniques. The degree of surface modification with the enhanced porosity of Zr–Pu was evident from the recorded scanning electron microscope (SEM) micrographs. The Brunauer-Emmett-Teller (BET) analysis confirmed the enhancement of the specific surface area of VPum after modification. The Fourier transform infrared (FTIR) examinations of VPum and Zr–Pu before and after adsorption did not reveal any significant spectrum changes. The pH drift method showed that VPum and Zr–Pu have positive charges at pH<sub>HPZC</sub> lower than 7.3 and 6.5, respectively. Zr–Pu yielded a higher adsorption capacity of 225 mg/kg (2.05 times the adsorption capacity of VPum: 110 mg/kg), at pH = 2 and volumetric flow rate (QO) of 1.25 mL/min. Breakthrough time increases with decreasing pH and flow rate. The experimental adsorption data was well-matched by the Thomas and Adams-Bohart models with correlation coefficients (R<sup>2</sup>) of  $\geq 0.980$  (Zr–Pu) and  $\geq 0.897$  (VPum), confirming that both models are suitable tools to design fixed-bed column systems using volcanic rock materials. Overall, coating pumice with zirconium improved the defluoridation capacity of pumice; hence, a Zr–Pu-packed fixed-bed can be applied for the defluoridation of excess fluoride from groundwater. However, additional investigations on, for instance, the influences of competing ions are advisable to draw explicit conclusions.

**Keywords:** adsorption; defluoridation; fluoride; VPum; Zirconium-coated pumice

### 3.1. Introduction

Fluoride is among the many vital trace elements required in drinking water within the allowable range ( $< 1.5$  mg/L) (Fawell et al., 2006) for the normal growth of humans and animal bones. Nevertheless, it is detrimental to bone development when ingested beyond the acceptable concentration limit ( $> 1.5$  mg/L) (Tao et al., 2020). Excess fluoride hurts bones because of its high electronegative value, enabling interrelations with calcium in bones. Hence, it causes dental fluorosis and/or skeletal fluorosis (bone cancer) (Kumari et al., 2021). Alzheimer's syndrome, arthritis, thyroid, etc., are additional adverse consequences of excess fluoride in drinking water (Kumari et al., 2019).

In several places around the globe, groundwater is the principal and favored source of potable water, as is the case for many communities in rural and urban areas in the African rift valley. However, over 200 million people around the globe, including East Africa, ingest groundwater with high fluoride concentrations, which has a serious effect on people's welfare (Geleta et al., 2021b; Zhang et al., 2019). Fluorosis is the most prevalent geochemical disease in the East African Rift, affecting over 80 million people (Geleta et al., 2021b; Kut et al., 2016; Mohan et al., 2017a). Ethiopia is one of the East African countries with a large community residing where excess fluoride is becoming a significant concern, especially along the country's central Rift (Rango et al., 2017; Žáček et al., 2015). The dissolution of fluoride-containing minerals has intensified excessive fluoride in the Ethiopian Rift in parent rocks and soils, which is usually linked to high bicarbonate and low calcium levels (Demelash et al., 2019; Rango et al., 2010). Levels of fluoride in wells in Ethiopia's Rift are typically up to ten times higher than that of the WHO norm, putting millions of Ethiopians at risk of severe fluoride ion toxicity (Rango et al., 2017; Tekle-Haimanot et al., 2006). Similar to Ethiopia, countries like India, China, Pakistan, and others, deal with similar issues. Hence, excess fluoride in drinking water is among the most pressing issues the world faces today; therefore, valuable and easy-to-apply techniques to maintain fluoride concentrations within the allowable standard are urgently required.

Despite several fluoride removal methods, economic, procedural, and environmental disadvantages restrict their wide usage in many parts of the world. Although reverse osmosis (Bejaoui et al., 2014; Shen & Schäfer, 2014), ultrafiltration (Liu & Liu, 2016), electrodialysis (Majewska-Nowak et al., 2015), and ion exchange (Castel et al., 2000; Jamhour, 2005; Li et al., 2016) have good fluoride removal efficiency and are fairly steady, their operating costs are prohibitively high for developing countries like Ethiopia. The coagulation sedimentation methods (Gan et al., 2019; Huang et al., 2017; López-Guzmán et al., 2019; Zhai et al., 2013) are simple to use, low cost and simple to apply; nevertheless, the dosage is too high and cannot be regenerated, causing secondary pollution and difficulty reducing fluoride to permissible levels. Adsorption using low-cost and locally available

materials has been considered a highly efficient and well-accepted fluoride removal process by researchers of recent decades ([Banerjee, 2015](#); [Chaudhary et al., 2019](#); [Teng et al., 2009](#); [Zhou et al., 2019](#)).

Adsorbent materials investigated for fluoride removal are numerous ([Abu Bakar et al., 2019](#); [Cai et al., 2018](#); [Chatterjee et al., 2018](#); [Chaudhary et al., 2019](#); [Ghanbarian et al., 2020](#); [Raj & Raj, 2019](#); [Wan et al., 2019](#); [Zhang et al., 2016](#)). However, many of the materials suffer from either time-consuming synthesis procedures, high manufacturing costs, scarcity of raw materials, or a short lifetime, making them impractical to apply in remote regions of Africa. Subsequently, efforts have been made to acquire readily available, long-lasting, inexpensive, and effective materials that can be utilized to purify polluted water in low-income countries. Surface modification of locally available materials to treat fluoride-laden water is also under review since this could have a capacity for cost minimization and increasing sustainability.

Pumice (VPum) is among the most encouraging and low-priced naturally available materials that have been broadly examined and applied for pollutant removal in water treatment ([Aregu et al., 2018](#); [Asgari et al., 2012](#); [Geleta et al., 2021b](#); [Mekonnen et al., 2021a](#)). Owing to the release of gasses during solidification, VPum has a light color and porous configuration. Good removal capabilities, mechanical strength, and absence of toxicity are the major benefits of VPum over other natural or synthetic adsorbents ([Asgari et al., 2012](#)). Many nations, including Spain, Greece, Turkey, Ethiopia, and Eritrea, have plenty of pumice deposits ([Aregu et al., 2018](#); [Geleta et al., 2021b](#)). From the previous report, it is generally recognized that natural adsorbents modified with multivalent metal cations, such as  $\text{Fe}^{3+}$ ,  $\text{Mn}^{4+}$ , and  $\text{Zr}^{4+}$ , may change the surface properties and the affinity of fluoride ([He et al., 2019](#)). Among these, zirconium ( $\text{Zr}^{4+}$ ) is paid more attention due to its non-toxicity, high binding affinity with fluoride ions, and acceptable cost ([Chaudhry et al., 2017](#); [ZHOU et al., 2014](#)). Studies have found that surface-modified pumice might perform better as an adsorbent for water contaminants ([Dehghani et al., 2017](#); [Geleta et al., 2021a](#); [Sepehr et al., 2013b](#)). Hence, research into zirconium-based adsorbents with good performance should be considered.

With the above issues in mind, fixed-bed columns packed with zirconium (IV) oxychloride octahydrate ( $\text{ZrOCl}_2 \cdot 8\text{H}_2\text{O}$ ) coated pumice (abbreviated as Zr–Pu hereafter), which was not previously tested to treat fluoride-contaminated water, the objectives of the present study were to (1) compare the defluoridation capacity of Zr–Pu and VPum in a fixed-bed column mode; (2) investigate the effect of solution pH and flow rate on the fluoride adsorption process; and (3) describe and analyze the adsorption processes employing well-known fixed-bed adsorption kinetic models such as the Thomas and Adams-Bohart model.

## 3.2. Materials and Methods

### 3.2.1. Adsorbent Preparations

#### 3.2.1.1. Natural Pumice

The natural pumice (VPum) used in this work was gathered from volcanic cones of the Main Rift Valley area of Oromia Regional State, East Showa Zone, Ethiopia, around 50–100 km East of Addis Ababa (Figure 3.1). VPum was repeatedly washed to eliminate possible attachments and other water-soluble substances from its surface. The washed VPum was dried in an oven at a temperature of 70 °C for 48 h, and subsequently, it was separated into four different mesh size fractions, as indicated in (Geleta et al., 2021b; Liu & Evett, 2003).

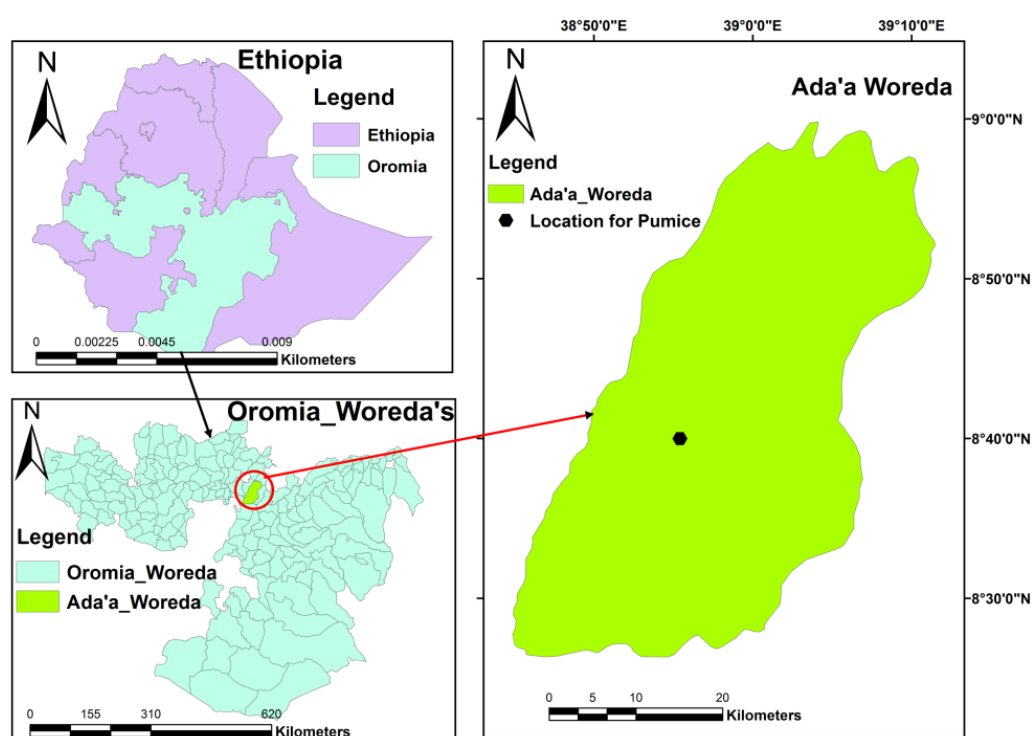


**Figure 3.1** The geographical location of natural pumice (VPum) sample collections

In our very recent study (Geleta et al., 2021b), VPum with a fine particle size (0.075–0.425 mm) revealed a good fluoride uptake performance compared to the other particle sizes. Hence, this fine particle size was used for coating with zirconium.

#### 3.2.1.2. Coating of VPum with Zirconium

The coating of VPum with zirconium was performed using 0.1 M  $\text{ZrOCl}_2 \cdot 8\text{H}_2\text{O}$  in accordance with the methods applied by Salifu et al. (2013), in which pumice was coated with aluminum (hydr) oxide. An adequate amount of  $\text{ZrOCl}_2 \cdot 8\text{H}_2\text{O}$  solution was added to completely soak the dried pumice in acid-washed cylindrical polyethylene wide-mouth plastic bottles. The mixture was shaken with a horizontal shaker (SM25, Edmund Bühler 7400 Tübinger, Germany) at 200 rpm for 12 h. The zirconium-coated

pumice (Zr–Pu) was decanted, dried in an electric oven at 70 °C for 48 h, and soaked in 2 M NH<sub>4</sub>OH. The Zr–Pu was washed repeatedly with deionized water, dried at 70 °C for 48 h, and stored in a plastic bag for subsequent experiment and characterization.

### 3.2.2. Chemicals and Reagents

All bottles and glassware were properly cleaned and rinsed with deionized water before use. All chemicals and reagents used in the experiments were of analytical quality. Zirconium oxychloride (IV) octahydrate (ZrOCl<sub>2</sub>·8H<sub>2</sub>O), ammonium hydroxide (NH<sub>4</sub>OH), sodium hydroxide (NaOH), and hydrochloric acid (HCl) were purchased from Merck KGaA, Darmstadt, Germany. A 1000 mg/L fluoride stock solution was made by dissolving 2.21 g of NaF in 1000 mL of deionized water and stored at 4 °C in a refrigerator. The synthetic solution for fixed-bed adsorption experiments was prepared by diluting the stock solution with deionized water to obtain the desired concentration. NaOH (0.1 M) and/or HCl (0.1 M) solutions were added to adjust the pH values of the fluoride solution.

### 3.2.3. Adsorbent Characterizations

#### 3.2.3.1. Crystalline Structure

The crystalline structure of VPum and Zr–Pu before and after the adsorption experiment was determined by an X-ray diffractometer (XRD-7000, Drawell, Shanghai, China) with Cu K $\alpha$  as a radiation source (1.54056 Å) generated at 30 kV using a 25mA instrument. The diffractogram was obtained with a step width of  $2\theta$  and a scan rate of 0.01°/min. The mineralogical buildup of the adsorbents was illustrated by contrasting the X-ray diffractogram with the database of the X'pert HighScore Plus software package (Version: 2.2b 2.2.2).

#### 3.2.3.2. Chemical Composition

The inductively coupled plasma-optical emission spectroscopy (ICP-OES) was employed to examine the elemental composition of the VPum and Zr–Pu. The oxide contents of VPum and Zr–Pu were analyzed by X-ray fluorescence (XRF) spectroscopy.

#### 3.2.3.3. Fourier Transform Infrared (FT-IR) Analysis

The Fourier Transform Infrared (FT-IR) analysis was run on KBr pellets to learn about the different functional groups of the samples. The spectra were recorded over a range of 5000 to 400 cm<sup>-1</sup> at a resolution of 0.1 cm<sup>-1</sup> in a PerkinElmer spectrometer (UNSW Sydney, Australia) using a lithium tantalite (LiTaO<sub>3</sub>) detector.

#### 3.2.3.4. Surface Area ( $S_{BET}$ ) and Pore-Size Distribution Analysis

The Brunauer-Emmett-Teller (BET) was used to analyze the surface area ( $S_{BET}$ ) of the adsorbents.

Barrett–Johner–Halenda (BJH) equation was used to determine the pore size distribution of the adsorbents.

#### 3.2.3.5. Scanning Electron Microscope (SEM) Analysis

A scanning electron microscope (SEM) (JCM-6000plus, Version 0.2, JEOL Ltd., Peabody, Massachusetts, USA), operated at 15 kV, was used to determine the morphologies of VPum, Zr–Pu before and after adsorption.

#### 3.2.3.6. pH and Point of Zero Charges ( $\text{pH}_{\text{PZC}}$ )

The pH of VPum, Zr–Pu before and after adsorption was determined using a pH meter in a 1:10 adsorbent/water ratio as per the standard method ([Appel & Ma, 2002](#); [Geleta et al., 2021b](#)). The point of zero charges ( $\text{pH}_{\text{PZC}}$ ) of the adsorbents was determined by the pH drift method ([Geleta et al., 2021b](#); [Newcombe et al., 1993](#)), using 0.01 M of NaCl solutions as an electrolyte and adding 0.1 M of NaOH or HCl solutions.

#### 3.2.3.7. Surface Acidity/Basicity Analysis

Boehm’s titration method ([Boehm, 1994](#)) was used to determine the surface acidity/ basicity of VPum and Zr–Pu. A dried adsorbent sample (0.1 g) was mixed with 50 mL of 0.05 M NaOH or 0.05 M HCl under the  $\text{N}_2$  atmosphere. The samples were shaken for 2 h and then filtered to remove the adsorbent. The excess base and acid were titrated with 0.05 M HCl and 0.05 M NaOH, respectively. The acidity and basicity of the surface were determined assuming that HCl and NaOH neutralize all basic groups and acidic groups, respectively.

#### 3.2.4. Fixed-Bed Column Adsorption Studies

The fluoride adsorption capacity of Zr–Pu for fluoride was evaluated by continuous up-flow column systems, as indicated in ([Geleta et al., 2021b](#)). A small-scale cylindrical filter column with an inner diameter of 8.1 cm and a height of 10 cm was used to conduct continuous up-flow adsorption experiments. A weighted amount of Zr–Pu was packed uniformly with care into the column as a fixed-bed absorber. One pore volume of deionized water was passed through the bed to avoid the potential occurrence of voids, channeling, or cracking. The fluoride solution as influent was pumped into the fixed-bed column in up-flow mode by a variable flow peristaltic pump (REGLO ICC, Ismatec, Cole-Parmer Barrington, IL, USA). All experiments were performed at a temperature of 298 K. An automatic fraction collector (RFI, MA-RON GmbH, Reichelt Chemietechnik GmbH + Co., Heidelberg, Germany) was used to collect effluent samples at the outlet of the column set-up. Ion chromatography (930 Compact IC Flex, Metrohm, Herisau, Switzerland) was employed to measure

the concentration of fluoride in the effluent samples. The desired breakthrough concentration ( $C_b$ ) was considered to be 1.5 mg/L (WHO, 2011). The exhaustion point was characterized as the point at which the fluoride concentration in the effluent was equal to 90% of the fluoride concentration in the influent (i.e.,  $0.9 C_t/C_0$ ).

The influence of experimental variables such as the pH of the feed solution (2, 4, and 6) and influent volumetric flow rate (1.25, 2.50, and 3.75 mL/min) on the shape of the breakthrough curves and amount of fluoride removed by Zr–Pu were tested at a constant fixed-bed column height of 10 cm and an initial fluoride concentration of 10 mg/L. The defluoridation performance of Zr–Pu was compared with the performance of VPum presented in our very recent study (Geleta et al., 2021b). The plots of experimental breakthrough curves were displayed only for Zr–Pu.

### 3.2.5. Analysis of Column Data

The shape of the breakthrough curve is an essential feature for describing the adsorption capacity of the adsorbent in a flow-through column. The breakthrough curves and breakthrough time ( $t_b$ ) are the characteristic features resulting from the adsorption dynamics and process design of the packed-bed column. These two parameters have a significant effect on the feasibility and economics of the adsorption process (Geleta et al., 2021b; Golie & Upadhyayula, 2016). The breakthrough parameters are influenced by the experimental conditions of the experiment, such as the initial flow rate and pH of the influent solution. The breakthrough curve is stated as the ratio of effluent to influent fluoride concentrations ( $C_t/C_0$ ) as a function of time. The exhaustion or saturation time and the breakthrough time are expressed by Equations (3.1) and (3.2), respectively.

$$t_e = \int_{t=0}^{t=t_{\text{total}}} \left(1 - \frac{C_t}{C_0}\right) dt \quad (3.1)$$

$$t_b = \int_{t=0}^{t_b} \left(1 - \frac{C_t}{C_0}\right) dt \quad (3.2)$$

where,  $t_e$  is the saturation time (min), and  $t_b$  is the breakthrough time (min) at which  $C_t = C_b$  (mg/L) (for the current system,  $C_b = 1.5$  mg/L).

The total amount of fluoride adsorbed ( $q_{\text{total}}$ : mg) in the column for a given feed concentration ( $C_t$ ), and initial flow rate ( $Q$ ) can be obtained from Equation (3.3) (Han et al., 2009).

$$q_{\text{total}} = \frac{QA}{1000} = \frac{Q \times C_0}{1000} \int_{t=0}^{t=t_{\text{total}}} \left(1 - \frac{C_t}{C_0}\right) dt \quad (3.3)$$

where  $Q$  (mL/min) is the volumetric flow rate, and 'A' is the area under the breakthrough curve.

The equilibrium fluoride uptake capacity ( $q_e$ : mg kg<sup>-1</sup>) of the packed-bed column is determined by dividing the total amount of fluoride adsorbed ( $q_{total}$ ) by the amount of dry mass of the adsorbent used ( $m$ ), Equation (3.4).

$$q_{eq} = \frac{q_{total}}{m} = \frac{C_o Q t_e}{m} \quad (3.4)$$

The experimental uptake capacity or amount of fluoride removed at  $t_b$  ( $q_b$ : mg kg<sup>-1</sup>) can be calculated from Equation (3.5).

$$q_b = \frac{C_o Q t_b}{m} \quad (3.5)$$

The volume of effluent ( $V_e$ ) and the volume of treated effluent or breakthrough volume ( $V_b$ ) of solution can be calculated from Equations (3.6) and (3.7), respectively.

$$V_e = Q t_e \quad (3.6)$$

$$V_b = Q t_b \quad (3.7)$$

where  $V_e$  is the total volume of the effluent until exhaustion/saturation time (mL) and  $V_b$  is the total volume of the effluent until the breakthrough time (mL).

The Mass Transfer Zone (MTZ) or unused bed length ( $H_{UNB}$ ) can be obtained from Equation (3.8) ([Futalan et al., 2020](#)).

$$MTZ = H_T \left( \frac{t_e - t_b}{t_e} \right) \quad (3.8)$$

where  $H_T$  is total bed height (cm),  $t_e$  (min) is exhaustion time, and  $t_b$  is breakthrough time (min).

The Empty Bed Contact Time (EBCT) is defined as the time of contact between the adsorbent and the adsorbate solution, which can be evaluated from Equation (3.9).

$$EBCT = \frac{V_B}{Q} \quad (3.9)$$

where  $V_B$  (mL) and  $Q$  (mL/min) designate the bed volume and the influent flow rate, respectively.

### 3.2.6. Breakthrough Curve Modeling

Before upscaling the study to a manufacturing application, the column data should be validated with



theoretical modeling. Different kinetic models have been tested for estimating the breakthrough performance of fixed-bed column adsorption systems (Adeyi et al., 2020; Chittoo & Sutherland, 2020). Besides, these kinetic models have been employed to evaluate the kinetic column parameters and uptake capacity of the column. In this work, to describe the dynamic behavior of fluoride adsorption using Zr–Pu in a fixed-bed column filter, the two most important and widely used mathematical models, the Thomas model and the Adams-Bohart model, were applied to the experimental data. The acquired model parameters for the defluoridation of water were compared with the Thomas model and Adams-Bohart model parameters obtained for the defluoridation of water onto VPum from our recent work (Geleta et al., 2021b).

#### 3.2.6.1. Thomas Model

The Thomas model is among the most common and highly employed dynamic models in a fixed-bed column performance operation. The model assumes that the process obeys Langmuir kinetics of adsorption-desorption with no axial dispersion, and the driving force obeys second-order reversible reaction kinetics (Thomas, 1944).

The Thomas model can be used to determine the maximum uptake of adsorbate and adsorption rate constants for the continuous adsorption process (Thomas, 1944). The non-linear form of the Thomas model is given by Equation (3.10).

$$\frac{C_t}{C_o} = \frac{1}{1 + \exp \left[ K_T q_o \frac{m}{Q} - K_T C_o t \right]} \quad (3.10)$$

where  $K_T$  is the Thomas rate constant (L/min mg),  $C_o$  (mg/L) is the inlet or initial concentration,  $C_t$  (mg/L) is the effluent fluoride concentration at the time,  $t$ ,  $Q$  (L/min) is the flow rate,  $q_o$  (mg/kg) is the equilibrium adsorbate uptake, and  $m$  (kg) is the amount of adsorbent (dry mass) in a fixed-bed.

#### 3.2.6.2. Adams-Bohart Model

The Adams–Bohart model (Bohart & Adams, 1920) was developed to analyze the dynamics of fixed-bed systems. It is based on the hypothesis that the adsorption rate is related to both the residual adsorbent and adsorbate concentration. For the estimation of breakthrough curves and model parameters, the non-linear form of the Adams–Bohart model (Equation (3.11)) (Chu, 2020) was applied.

$$\frac{C_t}{C_o} = \frac{1}{1 + \exp \left[ K_{AB} N_o \frac{Z}{v} - K_{AB} C_o t \right]} \quad (3.11)$$

where  $K_{AB}$  (L/mg. min) is the kinetic constant,  $v$  (mL/min) is the linear flow rate,  $Z$  (cm) is a column bed depth,  $N_0$  (mg/L) is the saturation concentration, and time  $t$  (min) ranges from the start to breakthrough points for fluoride. The linear flow rate (superficial velocity) was determined by Equation (3.12).

$$v = \frac{Q}{A} \quad (3.12)$$

where  $A$  is the cross-sectional area of the fixed-bed ( $\text{cm}^2$ ), and  $Q$  is the volumetric flow rate (mL/min).

The root-mean-squared error (RMSE) (Equation (3.13)) was used to measure the differences between the results predicted by the models and experimental data.

$$\text{RMSE} = \sqrt{\frac{1}{N} \sum_{i=1}^N (\text{predicted value} - \text{experimental value})^2} \quad (3.13)$$

where  $N$  is the number of data points.

### 3.3. Results and Discussions

#### 3.3.1. Characterization of Adsorbents

##### 3.3.1.1. Crystalline Structure

The crystalline structure of VPum and Zr–Pu before and after adsorption was explored by X-ray diffraction (XRD), as presented in Figure 3.2. The results showed that the dominant crystalline phases of VPum are silicon oxide ( $\text{SiO}_2$ ), Albite, calcian, low ( $(\text{Na}_{0.75}\text{Ca}_{0.25})(\text{Al}_{1.26}\text{Si}_{2.74}\text{O}_8)$ ), and Anorthite, Ordered ( $\text{CaAl}_2\text{Si}_2\text{O}_8$ ). Lemoyne ( $\text{Na}_2\text{CaZr}_2\text{Si}_{10}\text{O}_{26}(\text{H}_2\text{O})$ ), Baddeleyite ( $\text{ZrO}_2$ ), and Anorthite, Ordered ( $\text{CaAl}_2\text{Si}_2\text{O}_8$ ) are the main crystalline components of Zr–Pu before adsorption, while quartz ( $\text{SiO}_2$ ), Labradorite ( $\text{Na}_5\text{Ca}_5\text{Al}_{1.5}\text{Si}_{2.5}\text{O}_8$ ), and Oxonium Zirconium Fluoride Hydrate ( $\text{ZrF}_3\text{H}_3\text{O}(\text{H}_2\text{O})_2$ ) were the dominant components of Zr–Pu after adsorption. The existence of crystalline phases in VPum (Figure 3.2a) can be deduced from the peaks at  $2\theta = 13.88^\circ$ ,  $25.32^\circ$ ,  $28.12^\circ$ ,  $31.83^\circ$ ,  $35.30^\circ$ ,  $42.34^\circ$ , and  $42.34^\circ$ . The XRD patterns of Zr–Pu before adsorption (Figure 3.2b) showed peaks at  $2\theta = 13.99^\circ$ ,  $25.39^\circ$ ,  $27.99^\circ$ , and  $30.38^\circ$ ; while the peaks at  $2\theta = 13.96^\circ$ ,  $25.22^\circ$ ,  $27.94^\circ$ ,  $30.19^\circ$ ,  $42.36^\circ$ ,  $57.53^\circ$ , and  $62.48^\circ$  were observed for Zr–Pu after adsorption (Figure 3.2c). VPum (Figure 3.2a) had a main peak at  $28.12^\circ$  ( $2\theta$ ), which had the highest intensity corresponding to  $\text{SiO}_2$  (peak B). Zr–Pu before adsorption (Figure 3.2b) had a main peak at  $2\theta = 27.99^\circ$ , corresponding to  $\text{ZrO}_2$  (peak C) formed at the surface; while Zr–Pu after adsorption (Figure 3.2c) had a major peak at  $27.95^\circ$  ( $2\theta$ ), corresponding to  $\text{Na}_5\text{Ca}_5\text{Al}_{1.5}\text{Si}_{2.5}\text{O}_8$  (peak C). It is also worth noting that, in Figure

3.2b, the peaks of lower intensity observed in VPum at 35.30°, 42.34°, and 42.34° were almost undetectable in the XRD technique after the modification. This could be due to the growth of zirconium oxide over the surface (Chaudhary et al., 2019). Furthermore, some small peaks were detected after fluoride adsorption (Figure 3.2c). This could be because of a slight change in the structural framework of the adsorbent.

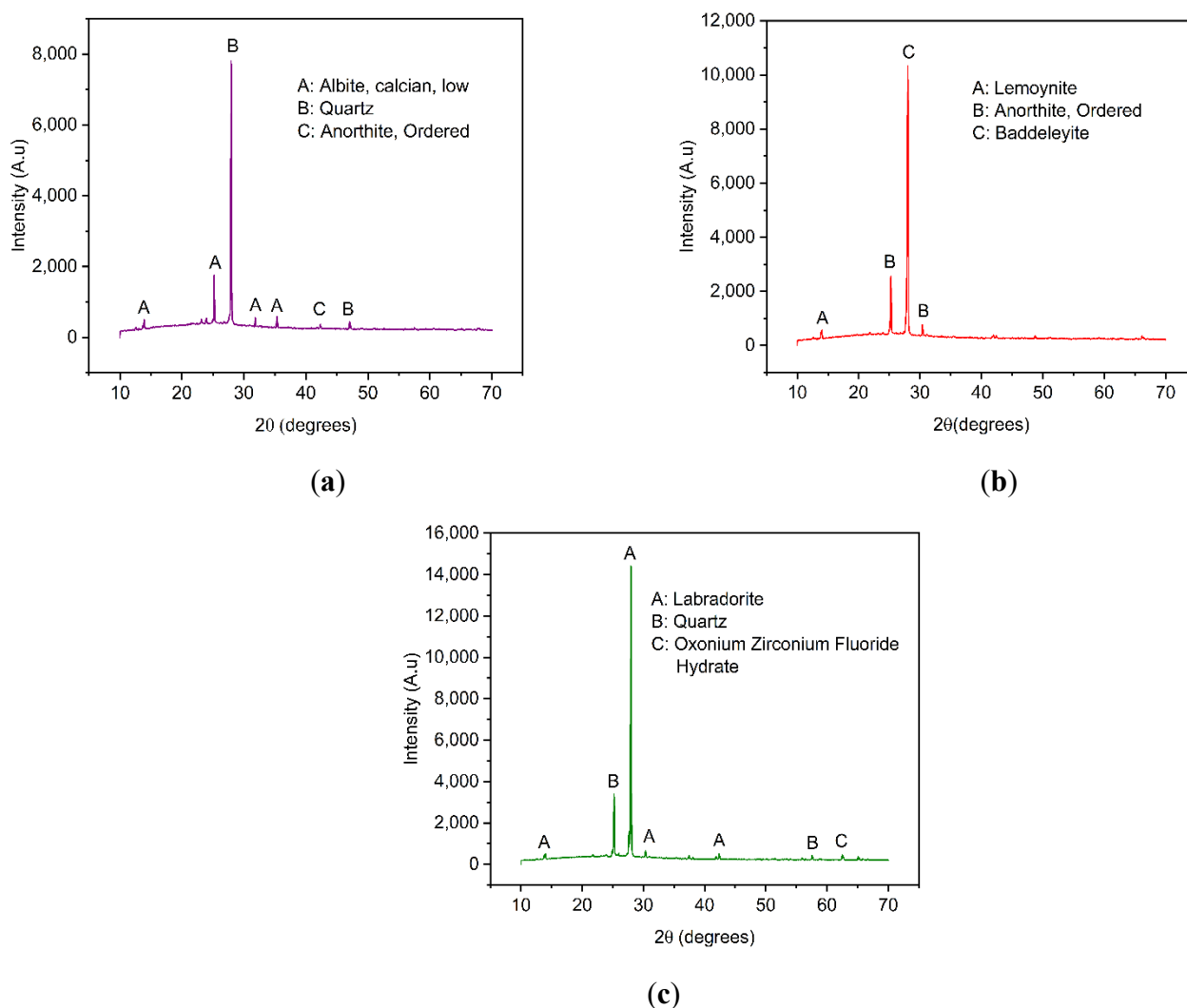


**Figure 3.2** XRD patterns for (a) VPum and Zirconium-coated pumice (Zr-Pu) (b) before and (c) after adsorption

### 3.3.1.2. Chemical Composition

The chemical analysis revealed that the major elements in VPum were Si, Al, K, and Fe (Table 3.1). Other elements were available in limited fractions or were below the instrument's detection limit.

Through XRF measurement, the main components of VPum are oxides of Si, Fe, K, and Al. A previous study has reported comparable values for natural pumice (Alemayehu & Lennartz, 2009).

The average amount of zirconium coated onto VPum was 3.9 % (wt). The XRF measurement

designated that 8.9 % (wt) (Table 3.1) of zirconium oxide was coated on VPum, enabling it to enhance its fluoride removal capacity.

**Table 3.1** Elemental and oxide compositions of natural pumice (VPum) and Zr–Pu

Elemental Content	VPum % (wt)	Zr–Pu % (wt)	Oxide Content	VPum% (wt)	Zr–Pu % (wt)
Si	27.1	26.3	SiO <sub>2</sub>	68.9	63.7
Al	5.3	5.5	Al <sub>2</sub> O <sub>3</sub>	11.7	10.9
Fe	3.4	3.1	Fe <sub>2</sub> O <sub>3</sub>	6.7	5.4
K	3.8	3.4	K <sub>2</sub> O	5.5	4.3
Ca	0.3	0.4	CaO	1.1	0.2
Na	1.2	1.0	Na <sub>2</sub> O	1.9	2.1
Mg	0.1	0.1	MgO	0.1	-
Zn	< 0.1	< 0.1	TiO <sub>2</sub>	0.2	-
Zr	< 0.1	3.9	ZrO <sub>2</sub>	-	8.9
Mn	< 0.1	< 0.1	MnO	0.1	0.2
Cr	< 0.1	< 0.1	ZnO	1.2	-
Cu	< 0.1	< 0.1	NiO	1.1	2.2
Co	< 0.1	< 0.1	CuO	1.6	1.7
Cd	< 0.1	< 0.1	-	-	-
Ni	< 0.1	< 0.1	-	-	-
Pb	< 0.1	< 0.1	-	-	-
As	< 0.1	< 0.1	-	-	-

### 3.3.1.3. Fourier Transform Infrared (FTIR) Analysis

The FTIR spectrums of VPum, Zr–Pu before adsorption and after adsorption at wavelengths between 400 cm<sup>-1</sup> and 5000 cm<sup>-1</sup> are shown in Figures 3.3a–c, respectively. Because of the Si-O-Si symmetric stretching vibration, the absorption band at ~1033 cm<sup>-1</sup> can be attributed to the (SiO<sub>4</sub>)<sup>2-</sup> groups. The peaks at ~775.75 and ~723.75 cm<sup>-1</sup> belong to the stretching and bending vibrations of the Si-O groups. Some peaks, like the broadening peak at ~3579.75 cm<sup>-1</sup> that belongs to the asymmetric stretching vibration of the H-O bond, can be allocated to adsorbed water molecules, and the peak at ~1640.75 cm<sup>-1</sup> can be allotted to the bending vibration of the H-O-H bond. In general, the IR spectrum of the natural pumice, Zr–Pu, before and after adsorption appeared approximately similar and consistent with those reported in previous studies (Li et al., 2010; Sepehr et al., 2014).

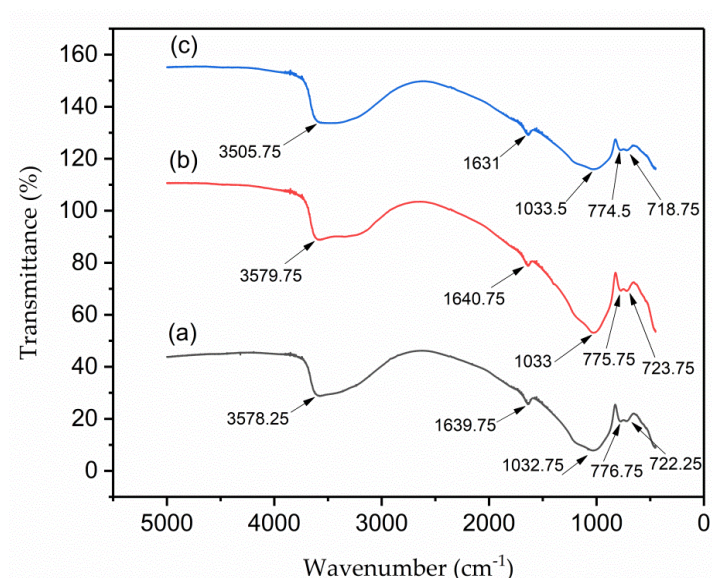


**Figure 3.3** Fourier–transform infrared (FT–IR) for (a) VPum; Zr–Pu (b) before and (c) after adsorption

#### 3.3.1.4. Surface Area ( $S_{\text{BET}}$ ) and Pore-Size Distribution Analysis

The BET specific surface area ( $S_{\text{BET}}$ ) of VPum and Zr–Pu was 3.45 and 9.63 ( $\text{m}^2/\text{g}$ ), respectively. It was observed that coating with zirconium enhanced the specific surface area of VPum (Table 3.2). A similar observation was made in the removal of pollutants using cerium-loaded pumice (Asere et al., 2017a). Based on the BJH method, the calculated pore size distribution resulted in an average pore size of 4.43 nm for VPum and 3.52 nm for Zr–Pu. This result showed that the adsorbents are a mesopore material by the IUPAC classification. As can be observed from Table 3.2, the pore size of VPum was changed after modification. The change in pore size reveals that zirconium oxide reached the internal pore. The ionic radius of fluoride is 0.133 nm, which is much smaller than the average pore size of VPum and Zr–Pu, confirming that the fluoride ions can easily penetrate the inner layers of the adsorbents.

**Table 3.2** Textural properties of VPum and Zr–Pu

Adsorbent	Specific Surface Area ( $\text{m}^2/\text{g}$ )	Average Pore Size (nm)
VPum	3.45	4.43
Zr–Pu	9.63	3.52

#### 3.3.1.5. Scanning Electron Microscope (SEM) Analysis

Scanning Electron Microscope analysis displayed the morphology of VPum and Zr–Pu before and after adsorption (Figure 3.4a–c). Figure 3.4a shows that VPum had an irregular texture with a rough surface and some pores. As seen from the SEM images of Zr–Pu before (Figure 3.4b) and after (Figure 3.4c) adsorption, the surface of the VPum was changed. The surface of Zr–Pu became dense, and

channels/pores can be noticed. The dense surface was attributed to the exterior surface of VPum, which was coated with zirconium. At the same time, the formation of pores originated from further removal of water-soluble compounds and dust by washing it repeatedly with deionized water. The improvements of the porous structure and adsorption for surface modification of pumice and salt treatment of zeolite were reported by Sepehr et al. (2013b) and Liang and Ni (2009), respectively. As seen from Zr–Pu’s micrographs after adsorption (Figure 3.4c), the pore morphology was altered, which produced a large but limited number of heterogeneous channels. This could elucidate the slight reduction in particle structure of VPum during modification and adsorption processes. Similar remarks were also drawn in a previous study (Liang & Ni, 2009).

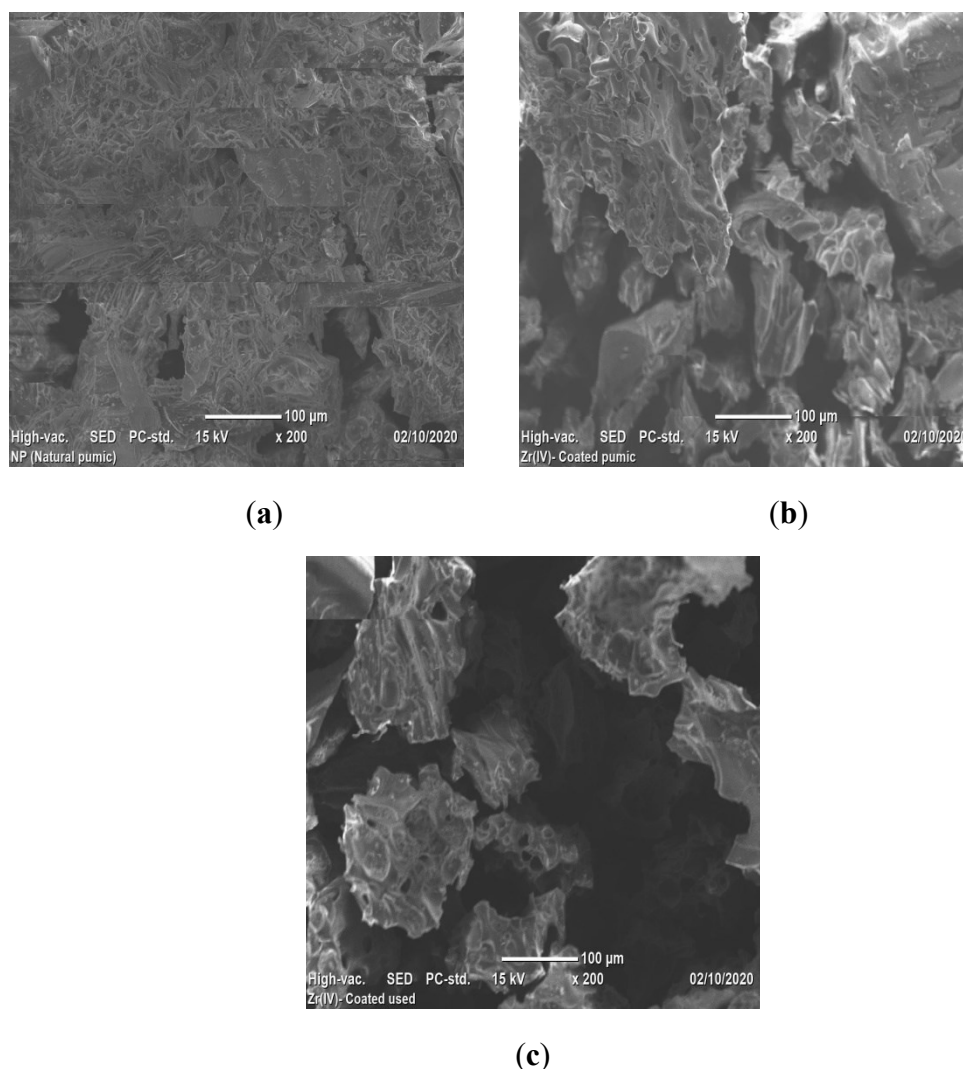


**Figure 3.4** SEM micrographs of (a) VPum; Zr– Pu (b) before and after (c) adsorption.

#### 3.3.1.6. pH and Point of Zero Charges ( $\text{pH}_{\text{PZC}}$ )

The pH in water and  $\text{pH}_{\text{PZC}}$  of VPum were found to be 8.8 and 7.3, respectively. These pH values are very close to values reported previously for VPum (Geleta et al., 2021b). The pH in water and  $\text{pH}_{\text{PZC}}$  for Zr–Pu were identified as 7.7 and 6.5, respectively. In the current study, both the pH in water and

the  $\text{pH}_{\text{PZC}}$  of Zr–Pu were found to be lower than that of VPum. A similar observation was reported for chitosan-pumice blends (Asere et al., 2017b). The adsorbent's surface charge was positive when the pH of the solution was below  $\text{pH}_{\text{PZC}}$  ((Zr)–Pu (6.5), VPum (7.3)). When the pH is lower than  $\text{pH}_{\text{PZC}}$ , fluoride can be adsorbed onto the surface of the adsorbents due to coulombic attraction (Ayoob & Gupta, 2009; Geleta et al., 2021b).

#### 3.3.1.7. Surface Acidity/Basicity Analysis

The acid-base character of VPum and Zr–Pu was obtained from Boehm's titration method. Acidity values of 0.805 and 0.875 (mmol/g) and basicity of 0.305 and 0.325 (mmol/g) were obtained for VPum and Zr–Pu, respectively. The notable observation is that VPum exhibits relatively lower acidity and basicity characteristics than Zr–Pu.

#### 3.3.2. Effect of Experimental Conditions on Fluoride Removal

##### 3.3.2.1. Initial Solution pH

The variation in defluoridation capacity of the adsorbents with respect to pH was evaluated at various pH values (2, 4, and 6) by a separate set of fixed-bed adsorption columns. The fluoride breakthrough curves obtained for Zr–Pu are presented in Figure 3.5 for a fixed inlet flow rate of 1.25 mL/min, influent fluoride concentration of 10 mg/L, and column bed depth of 10 cm. Sharper and earlier breakthrough curves emerged as the pH was raised from 2 to 6 (Figure 3.5).

The column adsorption parameters obtained for the uptake of fluoride onto Zr–Pu, and VPum are presented in Table 3.3. Reduced mass transfer zone values were found at a low pH level (pH 2), resulting in longer breakthrough and exhaustion times. Furthermore, a lower solution pH (pH 2) improved column performances, increased treated water volume, improved defluoridation efficacy, and enhanced adsorption capability at breakthrough and exhaustion time. The highest fluoride uptake capacity was 225 mg/kg by Zr–Pu, whereas the fluoride uptake was 110 mg/kg by VPum. This showed Zr–Pu removed 2.05 times fluoride compared to the VPum. The breakthrough capacity of Zr–Pu was 163 mg/kg (3.02 times that of VPum (54 mg/kg)). A breakthrough time of 3471 min for Zr–Pu and 1206 min for VPum; and an exhaustion time of 4781 min for Zr–Pu and 2339 min for VPum were achieved at a pH of 2. Hence, VPum has the quickest time to breakthrough and exhaustion, while Zr–Pu had the longest time to breakthrough and exhaustion and a better adsorption capacity. When the initial pH values of the solution were greater than two, the fluoride removal rate for Zr–Pu, and VPum decreased (Table 3.3). At pH values of four and six, the decrease in the fluoride uptake may be ascribed to the decrease in the amount of  $\text{H}^+$  or HF adsorption because of electrostatic attraction (Geleta et al., 2021b; Shang et al., 2019). The higher uptake capacity at pH 2 could be attributed to the fact that the



adsorbent surface has more positive charges at lower pH and electrostatically adsorbs fluoride ions (Shang et al., 2019). Hence, the adsorption of fluoride ions was due to an electrostatic phenomenon and surface complexation, which can occur alone or in combination with the fluoride ion's uptake on the adsorbents. In general, Zr–Pu, and VPum showed similar pH-dependent fluoride uptake performances. However, a noticeable performance enhancement was seen due to the zirconium coating, primarily because of the specific interaction between fluoride ions and zirconium (hydr) oxide. A similar observation was made in the removal of pollutants using cerium-loaded volcanic rocks (Asere et al., 2017a).

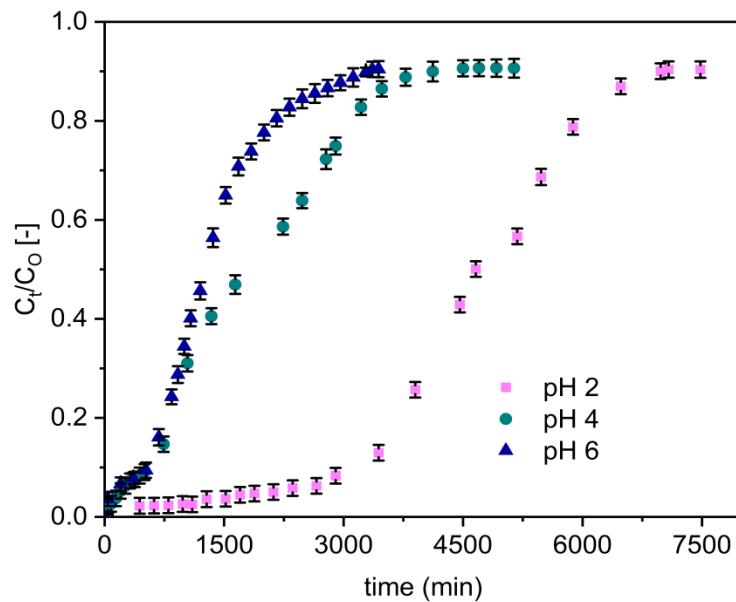


**Figure 3.5** Effect of solution pH on the breakthrough performance of fluoride onto Zr–Pu (initial fluoride concentration 10 mg/L ( $C_0$ : 10 mg/L); initial flow rate 1.25 mL/min ( $Q_0$ : 1.25 mL/min); bed depth 10 cm)

The breakthrough time was longer, and the volume of treated water was high at pH 2 for Zr–Pu. Accordingly, the pH of the solution was maintained at pH 2 in the subsequent experiment.

**Table 3.3** Fixed-bed column parameters obtained for defluoridation by zirconium–coated pumice (Zr–Pu) and on VPum (recent study) (Geleta et al., 2021b)

Parameter Studied	pH	$C_0$ (mg/L)	$Q_0$ (mL/min)	EBCT (min)	$t_b$ (min)	$t_e$ (min)	$V_b$ (mL)	$V_e$ (mL)	MTZ (cm)	$q_b$ (mg/kg)	$q_{tot}$ (mg)	$q_e$ (mg/kg)	Adsorbent
Variation of pH keeping $C_0$ and $Q_0$ constant	2	10	1.25	412	3471	4781	4338.94	5976.76	2.74	163.18	59.78	224.78	Zr–Pu
	4	10	1.25	412	689	2058	861.25	2572.50	6.65	32.39	25.73	96.75	
	6	10	1.25	412	604	1469	755.00	1836.25	5.89	28.39	18.36	69.06	
	2	10	1.25	412	1206	2339	1507.50	2923.70	4.84	54.20	29.24	110.00	VPum
	4	10	1.25	412	278	500	347.50	625.00	4.44	13.00	6.25	23.51	
	6	10	1.25	412	135	315	168.75	393.75	5.71	6.40	3.94	14.81	



	2	10	1.25	412	3471	4781	4338.94	5976.76	2.74	163.18	59.78	224.78	
	2	10	2.50	206	1807	1360	2717.50	3400.00	2.00	102.20	34.00	127.87	Zr–Pu
Variation of $Q_0$ keeping pH and $C_0$ constant	2	10	3.75	137	557	768	2088.75	2880.00	2.75	78.55	28.80	108.31	
	2	10	1.25	412	1206	2339	1507.50	2923.70	4.84	54.20	29.24	110.00	
	2	10	2.50	206	215	634	538.47	1585.16	6.60	20.30	7.93	29.80	VPum
	2	10	3.75	137	75	359	282.69	1346.42	7.90	7.10	4.49	16.89	

$t_b$  = breakthrough time,  $t_e$  = exhaustion time,  $V_b$  = total effluent volume at a breakthrough time,  $V_e$  = total effluent volume at exhaustion time MTZ = Mass Transfer Zone, EBCT = Empty Bed Contact Time,  $q_b$  = amount of fluoride removed at a breakthrough time per kg of adsorbent,  $q_{total}$  = total amount of fluoride adsorbed from the column,  $q_e$  = equilibrium fluoride uptake per kg of the adsorbent.

### 3.3.2.2. Flow Rate

Figure 6 presents the effect of various flow rates (1.25, 2.50, and 3.75 mL/min) on the fluoride breakthrough curves of Zr–Pu. When the flow rate increased from 1.25 to 3.75 mL/min, the breakthrough curves became steeper and occurred earlier (Figure 3.6). The breakthrough data displayed in Table 3.3 also confirmed that the flow rate rose from 1.25 to 3.75 mL/min resulted in the reduction of breakthrough time from 3471 to 557 min for Zr–Pu and from 1206 to 75 min for VPum. The exhaustion time also reduced from 4781 to 768 min and from 2339 to 359 min, Zr–Pu and VPum, respectively. At higher flow rates (higher hydraulic loading), the solution residence period in the column was shorter, hence less contact time between the adsorbate and adsorbent. The adsorbate ions exited the column before the equilibrium adsorption was reached, resulting in limited fluoride ion uptake. This assertion was backed up by MTZ (Table 3.3), which increases with increasing flow rate but narrows the utilized fractional bed (Lin et al., 2017). Thus, the column's maximum defluoridation capacity ( $q_e$ ) decreased from 225 to 108 mg/kg for Zr–Pu and 110 to 17 mg/kg for VPum with the rise in flow rate from 1.25 to 3.75 mL/min. Similarly, the defluoridation capacity at breakthrough time ( $q_b$ ) was reduced from 163 to 79 mg/kg for Zr–Pu and 54 to 7 mg/kg for VPum as the flow rate increased from 1.25 to 3.75 mL/min. The reduction in Empty Bed Contact Time (EBCT) values can also be observed in Table 3.3. Similar observations were made in other studies (Abdolali et al., 2017; Zhang et al., 2019). High flow rates reduced the contact time between the fluoride ions and the adsorbent surface, less fluoride was adsorbed, and the overall adsorption performance decreased. Although the influence of initial flow rate was similar for both Zr–Pu, and VPum, the zirconium coating resulted in a generally enhanced uptake of fluoride.

The best column performance was seen at the lowest flow rate (1.25 mL/min); consequently, all experiments except for the effect of flow rate were done at a flow rate of 1.25 mL/min.

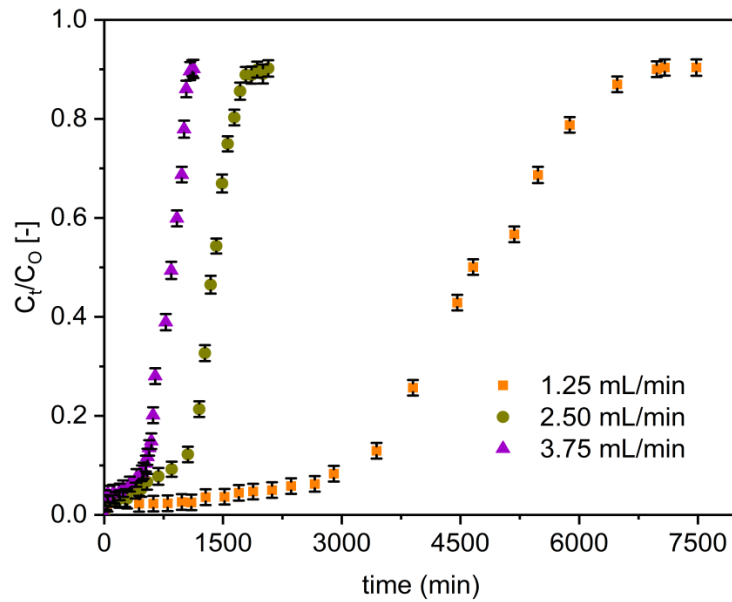


**Figure 3.6** Effect of initial flow rate on the breakthrough performance of fluoride onto Zr–Pu (pH 2;  $C_0$ : 10 mg/L; bed depth 10 cm)

Overall, the variation of column parameters, such as  $q_e$ ,  $q_b$ ,  $V_e$ , and  $V_b$ , obtained for fluoride removal onto Zr–Pu and VPum at experimental parameters showed that Zr–Pu has more activity than VPum towards fluoride (Table 3.3). The coating of natural pumice with zirconium could account for the improved activity and, hence, adsorption capacity.

### 3.3.3. Application of the Thomas Model

The Thomas model (Equation (3.10)) was fitted non-linearly to the experimental data (designated as exp.) for Zr–Pu at various initial pH values (Figure 3.7a) and initial flow rates (Figure 3.7b). For VPum, the according figures are not shown in this study but were reported previously (Geleta et al., 2021b). The Thomas model parameter values for the uptake of fluoride onto Zr–Pu, and VPum are summarized in Table 3.4. The slope and intercept data were used to evaluate the values of  $K_T$  and  $q_0$  for Zr–Pu and VPum. As the flow rates increased, the values of  $K_T$  increased, while the values of  $q_0$  decreased, implying that the Empty Bed Contact Time (EBCT) decreased. A decrease in  $q_0$  with increased flow rates resulted from a reduced interaction time among fluoride ions and adsorption sites (Ghosh et al., 2015; Ghosh et al., 2014b). As can be seen from Table 3.4, both adsorbents exhibited good adsorption capacity at pH 2, where  $K_T$  has the lowest value with 1.110 (L/min.mg) ( $\times 10^4$ ) for Zr–Pu and 1.44 (L/min.mg) ( $\times 10^4$ ) for VPum. The  $K_T$  value of Zr–Pu is smaller than that of VPum, revealing that the diffusion mass transfer is greater for Zr–Pu than VPum (Sivasankar et al., 2010). Nevertheless, the column adsorption capacity ( $q_0$ ) decreased from 226 to 64 (mg/kg) for Zr–Pu and from 110 to 13 (mg/kg) for VPum as the pH value increased from 2 to 6 while the other conditions were kept constant (Table 3.4). Overall, the Thomas model adequately represented the breakthrough

data for defluoridation by both adsorbents at various experimental conditions as indicated by the  $R^2$  values (Zr–Pu: 0.980–0.995; and VPum: 0.953–0.995). The values obtained by the Thomas model optimization confirmed that the zirconium coating enhanced the fluoride uptake capacity.

**Table 3.4** Thomas model parameter values for defluoridation by Zr–Pu, and VPum (Geleta et al., 2021b)

Parameter Studied	pH	$C_0$ (mg/L)	Q (mL/min)	Bed-Depth, $H_B$ (cm)	$K_T$ (L/min.mg) ( $\times 10^4$ )	$q_{O(cal.)}$ (mg/kg)	$q_{e(exp.)}$ (mg/kg)	$R^2$	RMSE	Adsorbent
Variation of pH keeping $C_0$ and $Q_0$ constant	2	10	1.25	10	1.110	226.31	224.78	0.994	0.0034	Zr–Pu
	4	10	1.25	10	1.270	93.54	96.75	0.986	0.0112	
	6	10	1.25	10	1.870	64.00	69.06	0.980	0.0082	
	2	10	1.25	10	1.440	110.00	110.00	0.993	0.0013	VPum
	4	10	1.25	10	8.289	17.83	23.51	0.977	0.0079	
	6	10	1.25	10	12.099	13.08	14.81	0.995	0.0034	
Variation of $Q_0$ keeping pH and $C_0$ constant	2	10	1.25	10	1.110	226.31	224.78	0.994	0.0034	Zr–Pu
	2	10	2.50	10	5.100	130.33	127.87	0.993	0.0047	
	2	10	3.75	10	10.000	78.07	108.31	0.992	0.0059	
	2	10	1.25	10	1.440	110.00	110.00	0.993	0.0013	VPum
	2	10	2.50	10	3.563	58.81	29.80	0.953	0.0167	
	2	10	3.75	10	5.000	45.82	16.90	0.962	0.0295	

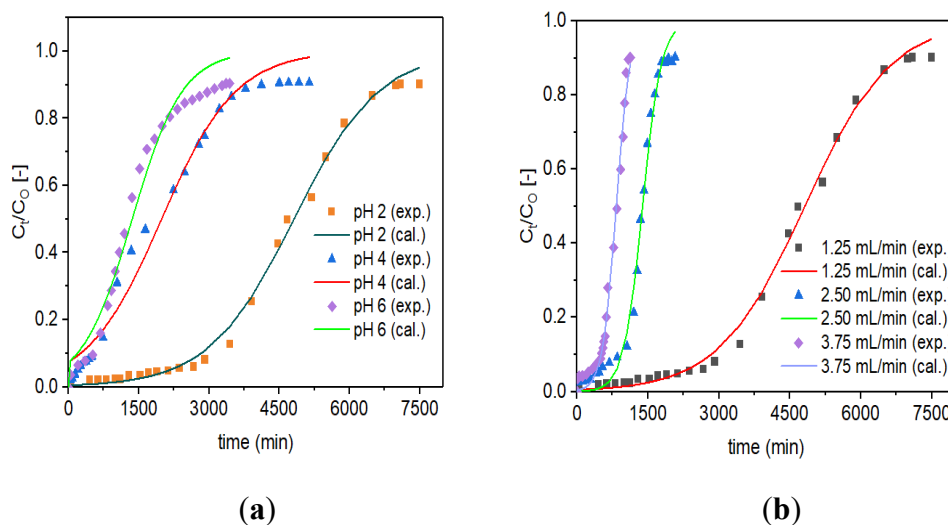


**Figure 3.7** Experimental (exp.) and simulated (cal.; Thomas model) breakthrough curves of fluoride for Zr–Pu at different (a) pH values ( $C_0$ : 10 mg/L;  $Q_0$ : 1.25 mL/min; bed depth 10 cm) and (b) initial flow rates,  $Q_0$  (pH 2;  $C_0$ : 10 mg/L; bed depth 10 cm)

### 3.3.4. Application of the Adams-Bohart Model

The plots for experimental (designated as exp.) and simulated (designated as cal.) breakthrough data based on the Adams-Bohart model are presented in Figure 3.8. Similar to the Thomas Model, the graphical plots for experimental data and simulated data are not shown for VPum, which were presented in our recent work (Geleta et al., 2021b). The optimized model parameter values such as  $K_{AB}$  and  $N_O$  are summarized in Table 3.5. Like the Thomas model, it can also be possible to deduce that the increase in  $K_{AB}$  with increased flow rates or decreased EBCT decreases the values of  $N_O$ . A decrease in  $N_O$  with increasing flow rates was attributed to EBCT reduction due to the direct proportion of the adsorption capacity to the interaction time. Similar observations were reported in previous studies (Ghosh et al., 2015; Sivasankar et al., 2010). Similar to the Thomas model, at pH 2, with a lower  $K_{AB}$  value ( $1.110 \text{ (L/min.mg)} (\times 10^4)$  for Zr–Pu and  $2.568 \text{ (L/min.mg)} (\times 10^4)$  for VPum), both materials showed good adsorption properties (Table 3.5).

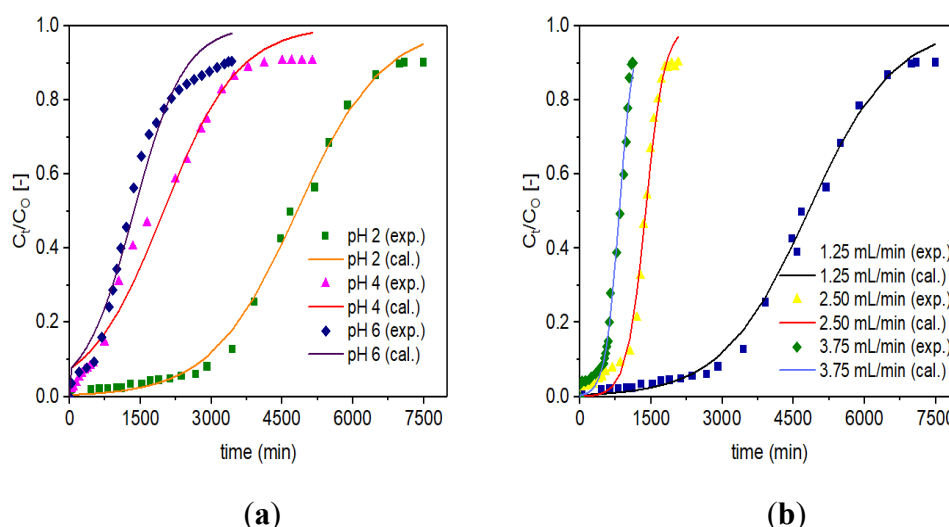


**Figure 3.8** Experimental (exp.) and simulated (cal.; Adams-Bohart model) breakthrough curves of fluoride for Zr–Pu at different (a) pH values ( $C_o$ : 10 mg/L;  $Q_o$ : 1.25 mL/min; bed depth 10 cm) and (b)  $Q_o$  (pH 2;  $C_o$ : 10 mg/L; bed depth 10 cm)

The lower value of  $K_{AB}$  for Zr–Pu than VPum suggests that the mass transfer by diffusion within the column packed with Zr–Pu was superior to VPum (Sivasankar et al., 2010). However, it is clear from Table 3.5 that the values of  $N_O$  decreased from 117 to 33 mg/L for Zr–Pu and from 46 to 8 mg/L for VPum as the pH value increased from 2 to 6, while the other conditions remained constant.

**Table 3.5** Adams-Bohart model parameter values for defluoridation by Zr–Pu, and VPum (Geleta et al., 2021b)

Parameter Studied	pH	$C_o$ (mg/L)	Q (mL/min)	Bed-Depth, $H_B$ (cm)	$K_{AB}$ (L/min.mg) ( $\times 10^4$ )	$N_{O(cal.)}$ (mg/L)	$R^2$	RMSE	Adsorbent
Variation of pH	2	10	1.25	10	1.110	116.98	0.996	0.0034	Zr–Pu

keeping $C_0$ and $Q_0$ constant	4	10	1.25	10	1.268	48.35	0.986	0.0112	
	6	10	1.25	10	1.874	33.08	0.980	0.0082	
	2	10	1.25	10	2.568	45.57	0.947	0.0013	
	4	10	1.25	10	7.772	11.03	0.980	0.0079	VPum
	6	10	1.25	10	11.220	7.75	0.980	0.0034	
Variation of $Q_0$ keeping pH and $C_0$ constant	2	10	1.25	10	1.110	116.98	0.996	0.0034	
	2	10	2.50	10	5.063	69.31	0.993	0.0047	Zr–Pu
	2	10	3.75	10	6.803	58.13	0.992	0.0059	
	2	10	1.25	10	2.568	45.57	0.947	0.0013	
	2	10	2.50	10	4.813	30.03	0.957	0.0167	VPum
	2	10	3.75	10	6.251	26.83	0.896	0.0295	

The values of  $R^2$  range from 0.980 to 0.996 for Zr–Pu and 0.896 to 0.996 for VPum, indicating the general applicability of the Adams-Bohart model for describing the experimental data (Table 3.5). The Adams-Bohart model did a good job of depicting the adsorption process and defluoridation by Zr–Pu and VPum packed fixed-beds at various experimental conditions. Similar to the Thomas model, the optimized model parameter values confirmed that zirconium coating improved the fluoride uptake capacity of VPum.

In general, the Thomas and Adams-Bohart models described the experimental data very well, revealing that the models are suitable tools for designing fixed-bed column systems using VPum and Zr–Pu.

### 3.3.5. Performance of various Adsorbents on Fluoride Uptake

The adsorbent (Zr–Pu) utilized in this work was compared to previously studied adsorbents for the uptake of fluoride in a flow-through fixed-bed column system, as shown in Table 3.6.

**Table 3.6** Fluoride adsorption capacity of various adsorbents

Adsorbents	Bed Height (cm)	Fluoride Level in (mg L <sup>-1</sup> )	Adsorption Capacity (mg g <sup>-1</sup> )	References
Granular acid-treated bentonite	28	6.34	0.190	(Ma et al., 2011)
Granular acid-treated bentonite	28	2.85	0.169	(Ma et al., 2011)
MnO <sub>2</sub> -coated Tamarind Fruit Shell	6	2	0.883	(Sivasankar et al., 2010)
Aluminum modified iron oxide	10.5	4	0.139	(García-sánchez et al., 2013)

Activated alumina (Grade OA-25)	10	5	0.74	(Ghorai & Pant, 2004)
Virgin Pumice (VPum)	10	10	0.110	(Geleta et al., 2021b)
Virgin Scoria (VSCO)	10	10	0.022	(Geleta et al., 2021b)
Zr–Pu	10	10	0.225	This study

The fluoride uptake capacity of Zr–Pu used in this study is higher than those of granular acid-treated bentonite, aluminum modified iron oxide, VPum, and VSCO. Above all, the raw material (VPum) is easily accessible and readily available, in contrast to some of the other substrates, confirming that Zr–Pu could be a promising candidate for the uptake of excess fluoride from water.

### 3.4. Conclusions

In this study, the defluoridation performance of the Zr–Pu-packed fixed-bed column systems were examined and compared with that of VPum. The XRD analysis showed that zirconium oxide was coated on the surface of VPum. The enhancement of the specific surface area was confirmed by the BET technique. The degree of surface modification with the improved porosity of Zr–Pu was evident from the recorded SEM image. The ICP-OES and XRF analysis were conducted for VPum and Zr–Pu to confirm the absence of harmful substances and to quantify the amount of zirconium coated onto the VPum. Fluoride adsorption was influenced by pH and input flow rate. The highest uptake capacity of fluoride by Zr–Pu was 225 mg/kg (2.05 times that of VPum: 110 mg/kg), at pH 2, input fluoride concentration of 10 mg/L, and an input flow rate of 1.25 mL/min. A fixed-bed column of 265 g Zr–Pu can generate a volume of 4339 mL (~2.9 times that of VPum: 1508 mL) treated water with an acceptable fluoride level of < 1.5 mg/L. Such enhanced performance is most likely associated with the coating of VPum with zirconium. The Thomas and Adams–Bohart models were employed to evaluate the breakthrough curves and obtain values for the kinetic parameters. Both models were capable of depicting the full range of the fluoride breakthrough curves, revealing that the models are suitable tools to design fixed-bed systems using VPum and Zr–Pu. This study demonstrated that the coating with zirconium enhances the fluoride adsorption capacity of VPum and that the Zr–Pu could be a promising candidate for the removal of high levels of fluoride from groundwater at a technical scale. However, additional investigations on, for instance, the influence of competing ions, regeneration of fluoride-laden adsorbents, and technical and economic analysis are advisable to draw explicit conclusions.

#### 4. Fixed-bed Adsorption: Comparisons of Virgin and Zirconium Oxide-Coated Scoria for the Removal of Fluoride from Water

Wondwosen Sime Geleta <sup>1,2,\*</sup>, Esayas Alemayehu <sup>3,4,\*</sup> and Bernd Lennartz <sup>2,\*</sup>

<sup>1</sup> School of Chemical Engineering, Jimma Institute of Technology, Jimma University, P.O. Box 378, Jimma, Oromia, Ethiopia

<sup>2</sup> Faculty of Agricultural and Environmental Sciences, University of Rostock, Justus-Von-Liebig-Weg 6, 18059 Rostock, Germany

<sup>3</sup> Faculty of Civil and Environmental Engineering, Jimma Institute of Technology, Jimma University, P.O. Box 378, Jimma, Oromia, Ethiopia

<sup>4</sup> Africa Center of Excellence for Water Management, Addis Ababa University, 1176 Addis Ababa, Ethiopia

\*Correspondence

***Molecules* (2022) 27: 2527**

**Abstract:** Many people worldwide are exposed to extreme levels of fluoride in drinking water. It is, therefore, critical to develop inexpensive, locally available, and environmentally friendly adsorbents for fluoride-laden water defluoridation. In the current study, virgin scoria (volcanic rock) from Ethiopia, was modified with zirconium oxide and used as an adsorbent in a fixed-bed column aiming at the removal of fluoride from water. The adsorption capability of zirconium oxide-coated scoria (ZrOCSc) was compared with unmodified virgin scoria (VSco). XRD, FTIR, XRF, SEM, ICP-OES, and the  $\text{pH}_{\text{PZC}}$  tests were evaluated to explore the adsorption mechanisms. Thermal analysis of VSco and ZrOCSc revealed lower total weight losses of 2.3 and 3.2 percent, respectively, owing to the removal of water molecules and OH species linked to metal oxides contained in the material. The effect of test conditions such as the pH of the solution and the influent flow rate on the adsorption capacity of the adsorbent was carefully studied. ZrOCSc exhibited the maximum removal capacity of 58 mg/kg, which was 4.46 times higher than the observations for VSco (13 mg/kg) at pH 2, and an initial flow rate of 1.25 mL/min. Breakthrough time increased with decreasing initial pH and flow rate. The adsorption experimental data under various test conditions were examined by the Thomas and Adams–Bohart models. Both models were found very effective in describing the experimental data with a correlation coefficient ( $R^2$ ) of  $\geq 0.976$  (ZrOCSc) and  $\geq 0.967$  (VSco). Generally, coating VSco with zirconium oxide improved the adsorption performance of VSco; hence, a ZrOCSc-packed fixed bed could be employed for the decontamination of high levels of fluoride from groundwater. However, further examination of the adsorbent using natural groundwater is advisable to produce a definitive conclusion.

**Keywords:** adsorption; fluoride; virgin scoria; zirconium oxide-coated scoria

#### 4.1. Introduction

Fluorine is the thirteenth most abundant element and makes up between 0.06% and 0.09% of the entire Earth's crust ([Armienta & Segovia, 2008](#); [Rasool et al., 2018](#)). Fluorine is always in a combined form of minerals such as fluoride. Fluoride levels in surface water ranged from 0.01 to 0.3 mg/L, while groundwater levels range from less than 1 to more than 35 mg/L ([Msonda et al., 2007](#); [Rasool et al., 2018](#)). Fluoride is thought to have beneficial effects in trace amounts in drinking water, but prolonged exposure to fluoride in drinking water, or combined effect with exposure to fluoride from other sources, could result in some negative effects ([Fawell et al., 2006](#); [Geleta et al., 2021a, 2021b, 2021c](#)). It can prevent the incidence of dental caries, particularly in children under the age of 8 years, if taken in drinking water at an optimum level ( $\sim 0.5\text{--}1.5$  mg/L) ([Whitford, 1996](#)). However, if the permissible level is exceeded, dental fluorosis or mottled enamel will appear, and if the concentration is greater than 3 mg/L, it will also cause skeletal fluorosis ([Dar et al., 2011](#)).

Groundwater is the safest and most economically viable option of all available drinking water sources for many communities around the world, as is the case for many communities in rural and urban areas of the main African rift valley ([Fawell et al., 2006](#); [Geleta et al., 2021b, 2021c](#)). In recent years, the entry of geogenic pollutants, such as fluoride, into groundwater aquifers has become a serious environmental problem worldwide. Over 200 million people around the world, including in East Africa, are drinking fluoride-containing groundwater beyond the permitted limit (1.5 mg/L), which has a significant impact on human well-being ([Geleta et al., 2021b, 2021c](#); [Y. Zhang et al., 2019](#)). Fluorosis is by far the most common geochemical disease in the East African rift, impacting more than 80 million individuals ([Geleta et al., 2021b](#); [Kut et al., 2016](#); [Mohan et al., 2017a](#)). Ethiopia is one of the most populous East African countries where excessive fluoride is becoming a growing issue, particularly along the main rift of the country ([Rango et al., 2017](#); [Žáček et al., 2015](#)). The fluoride concentrations in Ethiopian rift wells are usually 1 to 10 times higher than the WHO standard, which puts about 10 million Ethiopians at high risk of fluoride ion exposure ([Rango et al., 2017](#); [Tekle-Haimanot et al., 2006](#)).

High geogenic fluoride levels in groundwater are related to various geological climatic conditions such as arid climates, granitic basements, and alkaline volcanic rocks. In addition to the natural geological sources for fluoride enrichment in groundwater, numerous fluorochemical industries including aluminum smelting are also contributors to fluoride contamination. Alkaline volcanic areas, such as the East African Rift Valley, have some of the highest fluoride concentrations since high-fluoride hyper-alkaline volcanic rocks are present and fluoride is also introduced to groundwater through high-fluoride geothermal solutions ([Eawag, 2015](#); [Edmunds & Smedley, 2014](#)). Low calcium



levels can also cause too high fluoride levels in groundwater. The weathering of primary rocks and the leaching of fluoride-containing minerals in the soil exacerbate the problem of excessive fluoride in groundwater in the Ethiopian Rift, which is generally linked with a low calcium content and high concentrations of bicarbonate (Demelash et al., 2019; Rango et al., 2010). Therefore, a high concentration of fluoride in groundwater is among the most pressing problems that need to be addressed urgently.

Different treatment techniques such as ion exchange, membrane, precipitation, and adsorption have been employed for the uptake of fluoride (Chen et al., 2018). Among the existing techniques, adsorption remains the most widely employed and most suitable method because of its applicability for the uptake of fluoride even at small doses, economic feasibility, high efficiency, and simplicity of design (P. Chen et al., 2018; Geleta et al., 2021b, 2021c).

The adsorbent materials researched for fluoride uptake are abundant (Chen et al., 2010; Ghanbarian et al., 2020; Kennedy & Arias-Paic, 2020; Maliyekkal et al., 2006; Sarkar et al., 2006; Su et al., 2020). Nevertheless, many of them are suffering from either a time-taking synthesis procedure, high costs of processing, inaccessibility of raw materials, or short shelf life, which makes them unrealistic for use in the rift valleys' water (Geleta et al., 2021b, 2021c; Kumari et al., 2021). Thus, for sustainable defluoridation of drinking water, the search for suitable fluoride adsorbents is a critical concern for developing countries such as Ethiopia. Modifying the physicochemical properties of locally available adsorbents is also of interest, as it could have the potential for further cost reduction and applicability (Geleta et al., 2021c).

Volcanic rock (scoria) is one such indigenous material in many nations including Ethiopia that could be used as a raw material for producing an adsorbent for fluoride removal. Scoria has valuable features such as low cost, easy access, good mechanical strength, and availability in considerable quantities (Alemayehu & Lennartz, 2009; Geleta et al., 2021b; Mekonnen et al., 2021a). The possession of good mechanical strength could enable scoria to prevail over drawbacks such as clogging and/or low hydraulic conductivities in fixed-bed column adsorption techniques. However, the fluoride uptake capacity of natural scoria is limited, and surface modifications for improved performance appear not to have been well studied. Surface modification of natural adsorbents that may contribute to the available active sites for fluoride adsorption is expected to have good reactivity/affinity for fluoride ions (Geleta et al., 2021c; Salifu et al., 2016). From a previous study, it was generally noticed that natural materials modified with multivalent metal cations such as  $Mn^{4+}$ ,  $Zr^{4+}$ , and  $Fe^{3+}$  can change the surface properties and the affinity of fluoride (Geleta et al., 2021c; He et al., 2019). Among these, zirconium ( $Zr^{4+}$ ) is receiving more attention because of its high binding affinity to fluoride ions, non-

toxicity, and acceptable cost ([Chaudhry et al., 2017](#); [Dehghani et al., 2017](#); [Geleta et al., 2021c](#)). Therefore, the study of zirconium-based adsorbents with good performance is very important.

Taking the aforementioned problems into account, fixed-bed columns packed with zirconium (IV) oxychloride octahydrate ( $\text{ZrOCl}_2 \cdot 8\text{H}_2\text{O}$ )-coated scoria, hereinafter abbreviated as ZrOCSc, have not been tested for the treatment of fluoride-polluted water. Therefore, the aims of the current study were to (i) compare the adsorption properties of ZrOCSc with VSco, (ii) evaluate the processes of fluoride adsorption through variations in the solution pH and influent volumetric flow rate, and (iii) describe and analyze the adsorption processes using well-known fixed-bed adsorption models such as the Thomas and Adams–Bohart model.

## 4.2. Materials and Methods

### 4.2.1. Adsorbent Preparations

#### 4.2.2. Coating of Zirconium Oxide onto Virgin Scoria (VSco)

The virgin scoria (VSco) used as a base material in zirconium oxide coating for surface modification, was collected from volcanic cones (Figure 4.1) of the Main Rift Valley of Ethiopia; roughly 50 to 100 km East of Addis Ababa. The sample was washed multiple times with deionized water before being dried at 70 °C for 48 h. After cooling to room temperature, the sample was crushed and sieved to four different size fractions, as shown in ([Geleta et al., 2021b](#)). In our previous study ([Geleta et al., 2021b](#)), virgin scoria (VSco) with a silt size ( $< 0.075$  mm) showed a good fluoride removal performance compared to the remaining three particle sizes. However, some studied and reported defluoridation materials are either fine particles or powder which may make separation from an aqueous solution difficult. When used in fixed-bed adsorption systems, such materials could also cause clogging and/or low hydraulic conductivity ([Salifu et al., 2016](#)). To overcome these limitations, a fraction range of 0.075–0.425 mm was used for coating with zirconium oxide.

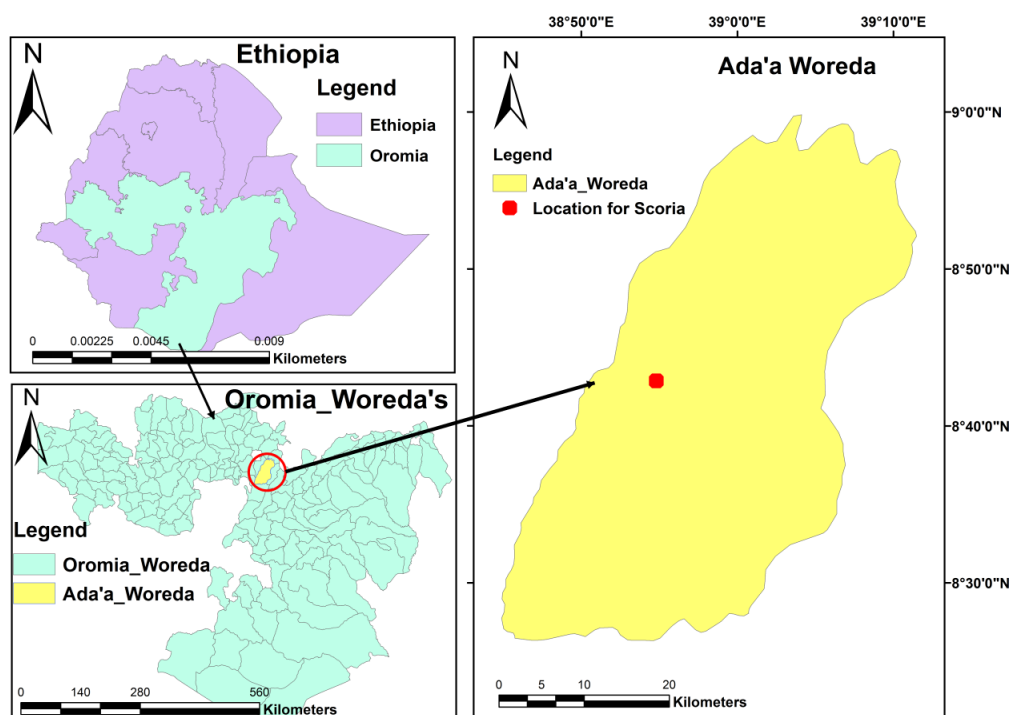


**Figure 4.1** Sampling site of virgin scoria (VSco)

VSco coating was accomplished by completely soaking the dried sample in a sufficient amount of 0.1 M  $\text{ZrOCl}_2 \cdot 8\text{H}_2\text{O}$  in acid-washed cylindrical polyethylene wide-mouth plastic bottles. The mixture was shaken with a horizontal shaker (SM25, Edmund Bühler 7400 Tübinger, Germany) at 200 rpm for 12 h. The zirconium oxide-coated scoria (ZrOCSc) was decanted, dried in an electric oven at 70 °C for 48 h, and soaked in 2 M  $\text{NH}_4\text{OH}$ . The ZrOCSc was washed repeatedly with deionized water and dried at 70 °C for 48 h (Geleta et al., 2021c; Salifu et al., 2013). The coated VSco (ZrOCSc) was then packed and stored in an airtight plastic bag for use.

#### 4.2.3. Chemicals and Reagents

All chemicals and reagents used in the experiments were of analytical grade. Zirconium oxychloride (IV) octahydrate ( $\text{ZrOCl}_2 \cdot 8\text{H}_2\text{O}$ ), ammonium hydroxide ( $\text{NH}_4\text{OH}$ ), sodium hydroxide ( $\text{NaOH}$ ), and hydrochloric acid ( $\text{HCl}$ ) were acquired from Merck KGaA, Darmstadt, Germany. 1000 mg/L of fluoride stock solution was gained by dissolving 2.21 g of  $\text{NaF}$  in 1000 mL of deionized water. The adsorbate solution concentration needed for the fixed-bed adsorption experiments was obtained by subsequent dilution of the stock solution with deionized water. The adsorbate solutions' pH values were calibrated with 0.1M  $\text{NaOH}$  and/or 0.1 M  $\text{HCl}$ .

#### 4.2.4. Characterizations of the Materials

The X-ray diffraction (XRD) patterns of ZrOCSc and VSco were gained by the XRD instrument

(XRD-7000, Drawell, Shanghai, China) with Cu K $\alpha$  as a radiation X-ray source (1.54056 Å) generated at 30 kV and 25 mA instrument. The diffractogram was achieved with a step width of  $2\theta$  in the range between  $10^\circ$  to  $70^\circ$  and a scan rate of  $0.01^\circ/\text{min}$ . The mineralogy content of the adsorbents was characterized by matching the diffractogram of VScO before adsorption and ZrOCSO before and after adsorption with the database of the X'pert HighScore Plus software package (Version: 2.2b (2.2.2)).

The oxide and elemental composition of the adsorbents were obtained by X-ray fluorescence (XRF, Mini-Pal 2 spectrometer, Panalytical, Malvern, Worcestershire, UK)) spectroscopy and inductively coupled plasma-optical emission spectroscopy (ICP-OES, Varian Vista MPX, Palo Alto, CA, USA), respectively.

The Fourier Transform Infrared (FTIR) spectra were recorded in a PerkinElmer spectrometer (UNSW Sydney, Australia) over a range of  $5000$  to  $400\text{ cm}^{-1}$  at a resolution of  $0.1\text{ cm}^{-1}$  using a lithium tantalite (LiTaO $_3$ ) detector.

The pH of the adsorbents was determined using a pH meter using a 1:10 adsorbent/water ratio according to the standard method. The point of zero charges (pH $_{\text{PZC}}$ ) of the adsorbents was determined using 0.01 M of NaCl solutions as an electrolyte and adding 0.1 M of NaOH or HCl solutions for pH adjustment (Geleta et al., 2021b, 2021c).

The scanning electron microscope (SEM) images were gained by NeoScope JCM-6000plus, Version 0.2, JEOL Ltd., Peabody, Massachusetts, USA, operated at 15 kV.

Simultaneous thermogravimetric and differential thermal analysis (TGA/DTA) of VScO and ZrOCSO were carried out using DTG-60H, SHIMADZU Corporation, Kyoto, Japan. An initial mass (about  $12 \pm 0.5\text{ mg}$ ) was placed in an aluminum crucible at a heating rate of  $15^\circ\text{C}/\text{min}$  from  $25$  to  $900^\circ\text{C}$  under nitrogen purging ( $50\text{ mL}/\text{min}$ ).

#### 4.2.5. Fixed-bed Column Adsorption Studies

Fixed-bed column tests of VScO and ZrOCSO were conducted in a small-scale cylindrical filter column (8.1 cm in diameter and 10 cm in height), as indicated in (Geleta et al., 2021b, 2021c). A weighted amount of material was packed carefully into the column. The bed was conditioned with one pore volume of deionized water to ensure a compact adsorbent (Geleta et al., 2021c). An adjustable variable flow peristaltic pump (REGLO ICC, Ismatec, Cole-Parmer Barrington, IL, USA) was utilized to set the flow rate. All column tests were performed at 298 K. Column effluent samples were collected regularly by the automatic fraction collector (RFI, MA-RON GmbH, Reichelt Chemietechnik GmbH + Co., Heidelberg, Germany). The effluent samples' fluoride concentration was measured by ion

chromatography (930 Compact IC Flex, Metrohm, Herisau, Switzerland). The WHO standard for the fluoride content in drinking water ( $< 1.5 \text{ mg/L}$ ) (WHO, 2011) was considered a breakthrough concentration ( $C_b$ ). The bed exhaustion/saturation point was considered when the fluoride level in the effluent was equal to 90 % of the fluoride level in the influent (i.e.,  $0.9 C_i/C_o$ ).

The influence of experimental parameters such as influent solution pH (2, 4, and 6) and influent volumetric flow rate (1.25, 2.50, and 3.75 mL/min) on the shape of the breakthrough curves and the amount of fluoride removed by the adsorbents was investigated at constant bed height (10 cm), and initial fluoride concentration (10 mg/L).

#### 4.2.6. Analysis of Column Data

##### 4.2.6.1. Breakthrough Curve

A breakthrough curve is used to assess the dynamic adsorption process of a system and to predict the performance of the fixed-bed column system (Sahu et al., 2020). The breakthrough time and breakthrough curve pattern are important indicators for operational adsorption techniques. The viability and economics of the adsorption process are primarily related to these two parameters (Geleta et al., 2021a, 2021b; Mekonnen et al., 2021b). The experimental conditions such as influent pH and influent flow rate influence the profile of the breakthrough curve and its parameters. To study the performance and scaling of the fixed bed column, it is very imperative to study these parameters through experimental tests. The breakthrough curve was expressed by plotting ( $C_t/C_o$ ) versus contact time,  $t$ . Where,  $C_o$  and  $C_t$  are the initial and the effluent fluoride concentration, respectively.

The time for exhaustion and the time for a breakthrough is given by the following Equations (4.1) and (4.2), respectively.

$$t_e = \int_{t=0}^{t=t_{\text{total}}} \left(1 - \frac{C_t}{C_o}\right) dt \quad (4.1)$$

$$t_b = \int_{t=0}^{t_b} \left(1 - \frac{C_{bt}}{C_o}\right) dt \quad (4.2)$$

where  $t_e$  is exhaustion time (min),  $t_b$  is the breakthrough time (min) at which  $C_t = C_b$  (mg/L) (for the present system,  $C_b = 1.5 \text{ mg/L}$ ).

The total amount of fluoride adsorbed in a fixed-bed column,  $q_{\text{total}}$  (mg) was evaluated from the area (A) under the breakthrough curve using Equation (4.3).

$$q_{\text{total}} = \frac{QA}{1000} = \frac{Q \times C_0}{1000} \int_{t=0}^{t=t_{\text{total}}} \left(1 - \frac{C_t}{C_0}\right) dt \quad (4.3)$$

where  $t_{\text{total}}$  and  $Q$  are the total flow time until saturation of the bed (min) and flow rate (mL/min), respectively.

The maximum fluoride removal capacity ( $q_e$ : mg kg<sup>-1</sup>) of the column is calculated using Equation (4.4).

$$q_{\text{eq}} = \frac{q_{\text{total}}}{m} = \frac{C_0 Q t_e}{m} \quad (4.4)$$

The amount of fluoride removed at  $t_b$  ( $q_b$ : mg kg<sup>-1</sup>) can be determined by Equation (4.5).

$$q_b = \frac{C_0 Q t_b}{m} \quad (4.5)$$

The effluent volume ( $V_e$ ) and treated effluent volume or breakthrough volume ( $V_b$ ) can be evaluated with Equations (4.6) and (4.7), respectively.

$$V_e = Q t_e \quad (4.6)$$

$$V_b = Q t_b \quad (4.7)$$

where  $V_e$  is the total effluent volume at saturation time (mL) and  $V_b$  is the total effluent volume at the breakthrough time (mL).

The Mass Transfer Zone (MTZ) or unused bed length ( $H_{\text{UNB}}$ ) can be evaluated from Equation (4.8).

$$\text{MTZ} = H_T \left( \frac{t_e - t_b}{t_e} \right) \quad (4.8)$$

where  $H_T$  is total bed height (cm),  $t_e$  (min) is exhaustion time, and  $t_b$  is breakthrough time (min).

The Empty Bed Contact Time (EBCT), which is defined as the contact time between the solid phase adsorbent and the liquid phase, can be determined from Equation (4.9).

$$\text{EBCT} = \frac{V_B}{Q} \quad (4.9)$$

where  $V_B$  is the volume of a fixed bed (mL) and  $Q$  is the flow rate (mL/min).

#### 4.2.7. Breakthrough Curve Modeling

The modeling of breakthrough curves can efficaciously avoid extensive studies on the pilot scale ([A.](#)

Hu et al., 2020). Various models have been reported to estimate breakthrough performance in the fixed-bed adsorption process (Mohan et al., 2017a). In this work, the two most common and widely employed mathematical models, the Thomas model and Adams–Bohart model, were used in the experimental data of the column to depict the dynamic behavior of fluoride uptake onto VScO and ZrOCSO packed fixed-bed column filter. The coefficient of determination ( $R^2$ ) was used to estimate the validity of the models. The mathematical descriptions of the models are given in the following sub-sections.

#### 4.2.7.1. Thomas Model

The Thomas model (Thomas, 1944) is among the most prominent models in fixed-bed column studies to anticipate the maximum adsorption capacity ( $q_o$ ) and the adsorption rate constant ( $K_T$ ). The model was also used to forecast effluent breakthrough curves. The model is based on the following assumptions (Hu et al., 2019): (i) the plug flow characteristic occurs in the fixed-bed; (ii) the external and internal diffusion constraints are insignificant; and (iii) the experimental data follow the Langmuir isotherm and second-order reversible reaction kinetics. The non-linear form of the Thomas model is given in Equation (4.10), as follows.

$$\frac{C_t}{C_o} = \frac{1}{1 + \exp \left[ K_T q_o \frac{m}{Q} - K_T C_o t \right]} \quad (4.10)$$

where  $C_o$  (mg/L) is the initial solute concentration,  $C_t$  (mg/L) is the solute concentration at the time,  $t$ ,  $Q$  (L/min) is the volumetric flow rate,  $q_o$  (mg/kg) is the adsorbed fluoride at equilibrium,  $K_T$  is the model kinetic constant (L/min mg), and  $m$  (kg) is the dry adsorbent mass.

#### 4.2.7.2. Adams-Bohart Model

The Adams–Bohart model (Bohart & Adams, 1920) was developed for the analysis of the dynamics of fixed-bed under the assumption that the adsorption rate is not instantaneous and that the adsorption rate is proportional to the residual adsorption capacity of the adsorbent and the concentration of adsorbate. The non-linear form of the Adams–Bohart model (Equation (4.11)) (Chu, 2020), was used to estimate the breakthrough curves and the model parameters.

$$\frac{C_t}{C_o} = \frac{1}{1 + \exp \left[ K_{AB} N_o \frac{Z}{v} - K_{AB} C_o t \right]} \quad (4.11)$$

Where  $K_{AB}$  (L/mg min) is the kinetic constant of the model,  $v$  (mL/min) is the linear flow rate,  $Z$  (cm) is the depth of the column bed, and  $N_o$  (mg/L) is the saturation concentration (adsorption capacity of

the adsorbent per unit volume of the bed), and time  $t$  (min).

The linear flow rate was determined using Equation (4.12).

$$v = \frac{Q}{A} \quad (4.12)$$

where  $Q$  (mL/min) is the volumetric flow rate, and  $A$  (cm<sup>2</sup>) is the cross-sectional area of the bed.

### 4.3. Results and Discussions

#### 4.3.1. Characterization of Adsorbents

The crystalline phases of VScO (before adsorption) and ZrOCSc before and after the fluoride scavenger were characterized using the XRD instrumental technique. The results showed that the main crystalline phases in VScO were Quartz, syn (SiO<sub>2</sub>) (ICSD, reference code: 01-083-2470), Silicon Oxide (SiO<sub>2</sub>) (ICSD, reference code: 01-082-1554), and Albite low (Na(AlSi<sub>3</sub>O<sub>8</sub>)) (ICSD, reference code: 01-076-1819); Zirconium Oxide (ZrO<sub>2</sub>) with monoclinic crystal structure (ICSD, reference code: 01-078-0047) and Albite ordered (NaAlSi<sub>3</sub>O<sub>8</sub>) (ICSD, reference code: 00-009-0466) are the main crystalline phases in ZrOCSc before adsorption while Anorthite, ordered (CaAl<sub>2</sub>Si<sub>2</sub>O<sub>8</sub>) (ICSD, reference code: 00-041-1486), quartz (SiO<sub>2</sub>) (ICSD, reference code: 01-078-0047), and Zirconium fluoride (ZrF<sub>4</sub>) (ICSD, reference code: 01-076-1023) are the dominant components of ZrOCSc after adsorption. The prominent XRD peaks for virgin scoria (VScO) were found at  $2\theta = 19.10^\circ, 22.14^\circ, 27.01^\circ, 27.95^\circ, 29.91^\circ, 35.75^\circ, 42.35^\circ, 48.48^\circ$ , and  $61.96^\circ$  (Figure 4.2a). The diffraction pattern of ZrOCSc before adsorption (Figure 4.2b) showed prominent peaks at  $2\theta = 22.13^\circ, 25.46^\circ, 28.19^\circ, 29.90^\circ, 35.78^\circ, 42.25^\circ$ , and  $64.49^\circ$ ; while the peaks at  $2\theta = 22.13^\circ, 23.81^\circ, 25.25^\circ, 27.90^\circ, 29.95^\circ, 35.75^\circ$ , and  $48.44^\circ$  were observed for ZrOCSc after adsorption (Figure 4.2c). The number and intensity of peaks in VScO were different from that of ZrOCSc before fluoride adsorption. The difference in the number and intensity of the peaks might be because the zirconium oxide particles had grown on the surface (Chaudhry et al., 2017; Geleta et al., 2021c).



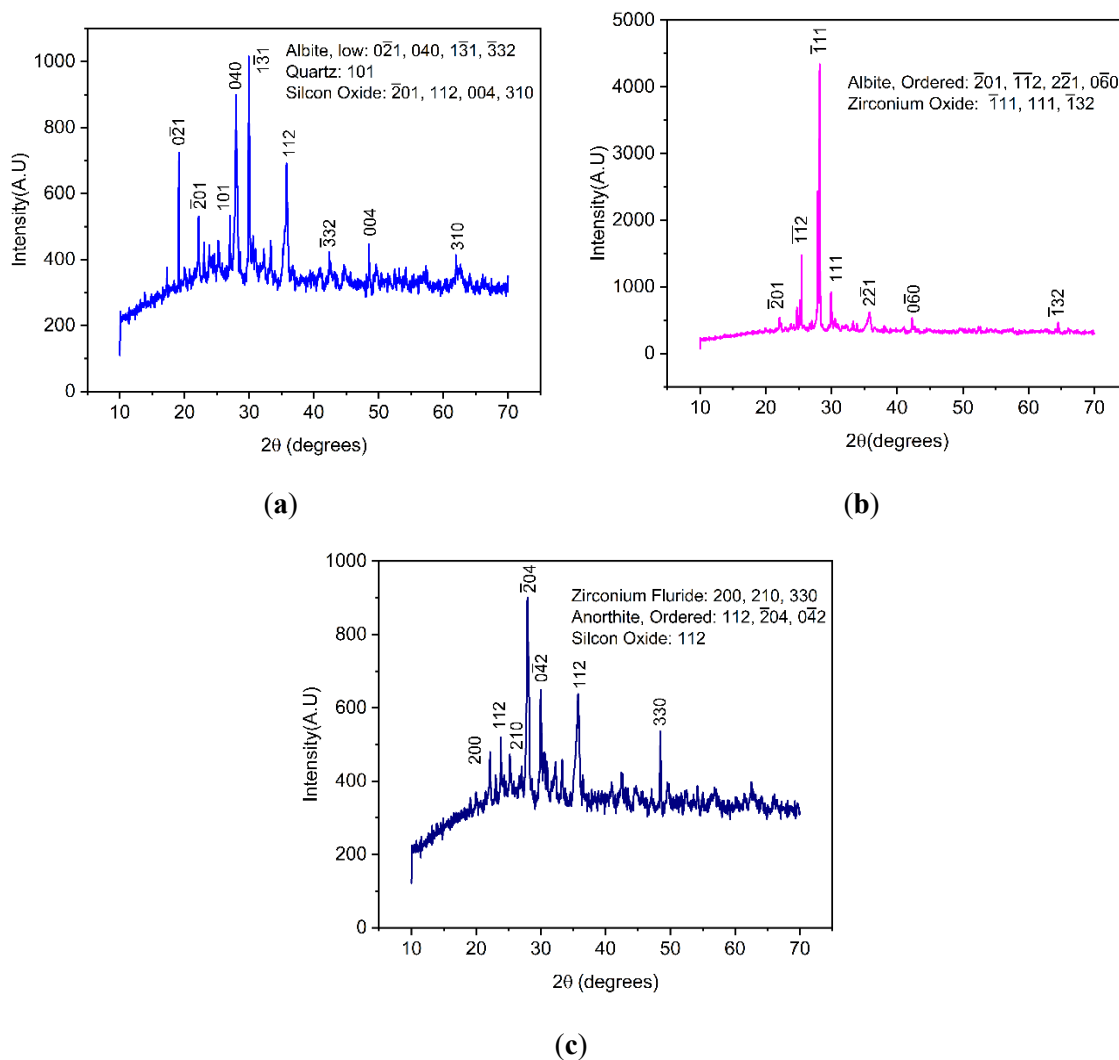


**Figure 4.2** XRD patterns for (a) VScO; zirconium oxide-coated scoria (ZrOCS) (b) before and (c) after adsorption experiment

As can be observed from the XRD patterns (Figure 4.2), the VScO (Figure 4.2a) had nine peaks with different intensities, with a major peak at  $2\theta = 29.90^\circ$  having the highest intensity, which corresponded to Na(AlSi<sub>3</sub>O<sub>8</sub>). ZrOCS before fluoride adsorption (Figure 4.2b) had seven prominent peaks and the major one at  $2\theta = 28.19^\circ$  having the highest intensity, which corresponded to ZrO<sub>2</sub> formed on the surface; while ZrOCS after adsorption (Figure 4.2c) had seven peaks and a major peak at  $27.90^\circ$  ( $2\theta$ ), corresponded to CaAl<sub>2</sub>Si<sub>2</sub>O<sub>8</sub>. The reduction in the number of peaks on coating might be due to the growth of zirconium oxide over the surface of VScO (Chaudhry et al., 2017; Geleta et al., 2021c). The number and intensities of the peaks decreased in spent adsorbent (Figure 4.2c) which could be due to an increase in the amorphous nature through surface co-precipitation during the adsorption of fluoride ions (Chaudhary et al., 2019; Lř et al., 2013) or due to a slight change in the adsorbent structural framework (Geleta et al., 2021c).

The FTIR spectrums of VScO, ZrOCS before and after fluoride adsorption at wavelengths between

400  $\text{cm}^{-1}$  and 5000  $\text{cm}^{-1}$  are presented in Figures 4.3a, b, and c respectively. The band located at  $\sim 1011.5$  and  $\sim 978$   $\text{cm}^{-1}$  can belong to the asymmetric stretching vibration of T-O-Si, T = Si or Al (Geleta et al., 2021b, 2021c; Pirsaeheb et al., 2018). The peaks at  $\sim 781$  and  $\sim 695.25$   $\text{cm}^{-1}$  belong to bending vibrations of the Si-O-Si bond (Geleta et al., 2021b, 2021c; Xu et al., 2012), while the band at  $\sim 767$   $\text{cm}^{-1}$  is related to the stretching vibration of 6-fold coordinated Al(VI)-OH and 6-fold coordinated Al(VI)-O (Djobo et al., 2014). The small peaks shown at  $\sim 550$   $\text{cm}^{-1}$  can be attributed to the symmetric stretching of Si-O-Si and Al-O-Si (Panias et al., 2007; Pirsaeheb et al., 2018). Although a clear diffraction peak for zirconium oxide and zirconium fluoride was detected in the XRD analysis of ZrOCS before and after adsorption, respectively, the expected bonds, i.e., a zirconium bridge to another zirconium atom via fluorine or oxygen bridges, were not detected in the FTIR spectrum. This could be due to the FTIR equipment's inability to detect such bonds. The inability of FTIR to detect Zr-F and F-Zr-F bending vibrations that occurs at  $\sim 375$ - $475$   $\text{cm}^{-1}$  and  $375$ - $475$   $\text{cm}^{-1}$ , respectively (Jere & Santhamma, 1977), was reported for hydrous zirconium oxide after fluoride adsorption (Dou et al., 2012). This finding is also comparable to previously reported studies (Geleta et al., 2021c; Sepehr et al., 2014; Sepehr et al., 2013a). However, additional investigation using complementary characterization techniques such as NMR/XPS should be considered in future work to draw strong evidence.

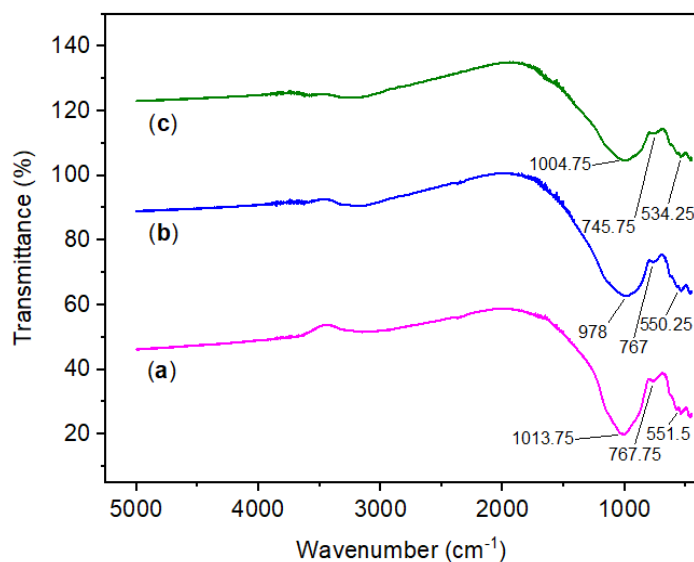


**Figure 4.3** Fourier-transform infrared (FT-IR) for (a) VSCO; ZrOCS (b) before, and (c) after adsorption experiment

The chemical analysis showed that aside from the major elements in VSCO (Si, Al, and Fe), as determined by ICP-OES (Table 4.1), Ca is the next high elemental component. Other elements were available in limited quantities or were below the device's detection limit. The main components of VSCO as measured by XRF were the oxides of Si, Fe, Ca, and Al. An earlier study reported comparable

values for VScO ([Alemayehu & Lennartz, 2009](#)). The lack of harmful components in the VScO suggested that ZrOCSc could be useful to treat excess fluoride-laden water. The average amount of zirconium oxide coated on VScO was 1.2 % (wt), while the XRF measurements showed that 8.3 % (wt) zirconium oxide was coated on VScO, enhancing its fluoride removal performance. This is in line with our recent study ([Geleta et al., 2021c](#)).

**Table 4.1** Elemental and oxide compositions of virgin scoria (VScO) and zirconium oxide-coated scoria (ZrOCSc)

Elemental Content	VScO % (wt)	ZrOCSc % (wt)	Oxide Content	VScO % (wt)	ZrOCSc % (wt)
Si	18.3	19.3	SiO <sub>2</sub>	47.4	44.8
Al	10.3	10.2	Al <sub>2</sub> O <sub>3</sub>	21.6	23.1
Fe	7.8	8.1	Fe <sub>2</sub> O <sub>3</sub>	8.9	5.8
K	0.4	0.4	K <sub>2</sub> O	0.5	0.3
Ca	6.4	6.2	CaO	12.4	11.9
Na	2.2	2.2	Na <sub>2</sub> O	3.0	2.6
Mg	2.8	2.7	MgO	3.3	2.0
Zn	< 0.1	< 0.1	TiO <sub>2</sub>	1.4	1.1
Zr	< 0.1	1.2	ZrO <sub>2</sub>	-	8.3
Mn	0.1	0.1	MnO	0.4	0.1
Cr	< 0.1	< 0.1	ZnO	0.2	0.2
Cu	< 0.1	< 0.1	NiO	0.1	0.2
Co	< 0.1	< 0.1	CuO	0.2	0.2
Cd	< 0.1	< 0.1	-	-	-
Ni	< 0.1	< 0.1	-	-	-
Pb	< 0.1	< 0.1	-	-	-
As	< 0.1	< 0.1	-	-	-

The pH in water and the pH<sub>PZC</sub> of VScO were found to be 9.3 and 8.7, respectively. These pH values are very close to the previous study ([Geleta et al., 2021b](#)). The pH in water and pH<sub>PZC</sub> for ZrOCSc was identified as 7.4 and 8.3, respectively. In the current study, both the pH in water and the pH<sub>PZC</sub> of ZrOCSc were found to be lower than those of VScO. A similar observation was reported for zirconium-coated pumice (Zr – Pu) ([Geleta et al., 2021c](#)). The surface charge of the adsorbent is positive when the pH of the solution is below pH<sub>PZC</sub> ((ZrOCSc (8.3), VScO (8.7)). Thus, fluoride could be adsorbed

onto the surface of adsorbents via coulombic attraction if the pH is less than  $pH_{PZC}$  (Geleta et al., 2021b, 2021c).

The SEM images of VScO and ZrOCSO before fluoride adsorption are shown in Figure 4.4a and Figure 4.4b, respectively.

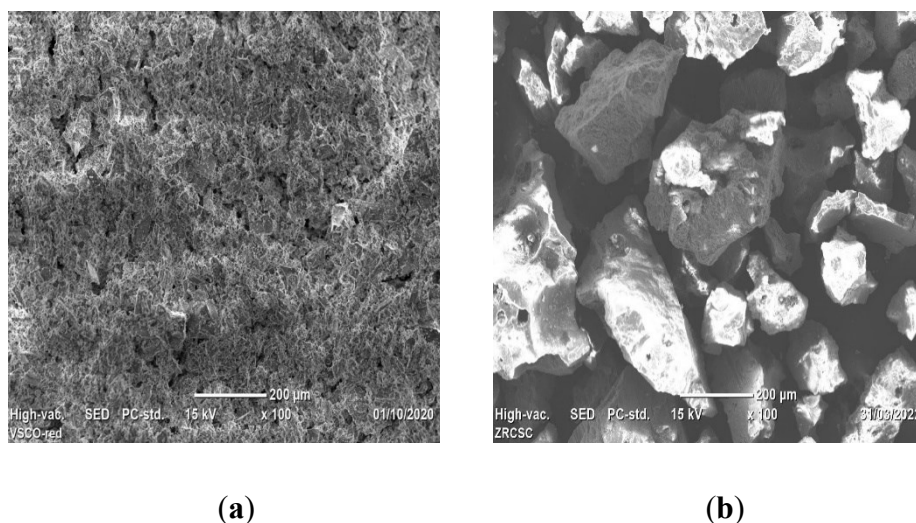


**Figure 4.4.** SEM image of (a) VScO and (b) ZrOCSO before adsorption experiments.

From Figure 4.4b, it can be seen that a large amount of irregularly shaped zirconium oxide (large clusters) is coated on the adsorbent surface and changes the surface structure of VScO. In our recent work, improvements in surface structure and adsorption for natural pumice surface modification (VPum) were reported (Geleta et al., 2021c).

Figure 4.5 depicts the thermal behavior of VScO (Figure 4.5a) and ZrOCSO (Figure 4.5b) at a heating rate of 15 °C/min from 25 to 900 °C under a nitrogen gas flow rate of 50 mL/min. The absorbable weight loss of about 2.3% of VScO (Figure 4.5a) between about 24 and 306 °C and 3.2% of ZrOCSO (Figure 4.5b) between 24 and 382 °C, is due to the removal of moistures as well as that of OH species linked to metal oxides and volatile organic impurities present at low levels. This demonstrates that the adsorbents could maintain their thermal stability up to 900 °C with insignificant weight gain, which could be attributed to the oxidation or reaction of the materials with nitrogen gas. An analogous observation was made in previous research (Alraddadi & Assaedi, 2021). The DTA thermogram of VScO (Figure 4.5a) showed a narrow and a broad exothermic peak in the ranges of about 25–73 °C and 204–900 °C, respectively, and an endothermic peak in the range of about 36–204 °C. A narrow and a broad exothermic peak in the region of about 25–52 °C and 185–900 °C, respectively, and an endothermic peak in the range of about 37–185 °C were also observed in the DTA analysis of ZrOCSO (Figure 4.5b).

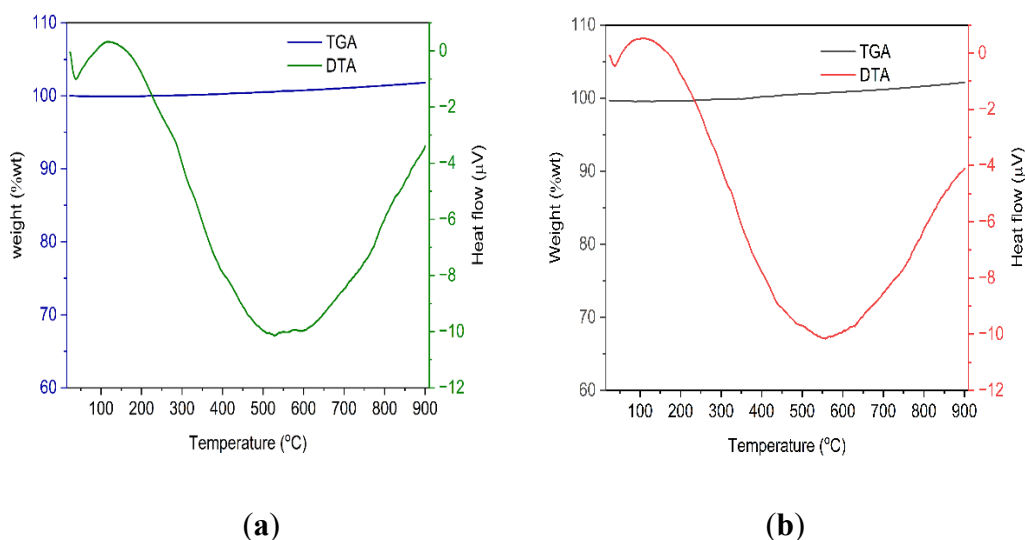


**Figure 4.5.** TGA-DTA thermograms of (a) VScO and (b) ZrOCSc before adsorption experiments.

#### 4.3.2. Influence of Experimental Parameters on Fluoride Removal

##### 4.3.2.1. Influence of Initial Solution pH

The pH-dependent disparity in the fluoride uptake performance of the adsorbents was evaluated at various pH values (2, 4, and 6) using a separate set of fixed-bed adsorption columns. The breakthrough curves are presented for VScO (Figure 4.6a) and ZrOCSc (Figure 4.6b) for a constant inlet flow rate (1.25 mL/min), initial fluoride concentration (10 mg/L), and column bed depth (10 cm). For both adsorbents, the breakthrough curves (Figure 4.6) appeared to move from right to left as the pH increased from 2 to 6.

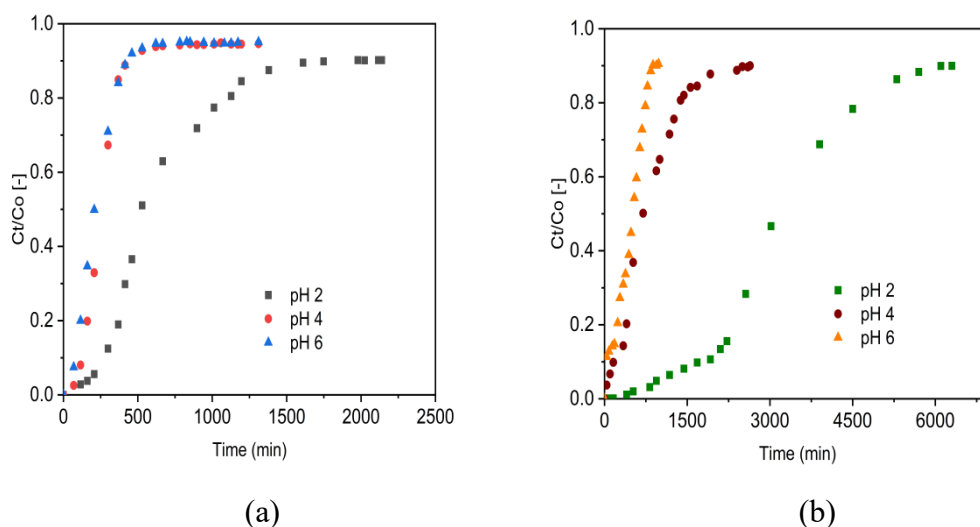


**Figure 4.6** Effect of solution pH on fluoride breakthrough (a) VScO and (b) ZrOCSc (initial fluoride concentration 10 mg/L (CO: 10 mg/L); initial flow rate 1.25 mL/min (QO: 1.25 mL/min); bed depth 10 cm)

The column adsorption parameters obtained for adsorption of fluoride onto ZrOCSc and VScO were

depicted in Table 4.2. Enhanced column performance was noticed at a lower initial solution pH including a higher volume of treated water, enhanced defluoridation efficacy, and enhanced adsorption capacity at breakthrough and exhaustion time. The highest defluoridation capacity of 58 mg/kg and 13 mg/kg was attained for ZrOCS and VSc, respectively. This revealed that ZrOCS scavenged 4.46 times fluoride compared to VSc. At a pH value of 2, the breakthrough capacity of 35 mg/kg (7 times that of VSc (5 mg/kg)) was achieved for ZrOCS. A breakthrough time of 2058 min for ZrOCS and 309 min for VSc; and an exhaustion time of 3425 min for ZrOCS and 753 min for VSc were also acquired at a pH of 2.

**Table 4.2** Fixed-bed column parameters obtained for defluoridation by VSc and ZrOCS

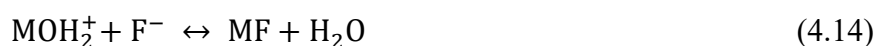
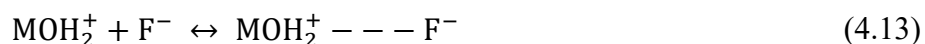
Parameter Studied	pH	C <sub>0</sub> (mg/L)	Q <sub>0</sub> (mL/min)	EBCT (min)	t <sub>b</sub> (min)	t <sub>e</sub> (min)	V <sub>b</sub> (mL)	V <sub>e</sub> (mL)	MTZ (cm)	q <sub>b</sub> (mg/kg)	q <sub>tot</sub> (mg)	q <sub>e</sub> (mg/kg)	Adsorbent
Variation of pH keeping C <sub>0</sub> and Q <sub>0</sub> constant	2	10	1.25	412	2058	3425	2572.50	4280.84	3.99	34.86	42.81	58	ZrOCS
	4	10	1.25	412	316	944	394.26	1180.41	6.66	5.34	11.80	16	
	6	10	1.25	412	161	495	200.89	618.75	6.75	2.72	6.19	8.39	
	2	10	1.25	412	309	783	386.25	941.25	5.60	5.23	9.41	12.76	VSc
	4	10	1.25	412	137	318	170	386.25	5.70	2.30	3.86	5.23	
	6	10	1.25	412	91	275	114.13	343.75	6.68	1.55	3.44	4.66	
Variation of Q <sub>0</sub> keeping pH and C <sub>0</sub> constant	2	10	1.25	412	2058	3425	2572.50	4280.84	3.99	34.86	42.81	58	ZrOCS
	2	10	2.50	206	721	1262	1803.05	3153.60	4.28	24.44	31.54	42.54	
	2	10	3.75	137	336.23	647.67	1260.86	2053.76	4.81	17.09	20.54	27.83	
	2	10	1.25	412	309	753	386.25	941.25	5.90	5.53	9.51	12.76	VSc
	2	10	2.50	206	155	353	386.58	881.58	5.61	5.24	8.82	11.95	
	2	10	3.75	137	65	217	243.41	813.49	7.01	3.30	8.15	11.02	

t<sub>b</sub> = breakthrough time, t<sub>e</sub> = exhaustion time, V<sub>b</sub> = total effluent volume at a breakthrough time, V<sub>e</sub> = total effluent volume at exhaustion time MTZ = Mass Transfer Zone, EBCT = Empty Bed Contact Time, q<sub>b</sub> = amount of fluoride removed at a breakthrough time per kg of adsorbent, q<sub>total</sub> = total amount of fluoride adsorbed from the column, q<sub>e</sub> = equilibrium fluoride uptake per kg of the adsorbent.

Thus, VSc has the briefest breakthrough and exhaustion time, whereas ZrOCS has the longest breakthrough and exhaustion time and, hence, improved adsorption performance. When the initial pH of the solution is greater than 2, the fluoride removal rate for ZrOCS and VSc decreases (Table 4.2). This may be assigned to the decrease in the amount of H<sup>+</sup> or HF adsorption due to electrostatic attraction (Geleta et al., 2021b, 2021c; Shang et al., 2019). Low pH promotes protonation of the adsorbent's surface. Increased protonation results in a greater number of positively charged sites per unit of surface area. Hence, the better adsorption performance at a pH of 2 might be corresponded to

the adsorbent surface having more positive charges at lower pH and electrostatically adsorbing fluoride ions (Shang et al., 2019). As a result, the fluoride ion sorption is caused by an electrostatic phenomenon and surface complexation, which can occur independently or in conjunction with the fluoride ion's adsorption on the adsorbents.

Furthermore, the pH value at the point of zero charges ( $pH_{PZC}$ ) of the adsorbents can be used to deduce this reality. The removal mechanism at  $pH < pH_{PZC}$  is possibly due to columbic attraction of fluoride by positive surface charges (Equation (4.13)) and/or ligand exchange reactions of fluoride with surface hydroxyl groups (Equation (4.14)).



Where, M represents Zr, Fe, Al, Si, Ca, etc.

In general, ZrOCSc and VScO depicted similar pH-dependent defluoridation performance. Nevertheless, the zirconium oxide coating significantly improved performance owing to the specific interaction between fluoride ions and the coated zirconium (hydr) oxide. A similar observation was witnessed in a recent study (Geleta et al., 2021c). At a pH of 2, the occurrence of the breakthrough time was longer and the volume of treated water was large. As a result, the pH of the solution was kept constant at a pH of 2 in the next experiment.

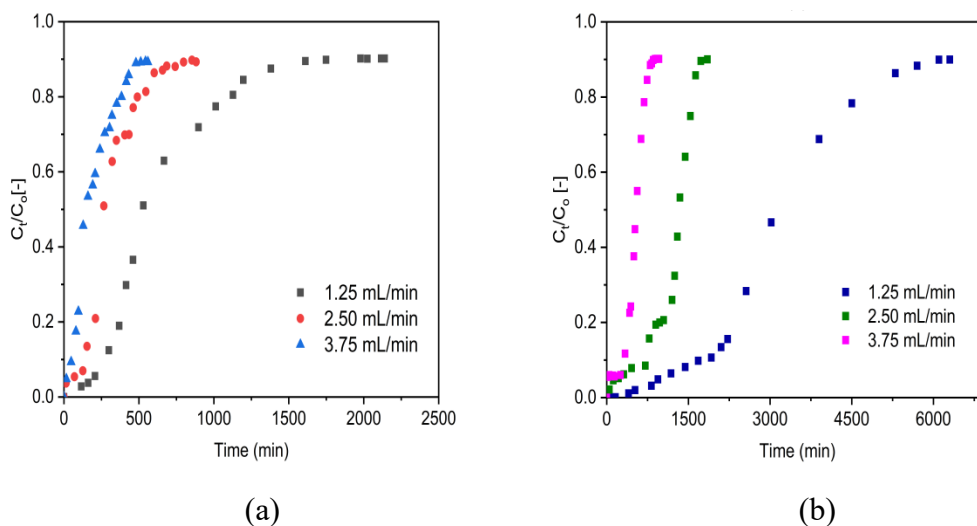
#### 4.3.2.2. Influence of Initial Flow Rate

Figure 4.7 depicts the breakthrough curves of VScO (Figure 4.7a) and ZrOCSc (Figure 4.7b) at various flow rates (1.25, 2.50, and 3.75 mL/min), and Table 4.2 displays their analysis results. As anticipated, as the flow rate increases, the breakthrough time is shortened, and the breakthrough curves become steeper. This means that the fluoride solution left the column before equilibrium was reached, resulting in limited fluoride ion removal. This characteristic is due to the short residence time in the column, and is also ascribed to the mass transfer zone (MTZ) (Table 4.2), which increases by increasing the flow rate, but narrows the fractional bed used (Geleta et al., 2021c; Lin et al., 2017). In addition, the breakthrough and exhaustion times were lowered with increasing the flow rate (Table 4.2). Accordingly, the breakthrough time observed was 2058, 721, and 336 min for ZrOCSc, and 309, 155, and 65 min for VScO corresponding to the volumetric flow rates of 1.25, 2.50, and 3.75 mL/min, respectively, and the exhaustion times were 3425, 1262, and 548 min for ZrOCSc, and 753, 353, and 217 min for VScO. At the breakthrough time, the amount of fluoride adsorbed (at constant initial concentration: 10 mg/L, pH: 2, and bed height: 10 cm) corresponded to 35, 24, and 17 mg/kg for



ZrOCSs, and 6, 5, and 3 mg/kg for VScO. The amounts adsorbed at exhaustion were 43, 32, and 21 mg/kg for ZrOCSs, and 10, 9, and 8 mg/kg for VScO. This can be illustrated by the fact that as the flow rate increased, an additional amount of fluoride in the solution was exposed to adsorbents. On the other hand, the decrease in the flow rates from 3.75 to 1.25 mL/min had a significant impact on the adsorption capacity at equilibrium, so that removal capacity increased from 27.83 to 58 mg/kg for ZrOCSs and 11.02 to 12.76 mg/kg for VScO. This may be ascribed to the fact that the fluoride ions have sufficient time to diffuse through the pores of the adsorbents and hence occupy more sites at a lower flow rate. The observations coincide with different studies (Geleta et al., 2021b, 2021c; Muthamilselvi et al., 2018). As the flow rate rose from 1.25 to 3.75 mL/min, the equilibrium adsorption capacity decreased, resulting in a decline in the residence time of the liquid. The empty bed contact time (EBCT) decreases due to the rise in the flow rate (Table 4.2), which means that at a lower flow rate, the interaction time between the adsorbent and the solution phase is longer than the larger flow rate. Our results are compatible with the findings of previous work (Fallah & Taghizadeh, 2020; Geleta et al., 2021b, 2021c).

Overall, the sensitivity of the adsorption to the flow rate of the solution can be related to the critical residence time of the solution in the column for each adsorption process. This means that the contact between the adsorbate solution and the adsorbents improved at a lower flow rate, leading to greater diffusion of fluoride ions onto the adsorbents bed and thus leading to maximum utilization of the sorption bed area.



**Figure 4.7** Effect of initial flow rate on the fluoride breakthrough (a) VScO and (b) ZrOCSs (pH 2;  $C_0$ : 10 mg/L; bed depth 10 cm)

This influence is also evidenced in improved bed performance and hence high fluoride uptake. Even though the influence of the initial flow rate was similar for both ZrOCSs and VScO, the zirconium



oxide coating showed significant improvement in fluoride adsorption capacity. The flow rate of 1.25 mL/min was observed to be optimal in this study, with a maximum fluoride uptake capacity of 58 mg/kg for ZrOCSc and 13 mg/kg for VScO, and was used in subsequent experiments.

In general, the variation of column parameters, such as  $q_e$ ,  $q_b$ ,  $V_e$ , and  $V_b$ , acquired for fluoride removal onto ZrOCSc and VScO under different experimental conditions demonstrated that ZrOCSc has higher activity than VScO towards fluoride (Table 4.2). The improved activity and thus adsorption performance could be ascribed to the coating of VScO with zirconium oxide.

#### 4.3.3. Application of the Thomas Model

For evaluation of the rate constant ( $K_T$ ) and the maximum adsorption capacity ( $q_0$ ), the experimental data (denoted as exp.) and simulated data (denoted as cal.) were fitted with the non-linear Thomas model (Equation (4.10)). The analysis of the experimental findings related to various pH (Figure 4.8a and 4.8b) and flow rates (Figure 4.9a and 4.9b) performed on the Thomas model was predicted.

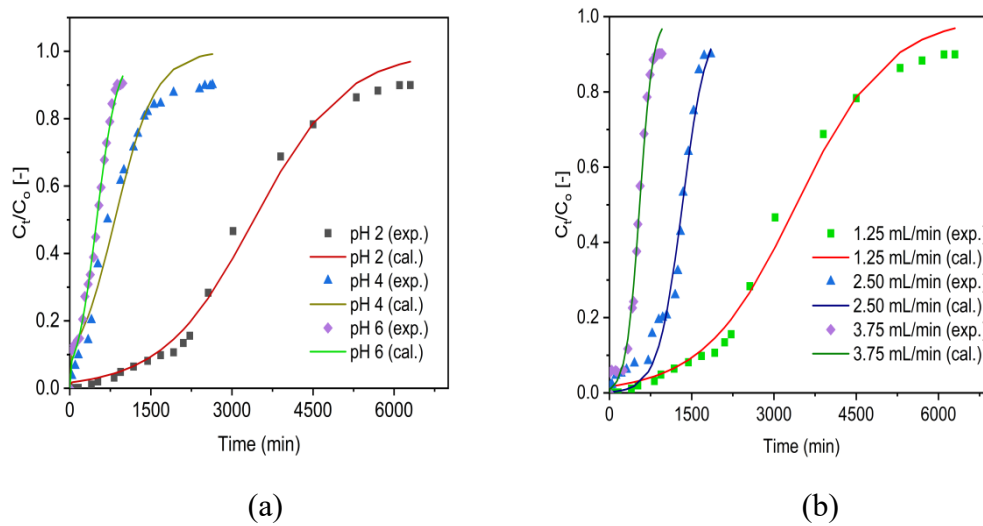


**Figure 4.8** Experimental (exp.) and simulated (cal.; Thomas model) breakthrough curves of fluoride for ZrOCSc at different (a) pH ( $C_0$ : 10 mg/L;  $Q_0$ : 1.25 mL/min; bed depth 10 cm) and (b) Initial flow rate,  $Q_0$  (pH 2;  $C_0$ : 10 mg/L; bed depth 10 cm)

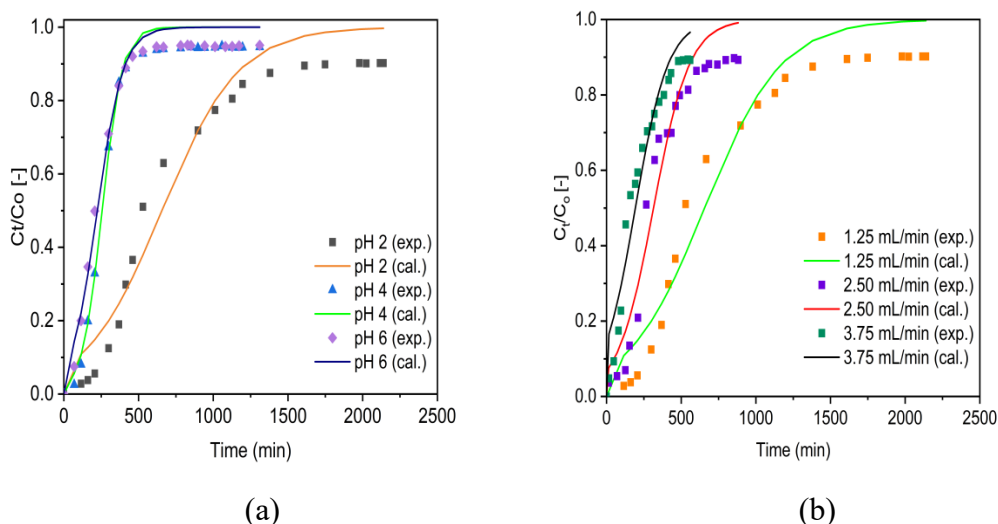


**Figure 4.9** Experimental (exp.) and simulated (cal.; Thomas model) breakthrough curves of fluoride for VScO at different (a) pH ( $C_0$ : 10 mg/L;  $Q_0$ : 1.25 mL/min; bed depth 10 cm) and (b) Initial flow rate,  $Q_0$  (pH 2;  $C_0$ : 10 mg/L; bed depth 10 cm)

The model parameters are depicted in Table 4.3. As can be noted from Figures 4.8 and 4.9, the breakthrough curves appeared to move from right to left as the pH and inlet flow rate increased from 2 to 6 and 1.25 to 3.75 mL/min, respectively. For both adsorbents (ZrOCS and VScO), the concentration values ( $q_0$ ) calculated by the Thomas model (Equation (4.10)) were comparable to the obtained experimental values ( $q_e$ ) (Table 4.3). The value of  $q_0$  decreased from 58 to 9 (mg/kg) for ZrOCS and from 11 to 4 (mg/kg) for VScO with increased pH (2 to 6) and flow rates (1.25 to 3.75 mL). A higher value of  $K_T$  indicated a faster approach to the equilibrium with an increasing inlet flow rate, while that of  $q_0$  showed an opposite trend, showing that the EBCT decreased (Geleta et al., 2021b, 2021c; Muthamilselvi et al., 2018). An increase in  $q_0$  with decreasing flow rates is the result of a longer interaction time between fluoride ions and adsorption sites (Geleta et al., 2021c; Ghosh et al., 2015; Ghosh et al., 2014a). Consequently, a lower flow rate results in a higher value of  $q_0$ . The regression coefficient,  $R^2$  being high (ranging from 0.976 to 0.996 for ZrOCS, and from 0.953 to 0.994 for VScO), as displayed in Table 4.3, advocated that the Thomas model exhibited a good fit to the experimental adsorption data gained in the present works. The values obtained from the optimization of the Thomas model confirmed that the zirconium oxide coating improved the fluoride removal performance of VScO.

**Table 4.3** Thomas model parameter values for the defluoridation by VScO and ZrOCS

Parameter studied	pH	$C_0$ (mg/L)	Q (mL/min)	Bed-depth, $H_B$ (cm)	$K_T$ (L/min.mg) ( $\times 10^4$ )	$q_0$ (cal.) (mg/kg)	$q_e$ (exp.) (mg/kg)	$R^2$	Adsorbent
Variation of pH	2	10	1.25	10	1.192	57.71	58	0.992	ZrOCS

keeping $C_0$ and $Q_0$ constant	4	10	1.25	10	2.642	14.13	16	0.976	VSco
	6	10	1.25	10	5.253	8.45	8.39	0.996	
	2	10	1.25	10	3.892	11.12	12.76	0.967	
	4	10	1.25	10	15.083	4.34	5.23	0.977	
	6	10	1.25	10	15.634	3.78	4.66	0.994	
Variation of $Q_0$ keeping pH and $C_0$ constant	2	10	1.25	10	1.192	57.71	58	0.992	ZrOCSc
	2	10	2.50	10	4.542	45.09	42.54	0.980	
	2	10	3.75	10	8.277	28.03	27.83	0.993	
	2	10	1.25	10	3.892	11.12	12.76	0.967	
	2	10	2.50	10	8.333	10.66	11.95	0.961	
	2	10	3.75	10	9.127	9.81	11.02	0.953	VSco

#### 4.3.4. Application of the Adams-Bohart Model

Plots for experimental (denoted as exp.) and simulated (denoted as cal.) breakthrough data based on the Adams-Bohart model for VSco and ZrOCSc at various initial pH values and initial flow rates are shown in Figures 4.10 and 4.11, respectively.

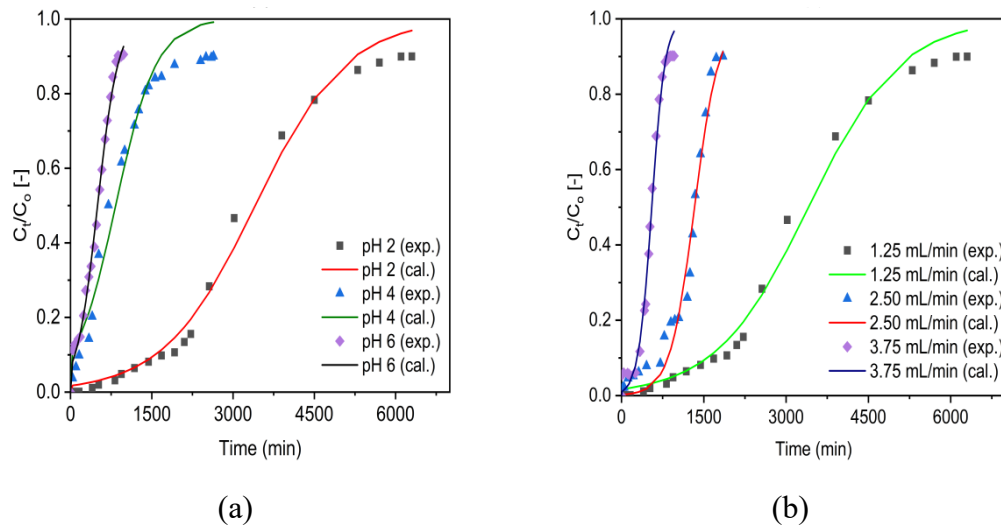


**Figure 4.10** Experimental (exp.) and simulated (cal.; Adams-Bohart model) breakthrough curves of fluoride for ZrOCSc at different (a) pH ( $C_0$ : 10 mg/L;  $Q_0$ : 1.25 mL/min; bed depth 10 cm) and (b)  $Q_0$  (pH 2;  $C_0$ : 10 mg/L; bed depth 10 cm).

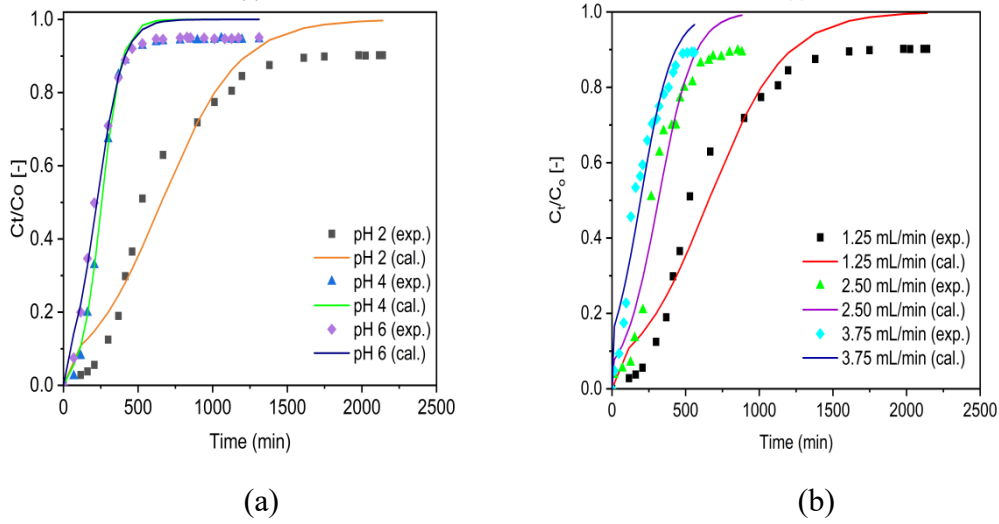


**Figure 4.11** Experimental (exp.) and simulated (cal.; Adams-Bohart model) breakthrough curves of fluoride for VSCO at different (a) pH ( $C_o$ : 10 mg/L;  $Q_o$ : 1.25 mL/min; bed depth 10 cm) and (b)  $Q_o$  (pH 2;  $C_o$ : 10 mg/L; bed depth 10 cm).

As can be seen from Figures 4.10 and 4.11, the breakthrough curves looked to move from right to left as the pH and inlet flow rate increased from 2 to 6 and 1.25 to 3.75 mL/min, respectively. The Adams-Bohart rate constant ( $K_{AB}$ ) and adsorption capacity of the adsorbents per unit volume of the bed ( $N_o$ ) predicted by the model are presented in Table 4.4. Similar to the Thomas model, as the initial flow rate is increased from 1.25 to 3.75 mL/min, the maximum volumetric adsorptive capacity of the bed ( $N_o$ ) decreased from 83 to 40 mg/L for ZrOCS and 16 to 14 mg/L for VSCO. Furthermore, the values of kinetics constant  $K_{AB}$  increased and values of EBCT decreased as the flow rate increased. This resulted in decreased  $N_o$  values. A decrease in  $N_o$  values with increasing flow rates is ascribed to the reduction in EBCT due to the direct proportion of the adsorption capacity to the interaction time. This is in agreement with previous studies (Geleta et al., 2021b, 2021c; A. Ghosh et al., 2015). As a result, the higher flow rate leads to a lower  $N_o$  value due to shorter interaction between the adsorbents and fluoride ions. The values of  $N_o$  decreased from 83 to 12 (mg/L) for ZrOCS and from 16 to 5 (mg/L) for VSCO with increased pH, while the other conditions remained constant (Table 4.4). The value of the coefficient of determination ( $R^2$ ) varies from 0.976 to 0.996 for ZrOCS, and from 0.953 to 0.993 for VSCO. The high values of  $R^2$  indicate the goodness of fit between the experimental data and the corresponding simulated data by the model. Thus, the model is suitable for depicting the adsorption behavior of fluoride in ZrOCS and VSCO. The results of the Adams-Bohart model optimization confirmed that the zirconium coating improved the defluoridation performance of VSCO.

On whole, the disparity of the Thomas and Adams-Bohart parameters for fluoride uptake onto ZrOCS and VSCO at different experimental parameters (as depicted in Table 4.3 and Table 4.4), indicated that

ZrOCSs performed better than VScs in defluoridation. This proved that the zirconium oxide coating positively affected the defluoridation potential of VScs.

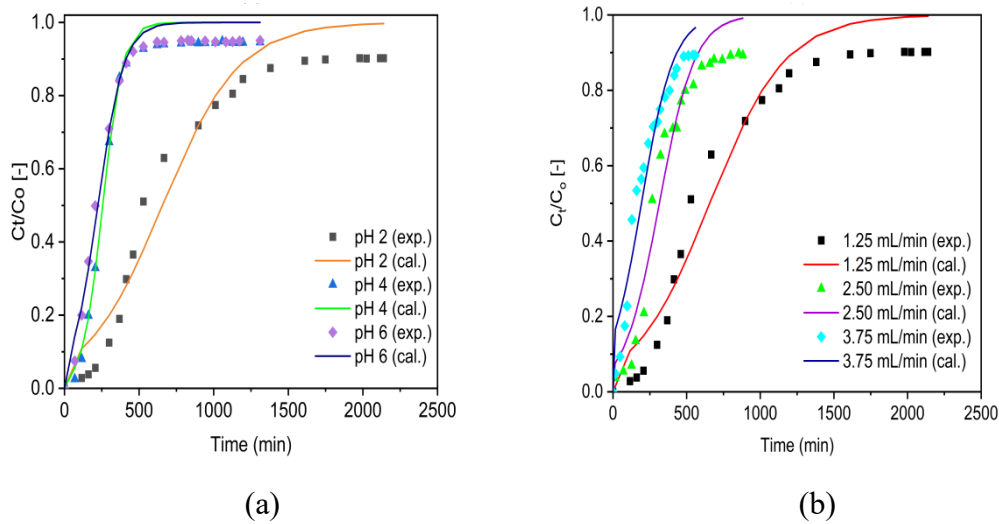


**Figure 4.12** Experimental (exp.) and simulated (cal.; Adams-Bohart model) breakthrough curves of fluoride for VScs at different (a) pH ( $C_o$ : 10 mg/L;  $Q_o$ : 1.25 mL/min; bed depth 10 cm) and (b)  $Q_o$  (pH 2;  $C_o$ : 10 mg/L; bed depth 10 cm).

**Table 4.4** Adams-Bohart model parameter values for defluoridation by ZrOCSs and VScs.

Parameter studied	pH	$C_o$ (mg/L)	Q (mL/min)	Bed-depth, $H_B$ (cm)	$K_{AB}$ (L/min.mg) ( $\times 10^4$ )	$N_{O(cal.)}$ (mg/L)	$R^2$	Adsorbent
Variation of pH keeping $C_o$ and $Q_o$ constant	2	10	1.25	10	1.192	82.78	0.992	ZrOCSs
	4	10	1.25	10	2.642	20.26	0.976	
	6	10	1.25	10	5.253	12.12	0.996	
	2	10	1.25	10	3.892	15.95	0.967	VScs
	4	10	1.25	10	15.083	6.23	0.977	
	6	10	1.25	10	11.634	5.43	0.994	
Variation of $Q_o$ keeping pH and $C_o$ constant	2	10	1.25	10	1.192	82.78	0.992	ZrOCSs
	2	10	2.50	10	4.542	64.55	0.980	
	2	10	3.75	10	8.277	40.16	0.993	
	2	10	1.25	10	3.892	15.95	0.967	VScs
	2	10	2.50	10	8.333	15.26	0.961	
	2	10	3.75	10	9.127	14.05	0.953	

#### 4.3.5. Fluoride Adsorption Performance of Different Adsorbents

Table 4.5 compares the adsorbent (ZrOCSs) used in this study with previously studied adsorbents for fluoride uptake in a flow-through fixed-bed column system.

**Table 4.5** Fluoride uptake capacity of some reported adsorbents

Adsorbents	Bed Height (cm)	Fluoride Level in (mg L <sup>-1</sup> )	Adsorption Capacity (mg g <sup>-1</sup> )	References
Granular acid-treated bentonite	28	6.34	0.190	(Ma et al., 2011)
Granular acid-treated bentonite	28	2.85	0.169	(Ma et al., 2011)
Aluminum-modified iron oxide	10.5	4	0.139	(García-sánchez et al., 2013)
Virgin Scoria (VSco*)	10	10	0.022	(Geleta et al., 2021b)
Virgin Scoria (VSco**)	10	10	0.013	(Geleta et al., 2021b)
ZrOCSc	10	10	0.058	This study

VSco\*: <0.075 mm; VSco\*\*: 0.075–0.425 mm.

Table 4.5 shows that the fluoride uptake capacity of ZrOCSc used in this study is greater than that of VSco\* and VSco\*\*. Furthermore, as shown in Table 4.5, ZrOCSc with a short bed height and a high initial fluoride concentration could be safely comparable with the adsorption performance of granular acid-treated bentonite and aluminum-modified iron, both of which have relatively long bed heights and low initial concentrations. Above all, unlike some of the other substrates, the raw material (VSco) is easily accessible and readily available, confirming that ZrOCSc could be a viable option for fluoride uptake from water. However, further investigation to improve its adsorption capacity might be considered.

#### 4.4. Conclusions

In this work, virgin scoria (VSco) and zirconium oxide-coated scoria (ZrOCSc) were examined for fluoride adsorption in fixed-bed column systems. The XRD analysis revealed that the VSco surface was coated with zirconium oxide. The absence of harmful substances on both adsorbents and the amount of zirconium oxide coated on VSco was evident from ICP-OES and XRF analysis. The FTIR analysis displayed there was an insignificant disparity between VSco; ZrOCSc spectrum before and after fluoride adsorption. The recorded SEM image clearly showed the degree of surface modification with improved porosity. Thermal analysis of VSco and ZrOCSc showed lower overall weight losses of 2.3 and 3.2 percent, respectively, due to the removal of water molecules and OH species bound to metal oxides contained in the material. The pH<sub>PZC</sub> analysis depicted that the surface charge of VSco and ZrOCSc was positive when the pH of the solution is below pH<sub>PZC</sub> of 8.3 and 8.7, respectively. The defluoridation capability of the ZrOCSc was 4.46 times greater than that of VSco under optimum

experimental conditions (pH 2 and influent flow rate of 1.25 mL/min). The breakthrough time of ZrOCSs was 6.66 times longer than that of VScs; consequently, the treated water volume at breakthrough for ZrOCSs was 2573 mL (6.66 times that of VScs). This improved performance could be ascribed to the zirconium oxide coating onto the VScs. The experimental results were well fitted by the Adams–Bohart and Thomas models, indicating that the attained models' parameters could be used to upscale the design of ZrOCSs and VScs-based defluoridation filters without the need for additional experimentation. According to this study, the coating of a low-cost adsorbent material, VScs, with zirconium oxide had a beneficial influence on its surface and improved its defluoridation performance. Therefore, ZrOCSs is a worthy material to eliminate high levels of fluoride in groundwater. However, further studies, such as regeneration and competing anions tests, are needed to conclude that the defluoridation of water with ZrOCSs is an economically viable and sustainable process.

## **5. Synthesis, General Outlook, Limitations, and Recommendations for Further study**

### **5.1. Overview**

Safe and potable drinking water for every individual by 2030 is one of the sustainable development goals of the United Nations Development Program. In recent years, groundwater contamination with high fluoride concentrations caused by geochemical reactions and geological or anthropogenic sources has resulted in a drinking water crisis globally ([Ahmad et al., 2022](#)). The presence of a high concentration of fluoride in groundwater, particularly in the East African Rift Valley (the main Ethiopian Rift Valley), is becoming the main challenge in terms of its utilization, leading to a serious health problem. Therefore, the treatment of fluoride-polluted water is a necessary and the only solution to avoid the consumption of excess fluoride as a protective measure. However, due to financial constraints, technical incapability, lack of awareness, and the lack of known effective treatment, excess fluoride concentration in drinking water in the main Ethiopian rift valley areas became a critical issue. Therefore, this study is conducted by considering different objectives with the main aim of investigating the unmodified and surface-modified adsorbents derived from low-cost and easily accessible volcanic rock materials for the treatment of fluoride-laden water in flow-through fixed-bed column adsorption systems. Further, how surface modification of raw adsorbents can improve fluoride adsorption performance was discussed. Furthermore, various physicochemical characteristics of the adsorbents before and after adsorption experiments have been evaluated to reveal the adsorption efficiency and mechanisms of the adsorbents. It has also evaluated how different experimental conditions, such as adsorbent particle size, initial solution pH, and initial flow rate, can affect the adsorption performance of the adsorbents. The Thomas and Adams-Bohart models, which are commonly used fixed-bed column models, were also used in the experimental breakthrough data to provide the necessary information for process design and optimization. The intention of this chapter (Chapter 5) is therefore to integrate all the findings from each specific objective, followed by a review of relevant results from previous studies, which link to a discussion of how this study addressed the research questions. Specific and detailed discussions and conclusions are already presented in the corresponding chapters. The general conclusions, general outlook, limitations, and recommendations for possible future work are also highlighted.

### **5.2. Synthesis**

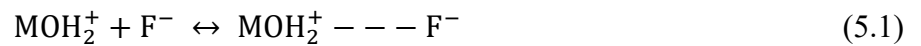
#### **5.2.1. Physiochemical Characteristics of the Adsorbents**

It is well understood that every purification agent must meet the basic characteristics of the filter media before it can be considered for use. Accordingly, the characterization of well-prepared unmodified and



surface-modified adsorbent materials before and after adsorption was carried out using various techniques such as X-ray diffraction (XRD), X-ray fluorescence (XRF) analysis, scanning electron microscopy (SEM), Fourier transform infrared (FTIR) analysis, Brunauer-Emmett-Teller (BET) specific surface area, inductively coupled plasma-optical emission spectroscopy (ICP-EOS), and pH point of zero charges ( $\text{pH}_{\text{PZC}}$ ) to demonstrate their physicochemical properties. The comparison of the X-ray diffractogram with the database of the X'pert HighScore Plus software package (version: 2.2b 2.2.2) showed that the main crystalline phases of VSco were Silicon Oxide ( $\text{SiO}_2$ ), Albite low ( $\text{Na}(\text{AlSi}_3\text{O}_8)$ ), whereas Hematite ( $\text{Fe}_2\text{O}_3$ ), Silicon Oxide ( $\text{SiO}_2$ ), and Albite high ( $\text{Na}(\text{AlSi}_3\text{O}_8)$ ) are the dominant components of VPum. The results obtained from XRD for surface-modified adsorbents (zirconium-coated pumice: Zr – Pu; and zirconium-oxide coated scoria: ZrOCSc) revealed that zirconium oxide was coated on the surface of unmodified rock materials, and consequently improved the defluoridation performance of the materials. Previous studies like Asere et al. (2017a) and Salifu et al. (2017) also demonstrated the same observations. The ICP-OES characterization investigation demonstrated that Si, Al, Fe, and K are the main elemental composition of VPum, whereas Si, Al, Fe, and Ca are the main elemental content of VSco. This confirmed the absence of harmful substances in both adsorbents which is consistent with previous research findings (Alemayehu et al., 2011; Asere et al., 2017a). The ICP-OES measurement also showed that the amount of zirconium coated on VPum and VSco was 3.9 % wt and 1.2 % wt, respectively, which could have improved the fluoride adsorption performance of the adsorbents. The recorded SEM images in Geleta et al. (2021b) revealed the presence of interconnected inner porous surfaces in VPum (Figure 2.3a) and the presence of dead zones in VSco (Figure 2.3b). The presence of interconnected inner porous surfaces in pumice in Asgari et al. (2012) and X. Li et al. (2010), whereas the presence of dead zones in scoria in Moradi et al. (2015), resembles the results in Geleta et al. (2021b) for VPum and VSco, respectively. The degree of surface modification with the enhanced porosity of Zr–Pu (Figure 3.4b) in Geleta et al. (2021c) and ZrOCSc (Figure 4.4b) in Geleta et al. (2022) was also evident from the recorded SEM micrographs. Sepehr et al. (2013) and Liang and Ni (2009) made similar observations for surface modification of pumice and salt treatment of zeolite, respectively, with a keen interest to develop inexpensive adsorbents. The oxides of Si, Fe, and Al as the main constituents of both VPum (Table 3.1) and VSco (Table 4.1) were revealed by XRF analysis. An earlier study found comparable values for VSco and VPum (Alemayehu & Lennartz, 2009). Moreover, the XRF analysis revealed that the amount of zirconium oxide coated on VPum was 8.9 % wt and 8.3 % on VSco, which was enough to improve fluoride uptake performance. The higher amount of zirconium oxide coated on VPum than VSco is due to VPum being more porous than VSco, which is similar to the results for cerium-loaded volcanic rocks reported by Asere et al. (2017a). The FTIR spectrum study confirmed the interaction of the

active adsorption site with fluoride ions. FTIR examinations, on the other hand, revealed a negligible difference in spectrum changes between unmodified and surface-modified adsorbents, which could be attributed to the equipment's inability to detect the difference. This finding is consistent with previous studies reported by Dou et al. (2012) and Sepehr et al. (2014). This demonstrates that the use of complementary characterization equipment such as NMR/XPS may be advantageous for future research. The BET specific surface area ( $S_{\text{BET}}$ ) analysis revealed that the specific surface area of VPum is larger than that of VSco. Furthermore, BET analysis demonstrated the enhancement of the specific surface area of the surface-modified VPum. The pore size distribution gained by the Barrett–Johner–Halenda (BJH) method showed that VPum and Zr–Pu are mesopore materials by the IUPAC classification; so, they can be appropriate adsorbents for the binding of fluoride ions (Fallah & Taghizadeh, 2020). The TGA/DTA analysis for VSco (see Figure 4.5a) and ZrOCSc (see Figure 4.5b) in Geleta et al. (2022) showed that the overall weight losses of both adsorbents were lower (2.3 % for VSco and 3.2 % for ZrOCSc), which could be attributed to the removal of moistures as well as that of OH species linked to metal oxides and volatile organic impurities present at low levels. This demonstrates that the adsorbents have good thermal durability up to 900 °C, which is consistent with Alraddadi & Assaedi (2021) findings for scoria and pumice volcanic rocks. Analysis of pH and  $\text{pH}_{\text{PZC}}$  revealed that the pH in water and the  $\text{pH}_{\text{PZC}}$  of the surface-modified adsorbents were lower than those of the unmodified adsorbents (Asere et al., 2017a). When the pH of the solution was lower than  $\text{pH}_{\text{PZC}}$ , the surface of the adsorbents is positively charged. This is because the hydroxyl groups on the surface of the adsorbents were protonated at lower pH (Wu et al., 2017). Therefore, the removal mechanism at  $\text{pH} < \text{pH}_{\text{PZC}}$  is possibly due to the columbic attraction of fluoride by positive surface charges (Equation (5.1)) and/or ligand exchange reactions of fluoride with surface hydroxyl groups (Equation (5.2)) (Chao et al., 2019).



Where M denotes the metal ion.

## 5.2.2. Effect of Experimental Conditions on Fluoride Removal

### 5.2.2.1. Effect of Adsorbent Particle Size

The effect of the particle size on the breakthrough behavior of fluoride was investigated for unmodified adsorbents (Chapter 2; Section 2.3.2) with grain size classes of silt to medium sand ( $< 0.075$ ,  $0.075$ – $0.425$ ,  $0.425$ – $2.00$  mm). On reducing the particle size from medium ( $0.425$ – $2.00$  mm) to silt ( $< 0.075$  mm) the breakthrough and exhaustion time noticeably increased for VSco, while the breakthrough and

exhaustion time was high for VPum at a fine particle size (0.075–0.425 mm) (Table 2.2). VPum was found to be effective in removing fluoride in an aqueous solution with a maximum uptake capacity ( $q_e$ ) of 110 mg/kg at a particle size of 0.075 – 0.425 mm, while the maximum removal capacity of VScO was 22 mg/kg at a particle size of < 0.075 mm (Figure 5.1).

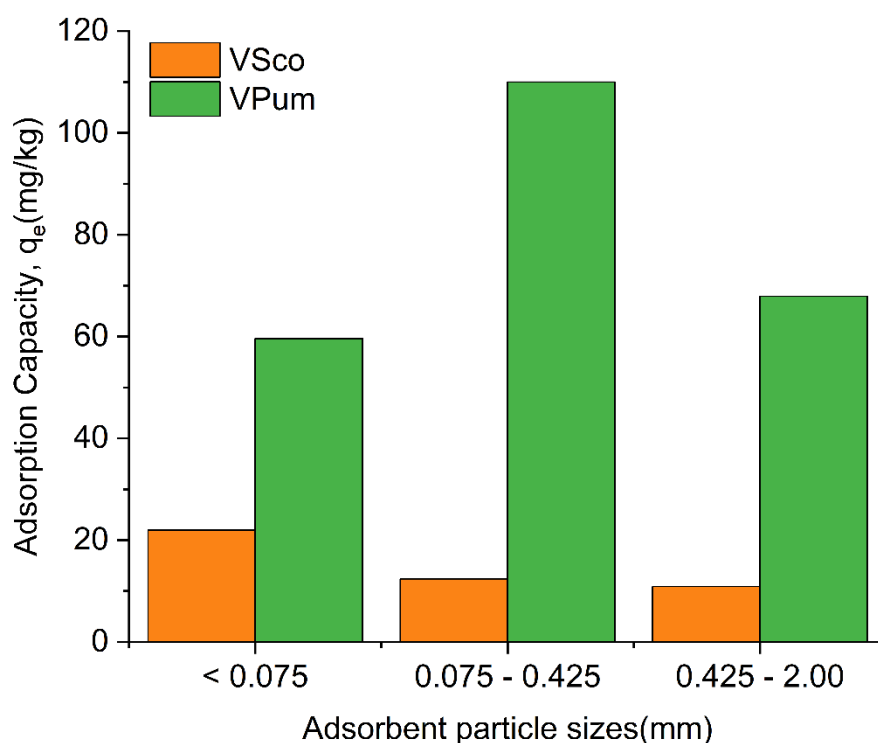


**Figure 5.1** Effects of particle sizes on the adsorption performance of VScO and VPum (pH 2.00;  $C_o$ : 10 mg/L;  $Q_o$ : 1.25 mL/min; bed depth 10 cm)

The reduction of particle size of an adsorbent, as shown in Figure 5.1, is a significant controlling factor in the fluoride–VScO system (at a particle size of < 0.075 mm the fluoride uptake was high). A similar effect was observed for VPum (at a particle size of 0.075–0.425 mm the fluoride sorption capacity was high). However, the effect of particle size on adsorption capacity is more pronounced for VScO than for VPum (see Figure 2.5 and Figure 5.1). This infers that VPum loses its internal porosity at the smallest particle size (< 0.075 mm) since the continuum pore space (skeletal structure) is damaged when compared to the fine particle size (0.075–0.425 mm) (see Figure 2.3a) and resulting in the smaller internal pore surface areas; consequently, the removal capacity of the adsorbent decreased. The aforementioned observation in Geleta et al. (2021b) was also observed by Alemayehu and Lennartz (2009) and X.Li et al. (2010).

#### 5.2.2.2. Effect of pH

The initial pH of the fluoride solution is also critical for fluoride adsorption. The chemically active

site of the adsorbents can be altered by changing the initial pH of the solution (Akafu et al., 2019). The effect of solution pH on fluoride adsorption using unmodified and surface-modified adsorbents was investigated at different pH (2.00, 4.00, and 6.00) by a separate set of fixed-bed adsorption columns. As can generally be observed in this thesis from Chapters 2-4 and also in Figure 5.2 below, the adsorption capacity of the adsorbents increased noticeably with decreasing pH. Furthermore, for all adsorbents used in the present study, the breakthrough curves (see Figures 2.6, 3.5, and 4.6) appeared to move from right to left as the pH increased from 2 to 6. The locally available unmodified materials have a defluoridation performance of 110 mg/kg (VPum: 0.075 – 0.425 mm) and 22 mg/kg (VScO: < 0.075 mm) at a solution pH of 2 and an initial flow rate of 1.25 mL/min (see Table 2.2). A defluoridation performance of 225 mg/kg was gained for Zr-Pu (2.05 times the adsorption capacity of VPum: 110 mg/kg) (see Table 3.3), whereas the defluoridation capacity of 58 mg/kg was achieved for ZrOCSc, which was 4.46 times higher than the adsorption capacity for VScO (13 mg/kg) at a solution pH of 2 and initial flow rate of 1.25 mL/min (see Table 4.2). The unmodified and surface-modified adsorbents were found to exhibit good fluoride adsorption performance at a lower pH of 2 (see Figure 5.2). As stated in this thesis (see Sections 2.3.3, 3.3.2.1, and 4.3.2.1), the higher uptake capacity at pH 2 could be attributed to the fact that the adsorbent surface has more positive charges at lower pH and electrostatically adsorbs fluoride ions. Other researchers have revealed similar observations (Akafu et al., 2019; Chao et al., 2019; Shang et al., 2019).

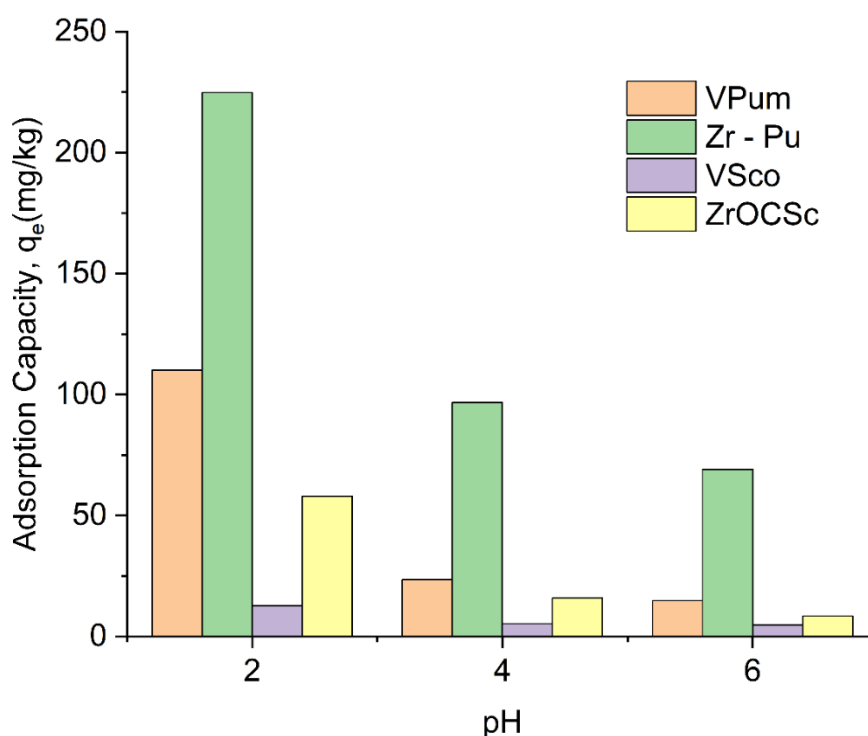


**Figure 5.2** Effects of solution pH on the adsorption performance of the adsorbents (particle sizes: 0.075 – 0.425 mm;  $C_0$ : 10 mg/L;  $Q_0$ : 1.25 mL/min; bed depth 10 cm)

Therefore, the adsorption of fluoride ions was due to an electrostatic phenomenon and surface complexation, which can occur alone or in conjunction with the uptake of fluoride ions on the adsorbents (Alemayehu et al., 2011; Fufa et al., 2013; Salifu et al., 2013). In general, the pH-dependent fluoride removal capacities of the unmodified and surface-modified adsorbents were comparable. However, a noticeable improvement observed for surface-modified adsorbents in Geleta et al. (2021c) and (2022) was due to the zirconium coating, because of the specific interaction between fluoride ions and zirconium (hydr) oxide. This type of observation was also stated by Asre et al. (2017a) for the adsorption of As (III) and As (V) from aqueous solution by cerium-loaded volcanic rocks.

#### 5.2.2.3. Effect of Flow Rate

The effect of inlet fluoride-polluted water sample flow rate on the adsorption of fluoride using unmodified and surface-modified adsorbents was investigated at various flow rates (1.25, 2.50, and 3.75 mL/min). As expected, as the flow rate rose from 1.25 to 3.75 mL/min, the breakthrough and exhaustion times declined (see Tables 2.2, 3.3, and 4.2) and their curves became steeper (see Figures 2.7, 3.6, and 4.7). This means that the fluoride solution has exited the fixed-bed column before an equilibrium occurs and consequently resulted in limited fluoride ions uptake. This behavior is due to an insufficient residence time of the solution in the column at higher flow rates (higher hydraulic loading) or it could be because of channeling or preferential flow. This finding was further confirmed by Mass Transfer Zone or Unused Bed Length (MTZ/ $H_{UNB}$ ), which increases with increasing flow rate but narrows the utilized fractional bed (Lin et al., 2017). The increase in flow rate had a significant impact on the equilibrium/maximum adsorption capacity of the adsorbents. Accordingly, the maximum defluoridation capacity ( $q_e$ ) of the unmodified adsorbents in the column decreased from 110 to 17 mg/kg (VPum: 0.075 – 0.425 mm), 13 to 11 mg/kg (VScO: 0.075 – 0.425 mm), and 22 to 4 mg/kg (VScO: < 0.075 mm) as the flow rate increased from 1.25 to 3.75 mL/min (see Figure 5.3). Similarly, as shown in Figure 5.3, the maximum adsorption performance of surface-modified adsorbents decreased from 225 to 108 mg/kg (Zr–Pu) and 58 to 28 mg/kg (ZrOCSc) as the flow rate increased from 1.25 to 3.75 mL/min. Thus, in this study, the flow rate of 1.25 mL/min was found to be the optimum flow rate for fluoride adsorption. The Empty Bed Contact Time (EBCT) decreased as the flow rate increased, indicating that at lower flow rates, the interaction time between the adsorbent and solution phase is longer than at higher flow rates. The current study revealed that high flow rates reduced the contact time between the fluoride ions and the adsorbent surface leading to less fluoride adsorption, and decreased overall adsorption performance. This corresponds to the finding of Muthamilselvi et al. (2018) and Fallah & Taghizadeh (2020). Although the initial flow rate had a similar effect on both unmodified and zirconium-modified adsorbents, the zirconium coating increased

fluoride uptake. Furthermore, when compared to the other adsorbents studied, zirconium-coated pumice (Zr-Pu) was shown to be the most effective and promising option, indicating that it could be a good potential for fluoride-laden groundwater in fluorotic areas of low-income countries, where pumice is abundant.

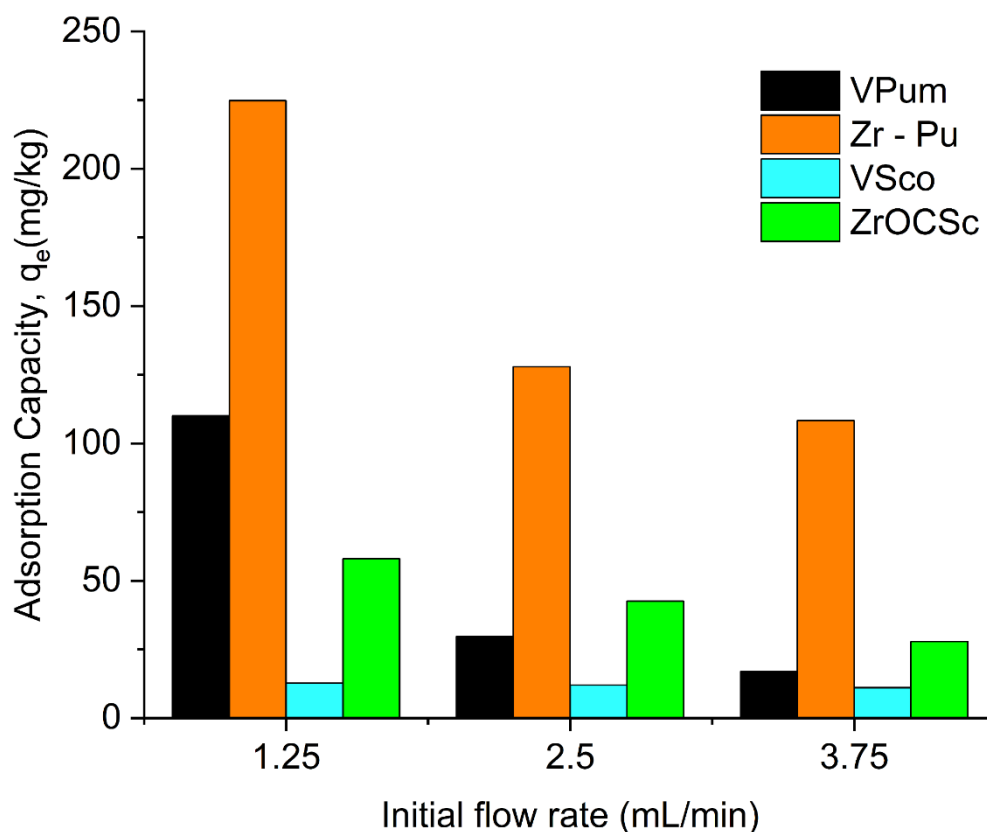


**Figure 5.3** Effects of initial flow rate on the adsorption performance of the adsorbents (particle sizes: 0.075 – 0.425 mm; pH: 2.00; bed depth 10 cm)

### 5.2.2. Application of the Thomas and Adams-Bohart Models

In this study, the Thomas model and the Adams-Bohart model were employed in the experimental data to describe the dynamic behavior of fluoride adsorption. The results of Geleta et al. (2021b), (2021c), and (2022) revealed that both models adequately described the experimental data at various experimental conditions (see Tables 2.3, 2.4, 3.4, 3.5, 4.3, and 4.4). Both models' breakthrough curves appeared to shift from the right to the left as the pH and inlet flow rate increased from 2 to 6 and 1.25 to 3.75 mL/min, respectively (see Figures A2.2, A2.3, 4.10, and 4.11). This indicates faster exhaustion of the adsorbents' bed, and hence lower fluoride removal performance of the adsorbents' bed (Salifu, 2017). The values of the Thomas rate constant ( $K_T$ ) and Adams-Bohart rate constant ( $K_{AB}$ ) decreased as the influent flow rate decreased. However, the adsorption capacity per unit mass of the bed of the adsorbents predicted by the Thomas model ( $q_0$ ; mg/kg) and the adsorption capacity per unit volume of the bed predicted by the Adams-Bohart model ( $N_0$ ; mg/L) increased as the flow rate decreased. An

increase in  $N_0$  and  $q_0$  values with decreasing flow rates is ascribed to the increase in the EBCT because of the direct proportion of the adsorption capacity to the interaction time. Similar observations were reported in previous studies (Ghosh et al., 2015; Sivasankar et al., 2010). Surface-modified adsorbents had the lowest rate constant values compared to unmodified adsorbents, indicating that diffusion mass transfer is greater for surface-modified adsorbents than for unmodified adsorbents (Sivasankar et al., 2010). The values obtained by the Thomas and Adams-Bohart models optimization confirmed that the zirconium coating enhanced the fluoride uptake capacity of VPum and VScO. In general, the Thomas and Adams-Bohart models described the experimental data very well at various experimental conditions with correlation coefficients ( $R^2$ )  $\geq 0.967$  and  $\geq 0.897$  for zirconium-modified adsorbents and unmodified adsorbents, respectively, revealing that the models are suitable tools for designing fixed-bed column systems using unmodified and surface-modified adsorbents, which can lead to the reduction of laboratory experimentation – saving time and cost (Hu et al., 2020).

Finally, based on the research described in this cumulative dissertation, the following conclusions (but not limited to) are generated:

- Variations of various process conditions such as particle sizes of adsorbents, influent flow rate, and initial solution pH; and variation of influent flow rate and initial solution pH have noticeably influenced the adsorption performance of unmodified and surface-modified adsorbents, respectively.
- The unmodified locally available materials have a defluoridation performance of 110 mg/kg (VPum: 0.075 – 0.425 mm) and 22 mg/kg (VScO: < 0.075 mm) at a pH of 2 and an initial flow rate of 1.25 mL/min. The effect of particle size on the adsorption capacity was more pronounced for VScO than VPum. This implies that VPum loses its internal porosity at the smallest particle size (< 0.075 mm) since the continuum pore space (skeletal structure) is damaged when compared to the fine particle size (0.075–0.425 mm) and resulting in smaller internal pore surface areas; consequently, the removal capacity of the adsorbent decreased.
- The zirconium-coated local materials with similar particle sizes (0.075 – 0.425 mm) were effective in scavenging excess fluoride from model water under flow-through continuous fixed-bed column systems. A defluoridation performance of 225 mg/kg was gained for Zr-Pu (2.05 times the adsorption capacity of VPum: 110 mg/kg), whereas the defluoridation capacity of ZrOCSO was 58 mg/kg (4.46 times the adsorption capacity of VScO: 13 mg/kg) at a pH of 2 and the initial flow rate of 1.25 mL/min.
- The comparison of the fluoride uptake capacity of the unmodified with the zirconium-modified locally available media of a similar particle size range (0.075 – 0.425 mm) showed

that the latter (i.e., zirconium modified media) had a significantly higher fluoride uptake capacity. A noticeable performance enhancement was seen due to the zirconium coating, primarily because of the specific interaction between fluoride ions and zirconium (hydr) oxide. However, zirconium-coated pumice (Zr-Pu) was found to be the most effective and promising candidate compared to the other adsorbents used in the current study, suggesting that it could be a good potential for fluoride-laden groundwater in fluorotic areas of low-income countries (with pumice availability).

- The unmodified and surface-modified adsorbents were found to exhibit good fluoride adsorption performance at a lower pH of 2 and a lower flow rate of 1.25 mL/min. This could be attributed to the adsorbent surface having more positive charges at lower pH and electrostatically adsorbing fluoride ions, and the interaction between the adsorbents and the adsorbate was longer at a lower flow rate. The longer breakthrough and exhaustion time was also obtained at lower values of pH and flow rate.
- The physicochemical characterization of the adsorbents was thoroughly investigated to reveal the adsorption mechanism. The XRD analysis showed that both unmodified and surface-modified adsorbents contain crystalline substances. Further, the XRD analysis presented that zirconium oxide was coated on the surface of VPum and VScO. The BET technique revealed that coating of VPum and VScO with zirconium oxide improved their specific surface area. The presence of interconnected inner porous surfaces in VPum, the presence of dead zones in VScO, as well as the degree of surface modification and enhanced porosity, were evident from the recorded SEM images. The FTIR examinations of the unmodified adsorbents, and modified adsorbents before/and after adsorption did not reveal any significant spectrum changes. This could be due to the inability of the FTIR equipment to detect the changes after modification and adsorption experiments. The ICP-OES analysis of both unmodified and surface-modified materials confirmed the absence of harmful substances. The XRF analysis showed that the major oxide compositions of the adsorbents were  $\text{SiO}_2$ ,  $\text{Al}_2\text{O}_3$ , and  $\text{Fe}_2\text{O}_3$ . Furthermore, XRF analysis revealed that the amount of zirconium oxide coated onto Zr – Pu and ZrOCSc was 8.9 % wt and 8.3 % wt, respectively, allowing for an enhanced defluoridation performance. TGA analysis of VScO and ZrOCSc revealed lower total weight losses of 2.3 and 3.2 percent, respectively, owing to the removal of water molecules and OH species linked to metal oxides contained in the material. The DTA thermogram of VScO and ZrOCSc demonstrated an endothermic peak as well as a narrow and broad exothermic peak.
- The fluoride uptake capacities of the natural and surface-modified adsorbent materials described in this thesis were found to be comparable to the capacities of some fluoride



adsorbents reported in the literature (see Sections 2.3.7, 3.3.5, and 4.3.5). Above all, the adsorbents used in the current study are widely available, inexpensive, and primarily part of the natural environment.

- The experimental adsorption data were well-matched by the Thomas and Adams-Bohart models with correlation coefficients ( $R^2$ ) of  $\geq 0.967$  (zirconium-modified adsorbents) and  $\geq 0.897$  (unmodified adsorbents). The parameters determined for these models can be helpful for engineers interested in optimizing the design of modified and surface-modified adsorbents column filters for the defluoridation of water which can lead to the reduction of laboratory experimentation – saving time and cost.

Finally, it can be concluded that the use of an unmodified and modification of the surface of the particles of locally available volcanic rocks (virgin pumice: VPum and virgin scoria: VSco) by zirconium coating was a useful approach for developing cost-effective and sustainable fluoride adsorbents. The information supplied would be helpful in the search for a potential adsorbent for the treatment of fluoride-contaminated groundwater, primarily in low-income countries like Ethiopia.

### 5.3. General Outlook, Limitations, and Recommendations for Further Study

The study aimed to investigate unmodified and surface-modified adsorbents derived from low-cost and easily accessible volcanic rock materials for the treatment of fluoride-laden groundwater in flow-through fixed-bed column adsorption systems. The outcome and conclusions of this research may be helpful to water providers for strategic planning for the provision of safe drinking, especially for the population residing in the rift valley area, to prevent the incidence of fluorosis and other fluoride-related health hazards. The research findings and conclusions also provide insight into the synthesis of fluoride adsorbents by modification of the surface properties of indigenous materials, using a zirconium coating process. The use of low-cost and easily available materials as base materials for the adsorbent synthesis can diminish production costs while improving long-term sustainability. Thus, the findings of this study may aid in the search for alternative suitable defluoridation materials that may be sustainable for the purification of fluoride-contaminated groundwater in low-income countries. The use of various high-tech equipment such as XRD, SEM, FTIR, XRF, BET, ICP-OES, and TGA/DTA for the characterizations of the adsorbents will advance the understanding of the adsorption mechanisms of the adsorbents and will also enhance their use for different applications. The use of different data analysis methods and fixed-bed column models for the interpretation of adsorption experimental data could also be helpful to researchers interested in the application of the adsorption technology for the purification of fluoride-laden water and the removal of other pollutants from the aqueous environment in general.

Although the research covered important areas concerning fluoride and the development of fluoride adsorbent materials, there are still many aspects that were either not covered or require further investigation as indicated below, and recommendations for future research studies:

- ✓ Further improvements to the adsorption capacity of the adsorbents, especially the capacity of raw scoria-based adsorbents, need to be explored.
- ✓ Representative samples of the rock materials have to be checked for possible composition changes induced over time as a result of weathering.
- ✓ Regeneration tests should be investigated as they may imply the economic viability of the system.
- ✓ Competing ion tests using real groundwater should be researched as the ions in groundwater can compete with fluoride for the same active sites which can impact the fluoride adsorption performance of the adsorbents.

Last, but not least, the raw materials used in this study are found in the same area, Ethiopia's Great Rift Valley, which has a high prevalence of fluorosis. The use of low-cost and locally available materials has implications for economic viability and sustainability. Fluoride treatment may be costly on a large scale for low-income countries, so water providers should focus on raising awareness, particularly among highly vulnerable communities, about the health effects of high fluoride levels in drinking water, and subsequently educating them to provide satisfactory and remedial technology. As a result, future research should concentrate on field pilot-scale studies that can aid in the development of easy-to-use household defluoridation units, particularly in the most fluorotic areas of the Great Ethiopian Rift Valley.

## References

- Abdolali, A., Ngo, H. H., Guo, W., Zhou, J. L., Zhang, J., Liang, S., Chang, S. W., Nguyen, D. D., & Liu, Y. (2017). Application of a breakthrough biosorbent for removing heavy metals from synthetic and real wastewaters in a lab-scale continuous fixed-bed column. *Bioresource Technology*, 229, 78–87. <https://doi.org/10.1016/j.biortech.2017.01.016>
- Abu Bakar, A. H., Abdullah, L. C., Mohd Zahri, N. A., & Alkhatib, M. (2019). Column Efficiency of Fluoride Removal Using Quaternized Palm Kernel Shell (QPKS). *International Journal of Chemical Engineering*, 2019, 5743590. <https://doi.org/10.1155/2019/5743590>
- Adeyi, A. A., Nurul, S., Jamil, A., Abdullah, L. C., Shean, T., Choong, Y., Lau, K. L., & Alias, N. H. (2020). Simultaneous Adsorption of Malachite Green and Methylene Blue Dyes in a Fixed-Bed Column Using Poly(Acrylonitrile-Co-Acrylic Acid) Modified with Thiourea. *Molecules*, 25(11), 2650. <https://doi.org/10.3390/molecules25112650>
- Ahmad, S., Singh, R., Arfin, T., & Neeti, K. (2022). Fluoride contamination, consequences and removal techniques in water: a review. *Environmental Science: Advances*, 94, 103916. <https://doi.org/10.1039/d1va00039j>
- Akafu, T., Chimdi, A., & Gomoro, K. (2019). Removal of Fluoride from Drinking Water by Sorption Using Diatomite Modified with Aluminum Hydroxide. *Journal of Analytical Methods in Chemistry*, 2019, 4831926. <https://doi.org/10.1155/2019/4831926>
- Aksu, Z., Çağatay, S. S., & Gönen, F. (2007). Continuous fixed bed biosorption of reactive dyes by dried *Rhizopus arrhizus*: Determination of column capacity. *Journal of Hazardous Materials*, 143(1–2), 362–371. <https://doi.org/10.1016/j.jhazmat.2006.09.039>
- Alemayehu, E., & Lennartz, B. (2009). Virgin volcanic rocks: Kinetics and equilibrium studies for the adsorption of cadmium from water. *Journal of Hazardous Materials*, 169, 395–401. <https://doi.org/10.1016/j.jhazmat.2009.03.109>
- Alemayehu, E., & Lennartz, B. (2010). Adsorptive removal of nickel from water using volcanic rocks. *Applied Geochemistry*, 25(10), 1596–1602. <https://doi.org/10.1016/j.apgeochem.2010.08.009>
- Alemayehu, E., Melak, F., Sharma, S. K., Bruggen, B. Van Der, & Lennartz, B. (2017). Use of porous volcanic rocks for the adsorptive removal of copper. *Water and Environmental Journal*, 2, 4–11. <https://doi.org/10.1111/wej.12234>
- Alemayehu, E., Thiele-Bruhn, S., & Lennartz, B. (2011). Adsorption behaviour of Cr (VI) onto macro and micro-vesicular volcanic rocks from water. *Separation and Purification Technology*, 78(1), 55–61. <https://doi.org/10.1016/j.seppur.2011.01.020>
- Alkurdi, S. S. A., Al-Juboori, R. A., Bundschuh, J., & Hamawand, I. (2019). Bone char as a green sorbent for removing health threatening fluoride from drinking water. *Environment International*, 127, 704–719. <https://doi.org/10.1016/j.envint.2019.03.065>
- Alraddadi, S., & Assaedi, H. (2021). Physical properties of mesoporous scoria and pumice volcanic rocks. *Journal of Physics Communications*, 5(11), 115018. <https://doi.org/10.1088/2399-6528/ac3a95>
- Aoudj, S., Khelifa, A., Drouiche, N., Belkada, R., & Miroud, D. (2015). Simultaneous removal of chromium(VI) and fluoride by electrocoagulation-electroflotation: Application of a hybrid Fe-

- Al anode. *Chemical Engineering Journal*, 267, 153–162.  
<https://doi.org/10.1016/j.cej.2014.12.081>
- Appel, C., & Ma, L. (2002). Concentration, pH, and Surface Charge Effects on Cadmium and Lead Sorption in Three Tropical Soils. *Journal of Environmental Quality*, 31(2), 581–589.  
<https://doi.org/10.2134/jeq2002.0581>
- Araga, R., Kali, S., & Sharma, C. S. (2019). Coconut-Shell-Derived Carbon/Carbon Nanotube Composite for Fluoride Adsorption from Aqueous Solution. *Clean - Soil, Air, Water*, 47(5), 1800286. <https://doi.org/10.1002/clen.201800286>
- Aregu, M. B., Asfaw, S. L., & Khan, M. M. (2018). Identification of two low-cost and locally available filter media (pumice and scoria) for removal of hazardous pollutants from tannery wastewater. *Environmental Systems Research*, 7, 10. <https://doi.org/10.1186/s40068-018-0112-2>
- Armienta, M. A., & Segovia, N. (2008). Arsenic and fluoride in the groundwater of Mexico. *Environmental Geochemistry and Health*, 30(4), 345–353. <https://doi.org/10.1007/s10653-008-9167-8>
- Asere, T. G., Verbeken, K., Tessema, D. A., Fufa, F., Stevens, C. V., & Du Laing, G. (2017a). Adsorption of As(III) versus As(V) from aqueous solutions by cerium-loaded volcanic rocks. *Environmental Science and Pollution Research*, 24(25), 20446–20458.  
<https://doi.org/10.1007/s11356-017-9692-z>
- Asere, T. G., Mincke, S., De Clercq, J., Verbeken, K., Tessema, D. A., Fufa, F., Stevens, C. V., & Du Laing, G. (2017b). Removal of arsenic (V) from aqueous solutions using chitosan–red scoria and chitosan–pumice blends. *International Journal of Environmental Research and Public Health*, 14(8), 895. <https://doi.org/10.3390/ijerph14080895>
- Asgari, G., Roshani, B., & Ghanizadeh, G. (2012). The investigation of kinetic and isotherm of fluoride adsorption onto functionalized pumice stone. *Journal of Hazardous Materials*, 217–218, 123–132. <https://doi.org/10.1016/j.jhazmat.2012.03.003>
- Ayoob, S., & Gupta, A. K. (2006). Fluoride in Drinking Water : A Review on the Status and Stress Effects. *Critical Reviews in Environmental Science and Technology*, 36(6), 433–487.  
<https://doi.org/10.1080/10643380600678112>
- Ayoob, S., & Gupta, A. K. (2007). Sorptive response profile of an adsorbent in the defluoridation of drinking water. *Chemical Engineering Journal*, 133(1–3), 273–281.  
<https://doi.org/10.1016/j.cej.2007.02.013>
- Ayoob, S., & Gupta, A. K. (2009). Performance evaluation of alumina cement granules in removing fluoride from natural and synthetic waters. *Chemical Engineering Journal*, 150, 485–491.  
<https://doi.org/10.1016/j.cej.2009.01.038>
- Ayoob, S., Gupta, A. K., & Bhat, V. T. (2008). A conceptual overview on sustainable technologies for the defluoridation of drinking water. *Critical Reviews in Environmental Science and Technology*, 38(6), 401–470. <https://doi.org/10.1080/10643380701413310>
- Banerjee, A. (2015). Groundwater fluoride contamination: A reappraisal. *Geoscience Frontiers*, 6(2), 277–284. <https://doi.org/10.1016/j.gsf.2014.03.003>
- Bejaoui, I., Mnif, A., & Hamrouni, B. (2014). Performance of Reverse Osmosis and Nanofiltration

- in the Removal of Fluoride from Model Water and Metal Packaging Industrial Effluent. *Separation Science and Technology (Philadelphia)*, 49(8), 1135–1145.  
<https://doi.org/10.1080/01496395.2013.878956>
- Bhatnagar, A., Kumar, E., & Sillanpää, M. (2011). Fluoride removal from water by adsorption-A review. *Chemical Engineering Journal*, 171(3), 811–840.  
<https://doi.org/10.1016/j.cej.2011.05.028>
- Birhane, M., Abebe, A., Alemayehu, E., & Mengistie, E. (2014). Efficiency of locally available filter media on fluoride and phosphate removal for household water treatment system. *Chinese Journal of Population Resources and Environment*, 12(2), 110–115.  
<https://doi.org/10.1080/10042857.2014.910873>
- Boehm, H. P. (1994). Some aspects of the surface chemistry of carbon blacks and other carbons. *Carbon*, 32(5), 759–769. [https://doi.org/https://doi.org/10.1016/0008-6223\(94\)90031-0](https://doi.org/https://doi.org/10.1016/0008-6223(94)90031-0)
- Bohart, G. S., & Adams, E. Q. (1920). Some aspects of the behavior of charcoal with respect to chlorine. *Journal of the American Chemical Society*, 42(3), 523–544.  
<https://doi.org/10.1021/ja01448a018>
- Cai, J., Zhang, Y., Pan, B., Zhang, W., Lv, L., & Zhang, Q. (2016). Efficient defluoridation of water using reusable nanocrystalline layered double hydroxides impregnated polystyrene anion exchanger. *Water Research*, 102, 109–116. <https://doi.org/10.1016/j.watres.2016.06.030>
- Cai, J., Zhang, Y., Qian, Y., Shan, C., & Pan, B. (2018). Enhanced Defluoridation Using Novel Millisphere Nanocomposite of La-Doped Li-Al Layered Double Hydroxides Supported by Polymeric Anion Exchanger. *Scientific Reports*, 8(1), 11741. <https://doi.org/10.1038/s41598-018-29497-1>
- Castel, C., Schweizer, M., Simonnot, M. O., & Sardin, M. (2000). Selective removal of fluoride ions by a two-way ion-exchange cyclic process. *Chemical Engineering Science*, 55(17), 3341–3352.  
[https://doi.org/10.1016/S0009-2509\(00\)00009-9](https://doi.org/10.1016/S0009-2509(00)00009-9)
- CDN (Catholic Diocese of Nakuru), & Müller, K. (2007). *CDN 'S EXPERIENCES IN PRODUCING BONE CHAR* (Vol. 2). Prepared jointly by CDN WQ and Eawag.
- Chao, C., Zhao, Y., Song, Q., Min, J., Wang, Z., Ma, H., & Li, X. (2019). Volcanic rock-based ceramsite adsorbent for highly selective fluoride removal: function optimization and mechanism. *Journal of Chemical Technology and Biotechnology*, 94(7), 2263–2273.  
<https://doi.org/10.1002/jctb.6014>
- Chatterjee, S., Mukherjee, M., & De, S. (2018). Defluoridation using novel chemically treated carbonized bone meal: batch and dynamic performance with scale-up studies. *Environmental Science and Pollution Research International*, 25(18), 18161–18178.  
<https://doi.org/10.1007/s11356-018-2025-z>
- Chaudhary, M., Rawat, S., Jain, N., Bhatnagar, A., & Maiti, A. (2019). Chitosan-Fe-Al-Mn metal oxyhydroxides composite as highly efficient fluoride scavenger for aqueous medium. *Carbohydrate Polymers*, 216, 140–148. <https://doi.org/10.1016/j.carbpol.2019.04.028>
- Chaudhry, S. A., Khan, T. A., & Ali, I. (2017). Zirconium oxide-coated sand based batch and column adsorptive removal of arsenic from water: Isotherm, kinetic and thermodynamic studies. *Egyptian Journal of Petroleum*, 26(2), 553–563.  
<https://doi.org/10.1016/j.ejpe.2016.11.006>

- Chen, I.-P., Kan, C.-C., Futralan, C., Calagui, M. J., Lin, S.-S., Tsai, W.-C., & Wan, M.-W. (2015). Batch and fixed bed studies: Removal of copper (II) using chitosan-coated kaolinite beads from aqueous solution. *Sustainable Environment Research*, 25(2), 73–81.
- Chen, N., Zhang, Z., Feng, C., Li, M., Chen, R., & Sugiura, N. (2011). Investigations on the batch and fixed-bed column performance of fluoride adsorption by Kanuma mud. *Desalination*, 268(1), 76–82. <https://doi.org/10.1016/j.desal.2010.09.053>
- Chen, N., Zhang, Z., Feng, C., Sugiura, N., Li, M., & Chen, R. (2010). Fluoride removal from water by granular ceramic adsorption. *Journal of Colloid and Interface Science*, 348(2), 579–584. <https://doi.org/10.1016/j.jcis.2010.04.048>
- Chen, P., Wang, T., Xiao, Y., Tian, E., Wang, W., Zhao, Y., Tian, L., Jiang, H., & Luo, X. (2018). Efficient fluoride removal from aqueous solution by synthetic Fe[sbnd]Mg[sbnd]La tri-metal nanocomposite and the analysis of its adsorption mechanism. *Journal of Alloys and Compounds*, 738, 118–129. <https://doi.org/10.1016/j.jallcom.2017.12.142>
- Chen, S., Yue, Q., Gao, B., Li, Q., Xu, X., & Fu, K. (2012). Adsorption of hexavalent chromium from aqueous solution by modified corn stalk: A fixed-bed column study. *Bioresource Technology*, 113, 114–120. <https://doi.org/10.1016/j.biortech.2011.11.110>
- Chitto, B. S., & Sutherland, C. (2020). Column breakthrough studies for the removal and recovery of phosphate by lime-iron sludge: Modeling and optimization using artificial neural network and adaptive neuro-fuzzy inference system. *Chinese Journal of Chemical Engineering*, 28(7), 1847–1859. <https://doi.org/10.1016/j.cjche.2020.02.022>
- Chu, K. H. (2020). Breakthrough curve analysis by simplistic models of fixed bed adsorption: In defense of the century-old Bohart-Adams model. *Chemical Engineering Journal*, 380, 122513. <https://doi.org/10.1016/j.cej.2019.122513>
- CSAE. (2017). *Drinking Water Quality in Ethiopia - Results from the 2016 Ethiopia Socioeconomic Survey*. CSAE Central Statistical Agency of Ethiopia. <https://washdata.org/.../Drinking-water-quality-ethiopia-ESS-2016.pdf>
- Dar, M. A., Sankar, K., & Dar, I. A. (2011). Fluorine contamination in groundwater: A major challenge. *Environmental Monitoring and Assessment*, 173(1–4), 955–968. <https://doi.org/10.1007/s10661-010-1437-0>
- Datturi, S., Kumsa, A., Kebede, S., & Steenbergen, Frank van and Beusekom, M. van. (2017). *The Right to Smile: Fluoride and Fluorosis in Central Rift Valley (Ethiopia)*. 3. [http://metameta.nl/wp-content/uploads/2017/02/GW3\\_Fluoride\\_SF.pdf](http://metameta.nl/wp-content/uploads/2017/02/GW3_Fluoride_SF.pdf)
- de Gennaro, B., Aprea, P., Liguori, B., Galzerano, B., Peluso, A., & Caputo, D. (2020). Zeolite-Rich Composite Materials for Environmental Remediation: Arsenic Removal from Water. *Applied Sciences*, 10(19), 6939. <https://doi.org/10.3390/app10196939>
- Dehghani, M. H., Faraji, M., Mohammadi, A., & Kamani, H. (2017). Optimization of fluoride adsorption onto natural and modified pumice using response surface methodology: Isotherm, kinetic and thermodynamic studies. *Korean Journal of Chemical Engineering*, 34(2), 454–462. <https://doi.org/10.1007/s11814-016-0274-4>
- Demelash, H., Beyene, A., Abebe, Z., & Melese, A. (2019). Fluoride concentration in groundwater and prevalence of dental fluorosis in Ethiopian Rift Valley: Systematic review and meta-analysis. *BMC Public Health*, 19(1), 1298. <https://doi.org/10.1186/s12889-019-7646-8>

- Djobo, J. N. Y., Tchadjié, L. N., Tchakoute, H. K., Kenne, B. B. D., & Elimbi, A. (2014). Synthesis of geopolymer composites from a mixture of volcanic scoria and metakaolin. *Journal of Asian Ceramic Societies*, 2(4), 387–398. <https://doi.org/10.1016/j.jascer.2014.08.003>
- Dou, X., Mohan, D., Pittman, C. U., & Yang, S. (2012). Remediating fluoride from water using hydrous zirconium oxide. *Chemical Engineering Journal*, 198–199(August), 236–245. <https://doi.org/10.1016/j.cej.2012.05.084>
- Dysart, A. (2008). *Investigation of Defluoridation Options for Rural and Remote Communities*. Report No.41, Cooperative Research Centre for Water Quality and Treatment.
- Eawag. (2015). *Geogenic contamination Contamination Handbook - Addressing arsenic and fluoride in drinking water* (A. B. C. Annette Johnson (ed.)). Swiss Federal Institute of Aquatic Science and Technology (Eawag).
- Edmunds, W. M., & Smedley, P. L. (2014). Fluoride in Natural Waters. In *Essentials of Medical Geology* (Vol. 51, Issue 08, pp. 311–336). Springer. <https://doi.org/10.5860/choice.51-4476>
- Fallah, N., & Taghizadeh, M. (2020). Continuous fixed-bed adsorption of Mo(VI) from aqueous solutions by Mo(VI)-IIP: Breakthrough curves analysis and mathematical modeling. *Journal of Environmental Chemical Engineering*, 8(5), 104079. <https://doi.org/10.1016/j.jece.2020.104079>
- Fawell, J., Bailey, K., Chilton, J., Dahi, E., Fewtrell, L., & Magara, Y. (2006). *Fluoride in Drinking-water*. World Health Organization (WHO) with IWA Publishing.
- Feenstra, L., Vasak, L., & Griffion, J. (2007). *Fluoride in groundwater: Overview and evaluation of removal methods* (Issue September). International Groundwater Resources Assessment Centre (igrac).
- Firempong, C., Nsiah, K., Awunyo-Vitor, D., & Dongsogo, J. (2013). SOLUBLE FLUORIDE LEVELS IN DRINKING WATER-A MAJOR RISK FACTOR OF DENTAL FLUOROSIS AMONG CHILDREN IN BONGO COMMUNITY OF GHANA. *Ghana Medical Journal*, 47(1), 16–23.
- Fufa, F., Alemayehu, E., & Lennartz, B. (2013). Defluoridation of groundwater using termite mound. *Water, Air, and Soil Pollution*, 224(5), 1552:1-1552:15. <https://doi.org/10.1007/s11270-013-1552-y>
- Futalan, C. M., Yang, J. H., Phatai, P., Chen, I. P., & Wan, M. W. (2020). Fixed-bed adsorption of copper from aqueous media using chitosan-coated bentonite, chitosan-coated sand, and chitosan-coated kaolinite. *Environmental Science and Pollution Research*, 27, 24659–24670. <https://doi.org/10.1007/s11356-019-06083-0>
- Gan, Y., Wang, X., Zhang, L., Wu, B., Zhang, G., & Zhang, S. (2019). Coagulation removal of fluoride by zirconium tetrachloride: Performance evaluation and mechanism analysis. *Chemosphere*, 218, 860–868. <https://doi.org/10.1016/j.chemosphere.2018.11.192>
- García-sánchez, J. J., Solache-ríos, M., Martínez-miranda, V., & Morelos, C. S. (2013). Removal of fluoride ions from drinking water and fluoride solutions by aluminum modified iron oxides in a column system. *Journal of Colloid and Interface Science*, 407, 410–415. <https://doi.org/10.1016/j.jcis.2013.06.031>
- Geleta, W. S., Alemayehu, E., & Lennartz, B. (2021a). Enhanced Defluoridation from Aqueous Solutions using Zirconium-coated Pumice in Fixed-bed Column Systems. *Proceedings of the*

- Geleta, W. S., Alemayehu, E., & Lennartz, B. (2021b). Volcanic Rock Materials for Defluoridation of Water in Fixed-Bed Column Systems. *Molecules*, 26(4), 977. <https://doi.org/10.3390/molecules26040977>
- Geleta, W. S., Alemayehu, E., & Lennartz, B. (2021c). Enhanced Defluoridation of Water Using Zirconium—Coated Pumice in Fixed-Bed Adsorption Columns. *Materials*, 14(20), 6145. <https://doi.org/10.3390/MA14206145>
- Geleta, W. S., Alemayehu, E., & Lennartz, B. (2022). Fixed-Bed Adsorption: Comparisons of Virgin and Zirconium Oxide-Coated Scoria for the Removal of Fluoride from Water. *Molecules*, 27(8), 2527. <https://doi.org/https://doi.org/10.3390/molecules27082527>
- Ghanbarian, M., Ghanbarian, M., Mahvi, A. H., & Tabatabaie, T. (2020). Enhanced fluoride removal over MgFe<sub>2</sub>O<sub>4</sub>–chitosan–CaAl nanohybrid: Response surface optimization, kinetic and isotherm study. *International Journal of Biological Macromolecules*, 148, 574–590. <https://doi.org/10.1016/j.ijbiomac.2020.01.143>
- Ghorai, S., & Pant, K. K. (2004). Investigations on the column performance of fluoride adsorption by activated alumina in a fixed-bed. *Chemical Engineering Journal*, 98(1–2), 165–173. <https://doi.org/10.1016/j.cej.2003.07.003>
- Ghorai, S., & Pant, K. K. (2005). Equilibrium, kinetics and breakthrough studies for adsorption of fluoride on activated alumina. *Separation and Purification Technology*, 42, 265–271. <https://doi.org/10.1016/j.seppur.2004.09.001>
- Ghosh, A., Chakrabarti, S., & Ghosh, U. C. (2014a). Fixed-bed column performance of Mn-incorporated iron(III) oxide nanoparticle agglomerates on As(III) removal from the spiked groundwater in lab bench scale. *Chemical Engineering Journal*, 248, 18–26. <https://doi.org/10.1016/j.cej.2014.03.010>
- Ghosh, A., Chakrabarti, S., Biswas, K., & Ghosh, U. C. (2014b). Agglomerated nanoparticles of hydrous Ce(IV) + Zr(IV) mixed oxide: Preparation, characterization and physicochemical aspects on fluoride adsorption. *Applied Surface Science*, 307, 665–676. <https://doi.org/10.1016/j.apsusc.2014.04.095>
- Ghosh, A., Chakroborty, S., Biswas, K., & Ghosh, U. C. (2015). Column performances on fluoride removal by agglomerated Ce (IV) – Zr (IV) mixed oxide nanoparticles packed fixed-beds. *Journal of Environmental Chemical Engineering*, 3(2), 653–661. <https://doi.org/10.1016/j.jece.2015.02.001>
- Ghosh, D., Medhi, C. R., & Purkait, M. K. (2008). Treatment of fluoride containing drinking water by electrocoagulation using monopolar and bipolar electrode connections. *Chemosphere*, 73(9), 1393–1400. <https://doi.org/10.1016/j.chemosphere.2008.08.041>
- Gill, T., Tiwari, S., & Kumar, P. A. (2014). A Review on Feasibility of Conventional Fluoride Removal Techniques in Urban Areas. *International Journal of Environmental Research and Development*, 4(2), 179–182. [https://www.ripublication.com/ijerd\\_spl/ijerv4n2spl\\_13.pdf](https://www.ripublication.com/ijerd_spl/ijerv4n2spl_13.pdf)
- Golie, W. M., & Upadhyayula, S. (2016). Continuous fixed-bed column study for the removal of nitrate from water using chitosan/alumina composite. *Journal of Water Process Engineering*, 12, 58–65. <https://doi.org/10.1016/j.jwpe.2016.06.007>



- Govindan, K., Raja, M., Uma Maheshwari, S., Noel, M., & Oren, Y. (2015). Comparison and understanding of fluoride removal mechanism in  $\text{Ca}^{2+}$ ,  $\text{Mg}^{2+}$  and  $\text{Al}^{3+}$  ion assisted electrocoagulation process using Fe and Al electrodes. *Journal of Environmental Chemical Engineering*, 3(3), 1784–1793. <https://doi.org/10.1016/j.jece.2015.06.014>
- Gupta, A. K., & Ayoob, S. (2016). *Fluoride in Drinking Water: Status, Issues, and Solutions* (first edit). CRC Press. <https://doi.org/10.1201/b21385>
- Gwala, P., Andey, S., Mhaisalkar, V., Labhasetwar, P., Pimpalkar, S., & Kshirsagar, C. (2011). Lab scale study on electrocoagulation defluoridation process optimization along with aluminium leaching in the process and comparison with full scale plant operation. *Water Science and Technology*, 63(12), 2788–2795. <https://doi.org/10.2166/wst.2011.475>
- Han, R., Wang, Y., Yu, W., Zou, W., Shi, J., & Liu, H. (2007). Biosorption of methylene blue from aqueous solution by rice husk in a fixed-bed column. *Journal of Hazardous Materials*, 141(3), 713–718. <https://doi.org/10.1016/j.jhazmat.2006.07.031>
- Han, R., Zou, L., Zhao, X., Xu, Y., Xu, F., Li, Y., & Wang, Y. (2009). Characterization and properties of iron oxide-coated zeolite as adsorbent for removal of copper (II) from solution in fixed bed column. *Chemical Engineering Journal*, 149, 123–131. <https://doi.org/10.1016/j.cej.2008.10.015>
- He, Y., Zhang, L., An, X., Wan, G., Zhu, W., & Luo, Y. (2019). Enhanced fluoride removal from water by rare earth (La and Ce) modified alumina: Adsorption isotherms, kinetics, thermodynamics and mechanism. *Science of the Total Environment*, 688, 184–198. <https://doi.org/10.1016/j.scitotenv.2019.06.175>
- Hem, J. D. (1985). *Study and Interpretation of the Chemical Characteristics of Natural Water*. U.S. Geological Survey Water Supply-Supply.
- Hu, A., Ren, G., Che, J., Guo, Y., Ye, J., & Zhou, S. (2020). Phosphate recovery with granular acid-activated neutralized red mud: Fixed-bed column performance and breakthrough curve modelling. *Journal of Environmental Sciences (China)*, 90, 78–86. <https://doi.org/10.1016/j.jes.2019.10.018>
- Hu, C.-Y., Lo, S.-L., Kuan, W.-H., & Lee, Y.-D. (2008). Treatment of high fluoride-content wastewater by continuous electrocoagulation-flotation system with bipolar aluminum electrodes. *Separation and Purification Technology*, 60(1), 1–5. <https://doi.org/10.1016/j.seppur.2007.07.040>
- Hu, Q., Xie, Y., Feng, C., & Zhang, Z. (2019). Fractal-like kinetics of adsorption on heterogeneous surfaces in the fixed-bed column. *Chemical Engineering Journal*, 358, 1471–1478. <https://doi.org/10.1016/j.cej.2018.10.165>
- Huang, H., Liu, J., Zhang, P., Zhang, D., & Gao, F. (2017). Investigation on the simultaneous removal of fluoride, ammonia nitrogen and phosphate from semiconductor wastewater using chemical precipitation. *Chemical Engineering Journal*, 307, 696–706. <https://doi.org/10.1016/j.cej.2016.08.134>
- Jamhour, R. M. A. Q. (2005). New Inorganic Ion-exchange Material for Selective Removal of Fluoride from Potable Water Using Ion-selective Electrode. *American Journal of Environmental Sciences*, 1(1), 1–4. <https://doi.org/10.3844/ajessp.2005.1.4>
- Jere, G. V., & Santhamma, M. T. (1977). IR and Laser Raman studies on Peroxo Fluoro Species of

- Zirconium. *Inorganica Chimica Acta*, 24, 57–61. [https://doi.org/10.1016/S0020-1693\(00\)93851-9](https://doi.org/10.1016/S0020-1693(00)93851-9)
- Kang, W. H., Kim, E. I., & Park, J. Y. (2007). Fluoride removal capacity of cement paste. *Desalination*, 202(1–3), 38–44. <https://doi.org/10.1016/j.desal.2005.12.036>
- Kennedy, A. M., & Arias-Paic, M. (2020). Fixed-Bed Adsorption Comparisons of Bone Char and Activated Alumina for the Removal of Fluoride from Drinking Water. *Journal of Environmental Engineering*, 146(1), 04019099. [https://doi.org/10.1061/\(asce\)ee.1943-7870.0001625](https://doi.org/10.1061/(asce)ee.1943-7870.0001625)
- Kumari, U., Behera, S. K., & Meikap, B. C. (2019). Defluoridation of synthetic and industrial wastewater by using acidic activated alumina adsorbent: characterization and optimization by response surface methodology. *Journal of Environmental Science and Health - Part A Toxic/Hazardous Substances and Environmental Engineering*, 54(1), 79–88. <https://doi.org/10.1080/10934529.2018.1521674>
- Kumari, U., Behera, S. K., Siddiqi, H., & Meikap, B. C. (2020). Facile method to synthesize efficient adsorbent from alumina by nitric acid activation: Batch scale defluoridation, kinetics, isotherm studies and implementation on industrial wastewater treatment. *Journal of Hazardous Materials*, 381(April 2019), 120917. <https://doi.org/10.1016/j.jhazmat.2019.120917>
- Kumari, U., Mishra, A., Siddiqi, H., & Meikap, B. C. (2021). Effective defluoridation of industrial wastewater by using acid modified alumina in fixed-bed adsorption column: Experimental and breakthrough curves analysis. *Journal of Cleaner Production*, 279, 123645. <https://doi.org/10.1016/j.jclepro.2020.123645>
- Kut, K. M. K., Sarswat, A., Srivastava, A., Pittman Jr., C. U., & Mohan, D. (2016). A review of fluoride in African groundwater and local remediation methods. *Groundwater for Sustainable Development*, 2–3, 190–212. <https://doi.org/10.1016/j.gsd.2016.09.001>
- Kwon, J.-S., Yun, S.-T., Lee, J.-H., Kim, S.-O., & Jo, H. Y. (2010). Removal of divalent heavy metals (Cd, Cu, Pb, and Zn) and arsenic (III) from aqueous solutions using scoria: Kinetics and equilibria of sorption. *Journal of Hazardous Materials*, 174(1–3), 307–313. <https://doi.org/10.1016/j.jhazmat.2009.09.052>
- Li, Q., Wang, B., Li, W., Wang, C., Zhou, Q., Shuang, C., & Li, A. (2016). Performance evaluation of magnetic anion exchange resin removing fluoride. *Journal of Chemical Technology and Biotechnology*, 91(6), 1747–1754. <https://doi.org/10.1002/jctb.4764>
- Li, X., Yang, W., Zou, Q., & Ph, DZuo, Y. (2010). Investigation on Microstructure, Composition, and Cytocompatibility of Natural Pumice for Potential Biomedical Application. *Tissue Engineering: Part C*, 16(3), 427–434. <https://doi.org/10.1089=ten.tec.2009.0285>
- Liang, Z., & Ni, J. (2009). Improving the ammonium ion uptake onto natural zeolite by using an integrated modification process. *Journal of Hazardous Materials*, 166, 52–60. <https://doi.org/10.1016/j.jhazmat.2008.11.002>
- Lin, X., Huang, Q., Qi, G., Shi, S., Xiong, L., Huang, C., Chen, X., Li, H., & Chen, X. (2017). Estimation of fixed-bed column parameters and mathematical modeling of breakthrough behaviors for adsorption of levulinic acid from aqueous solution using SY-01 resin. *Separation and Purification Technology*, 174, 222–231. <https://doi.org/10.1016/j.seppur.2016.10.016>
- Liu, C. C., & Liu, J. C. (2016). Coupled precipitation-ultrafiltration for treatment of high fluoride-

- content wastewater. *Journal of the Taiwan Institute of Chemical Engineers*, 58, 259–263. <https://doi.org/10.1016/j.jtice.2015.05.038>
- Liu, C., & Evett, J. B. (2003). *Soil properties-testing, measurement, and evaluation*. Banta Book Company.
- Liu, J., Yue, X., Lu, X., & Guo, Y. (2018). Uptake Fluoride from Water by Starch Stabilized Layered Double Hydroxides. *Water*, 10, 745. <https://doi.org/10.3390/w10060745>
- López-Guzmán, M., Alarcón-Herrera, M. T., Irigoyen-Campuzano, J. R., Torres-Castañón, L. A., & Reynoso-Cuevas, L. (2019). Simultaneous removal of fluoride and arsenic from well water by electrocoagulation. *Science of the Total Environment*, 678, 181–187. <https://doi.org/10.1016/j.scitotenv.2019.04.400>
- Lǔ, J., Liu, H., Liu, R., Zhao, X., Sun, L., & Qu, J. (2013). Adsorptive removal of phosphate by a nanostructured Fe-Al-Mn trimetal oxide adsorbent. *Powder Technology*, 233, 146–154. <https://doi.org/10.1016/j.powtec.2012.08.024>
- Ma, Y., Shi, F., Zheng, X., Ma, J., & Gao, C. (2011). Removal of fluoride from aqueous solution using granular acid-treated bentonite (GHB): Batch and column studies. *Journal of Hazardous Materials*, 185(2–3), 1073–1080. <https://doi.org/10.1016/j.jhazmat.2010.10.016>
- MacDonald, A., Dochartaigh, B. Ó., & Welle, K. (2009). *Mapping for Water Supply and Sanitation ( WSS ) in Ethiopia Research-inspired Policy Ethiopia and the Nile region Mapping for Water Supply and Sanitation ( WSS ) in Ethiopia* (Issue January).
- Majewska-Nowak, K., Grzegorzec, M., & Kabsch-Korbutowicz, M. (2015). Removal of fluoride ions by batch electrodialysis. *Environment Protection Engineering*, 41(1), 67–81. <https://doi.org/10.5277/epe150106>
- Maliyekkal, S. M., Sharma, A. K., & Philip, L. (2006). Manganese-oxide-coated alumina: a promising sorbent for defluoridation of water. *Water Research*, 40(19), 3497–3506. <https://doi.org/10.1016/j.watres.2006.08.007>
- Manna, S., Saha, P., Roy, D., Adhikari, B., & Das, P. (2018). Fixed bed column study for water defluoridation using neem oil-phenolic resin treated plant bio-sorbent. *Journal of Environmental Management*, 212, 424–432. <https://doi.org/10.1016/j.jenvman.2018.02.037>
- Manville, V., White, J. D. L., Houghton, B. F., & Wilson, C. J. N. (1998). The saturation behaviour of pumice and some sedimentological implications. *Sedimentary Geology*, 119(1–2), 5–16. [https://doi.org/10.1016/S0037-0738\(98\)00057-8](https://doi.org/10.1016/S0037-0738(98)00057-8)
- Meenakshi, & Maheshwari, R. C. (2006). Fluoride in drinking water and its removal. *Journal of Hazardous Materials*, 137(1), 456–463. <https://doi.org/10.1016/j.jhazmat.2006.02.024>
- Mekonnen, D. T., Alemayehu, E., & Lennartz, B. (2021a). Adsorptive Removal of Phosphate from Aqueous Solutions Using Low-Cost Volcanic Rocks: Kinetics and Equilibrium Approaches. *Materials*, 14(5), 1312. <https://doi.org/10.3390/ma14051312> Academic
- Mekonnen, D. T., Alemayehu, E., & Lennartz, B. (2021b). Fixed-Bed Column Technique for the Removal of Phosphate from Water Using Leftover Coal. *Materials*, 14(19), 5466.
- Mengistu, T. D., Chung, I. M., Chang, S. W., Yifru, B. A., Kim, M. G., Lee, J., Ware, H. H., & Kim, I. H. (2021). Challenges and Prospects of Advancing Groundwater Research in Ethiopian Aquifers: A Review. *Sustainability*, 13(20), 11500. <https://doi.org/10.3390/su132011500>

- Mjengera, H., & Mkongo, G. (2003). Appropriate defluoridation technology for use in flourotic areas in Tanzania. *Physics and Chemistry of the Earth*, 28, 1097–1104. <https://doi.org/10.1016/j.pce.2003.08.030>
- Mohan, S., Kumar, V., Singh, D. K., & Hasan, S. H. (2016). Synthesis and characterization of rGO/ZrO<sub>2</sub> nanocomposite for enhanced removal of fluoride from water: Kinetics, isotherm, and thermodynamic modeling and its adsorption mechanism. *RSC Advances*, 6(90), 87523–87538. <https://doi.org/10.1039/c6ra15460c>
- Mohan, S., Singh, D. K., Kumar, V., & Hasan, S. H. (2017a). Effective removal of Fluoride ions by rGO/ZrO<sub>2</sub> nanocomposite from aqueous solution: Fixed bed column adsorption modelling and its adsorption mechanism. *Journal of Fluorine Chemistry*, 194, 40–50. <https://doi.org/10.1016/j.jfluchem.2016.12.014>
- Mohan, S., Singh, D. K., Kumar, V., & Hasan, S. H. (2017b). Modelling of fixed bed column containing graphene oxide decorated by MgO nanocubes as adsorbent for Lead ( II ) removal from water. *Journal of Water Process Engineering*, 17, 216–228. <https://doi.org/10.1016/j.jwpe.2017.03.009>
- Monash, P., & Pugazhenth, G. (2010). Removal of crystal violet dye from aqueous solution using calcined and uncalcined mixed clay adsorbents. *Separation Science and Technology*, 45(1), 94–104. <https://doi.org/10.1080/01496390903256174>
- Moradi, M., Mansouri, A. M., Azizi, N., & Amini, J. (2015). Adsorptive removal of phenol from aqueous solutions by copper (Cu) - modified scoria powder: process modeling and kinetic evaluation. *Desalination and Water Treatment*, 57(25), 1–15. <https://doi.org/10.1080/19443994.2015.1054311>
- Msonda, K. W. M., Masamba, W. R. L., & Fabiano, E. (2007). A study of fluoride groundwater occurrence in Nthenje, Lilongwe, Malawi. *Physics and Chemistry of the Earth*, 32(15–18), 1178–1184. <https://doi.org/10.1016/j.pce.2007.07.050>
- Muthamilselvi, P., Karthikeyan, R., Kapoor, A., & Prabhakar, S. (2018). Continuous fixed-bed studies for adsorptive remediation of phenol by garlic peel powder. *International Journal of Industrial Chemistry*, 9(4), 379–390. <https://doi.org/10.1007/s40090-018-0166-z>
- Nehra, S., Raghav, S., & Kumar, D. (2020). Biomaterial Functionalized Cerium Nanocomposite for Removal of Fluoride using Central Composite Design Optimization Study. *Environmental Pollution*, 258, 113773. <https://doi.org/10.1016/j.envpol.2019.113773>
- Newcombe, G., Hayes, R., & Drikas, M. (1993). Granular activated carbon: Importance of surface properties in the adsorption of naturally occurring organics. *Colloids and Surfaces A: Physicochemical and Engineering Aspects*, 78, 65–71. [https://doi.org/10.1016/0927-7757\(93\)80311-2](https://doi.org/10.1016/0927-7757(93)80311-2)
- Obijole, O. A., Gitari, M. W., & Ndungu, P. G. (2019). Mechanochemically Activated Aluminosilicate Clay Soils and their Application for Defluoridation and Pathogen Removal from Groundwater. *International Journal of Environmental Research and Public Health*, 16, 2:654-19:654. <https://doi.org/10.3390/ijerph16040654>
- Panias, D., Giannopoulou, I. P., & Perraki, T. (2007). Effect of synthesis parameters on the mechanical properties of fly ash-based geopolymers. *Colloids and Surfaces A: Physicochemical and Engineering Aspects*, 301(1–3), 246–254. <https://doi.org/10.1016/j.colsurfa.2006.12.064>

- Patel, H. (2019). Fixed - bed column adsorption study: a comprehensive review. *Applied Water Science*, 9, 45. <https://doi.org/10.1007/s13201-019-0927-7>
- Paudyal, H., Pangeni, B., Inoue, K., Kawakita, H., Ohto, K., & Alam, S. (2013). Adsorptive removal of fluoride from aqueous medium using a fixed bed column packed with Zr (IV) loaded dried orange juice residue. *Bioresource Technology*, 146, 713–720. <https://doi.org/10.1016/j.biortech.2013.07.014>
- Pirsaheb, M., Mohammadi, H., Sharafi, K., & Asadi, A. (2018). Fluoride and nitrate adsorption from water by Fe(III)-doped scoria: optimizing using response surface modeling, kinetic and equilibrium study. *Water Science and Technology: Water Supply*, 18(3), 1117–1132. <https://doi.org/10.2166/ws.2017.185>
- Quintelas, C., Pereira, R., Kaplan, E., & Tavares, T. (2013). Removal of Ni(II) from aqueous solutions by an *Arthrobacter viscosus* biofilm supported on zeolite: From laboratory to pilot scale. *Bioresource Technology*, 142, 368–374. <https://doi.org/10.1016/j.biortech.2013.05.059>
- Raj, R. M., & Raj, V. (2019). Electrosynthesis of Zr-loaded copolymer coatings on Al for defluoridation of water and its corrosion protection ability. *Progress in Organic Coatings*, 137, 105065. <https://doi.org/10.1016/j.porgcoat.2019.04.039>
- Rajkumar, S., Murugesh, S., Sivasankar, V., Darchen, A., Msagati, T. A. M., & Chaabane, T. (2019). Low-cost fluoride adsorbents prepared from a renewable biowaste: Syntheses, characterization and modeling studies. *Arabian Journal of Chemistry*, 12(8), 3004–3017. <https://doi.org/10.1016/j.arabjc.2015.06.028>
- Rango, T., Bianchini, G., Beccaluva, L., & Tassinari, R. (2010). Geochemistry and water quality assessment of central Main Ethiopian Rift natural waters with emphasis on source and occurrence of fluoride and arsenic. *Journal of African Earth Sciences*, 57(5), 479–491. <https://doi.org/10.1016/j.jafrearsci.2009.12.005>
- Rango, T., Vengosh, A., Jeuland, M., Whitford, G. M., & Tekle-Haimanot, R. (2017). Biomarkers of chronic fluoride exposure in groundwater in a highly exposed population. *Science of the Total Environment*, 596–597, 1–11. <https://doi.org/10.1016/j.scitotenv.2017.04.021>
- Rasool, A., Farooqi, A., Xiao, T., Ali, W., Noor, S., Abiola, O., Ali, S., & Nasim, W. (2018). A review of global outlook on fluoride contamination in groundwater with prominence on the Pakistan current situation. *Environmental Geochemistry and Health*, 40(4), 1265–1281. <https://doi.org/10.1007/s10653-017-0054-z>
- Rowe, M. C., & Brewer, B. J. (2018). AMORPH : A statistical program for characterizing amorphous materials by X-ray diffraction 1. *Computer and Geoscience*, 120, 24–31. <https://doi.org/10.1016/j.cageo.2018.07.004>
- Sahu, N., Bhan, C., & Singh, J. (2020). Removal of fluoride from an aqueous solution by batch and column process using activated carbon derived from iron infused *Pisum sativum* peel: characterization, Isotherm, kinetics study. *Environmental Engineering Research*, 26(4), 200241. <https://doi.org/10.4491/eer.2020.241>
- Salifu, A. (2017). Laboratory-Scale column filter studies for fluoride removal with aluminium (hydr) oxide coated pumice, regeneration and disposal. In *Fluoride Removal from Groundwater by Adsorption Technology: The occurrence, adsorbent synthesis, regeneration and disposal* (1st ed., pp. 127–129). CRC Press/Balkema.

- Salifu, A., Petrusevski, B., Ghebremichael, K., Modestus, L., Buamah, R., Aubry, C., & Amy, G. L. (2013). Aluminum (hydr) oxide coated pumice for fluoride removal from drinking water: Synthesis, equilibrium, kinetics and mechanism. *Chemical Engineering Journal*, 228, 63–74. <https://doi.org/10.1016/j.cej.2013.04.075>
- Salifu, A., Petrusevski, B., Mwampashi, E. S., Pazi, I. A., Ghebremichael, K., Buamah, R., Aubry, C., Amy, G. L., & Kenedy, M. D. (2016). Defluoridation of groundwater using aluminum-coated bauxite: Optimization of synthesis process conditions and equilibrium study. *Journal of Environmental Management*, 181, 108–117. <https://doi.org/10.1016/j.jenvman.2016.06.011>
- Sarkar, M., Banerjee, A., Pramanick, P. P., & Sarkar, A. R. (2006). Use of laterite for the removal of fluoride from contaminated drinking water. *Journal of Colloid and Interface Science*, 302(2), 432–441. <https://doi.org/10.1016/j.jcis.2006.07.001>
- Sarkar, M., Banerjee, A., Pramanick, P. P., & Sarkar, A. R. (2007). Design and operation of fixed bed laterite column for the removal of fluoride from water. *Chemical Engineering Journal*, 131(1–3), 329–335. <https://doi.org/10.1016/j.cej.2006.12.016>
- Sepehr, M. N., Amrane, A., Karimaian, K. A., Zarrabi, M., & Ghaffari, H. R. (2014). Potential of waste pumice and surface modified pumice for hexavalent chromium removal: Characterization, equilibrium, thermodynamic and kinetic study. *Journal of the Taiwan Institute of Chemical Engineers*, 45(2), 635–647. <https://doi.org/10.1016/j.jtice.2013.07.005>
- Sepehr, M. N., Sivasankar, V., Zarrabi, M., & Kumar, M. S. (2013b). Surface modification of pumice enhancing its fluoride adsorption capacity: An insight into kinetic and thermodynamic studies. *Chemical Engineering Journal*, 228, 192–204. <https://doi.org/10.1016/j.cej.2013.04.089>
- Sepehr, M. N., Zarrabi, M., Kazemian, H., Amrane, A., Yaghmaian, K., & Ghaffari, H. R. (2013a). Removal of hardness agents, calcium and magnesium, by natural and alkaline modified pumice stones in single and binary systems. *Applied Surface Science*, 274, 295–305. <https://doi.org/10.1016/j.apsusc.2013.03.042>. hal-00915133
- Shang, Y., Wang, Z., Xu, X., Cheng, C., Gao, B., Yue, Q., Liu, S., & Han, C. (2019). Enhanced fluoride uptake by bimetallic hydroxides anchored in cotton cellulose/graphene oxide composites. *Journal of Hazardous Materials*, 376, 91–101. <https://doi.org/10.1016/j.jhazmat.2019.05.039>
- Shen, F., Chen, X., Gao, P., & Chen, G. (2003). Electrochemical removal of fluoride ions from industrial wastewater. *Chemical Engineering Science*, 58(3–6), 987–993. [https://doi.org/10.1016/S0009-2509\(02\)00639-5](https://doi.org/10.1016/S0009-2509(02)00639-5)
- Shen, J., & Schäfer, A. (2014). Removal of fluoride and uranium by nanofiltration and reverse osmosis: A review. *Chemosphere*, 117(1), 679–691. <https://doi.org/10.1016/j.chemosphere.2014.09.090>
- Shen, J., & Schäfer, A. I. (2015). Factors affecting fluoride and natural organic matter (NOM) removal from natural waters in Tanzania by nanofiltration/reverse osmosis. *Science of the Total Environment*, 527–528, 520–529. <https://doi.org/10.1016/j.scitotenv.2015.04.037>
- Singh, T. P., Ghosh, S., & Cb, M. (2016). Adsorption of fluoride from industrial wastewater in fixed bed column using java plum (*Syzygium Cumini*). *Asian Journal of Pharmaceutical and Clinical Research*, 9(3), 320–327. <https://doi.org/10.22159/ajpcr.2016.v9s3.12613>

- Sivasankar, V., Ramachandramoorthy, T., & Chandramohan, A. (2010). Fluoride removal from water using activated and MnO<sub>2</sub>-coated Tamarind Fruit ( *Tamarindus indica*) shell: Batch and column studies. *Journal of Hazardous Materials*, 177(1–3), 719–729. <https://doi.org/10.1016/j.jhazmat.2009.12.091>
- Smedley, P. L., Nkotagu, H., Pelig-Ba, K., MacDonald, A. M., TylerWhittle, R., Whitehead, E. J., & Kinniburgh, D. G. (2002). *Fluoride in groundwater from high-fluoride areas of Ghana and Tanzania*. British Geological Survey Groundwater Systems and Water Quality Programme, Commissioned Report CR/02/316.
- Souza, R. F., Brandão, P. R. G., & Paulo, J. B. A. (2012). Effect of chemical composition on the Zeta -potential of chromite. *Minerals Engineering*, 36–38, 65–74. <https://doi.org/10.1016/j.mineng.2012.02.012>
- Su, T., Song, Y., Lan, X., & Gao, W. (2020). Optimization for removal efficiency of fluoride using La (III) – Al (III) - activated carbon modified by chemical route. *Green Processing and Synthesis*, 9, 405–415.
- Susheela, A. K., & Bhatnagar, M. (2002). Reversal of fluoride induced cell injury through elimination of fluoride and consumption of diet rich in essential nutrients and antioxidants. *Molecular and Cellular Biochemistry*, 234/235(1–2), 335–340.
- Tao, W., Zhong, H., Pan, X., Wang, P., Wang, H., & Huang, L. (2020). Removal of fluoride from wastewater solution using Ce-ALOOH with oxalic acid as modification. *Journal of Hazardous Materials*, 384, 121373. <https://doi.org/10.1016/j.jhazmat.2019.121373>
- Tekle-Haimanot, R., Melaku, Z., Kloos, H., Reimann, C., Fantaye, W., Zerihun, L., & Bjorvatn, K. (2006). The geographic distribution of fluoride in surface and groundwater in Ethiopia with an emphasis on the Rift Valley. *Science of the Total Environment*, 367(1), 182–190. <https://doi.org/10.1016/j.scitotenv.2005.11.003>
- Teng, S. X., Wang, S. G., Gong, W. X., Liu, X. W., & Gao, B. Y. (2009). Removal of fluoride by hydrous manganese oxide-coated alumina: Performance and mechanism. *Journal of Hazardous Materials*, 168(2–3), 1004–1011. <https://doi.org/10.1016/j.jhazmat.2009.02.133>
- Thomas, H. C. (1944). Heterogeneous Ion Exchange in a Flowing System. *Journal of the American Chemical Society*, 66(10), 1664–1666. <https://doi.org/10.1021/ja01238a017>
- UNICEF. (2009). *UNICEF's Position on Water Fluoridation*. Water, Environment, and Sanitation. [http://www.nofluoride.com/UNICEF\\_fluor.htm](http://www.nofluoride.com/UNICEF_fluor.htm)
- UNICEF & WHO. (2019). *Progress on household drinking water, sanitation and hygiene 2000-2017: Special focus on inequalities*.
- US EPA. (1983). *Control of organic substances in water and wastewater* (Document No.: U.S. EPA-600/8-83-011). U.S. Environmental Protection Agency.
- Viswanathan, N., & Meenakshi, S. (2010). Enriched fluoride sorption using alumina/chitosan composite. *Journal of Hazardous Materials*, 178(1–3), 226–232. <https://doi.org/10.1016/j.jhazmat.2010.01.067>
- Waghmare, S. S., & Arfin, T. (2015). Fluoride Removal from Water by various techniques: Review. *International Journal of Innovative Science, Engineering & Technology*, 2(9), 560–571. [ijiset.com/vol2/v2s9/IJSET\\_V2\\_I9\\_67.pdf](http://ijiset.com/vol2/v2s9/IJSET_V2_I9_67.pdf)



- Wan, S., Lin, J., Tao, W., Yang, Y., Li, Y., & He, F. (2019). Enhanced Fluoride Removal from Water by Nanoporous Biochar-Supported Magnesium Oxide [Research-article]. *Industrial and Engineering Chemistry Research*, 58(23), 9988–9996. <https://doi.org/10.1021/acs.iecr.9b01368>
- Warner, M. (1990). Basalts, water, or shear zones in the lower continental crust? *Tectonophysics*, 173(1–4), 163–174. [https://doi.org/10.1016/0040-1951\(90\)90214-S](https://doi.org/10.1016/0040-1951(90)90214-S)
- Whitford, G. M. (1996). The metabolism and toxicity of fluoride. In *Monographs in oral science* (2nd ed., Vol. 16). [https://doi.org/10.1016/0300-5712\(92\)90111-o](https://doi.org/10.1016/0300-5712(92)90111-o)
- WHO. (2002). The World Health Organization Report 2002: reducing risks, promoting healthy life. In *WHO Library Cataloguing in Publication Data*. WHO.
- WHO. (2011). *Guidelines for Drinking-water Quality* (4th ed.). WHO World Health Organization.
- WHO and UNICEF. (2004). *WHO and UNICEF, Meeting the MDG Drinking Water Sanitation Target: A Mid-Term Assessment of Progress*. WHO Geneva and UNICEF.
- WHO and UNICEF. (2015). *Progress on Sanitation and Drinking water-2015 Update and MDG Assessment*. WHO Press.
- Worch, E. (2012). *Adsorption Technology in Water Treatment: Fundamentals, Processes, and Modeling*. Walter de Gruyter and Co.KG.
- Wu, H., Zhang, H., Yang, Q., Wang, D., Zhang, W., & Yang, X. (2017). Calcined chitosan-supported layered double hydroxides: An efficient and recyclable adsorbent for the removal of fluoride from an aqueous solution. *Materials*, 10(11), 1320. <https://doi.org/10.3390/ma10111320>
- Xu, X., Li, Q., Cui, H., Pang, J., An, H., Wang, W., & Zhai, J. (2012). Column-mode fluoride removal from aqueous solution by magnesia-loaded fly ash cenospheres. *Environmental Technology (United Kingdom)*, 33(12), 1409–1415. <https://doi.org/10.1080/09593330.2011.630424>
- Yadav, K. K., Gupta, N., Kumar, V., Khan, S. A., & Kumar, A. (2018). A review of emerging adsorbents and current demand for defluoridation of water: Bright future in water sustainability. *Environment International*, 111, 80–108. <https://doi.org/10.1016/j.envint.2017.11.014>
- Yagub, M. T., Sen, T. K., Afroze, S., & Ang, H. M. (2015). Fixed-bed dynamic column adsorption study of methylene blue (MB) onto pine cone. *Desalination and Water Treatment*, 55(4), 1026–1039. <https://doi.org/10.1080/19443994.2014.924034>
- Ye, Y., Yang, J., Jiang, W., Kang, J., Hu, Y., Ngo, H. H., Guo, W., & Liu, Y. (2018). Fluoride removal from water using a magnesia-pullulan composite in a continuous fixed-bed column. *Journal of Environmental Management*, 206, 929–937. <https://doi.org/10.1016/j.jenvman.2017.11.081>
- Žáček, V., Rapprich, V., Šíma, J., Škoda, R., Laufek, F., & Legesa, F. (2015). Kogarkoite, Na<sub>3</sub>(SO<sub>4</sub>)F, from the Shalo hot spring, Main Ethiopian Rift: Implications for F-enrichment of thermal groundwater related to alkaline silicic volcanic rocks. *Journal of Geosciences (Czech Republic)*, 60(3), 171–179. <https://doi.org/10.3190/jgeosci.195>
- Zhai, L. Z., Sun, Y. H., & He, C. (2013). Research on coagulation/sedimentation process for simulation of fluorine-containing wastewater treatment. *Applied Mechanics and Materials*, 361–363, 755–759. <https://doi.org/10.4028/www.scientific.net/AMM.361-363.755>



- Zhang, J., & Stanforth, R. (2005). Slow adsorption reaction between arsenic species and goethite ( $\alpha$ -FeOOH): Diffusion or heterogeneous surface reaction control. *Langmuir*, 21(7), 2895–2901. <https://doi.org/10.1021/la047636e>
- Zhang, T., Yu, H., Zhou, Y., Rong, J., Mei, Z., & Qiu, F. (2016). Enhanced adsorption of fluoride from aqueous solutions by hierarchically structured Mg-Al LDHs/Al<sub>2</sub>O<sub>3</sub> composites. *Korean Journal of Chemical Engineering*, 33(2), 720–725. <https://doi.org/10.1007/s11814-015-0181-0>
- Zhang, Y., Xiong, L., Xiu, Y., & Huang, K. (2019). Defluoridation in fixed bed column filled with Zr(IV)-loaded garlic peel. *Microchemical Journal*, 145, 476–485. <https://doi.org/10.1016/j.microc.2018.11.007>
- Zhao, X., Zhang, B., Liu, H., & Qu, J. (2011). Simultaneous removal of arsenite and fluoride via an integrated electro-oxidation and electrocoagulation process. *Chemosphere*, 83(5), 726–729. <https://doi.org/10.1016/j.chemosphere.2011.01.055>
- ZHOU, H., CHEN, W., GAO, Z. Y. and, & CHEN, D. (2014). Removal of Fluoride from Aqueous Media by Zirconium Modified Zeolite. *Asian Journal of Chemistry*, 26(23), 8062–8068.
- Zhou, J., Yu, J., Liao, H., Zhang, Y., & Luo, X. (2019). Facile fabrication of bimetallic collagen fiber particles via immobilizing zirconium on chrome-tanned leather as adsorbent for fluoride removal from groundwater near hot spring. *Separation Science and Technology (Philadelphia)*, 55, 658–671. <https://doi.org/10.1080/01496395.2019.1574826>
- Zuo, Q., Chen, X., Li, W., & Chen, G. (2008). Combined electrocoagulation and electroflotation for removal of fluoride from drinking water. *Journal of Hazardous Materials*, 159(2–3), 452–457. <https://doi.org/10.1016/j.jhazmat.2008.02.039>

### Article

## Volcanic Rock Materials for Defluoridation of Water in Fixed-Bed Column Systems

Wondwosen Sime Geleta <sup>1,2</sup> , Esayas Alemayehu <sup>3,4,\*</sup> and Bernd Lennartz <sup>2,5</sup> 

<sup>1</sup> School of Chemical Engineering, Jimma Institute of Technology, Jimma University,

P.O. Box 378, Jimma, Oromia, Ethiopia; wondeto@gmail.com

<sup>2</sup> Faculty of Agricultural and Environmental Sciences, University of Rostock, Justus-Von-Liebig-Weg 6,

18059 Rostock, Germany

<sup>3</sup> Faculty of Civil and Environmental Engineering, Jimma Institute of Technology, Jimma University,

P.O. Box 378, Jimma, Oromia, Ethiopia

<sup>4</sup> Africa Center of Excellence for Water Management, Addis Ababa University, 1176 Addis Ababa, Ethiopia

<sup>5</sup> Correspondence: esayas16@yahoo.com (E.A.); bernd.lennartz@uni-rostock.de (B.L.);

Tel.: +251-91-701-7002 (E.A.); +49-381-496-3180 (B.L.)

**Abstract:** Consumption of drinking water with a high concentration of fluoride (>1.5 mg/L) causes detrimental health problems and is a challenging issue in various regions around the globe. In this study, a continuous fixed-bed column adsorption system was employed for defluoridation of water using volcanic rocks, virgin pumice (VPum) and virgin scoria (VSco), as adsorbents. The XRD, SEM, FTIR, BET, XRF, ICP-OES, and pH Point of Zero Charges (pH<sub>PZC</sub>) analysis were performed for both adsorbents to elucidate the adsorption mechanisms and the suitability for fluoride removal. The effects of particle size of adsorbents, solution pH, and flow rate on the adsorption performance of the column were assessed at room temperature, constant initial concentration, and bed depth. The maximum removal capacity of 110 mg/kg for VPum and 22 mg/kg for VSco were achieved at particle sizes of 0.075–0.425 mm and <0.075 mm, respectively, at a low solution pH (2.00) and flow rate (1.25 mL/min). The fluoride breakthrough occurred late and the treated water volume was higher at a low pH and flow rate for both adsorbents. The Thomas and Adams–Bohart models were utilized and fitted well with the experimental kinetic data and the entire breakthrough curves for both adsorbents. Overall, the results revealed that the developed column is effective in handling water containing excess fluoride. Additional testing of the adsorbents including regeneration options is, however, required to confirm that the defluoridation of groundwater employing volcanic rocks is a safe and sustainable method.

**Keywords:** adsorption; breakthrough curve; defluoridation; up-flow mode; volcanic rocks



**Citation:** Geleta, W.S.; Alemayehu, E.; Lennartz, B. Volcanic Rock Materials for Defluoridation of Water in Fixed-Bed Column Systems. *Molecules* **2021**, *26*, 977. <https://doi.org/10.3390/molecules26040977>

Academic Editor: Giorgio Vilardi

Received: 7 December 2020

Accepted: 8 February 2021

Published: 12 February 2021

**Publisher's Note:** MDPI stays neutral with regard to jurisdictional claims in published maps and institutional affiliations.



Copyright © 2021 by the authors. Licensee MDPI, Basel, Switzerland. This article is an open access article distributed under the terms and conditions of the Creative Commons Attribution (CC BY) license (<https://creativecommons.org/licenses/by/4.0/>).

### 1. Introduction

Credible evidence from scientific literature substantiates both beneficial and detrimental effects of fluoride on human health with only a narrow range between intake associated with these effects [1,2]. Consumptions of fluoride in low concentrations (<1.0 mg/L) is an essential micronutrient for the healthy development of bone and dental enamel [3]; however, it leads to the development of fluorosis if it is consumed beyond the permissible limit (>1.5 mg/L) [4].

In many parts of the world, groundwater sources are the single largest supply of drinking water. For many rift communities, it may be the only economically viable option for drinking water. In the Ethiopian rift valley, about 40% of deep and shallow wells are contaminated with up to 26 mg/L of fluoride [5,6]. The weathering of primary rocks and leaching of fluoride-containing minerals in soils yield fluoride-rich groundwater in the Ethiopian Rift, which is generally associated with a low calcium content and high bicarbonate concentrations [7,8].

Article

# Enhanced Defluoridation of Water Using Zirconium—Coated Pumice in Fixed-Bed Adsorption Columns

Wondwosen Sime Geleta <sup>1,2</sup>, Esayas Alemayehu <sup>3,4,\*</sup> and Bernd Lennartz <sup>2,5</sup>

<sup>1</sup> School of Chemical Engineering, Jimma Institute of Technology, Jimma University, Jimma P.O. Box 378, Ethiopia; wondet@gmail.com

<sup>2</sup> Faculty of Agricultural and Environmental Sciences, University of Rostock, Justus-Von-Liebig-Weg 6, 18059 Rostock, Germany

<sup>3</sup> Faculty of Civil and Environmental Engineering, Jimma Institute of Technology, Jimma University, Jimma P.O. Box 378, Ethiopia

<sup>4</sup> Africa Center of Excellence for Water Management, Addis Ababa University, Addis Ababa 1176, Ethiopia

\* Correspondence: esayas16@yahoo.com (E.A.); bernd.lennartz@uni-rostock.de (B.L.); Tel.: +49-381-498-3180 (B.L.)

**Abstract:** Millions of people across the globe suffer from health issues related to high fluoride levels in drinking water. The purpose of this study was to test modified pumice as an adsorbent for the purification of fluoride-containing waters. The adsorption of fluoride onto zirconium-coated pumice (Zr-Pu) adsorbent was examined in fixed-bed adsorption columns. The coating of zirconium on the surface of VPum was revealed by X-ray diffractometer (XRD), inductively coupled plasma-optical emission spectroscopy (ICP-OES), and X-ray fluorescence (XRF) techniques. The degree of surface modification with the enhanced porosity of Zr-Pu was evident from the recorded scanning electron microscope (SEM) micrographs. The Brunauer-Emmett-Teller (BET) analysis confirmed the enhancement of the specific surface area of VPum after modification. The Fourier transform infrared (FTIR) examinations of VPum and Zr-Pu before and after adsorption did not reveal any significant spectrum changes. The pH drift method showed that VPum and Zr-Pu have positive charges at  $pH_{ZPC}$  lower than 7.3 and 6.5, respectively. Zr-Pu yielded a higher adsorption capacity of 225 mg/kg (2.05 times the adsorption capacity of VPum: 110 mg/kg), at  $pH = 2$  and volumetric flow rate ( $Q_V$ ) of 1.25 mL/min. Breakthrough time increases with decreasing pH and flow rate. The experimental adsorption data was well-matched by the Thomas and Adams-Bohart models with correlation coefficients ( $R^2$ ) of  $\geq 0.980$  (Zr-Pu) and  $\geq 0.897$  (VPum), confirming that both models are suitable tools to design fixed-bed column systems using volcanic rock materials. Overall, coating pumice with zirconium improved the defluoridation capacity of pumice; hence, a Zr-Pu-packed fixed-bed can be applied for defluoridation of excess fluoride from groundwater. However, additional investigations on, for instance, the influences of competing ions are advisable to draw explicit conclusions.

**Keywords:** adsorption; defluoridation; fluoride; VPum; zirconium-coated pumice



**Citation:** Geleta, W.S.; Alemayehu, E.; Lennartz, B. Enhanced Defluoridation of Water Using Zirconium—Coated Pumice in Fixed-Bed Adsorption Columns. *Materials* **2021**, *14*, 4345. <https://doi.org/10.3390/ma14204345>

**Academic Editors:** Agnieszka Gladysz-Plaska and Ewa Skoczniak

Received: 1 September 2021

Accepted: 13 October 2021

Published: 16 October 2021

**Publisher's Note:** MDPI stays neutral with regard to jurisdictional claims in published maps and institutional affiliations.



Copyright © 2021 by the authors. Licensee MDPI, Basel, Switzerland. This article is an open access article distributed under the terms and conditions of the Creative Commons Attribution (CC BY) license (<https://creativecommons.org/licenses/by/4.0/>).

## 1. Introduction

Fluoride is among the many vital trace elements required in drinking water within the allowable range ( $<1.5$  mg/L) [1] for the normal growth of humans and animal bones. Nevertheless, it is detrimental to bone development when ingested beyond the acceptable concentration limit ( $>1.5$  mg/L) [2]. Excess fluoride hurts bones because of its high electronegative value, enabling interrelations with calcium in bones. Hence, it causes dental fluorosis and/or skeletal fluorosis (bone cancer) [3]. Alzheimer's syndrome, arthritis, thyroid, etc., are additional adverse consequences of excess fluoride in drinking water [4].

In several places around the globe, groundwater is the principal and favored source of potable water, as is the case for many communities in rural and urban areas in the African rift valley. However, over 200 million people around the globe, including East

Article

# Fixed-Bed Adsorption: Comparisons of Virgin and Zirconium Oxide-Coated Scoria for the Removal of Fluoride from Water

Wondrosen Sime Geleta <sup>1,2,\*</sup>, Esayas Alemayehu <sup>3,4,\*</sup> and Bernd Lennartz <sup>2,5</sup>

<sup>1</sup> School of Chemical Engineering, Jimma Institute of Technology, Jimma University, Jimma P.O. Box 378, Ethiopia

<sup>2</sup> Faculty of Agricultural and Environmental Sciences, University of Rostock, Justus-Von-Liebig-Weg 6, 18099 Rostock, Germany

<sup>3</sup> Faculty of Civil and Environmental Engineering, Jimma Institute of Technology, Jimma University, Jimma P.O. Box 378, Ethiopia

<sup>4</sup> Africa Center of Excellence for Water Management, Addis Ababa University, Addis Ababa P.O. Box 1176, Ethiopia

<sup>5</sup> Correspondence: wondrosen@gmail.com (W.S.G.); esayas16@yahoo.com (E.A.); bernd.lennartz@uni-rostock.de (B.L.); Tel.: +251-911792335 (W.S.G.); +251-917017002 (E.A.); +49-381-498-3180 (B.L.)



Citation: Geleta, W.S.; Alemayehu, E.; Lennartz, B. Fixed-Bed Adsorption: Comparisons of Virgin and Zirconium Oxide-Coated Scoria for the Removal of Fluoride from Water. *Molecules* **2022**, *27*, 2527. <https://doi.org/10.3390/molecules27082527>

Academic Editors: Monika Wronkiewicz and Anna Włodarczyk

Received: 14 March 2022

Accepted: 12 April 2022

Published: 14 April 2022

Publisher's Note: MDPI stays neutral with regard to jurisdictional claims in published maps and institutional affiliations.



Copyright: © 2022 by the authors. Licensee MDPI, Basel, Switzerland. This article is an open access article distributed under the terms and conditions of the Creative Commons Attribution (CC BY) license (<https://creativecommons.org/licenses/by/4.0/>).

**Abstract:** Many people worldwide are exposed to extreme levels of fluoride in drinking water. It is, therefore, critical to develop inexpensive, locally available, and environmentally friendly adsorbents for fluoride-laden water defluoridation. In the current study, virgin scoria (volcanic rock) from Ethiopia, was modified with zirconium oxide and used as an adsorbent in a fixed-bed column aiming at the removal of fluoride from water. The adsorption capability of zirconium oxide-coated scoria (ZrOCS) was compared with unmodified virgin scoria (VSc). XRD, FTIR, XRF, SEM, ICP-OES, and the pH<sub>ZPC</sub> tests were evaluated to explore the adsorption mechanisms. Thermal analysis of VSc and ZrOCS revealed lower total weight losses of 2.3 and 3.2 percent, respectively, owing to the removal of water molecules and OH species linked to metal oxides contained in the material. The effect of test conditions such as the pH of the solution and the influent flow rate on the adsorption capacity of the adsorbent was carefully studied. ZrOCS exhibited the maximum removal capacity of 58 mg/kg, which was 4.46 times higher than the observations for VSc (13 mg/kg) at pH 2, and an initial flow rate of 1.25 mL/min. Breakthrough time increased with decreasing initial pH and flow rate. The adsorption experimental data under various test conditions were examined by the Thomas and Adams-Bohart models. Both models were found very effective in describing the experimental data with a correlation coefficient ( $R^2$ ) of  $\geq 0.976$  (ZrOCS) and  $\geq 0.967$  (VSc). Generally, coating VSc with zirconium oxide improved the adsorption performance of VSc; hence, a ZrOCS-packed fixed bed could be employed for the decontamination of high levels of fluoride from groundwater. However, further examination of the adsorbent using natural groundwater is advisable to produce a definitive conclusion.

**Keywords:** adsorption; fluoride; virgin scoria; zirconium oxide-coated scoria

## 1. Introduction

Fluorine is the thirteenth most abundant element and makes up between 0.06% and 0.09% of the entire Earth's crust [1,2]. Fluorine is always in a combined form of minerals such as fluoride. Fluoride levels in surface water ranged from 0.01 to 0.3 mg/L, while groundwater levels range from less than 1 to more than 35 mg/L [2,3]. Fluoride is thought to have beneficial effects in trace amounts in drinking water, but prolonged exposure to fluoride in drinking water, or combined effect with exposure to fluoride from other sources, could result in some negative effects [4–7]. It can prevent the incidence of dental caries, particularly in children under the age of 8 years, if taken in the drinking water at an



## Annex 2: Supplementary materials to Chapter 2

**Table A2.1** Elemental composition and oxide content of VPum and VSco

Elements	VPum % (wt)	VSco % (wt)	Oxides	VPum % (wt)	VSco % (wt)
Si	27.1	18.3	SiO <sub>2</sub>	68.6	47.4
Al	5.3	10.3	Al <sub>2</sub> O <sub>3</sub>	8.9	21.6
Fe	3.4	7.8	Fe <sub>2</sub> O <sub>3</sub>	4.9	8.9
K	3.8	0.4	K <sub>2</sub> O	5.5	0.5
Ca	0.3	6.4	CaO	1.8	12.4
Na	1.2	2.2	Na <sub>2</sub> O	4.1	3.0
Mg	0.1	2.8	MgO	0.2	3.3
Zn	<0.1	<0.1	TiO <sub>2</sub>	0.3	1.2
Mn	<0.1	0.1	Others	5.7	1.2
Cr	<0.1	<0.1			
Cu	<0.1	<0.1			
Co	<0.1	<0.1			
Cd	<0.1	<0.1			
Ni	<0.1	<0.1			
Pb	<0.1	<0.1			
As	<0.1	<0.1			

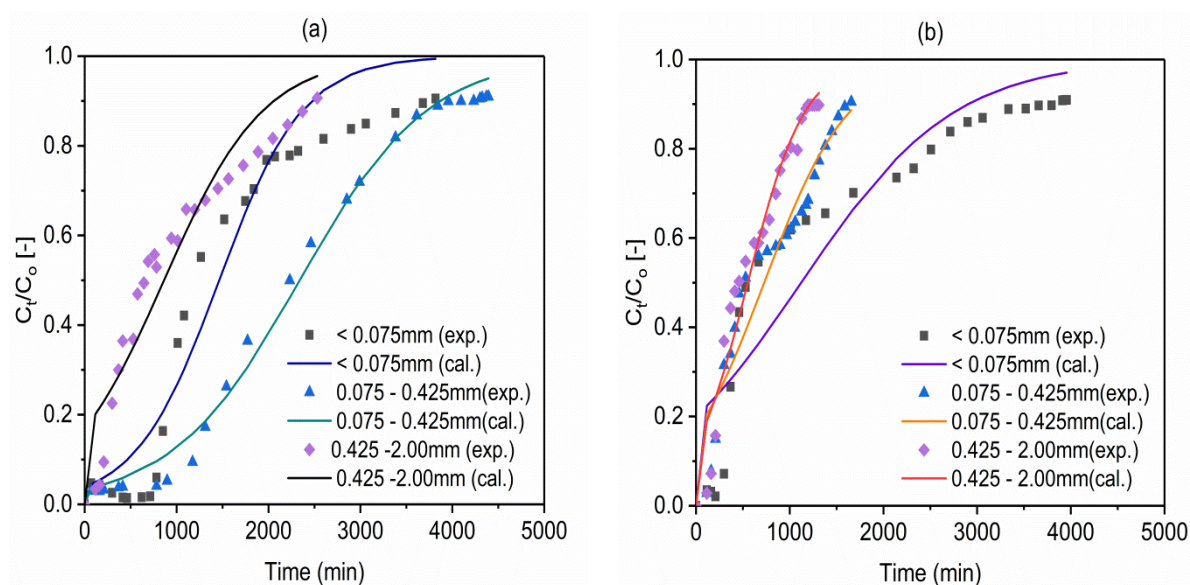


**Figure A2.1** Experimental (exp.) and simulated (cal.; Thomas model) breakthrough curves of fluoride at different particle sizes for (a) VPum and (b) VSco (pH 2.00; C<sub>o</sub>: 10 mg/L; Q<sub>o</sub>: 1.25 mL/min; bed depth 10 cm)

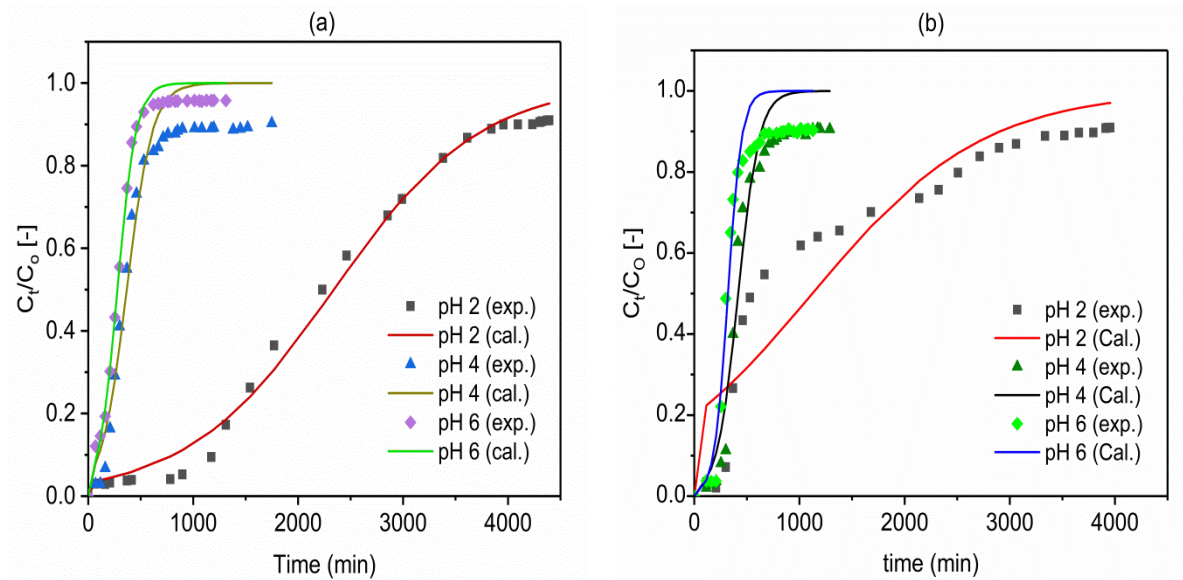


**Figure A2.2** Experimental and simulated (Thomas model) breakthrough curves of fluoride at different pH for (a) VPum: 0.075 – 0.425 mm (b) VSc0: < 0.075 mm ( $C_0$ : 10 mg/L;  $Q_0$ : 1.25 mL/min; bed depth 10 cm)

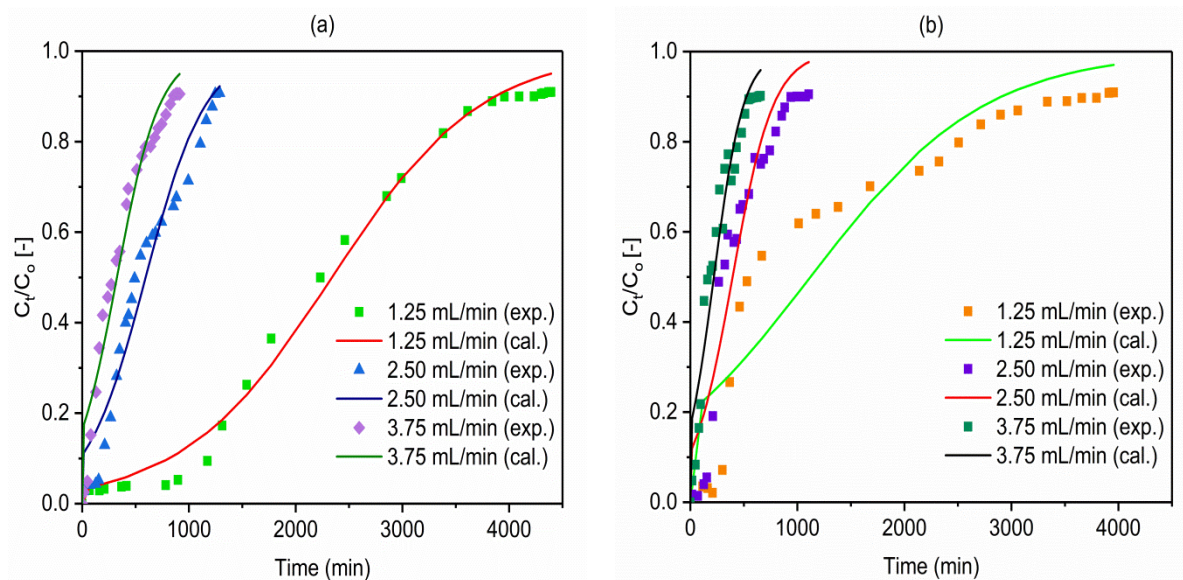


**Figure A2.3** Experimental and simulated (Thomas model) breakthrough curves of fluoride at different influent flow rates for (a) VPum: 0.075 – 0.425 mm and (b) VSc0: < 0.075 mm (pH 2.00;  $C_0$ : 10 mg/L; bed depth 10 cm)

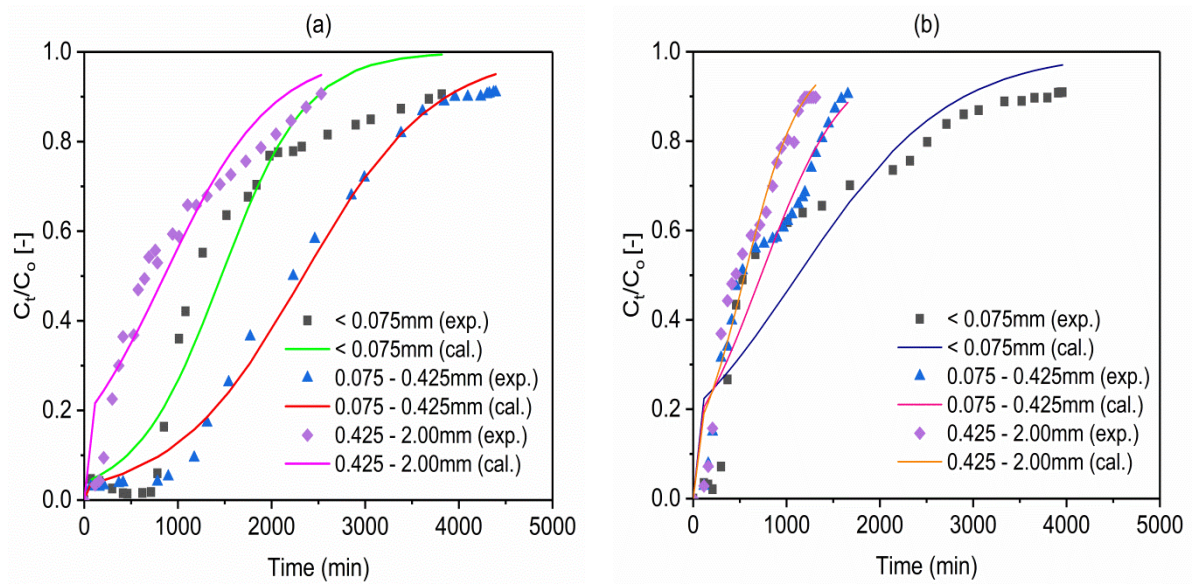


**Figure A2.4** Experimental (exp.) and simulated (cal.; Adams-Bohart model) breakthrough curves of fluoride at different particle sizes for (a) VPum and (b) VSCO (pH 2;  $C_o$ : 10 mg/L;  $Q_o$ : 1.25 mL/min; bed depth 10 cm)

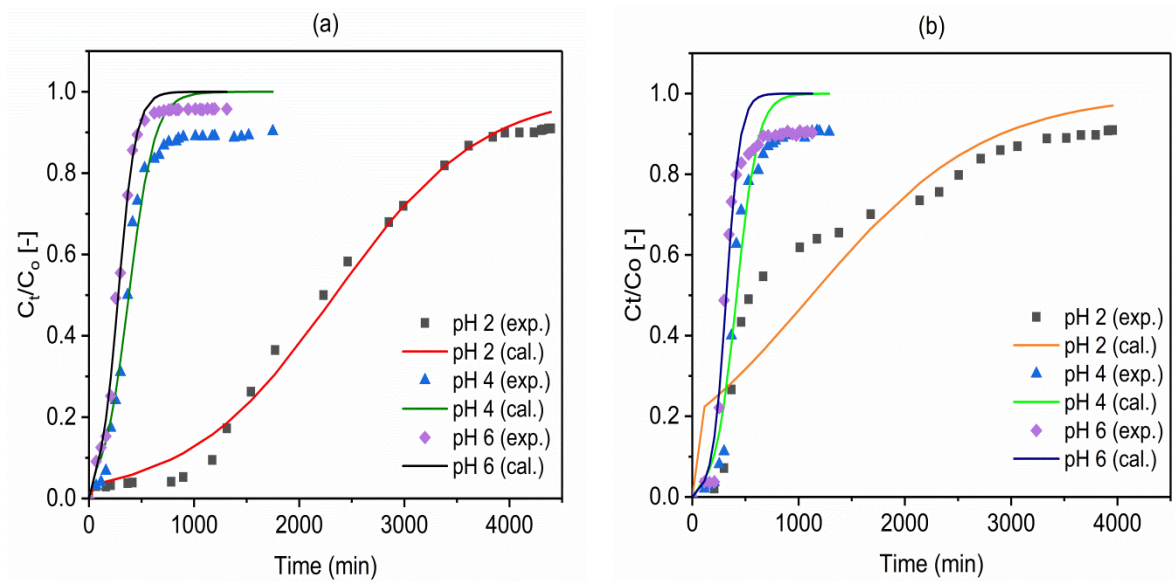


**Figure A2.5** Experimental and simulated (Adams-Bohart model) breakthrough curves of fluoride at different pH for (a) VPum: 0.075 – 0.425 mm and (b) VSCO: < 0.075 mm ( $C_o$ : 10 mg/L;  $Q_o$ : 1.25 mL/min; bed depth 10 cm)

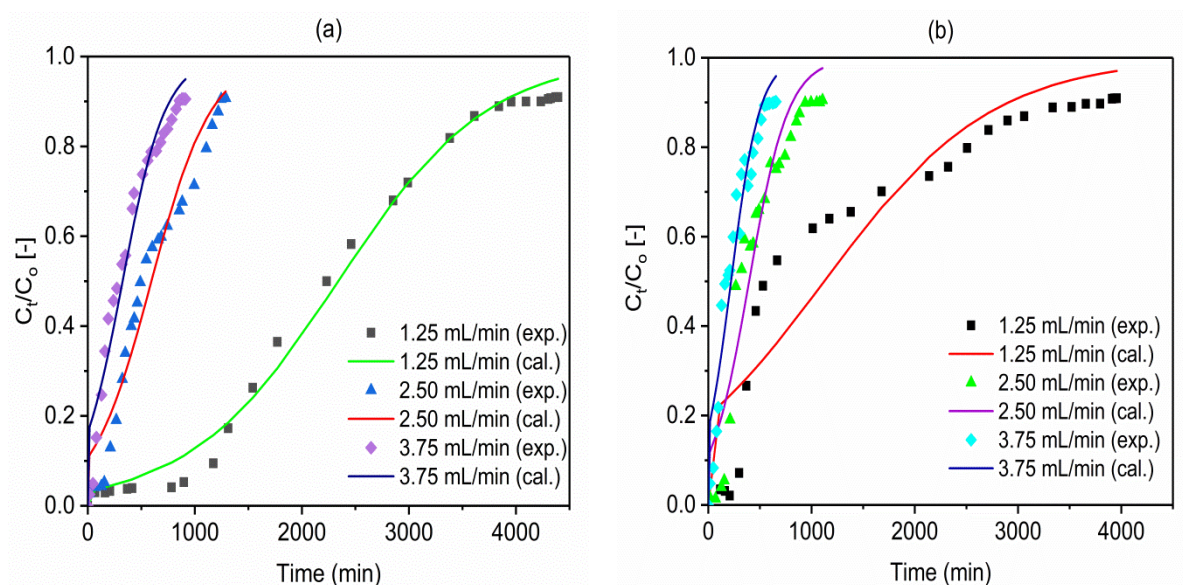


**Figure A2.6.** Experimental and simulated (Adams-Bohart model) breakthrough curves of fluoride at different flow rates for (a) VPum: 0.075 – 0.425 mm and (b) VSc0: < 0.075 mm (pH 2.00;  $C_0$ : 10 mg/L; bed depth 10 cm)



### **Annex 3: Curriculum Vitae (CV)**

#### **Wondwosen Sime Geleta**

Jimma University

P.O. Box: 378 Jimma, Ethiopia

Cellphone: +251-91-179-2335

Personal Email: [wondeto@gmail.com](mailto:wondeto@gmail.com)

Institutional Email: [wondwosen.sime@ju.edu.et](mailto:wondwosen.sime@ju.edu.et)

Google Scholar: Wondwosen Sime Geleta

ResearchGate: Wondwosen Sime

ORCID: <https://orcid.org/0000-0002-2879-9622>



#### **Personal data**

---

Date of Birth: June 30, 1983

Place of birth: Fitcha/North Showa/Oromia/Ethiopia

Sex: Male

Marital Status: Single

Nationality: Ethiopian

#### **Summary**

---

Mr. Geleta has a Bachelor of Science Degree from Bahir Dar University in 2007, a Master's Degree in Chemical Engineering in 2012, and has creditable knowledge and experience in Teaching, Research, Community Service, and leadership.

#### **Software and Skills**

---

Microsoft Office (Basic), E-draw, ChemCAD, Origin Pro., X'Pert HighScore Plus, Mendeley, Design Expert, EndNote

#### **Education**

---

**University of Rostock, Rostock, Germany (October 2018 – onwards)**

Ph.D. candidate, Faculty of Agriculture and Environmental Sciences.

Research area: Water/treatment and pollutant removal, Pollution Control, Environmental Engineering, and sciences, Reaction Engineering/Chemical Engineering

**Addis Ababa University, Addis Ababa, Ethiopia (2010– 2012)**

Master's Degree in Chemical Engineering

Masters Project title: Production of maleic anhydride by oxidation of benzene

**Bahir Dar University, Bahir Dar, Ethiopia (2002– 2007)**

Bachelor of Science in Chemical Engineering

Final year project title: Efficient Utilization of Energy in Brewery Industry: the case of Meta Abo Brewery Factory.

**Employment History**

---

Assistant Professor, School of Chemical Engineering, Jimma Institute of Technology, Jimma University, Jimma, Ethiopia **Since December 2017**

Achievements and responsibilities:

- ❖ Instructed different undergraduate courses (Fluid mechanics for Chemical Engineers, Fundamental of Chemical Engineering, Chemical Reaction Engineering (Kinetics and Reactor Design), Engineering Professions, Reaction Engineering Lab) and postgraduate in Chemical engineering (Advanced Process Control, Advanced Reaction Engineering)
- ❖ Project advisor for undergraduate as part of the BSc curriculum for the final year thesis
- ❖ Coordinator, Pre-Engineering Office (from October 2012 to December 2013) at College of Engineering and Technology, Samara University, Samara, Ethiopia
- ❖ Head, Department of Chemical Engineering (from December 2013 to August 2015) at College of Engineering and Technology, Samara University, Samara, Ethiopia
- ❖ Program Officer (October 2015 to September 2017), Ethiopian Society of Chemical Engineers, Addis Ababa, Ethiopia
- ❖ Coordinator, School Transformation, Academic Quality Assurance, Internship, and Community based Education (May 2016 to January 2017) at the School of Chemical Engineering, Jimma Institute of Technology, Jimma University, Jimma Ethiopia
- ❖ Head, School of Chemical Engineering (from January 2017 to September 2018) at Jimma Institute of Technology, Jimma University, Jimma Ethiopia

**Projects and researches**

- 
- ❖ Coordinator on Megaproject entitled “waste resource utilization as energy”
  - ❖ Involved in multiple community-based research projects undertaken by students as an advisor at various times.

**Training and Workshops**

- 
- Participated in different pieces of training and workshops in Ethiopia as well as in Germany

## **Publications and conferences**

---

1. Geleta, W.S.; Alemayehu, E.; Lennartz, B. Volcanic Rock Materials for Defluoridation of Water in Fixed-Bed Column Systems. *Molecules* **2021**, *26*, 977. <https://doi.org/10.3390/molecules26040977>
2. Geleta, W.S.; Alemayehu, E.; Lennartz, B. Enhanced Defluoridation of Water Using Zirconium-Coated Pumice in Fixed-Bed Adsorption Columns. *Materials* **2021**, *14*, 6145. <https://doi.org/10.3390/ma14206145>
3. Geleta, W.S.; Alemayehu, E.; Lennartz, B. Fixed-Bed Adsorption: Comparisons of Virgin and Zirconium Oxide-Coated Scoria for the Removal of Fluoride from Water. *Molecules* **2022**, *27*, 2527. <https://doi.org/10.3390/molecules27082527>
4. Geleta, W. S., Alemayehu, E., & Lennartz, B. Enhanced Defluoridation from Aqueous Solutions using Zirconium-coated Pumice in Fixed-bed Column Systems. *Proceedings of the MOL2NET 2021, International Conference on Multidisciplinary Sciences*, (7th edition, 25 January 2021–30 January 2022), 1–5. <https://doi.org/10.3390/mol2net-07-10687>

## **References**

---

### **Prof. Dr. Bernd Lennartz**

Professor of Soil physics, Faculty of Agriculture and Environmental Sciences, University of Rostock  
Justus Von-Liebig Weg 6, 18051 Rostock, Germany

Telephone: +49-381-498-3180

E-mail: [bernd.lennartz@uni-rostock.de](mailto:bernd.lennartz@uni-rostock.de)

### **Prof. Dr. -Ing Esayas Alemayehu**

Professor of Water and Environmental Engineering, Faculty of Civil and Environmental Engineering, Jimma  
Institute of Technology, Jimma University, P.O. Box 378 Jimma, Ethiopia

Cellphone: +251-91-701-7002

E-Mail: [esayas16@yahoo.com](mailto:esayas16@yahoo.com)

### **Dr. -Ing Nigus Gabbiye (Asso. Prof.)**

Bahir Dar Institute of Technology, Bahir Dar University, P.O. Box. 79, Bahir Dar, Ethiopia

Cellphone: +251-92-257-4439

E-Mail: [nigus\\_g@yahoo.com](mailto:nigus_g@yahoo.com)